Investigation into Branching in Acrylate Polymerization: Advanced Characterization and Kinetics

A thesis submitted in partial fulfilment of the requirements for the degree of Doctor of Philosophy in Chemistry at the University of Canterbury, Christchurch, New Zealand

Jean-Baptiste Lena

2018

Declaration

This thesis has not been previously submitted, in whole or in part, for any degree at this or any other university. This work is original and my own, carried out under the supervision of Dr Sarah Masters, A/Prof Greg Russell, Dr Patrice Castignolles and Dr Marion Gaborieau. where this is not so, credit has been duly given.

(Jean-Baptiste Lena)

Acknowledgements

I would firstly like to thank all my supervisory team, Sarah Masters, Greg Russell, Patrice Castignolles and Marion Gaborieau, for the opportunity to take this project, for proof reading this thesis as well as abstracts, publications, progress reports and grant applications. They pushed me to try my best and to be confident. I also thank Mike Reid for his continued support. Over my PhD studies, my anxiety could have taken over my work if they had not been here to keep me on track.

My PhD work involved a lot of lab experiments. I would not have been able to successfully carry out the experimental part without the outstanding support of Matt Polson, who was always available for advice and spent time with me in the lab. I also thank Samantha Bodman, Will Kerr and Nic Bason for their everyday help in an organic chemistry lab. Different analyses needed to be done over the last four years. I would like to thank Alexander Goroncy and Marie Squire for their training in the NMR room and for successfully performing the mass spectrometry experiments.

As my PhD required advanced characterization of complex polymers, some specific analyses needed to be done and the equipment at UC was not sufficient. I would like to thank Patrice Castignolles and Marion Gaborieau for generously making the capillary electrophoresis equipment available to me, and for training me to use the instruments at the Western Sydney University. In this instance, I also give a big thank you to Alison Maniego, Joel Thevarajah, Hai Feng, James Lee, Mathew Van Leeuwen and Adam Sutton for their help in the capillary electrophoresis lab. Hank de Bruyn and Natasha Sciortino are acknowledged for having successfully performed TGA and DSC analyses in their lab, at the University of Sydney. I would particularly like to thank Michael Deschamps for performing melt-state NMR spectroscopy (at high temperature and very high magnetic field, in the CNRS of Orleans) of hydrophobic polymers. This equipment is not available in New Zealand.

Over the four years of study here and my previous years of Master's degree in Montpellier, I have had the opportunity to meet researchers in polymer science and to develop personal contact with them. I would like to thank Chris Fellows, Cedric Loubat, Nathalie Delaunay, Per Zetterlund, Denis Bertin, and Ghislain David for providing advice and feedback on my work when I contacted them.

Finally, I would like to express my love and gratitude to my parents, Isabelle Pitchal and Jacques Lena, for their moral and financial support over my years of study.

Abstract

Branching has been investigated in poly(acrylic acid) (PAA) and poly(2-ethylhexyl acrylate) (P2EHA) synthesized by conventional radical polymerization with and without chain transfer agent (CTA) at different temperatures and initial monomer concentrations. The average number of branches per monomer unit (i.e., degree of branching) was quantified by solution-state ^{13}C NMR spectroscopy (solution-state and melt-state for PAA and P2EHA respectively). The heterogeneity of branching in PAA (dispersity of the electrophoretic mobility distributions) was measured by capillary electrophoresis in the critical conditions (CE-CC). For PAA, the degree of branching (*DB*) increases with the reaction temperature due to a rise in the frequency of reactions leading to branches, while the heterogeneity of branching remains steady. *DB* is lower in polymer synthesized with CTA. This decrease is due to either the CTA quenching the mid-chain radicals or a reduction of the rate of chain transfer to polymer relative to (chain-end) propagation. No influence of initial monomer concentration on *DB* and on the heterogeneity of branching was observed. Results were slightly different for the P2EHA. Electrospray ionization-mass spectrometry analyses have revealed the occurrence of β-scission and of termination products, which was not the case for PAA. The *DB* of P2EHA is also reduced by the presence of a CTA but its increase with temperature is not observed anymore when the β-scission becomes important. Backbiting rate coefficients of PAA and P2EHA were evaluated from the *DB* values. Further characterization of PAA by CE-CC was carried out. The mechanism of separation has been studied in depth. The effects of ionic strength and the addition of silver on the selectivity of separation were investigated. The optimal separation of branched poly(sodium acrylate) (PNaA) was obtained at high sodium borate buffer concentration, as the different peaks (corresponding to different branching densities) in a sample are completely resolved in electropherograms and no adsorption of polymer on the capillary was observed. No influence of the addition of silver on the selectivity of separation was observed. The potential complexation between PNaA and buffer and its effect on the analysis were investigated. The improvement of separation of PNaA by branching has allowed new findings on the dispersity of electrophoretic mobility distribution that were not previously observable. Finally, alternative methods to size exclusion chromatography (SEC) were tested on PAA to obtain size-based characterization: diffusion coefficients and hydrodynamic radii of PAAs can be obtained by Taylor dispersion analysis and the M_n can be obtained by quantification of end groups with ^{1}H solution-state NMR spectroscopy.

UNIVERSITY OF CANTERBURY
Te Whare Wānanga o Waitaha
CHRISTCHURCH NEW ZEALAND

Deputy Vice-Chancellor's Office
Postgraduate Office

Co-Authorship Form

This form is to accompany the submission of any thesis that contains research reported in co-authored work that has been published, accepted for publication, or submitted for publication. A copy of this form should be included for each co-authored work that is included in the thesis. Completed forms should be included at the front (after the thesis abstract) of each copy of the thesis submitted for examination and library deposit.

Please indicate the chapter/section/pages of this thesis that are extracted from co-authored work and provide details of the publication or submission from the extract comes:

Chapter 2 contains work from a journal article that has been published in *Polymer*

J.-B. Lena, A.K. Goroncy, J.J. Thevarajah, A.R. Maniego, G.T. Russell, P. Castignolles, M. Gaborieau, *Polymer*, 114 (2017) 209-220.

Chapter 4 contains work from a manuscript that has been submitted to *Macromolecular Chemistry & Physics*

J.-B. Lena, M. Deschamps, N.F. Sciortino, S.L. Masters, M.A. Squire, G.T. Russell, *Macromolecular Chemistry & Physics*, accepted (macp.201700579)

Please detail the nature and extent (%) of contribution by the candidate:

For the first publication, experimental data were collected by the candidate (except one NMR analysis that was obtained by Alison R. Maniego, a Western Sydney University Ph.D. candidate, and the manuscript was written by the candidate.

For the submitted manuscript, melt-state NMR analyses were carried out by Prof. Michael Deschamps (CNRS Orleans, France) and the DSC and some TGA analyses were conducted by Dr. Hank de Bruyn and Dr. Natasha Sciortino (University of Sydney). The other analyses were carried out by the candidate. The manuscript was written by the candidate and the candidate also undertook analyses and interpretation of all experimental data.

Certification by Co-authors:
If there is more than one co-author then a single co-author can sign on behalf of all
The undersigned certifys that:

- The above statement correctly reflects the nature and extent of the PhD candidate's contribution to this co-authored work
- In cases where the candidate was the lead author of the co-authored work he or she wrote the text

Name: Sarah Masters Signature: 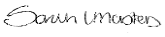 Date: *01/03/2018*

Table of content

Chapter 1

Introduction

1.1 General Introduction

Polymer chemists have always been interested in the structural characterization of polymers and the determination of rate coefficients in radical polymerization. Size, presence of branches, dispersity of molar mass and heterogeneity of branching all strongly influence physical and chemical properties of polymers. Short branches influence mainly physical properties e.g. glass transition temperature or melting point whilst long branches affect rheology [1]. Furthermore, accurate knowledge of the kinetics of radical polymerization is useful for fundamental and industry-oriented applications.

In recent years, different methods have been developed to characterize the structure of a polymer and determine different kinetic rate coefficients. The size and the dispersity of molar mass of polymers are generally determined using size exclusion chromatography (SEC) [2, 3], while the degree of branching (i.e. number of branches per monomer unit) is determined by ^{13}C NMR spectroscopy [4, 5]. The heterogeneity of branching can be obtained using free solution capillary electrophoresis in the critical conditions (CE-CC) [6]. Propagation and termination rate coefficients can be determined by pulsed-laser polymerization (PLP) coupled with SEC [7] and with EPR spectroscopy respectively [8]. The backbiting rate coefficient can be determined by frequency-tuned PLP coupled with SEC (ft-PLP-SEC) and by electron paramagnetic resonance (EPR) spectroscopy [9]. It can also be calculated from the degree of branching, as obtained by NMR [5].

Even though all these methods were used and developed over the last thirty years, some of them are not accurate, or they are expensive, and therefore not available in all research institutes. For instance, the molar mass determination of poly(acrylic acid) (PAA) and poly(2-ethylhexyl acrylate) (P2EHA) using SEC shows up to 100% error [3, 10]. Ft-PLP-SEC and EPR spectroscopy are expensive and hard to use. On the other hand, CE-CC is a cheap, straightforward and efficient method that can be used to separate water-soluble polyelectrolytes by branching [11]. This is the case even though the mechanism of separation of branched polyelectrolytes is not yet fully understood, and only incomplete knowledge of the heterogeneity of branching is available. The degree of branching can easily be determined using different ^{13}C NMR spectroscopy methods (solution-state and melt-state).

Moreover, these polymers present different properties which allow interesting commercial uses. PAA is a hydrophilic polymer that can be used as a scale control agent [12] and water

purifier while P2EHA is an hydrophobic polymer used as a waterborne coating [13] or in pressure sensitive adhesives [14].

Consequently, this thesis deals with the determination of the degree of branching of PAA and of P2EHA of different size by ^{13}C NMR spectroscopy, and from this the calculation of the backbiting rate coefficients in these polymerizations. This will allow to compare the transfer to polymer reactions for hydrophilic and hydrophobic polymers. P2EHA has been chosen as it has a low T_g (between –60 °C and –90 °C) due to its long ester side group. This will allow branching measurements by melt state NMR below 100 °C, which fit with the available equipment. More details will be given in Chapter 4.

As PAA is a hydrophilic polymer, its base, poly(sodium acrylate) (PNaA) can be characterized by CE-CC. The mechanism of separation of PNaA by branching will be studied in depth and the heterogeneity of branching of PNaA will be estimated and compared with previous results. Finally, some other methods of size-based characterization will be tested: the determination of the fraction of chain-ends using ^{1}H NMR spectroscopy and the Taylor dispersion analysis using CE equipment. In all cases, the precision and accuracy of the method will be provided.

1.2 Kinetics of radical polymerization

Radical polymerization is a chain polymerization in which polymers are formed by successive addition of monomer building blocks. The mechanism consists of different steps: initiation, propagation, termination and sometimes chain transfer. It is used to obtain a wide variety of polymer and composite materials.

1.2.1 Initiation, propagation and termination

Three core reactions always occur in radical polymerization:

- Initiation: radicals are formed from an initiator. Each radical may react with a monomer to form a radical monomer. The initiator can decompose into radicals by various paths. The two most common ways are photolytic cleavage (or photoinitiation), in which (typically) UV rays lead to a homolytic scission in a photoinitiator, and thermal decomposition, in which heating leads to homolytic scission in a (so-called) chemical

initiator. Less commonly, redox processes may be used to generate radicals. Photo and redox initiations are known to be efficient at low temperature. On the other hand, so called autoiniation – the generation of radicals directly from monomer – comes into play at high temperatures.

- Propagation: radicals react with further monomer to sustain and grow a living chain.
- Termination: two radicals either combine together to form a single chain of cumulative length or they disproportionate to form dead chains of the size of each radical. Dead chains may also be formed by transfer of the radical activity to another molecule, but this is usually regarded as a different type of reaction, because it does not eliminate radical activity.

The general mechanism of the above steps is represented in Scheme 1.1.

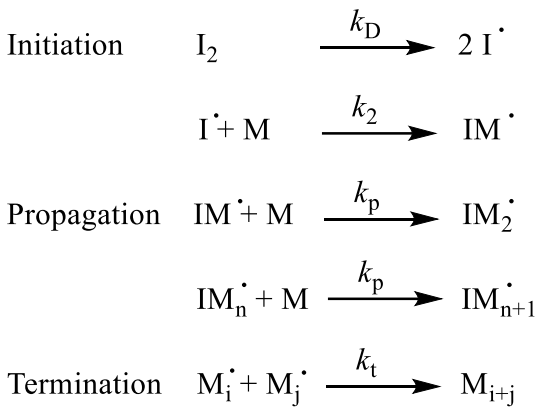

Scheme 1.1: Main steps of the mechanism of radical polymerization. The termination in this scheme is by combination. (Note that I_2 represents an initiator molecule, not molecular iodine.)

To define the initiation rate R_i, the factor f (initiator efficiency) must be taken into account. This represents a solvent‐related factor for escape of radicals from geminate recombination, and is a value between 0 and 1. Thus, R_i is expressed according to Eq. (1.1):

$$R_i = 2fk_d[I_2] \tag{1.1}$$

The polymerization rate is defined as the rate of disappearance of monomer (see Eq. (1.2)):

$$R_p = -\frac{d[M]}{dt} \tag{1.2}$$

In order to calculate R_p, the quasi-steady state approximation (QSSA) is often considered. This is an approximation which states that the concentration of the active growing chains remains constant, i.e. the rate of initiation and termination is the same. Figure 1.1 (from [15]) illustrates attainment of steady-state conditions, and thus validity of the QSSA.

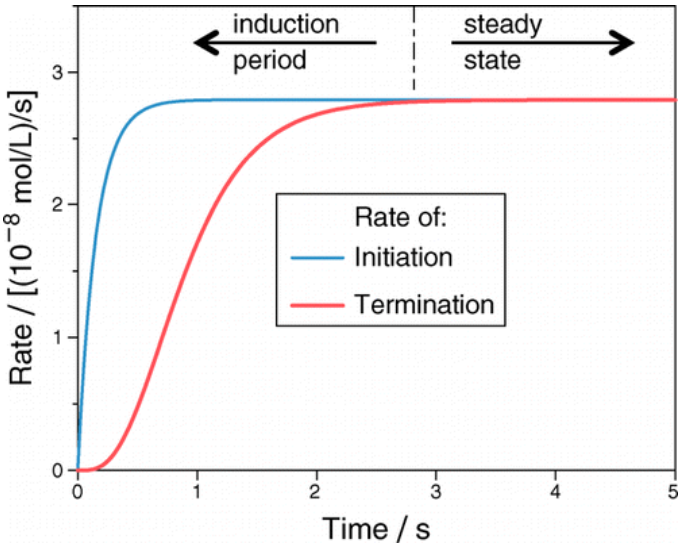

Figure 1.1: Rates of initiation and termination (as indicated) versus time, *t*, for a radical polymerization reaction. Reprinted with permission from [15]. Copyright 2014 American Chemical Society.

After a certain time called the 'induction period', the initiation rate becomes equal to the termination rate, at which point there is a steady state in radical concentration. As this time is usually very fast – between 2 and 3 seconds in Figure 1.1 – compared with the overall polymerization time, which is typically hours, the QSSA essentially holds throughout a polymerization. Consequently, when the QSSA is reached, Eq. (1.3), (1.4) and (1.5) apply:

$$\frac{d[I\cdot]}{dt} = 0 \tag{1.3}$$

$$\frac{d[M\cdot]}{dt} = 0 \tag{1.4}$$

$$2fk_d[I_2] = 2k_t[M\cdot]^2 \tag{1.5}$$

Note that $[M\cdot] = \sum_{i=1}^{\infty}[M_i]$ and is the overall concentration in polymer radicals. From Equation 5 it can be expressed as in Eq. (1.6):

$$[M^{\cdot}] = \sqrt{\frac{f k_d [I_2]}{k_t}} \tag{1.6}$$

Eq. (1.7) gives the kinetics of initiator decomposition, which follow from this being a unimolecular reaction:

$$[I_2] = [I_2]_0 e^{-k_d t} \tag{1.7}$$

It is also assumed that k_p *[M·]* >> k_2 *[I·]*: this is the so-called long-chain approximation. Consequently, $R_p = k_p$ *[M][M·]*, leading to the following analytical expressions providing the monomer concentration (Eq. (1.8)), monomer conversion (Eq. (1.9)), and the kinetic chain length (Eq. (1.10)) as a function of time.

$$[M] = [M]_0 e^{\frac{2k_p}{k_d}\sqrt{\frac{2f k_d [I_2]}{k_t}}\left(e^{\frac{-k_d t}{2}}-1\right)} \tag{1.8}$$

$$X = 1 - \frac{[M]}{[M]_0} = 1 - e^{-k_p t\sqrt{\frac{f k_d [I]}{k_t}}} \tag{1.9}$$

$$\nu = \frac{R_p}{R_i} = \frac{k_p [M]}{2\sqrt{f k_d [I_2] k_t}} \tag{1.10}$$

ν is the average number of propagation events a radical undergoes before terminating. These equations make it clear that to understand and model polymerization kinetics and product properties, rate coefficients must be known [16, 17].

1.2.2 Backbiting and chain transfer

In radical polymerization, a chain transfer is defined as a polymerization reaction in which the activity of a growing radical in transferred elsewhere, either to another molecule or to another site on the same molecule. Chain transfer can be either introduced deliberately, using a chain transfer agent, or be a side reaction (transfer to monomer, transfer to solvent, transfer to polymer leading to branching). With the exception of chain transfer to polymer, a chain transfer reaction reduces the average chain length of a polymer. As the branching in radical polymerization as well as the impact of a chain transfer agent on the polymer structure constitute an important part of this Ph.D., transfer to polymer and to a chain transfer agent will now be detailed.

1.2.2.1 Transfer to polymer

In some cases, intra- and intermolecular chain transfer to polymer occurs, which has ramifications. Long chain branching (LCB) results from intermolecular and random intramolecular chain transfer, while short chain branching (SCB) results from intramolecular chain transfer. The dominant process in the formation of branches is intramolecular transfer, also called backbiting, which proceeds as a pericyclic reaction reaction, as shown below.

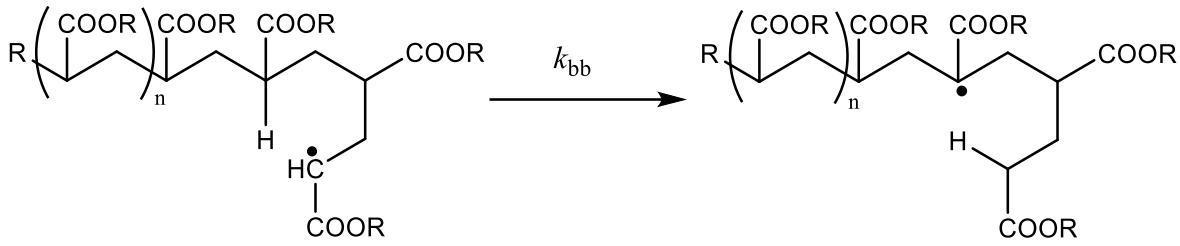

Scheme 1.2: Intramolecular chain transfer in polyacrylates.

As can be observed, a secondary propagating radical (SPR) is transformed into a tertiary midchain radical (MCR), with a backbiting rate coefficient k_{bb}. An MCR can become an SPR again via propagation (addition to monomer) leading to branches. MCRs propagate with a kinetic rate coefficient k_p^t that is much lower than k_p. Thus their presence strongly affects the polymerization kinetics. As the propagation frequency varies with monomer concentration, the fraction of MCRs, X^{MCR}, varies with the monomer concentration, and thus the monomer conversion [18]. Experimental results have shown. that the occurrence of backbiting raises the order of reaction with respect to [M] from 1 to a value of between 1.4 and 1.8 [19]. The different elementary processes in the case of backbiting are presented below.

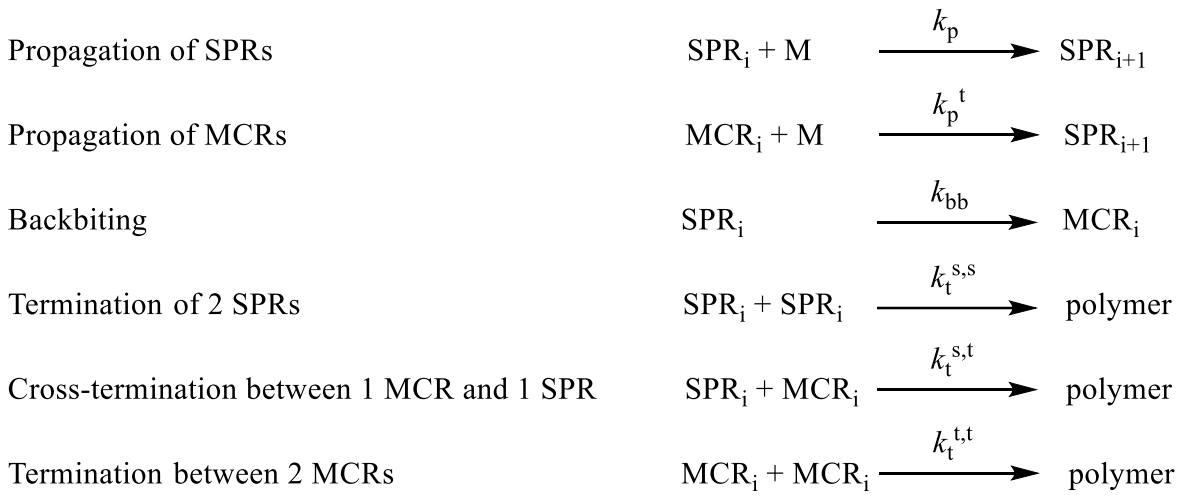

Scheme 1.3: Steps in radical polymerization process when backbiting occurs.

The last of these reactions is thought to be negligible in rate because the rate coefficient is very low due to steric hindrance. In the case of poly(acrylic acid) and poly(alkyl acrylate)s, intramolecular chain transfer occurs above 20 °C [18]. Thus its complicating effect on kinetics – see above – must routinely be considered.

Intermolecular chain transfer is an exchange of H atom between a living radical and a dead chain. It is more prominent at high conversion because the polymer concentration is so high [20].

As previously discussed, branching strongly influences the properties of the polymer. SCB mainly influences physical properties such as melting point and glass transition temperature, whilst LCB affects viscoelastic properties [1]. One consequence of branching can be inaccurate determination of the propagation rate coefficient, k_p, by pulse-laser polymerization (PLP) coupled with size exclusion chromatography (SEC) [21]. Long-chain branching (LCB) was detected even at low conversion and it was shown that it can decrease the accuracy of the molar mass determined by SEC, and hence the k_p obtained is less accurate (up to 100 % error) [10]. The molar masses of PAAs determined by SEC showed low accuracy [3], potentially due to long-chain branching. That will be discussed at a later stage. Short-chain branching also has an important effect on PLP-SEC, in that the obtained k_p is an average over the SPR and MCR fractions.

1.2.2.2 Transfer to a chain transfer agent

Chain transfer to a small molecule reduces the average length of the polymer. Such chain transfer can either be introduced deliberately into a polymerization reaction or occur as a side reaction with various component of the polymerization, most notably solvent, monomer or even initiator.

A chain transfer agent is a molecule with at least one weak chemical bond, which facilitates the transfer reaction. Commonly used chain transfer agents include thiols and halocarbons [22].

Of course the presence of a chain transfer agent (CTA) influences the outcome of a radical polymerization. A brief summary of the effect of CTA on the mechanism is detailed below. Scheme 1.4 shows the mechanism of radical polymerization in the presence of a CTA.

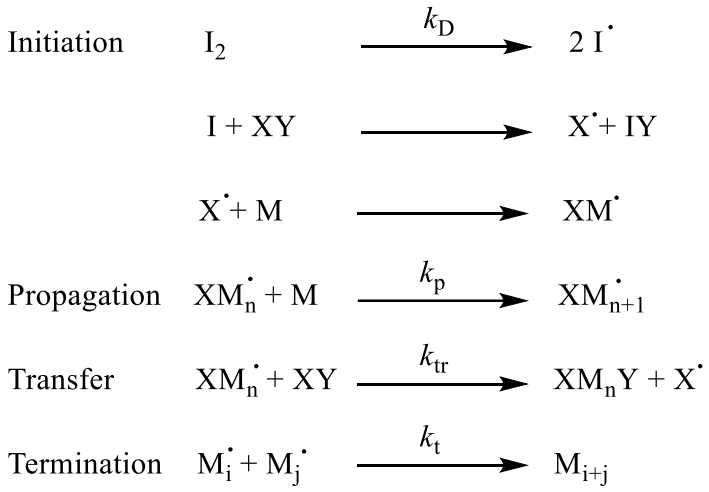

Scheme 1.4: Mechanism of radical polymerization in the presence of a chain transfer agent, XY. (Note that I_2 represents an initiator molecule, not molecular iodine.)

The number-average degree of polymerization in absence of CTA, DP_n^0, can be expressed according to Equation 11:

$$\overline{DP_n^0} = (1 + a)\nu \tag{1.11}$$

Here ν is the kinetic chain length (given by Eq. (10)) and a is the fraction of dead chain formed by combination. In the cases of radical polymerization of acrylic acid and alkyl acrylate, a can

be considered as equal to unity, as the fraction of chain formed by disproportionation is negligible.

The number-average degree of polymerization in the presence of a CTA, DP_n, is expressed as in Eq. (1.12):

$$\overline{DP_n} = \frac{R_p}{(1+a)R_i + R_{tr}} \tag{1.12}$$

From Eq. (1.10), (1.11) and (1.12):

$$\frac{1}{\overline{DP_n}} = \frac{2\sqrt{fk_D k_t}}{(1+a)k_p}\frac{\sqrt{[I_2]}}{[M]} + \frac{k_{tr}}{k_p}\frac{[XY]}{[M]} \tag{1.13}$$

$$\frac{1}{\overline{DP_n}} = \frac{1}{\overline{DP_n^0}} + C_T\frac{[XY]}{[M]}, C_T = \frac{k_{tr}}{k_p} \tag{1.14}$$

The transfer constant C_T can be determined using either the Mayo method [23] or, less commonly, O'Brian's method [24]. These are detailed in the literature.

Some literature values are given in Table 1.1.

Table 1.1: Values of C_T for various thiols, as taken from the literature. AA stands for acrylic acid while MMA stands for methyl methacrylate.

CTA	monomer	solvent	Temperature	$\boldsymbol{C_T}$	Ref.
Thioglycolic acid	AA	water	65 °C	0.5	[25]
Thioglycolic acid	AA	Water/THF (8/2)	65 °C	1	[25]
Mercaptoethanol	AA	water	50 °C	0.28	[5]
Dodecanethiol	MMA	bulk	40 °C	0.63-0.85	[26]
Dodecanethiol	MMA	bulk	60 °C	0.97-1.51	[26]

1.3 Hydrophilic and hydrophobic polymers studied in this Ph.D.

It is known that PAA is a hydrophilic polymer due to the presence of COOH groups. All poly(alkyl acrylates) are hydrophobic due to the absence of groups able to form H-bonds with water molecules. Even though different poly(alkyl acrylates) have been subject to an important number of research studies, the literature about characterization of PAA and kinetics of radical polymerization of acrylic acid is still incomplete and can be improved.

A brief introduction to PAA and P2EHA is provided below (structure, properties and main applications).

1.3.1 Poly(acrylic acid)

PAA is a water-soluble polymer with a wide range of applications, for example as a superabsorbent [27], water purification aid [28], drug carrier [29, 30] and scale control agent [12]. The chemical structure of PAA is shown below, including the effect of pH. Its capacity to form H-bond with water molecules makes evident why it is hydrophilic.

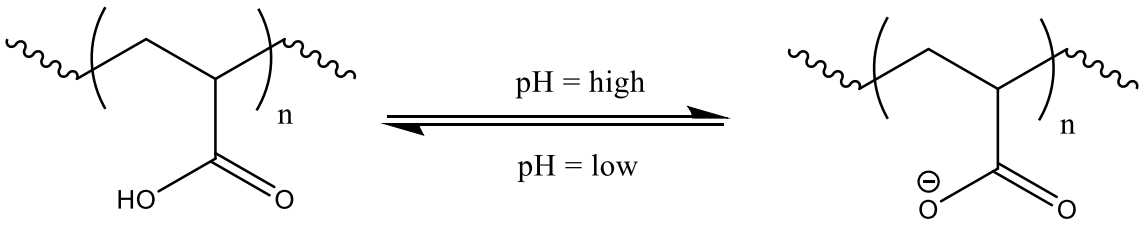

Scheme 1.4: Structure of poly(acrylic acid). The equilibrium lies to the right at high pH and to the left at low pH.

Even if it is not always acknowledged, PAA is branched when produced by radical polymerization [11, 31, 32]. The rate coefficients of radical polymerization of water-soluble monomers such as acrylic acid (AA) must be known for fundamental and application-oriented interests [16] as it provides useful information on its synthesis and structure.

1.3.2 Poly(2-ethyl hexyl acrylate)

P2EHA is a hydrophobic polymer with a large pendant group, which lowers its glass transition temperature (T_g). This allows applications in pressure sensitive adhesives [14]. As the polymer becomes softer when the end group size increases, such poly(alkyl acrylates) can be used as basic components of acrylic latex [33]. It also has applications in nanocomposites [34]. Its structure is given in Figure 1.2.

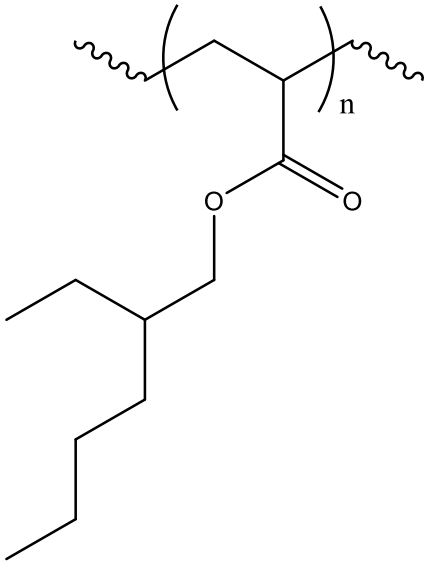

Figure 1.2: Structure of poly(2-ethyl hexyl acrylate).

Like PAA, P2EHA contains tertiary C-H bonds (on the polymer backbone) that are α to a carbonyl group. For this reason they can both undergo backbiting and intermolecular chain transfer to polymer. The occurrence of branching in P2EHA synthesized in bulk [35], solution [4, 36] and emulsion [33] has already been proven.

1.4 Determination of kinetic rate coefficients

For fundamental and industry-oriented applications, it is important to evaluate the different kinetic rate coefficients in radical polymerization. Even though only determination of the backbiting rate coefficients, k_{bb}, are carried out in this Ph.D., values of propagation and termination rate coefficients, k_p and k_t respectively, are useful for the interpretation of different results. Consequently, details on the previous work on k_p and k_t determination for PAA and poly(alkyl acrylates) are given below.

1.4.1 Propagation rate coefficient, k_p

Pulsed-laser polymerization (PLP) coupled with analysis of the molecular weight distribution (MWD) of the resulting polymer by size-exclusion-chromatography (SEC) has been recommended by the IUPAC Working Party on *Modeling of Polymerization Kinetics and Processes* as the method of choice to determine propagation rate coefficients, k_p.

It is relatively easy to see that when chain transfer is negligible, the average chain length (or degree of polymerization), L, of polymer obtained in the time between laser pulses, t_d, is given by Eq. (1.15):

$$L = k_p[M]t_d \tag{1.15}$$

This is because in (multiple-pulse) PLP, laser pulses strike at regular intervals. When a new pulse arrives, radicals will be distributed in a relatively monodisperse population of sizes $k_p[M]t_d$, $2k_p[M]t_d$, $3k_p[M]t_d$… from previous pulses. After a new pulse, these populations will be subject to a much higher frequency of termination due to the creation of a whole crowd of new radicals. Consequently, dead chains predominantly of size $k_p[M]t_d$, $2k_p[M]t_d$, $3k_p[M]t_d$… will be obtained. Therefore, if the chain length is determined by SEC, it becomes easy to determine k_p, as t_d (inverse of laser frequency) and $[M]$ ($\approx [M]_0$, as the monomer conversion is very low with PLP-SEC) are known. This concept was first published by Olaj and co-workers in 1987 [7]. The chain length L is determined from SEC analysis, as exemplified below:

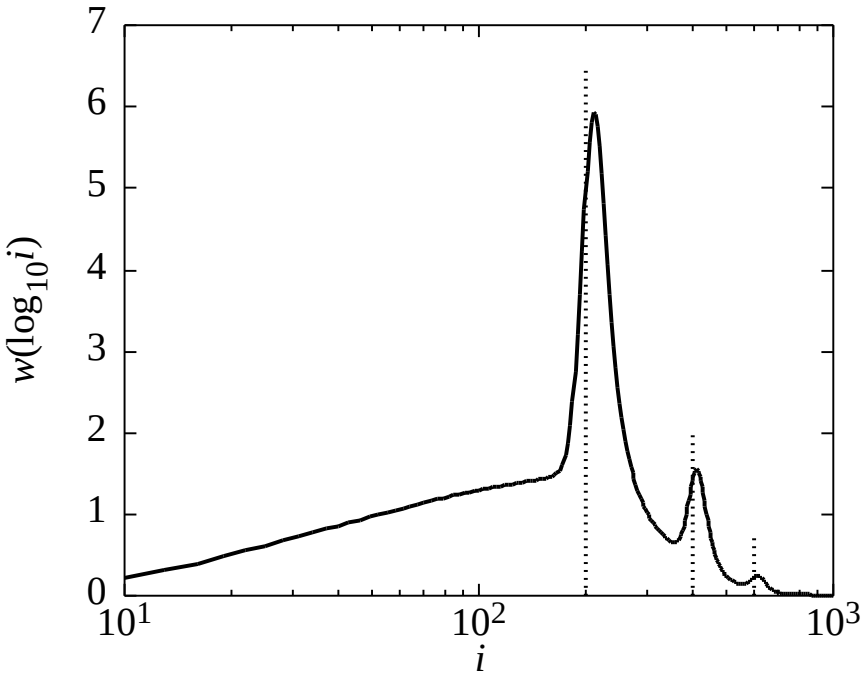

Figure 1.3: Chain length distribution, presented as $w(\log_{10} i)$, where w is the weight fraction and i is the chain length, from simulation of a multiple-pulse PLP [8]. The dotted vertical lines represent $k_p[M]t_d$, $2k_p[M]t_d$, $3k_p[M]t_d$ for the simulation. Copyright 2017 Willey.

L best corresponds to the point of inflection on the low molecular weight side of each MWD peak, as shown in Figure 1.3 [8].

When setting up a PLP-SEC experiment to determine k_p of a polymerization, some consistency criteria must be fulfilled [37]:

- Reproducibility
- Independence of k_p from the laser pulse repetition rate
- Consistency of k_p from at least the 2 first points of inflection of the distribution

In the case of systems with backbiting, if the chosen pulse separation time is too high, growing radicals are subject to several backbiting events during that time, meaning that the apparent k_p is lowered because of the much slower propagation of MCRs. The mean lifetime of a secondary radical before it undergoes a backbiting event is given by Eq. (1.16):

$$\tau_{bb} = 1/k_{bb} \tag{1.16}$$

The time between two laser-pulses must be smaller than this so as to avoid backbiting and thus obtain a reliable k_p for SPRs. As the activation energy of backbiting is greater than that of propagation, an increase in temperature results in backbiting becoming more prominent [38].

Some literature values of k_p obtained by PLP-SEC are given in Table 1.2.

Table 1.2: Propagation rate coefficient values of AA and 2EHA from the literature.

monomer	Monomer content	Solvent	k_p (L mol^{-1} s^{-1})	Ref
AA	20 %	Water	$1.20 \times 10^7 e^{-\frac{1437}{T}}$	[16]
AA	40 %	Water	$8.89 \times 10^6 e^{-\frac{1468}{T}}$	[16]
AA	-	Water	$3.20 \times 10^7 e^{-\frac{1564}{T}}\left(0.11 + (1-0.11)e^{-3w'_{AA}}\right)^*$	[5]
2EHA	-	bulk	$9.1 \times 10^6 e^{-\frac{1901}{T}}$ $(10\,°C < T < 60\,°C)$	[39]
2EHA	-	bulk	$13.1 \times 10^6 e^{-\frac{2034}{T}}$ $(-35\,°C < T < 25\,°C)$	[39]
2EHA	-	bulk	$17.0 \times 10^6 e^{-\frac{2158}{T}}$ $(-25\,°C < T < 10\,°C)$	[40]

*w' represents the weight fraction of polymer

1.4.2 Termination rate coefficient, k_t

In 1986, Buback established that it was possible to determine the termination rate coefficient via monitoring of the monomer concentration by near infrared spectroscopy (NIR) on a sub-second timescale after a single (laser) pulse (SP). Accordingly, the technique is named SP-PLP-NIR. After a laser pulse, the rate of initiation is equal to 0. Consequently, it can be established that:

$$\frac{d[M\cdot]}{dt} = -2k_t[M\cdot]^2 \tag{1.16}$$

From Eq. (1.16) [8]:

$$\frac{[M]}{[M]_0} = (2k_t[M\cdot]_0 t + 1)^{-k_p/2k_t} \tag{1.17}$$

So if [M], the monomer concentration, is monitored via NIR, both k_p/k_t and $k_t[M^{\cdot}]_0$ can be determined by fitting the data, where $[M^{\cdot}]_0$ is the concentration of radicals produced by a laser pulse. As discussed previously, k_p is accessible via PLP-SEC. Consequently, k_t can be calculated [41, 42]. An example of this is given below [43].

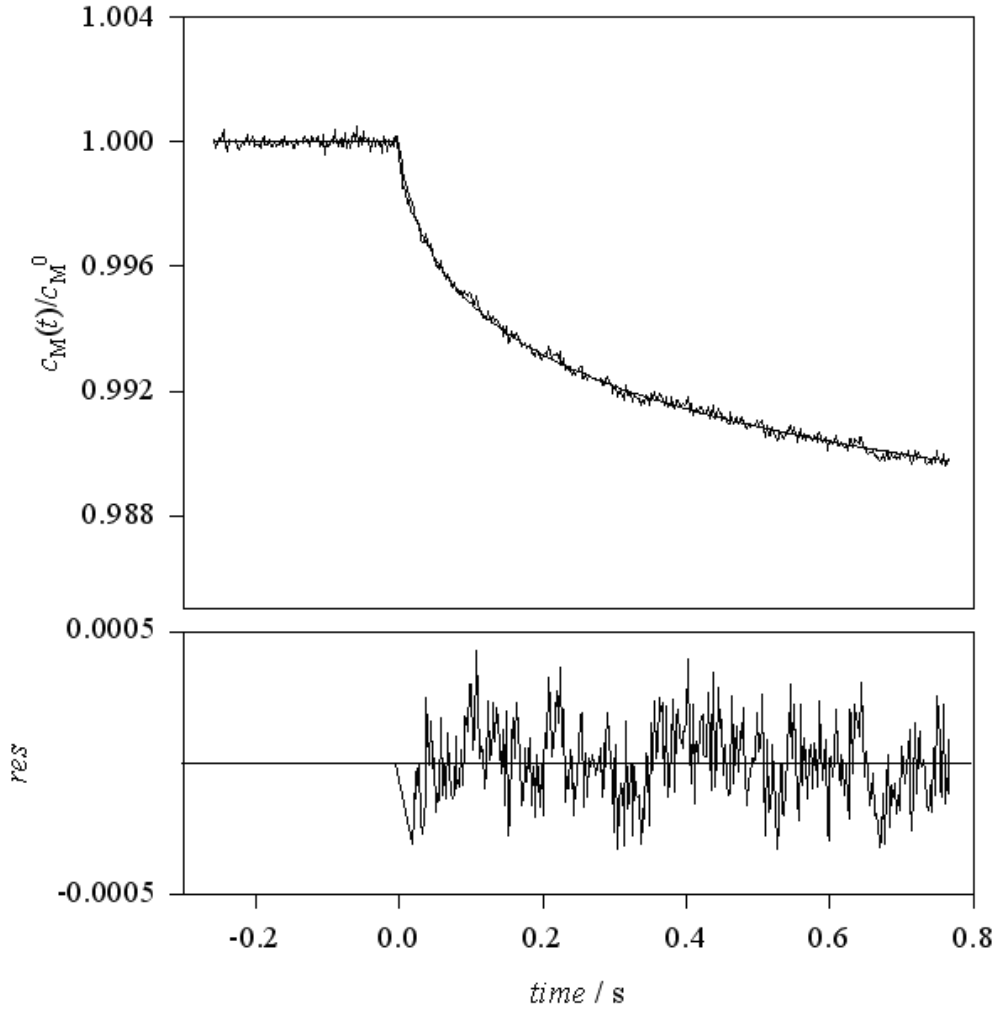

Figure 1.4: Illustrating the SP-PLP-NIR technique for determining k_t: relative monomer concentration, $[M]/[M]_0$, vs time for SP-PLP involving copolymerization of methyl acrylate and dodecyl acrylate is fitted to obtain k_p/k_t, from which the independent knowledge of k_p yields k_t [8]. Copyright 2017 Willey.

It needs to be stressed that there are many methods for determining k_t. The above has been chosen as an illustrative example because it is the easiest and most understandable method. Even better is the coupling of SP PLP with EPR spectroscopy [8].

1.4.3 Backbiting rate coefficient, k_{bb}

At modest laser pulse frequency and above 30 °C, the PLP-SEC technique provides featureless MWDs. In this event, no reliable k_p can be deduced, because intramolecular chain transfer (backbiting) is occurring. Different methods have been established to monitor SPR and MCR concentration, and thus determine backbiting rate coefficients, k_{bb}, and propagation rate coefficient for MCRs, k_p^t. Gilbert et al. were the first to detect MCRs by electron paramagnetic resonance (EPR) spectroscopy [44]. ^{13}C NMR was first used to determine k_{bb} via the degree of branching of polymer. However, this method can suffer from poor signal-to-noise ratio [45]. More recently, two methods have been developed:

- Frequency-tuned PLP in conjunction with SEC analysis (ft-PLP-SEC) [46]
- Time-resolved EPR monitoring of SPR and MCR concentrations after a single pulse (SP-PLP-EPR) [47]

The two last methods allow determination of [MCR] and [SPR], meaning k_{bb} and k_p^t are accessible via kinetic modeling; this is often done with a software package called PREDICI [47].

The backbiting rate coefficient k_{bb} can also be evaluated from the degree of branching (*DB*), defined as the percent of branches per monomer unit. At low monomer conversion, it can be reasonably assumed that the amount of MCRs lost by transfer, *β*-scission, and termination is negligible. Consequently, it can be considered that every backbiting event leads to a branching point and *DB* can be expressed as the ratio of the rate of backbiting to the rate of propagation as in Eq. (1.18) [5]:

$$DB\ (\%) = \frac{R_{bb} \times 100}{R_p} = \frac{100 \times k_{bb}[M^{\cdot}]X_{SPR}}{k_p[M][M^{\cdot}]X_{SPR} + k_p^t[M][M^{\cdot}]X_{MCR}} \tag{1.18}$$

Moreover, as the consumption of monomer by a MCR is assumed to be negligible, i.e., $k_p^s[M][M^{\cdot}]X_{SPR} >> k_p^t[M][M^{\cdot}]X_{MCR}$, Eq. (1.18) can be simplified to

$$DB\ (\%) = \frac{100 \times k_{bb}}{k_p[M]} \tag{1.19}$$

Eq. (1.19) holds for instantaneous *DB* and assumes the branching due to intermolecular transfer is negligible. In 2009, Nikitin et al. were able to link the cumulative *DB* to the ratio of backbiting and propagation rate coefficients, deriving Equation 20 that takes into account how

instantaneous *DB* changes as monomer concentration changes (see Eq. (1.19)) [48]. Thus the following equation should be used where appreciable conversion takes place in an experiment for measuring *DB*:

$$DB\ (\%) = \frac{100 \times k_{bb} ln\left(\frac{[M]_0}{[M]_e}\right)}{k_p([M]_0 - [M]_e)} \tag{1.20}$$

Values of k_{bb} (from the literature) for acrylic acid and *n*-butyl acrylate are given in Table 1.3.

Table 1.3: Backbiting rate coefficients of acrylic acid and alkyl acrylates.

Monomer	Solvent	$Wt_{monomer}$ (%)	k_{bb} (s^{-1})	Ref.
AA	Water	independent	$9.94 \times 10^8 e^{-\frac{4576}{T}}$	[5]
AA	Water	10	$4.3 \times 10^8 e^{-\frac{4331}{T}}$	[47]
AA	Water	50	$2.9 \times 10^8 e^{-\frac{3723}{T}}$	[47]
Methyl (MA)	toluene	independant	$1.5 \times 10^8 e^{-\frac{3993}{T}}$	[49]
nBA	bulk	-	$4.84 \times 10^7 e^{-\frac{3815}{T}}$	[46]
nBA	heptane	independent	$3.5 \times 10^7 e^{-\frac{3524}{T}}$	[45]
nBA	toluene	independent	$1.6 \times 10^8 e^{-\frac{4174}{T}}$	[50]
Dodecyl (DA)	toluene	independent	$2.1 \times 10^8 e^{-\frac{4234}{T}}$	[49]

1.5 Methods of characterization

Three different methods of characterization were mainly used in this work: (1) Electrospray ionization-mass spectrometry was used to study the end groups of PAA and P2EHA. (2) Capillary electrophoresis was used to separate poly(sodium acrylate)s (PNaA) by branching and to study the heterogeneity of branching. (3) ^{13}C NMR spectroscopy (solution and melt-state) was used determine the average degree of branching in PAA and P2EHA. These are all introduced below.

Size exclusion chromatography (SEC) was not used, but of course it is a very important method of characterization, and is used to determine the molecular weight and the local dispersity of a polymer sample, as well as to separate polymers by hydrodynamic volume (which varies with the branching). As the results obtained over this Ph.D. are compared with previous results obtained by SEC, a brief introduction to this method is given below, including its limitations.

1.5.1 Electrospray ionization-mass spectrometry (ESI-MS)

Mass spectrometry (MS) is a technique that ionizes chemical species based on their mass to charge ratio. First of all a sample is ionized, for instance by bombarding with ions, and then the resulting charged adducts are separated by their mass-to-charge ratios. Historically this was done by accelerating them in an electric field. Ions of the same mass-to-charge ratio would undergo the same amount of deflection. Adducts were detected using a mechanism capable of detecting charged particles. A mass spectrum shows the relative abundance of detected ions as a function of mass-to-charge ratio.

This traditional version of MS fails for large molecules as they are not ionized as easily as small molecules. Electrospray ionization (ESI) is a method used to produce adducts via a so-called electrospray, in which a high voltage is applied to a liquid to create an aerosol. This method is adequate for characterizing macromolecules such as polymers, as it overcomes their tendency to fragment under traditional methods of ionization.

The development of ESI-MS has been useful to determine the product spectrum of a polymer sample and its changes within the chain length distribution [51]. A higher level of polymer characterization has become available, in that polymer chains can be ‘visualized’ precisely according to their end groups and chain length. The influence of temperature and of chain transfer-agent (CTA) concentration on the structure of poly(*n*-alkyl acrylate)s has been studied by ESI-MS [52, 53]. The amount of β-scission increased with temperature and decreased with CTA concentration.

Tables 1.4 and 1.5 sum up the conditions used to characterize PAA and poly(alkyl acrylate)s by ESI-MS. Figure 1.5 is an example ESI-MS spectrum of poly(*n*-butyl acrylate).

Table 1.4: Conditions used to analyse PAA by ESI-MS in the literature.

References	**[54]**	**[55]**	**[56]**	**[57]**
Sample	0.001 g L^{-1} in MeOH/H_2O (1/1 v/v)	Not mentioned	0.01 g L^{-1} (pure MeOH)	Not mentioned
System	Finnigan Mat LCQ MS detector with Finnigan LCQ Data Processing and Instrument Control Software	Agilent 1200 pump	Finnigan LCQ MS Detector with Finnigan LCQ Data Processing using Instrument Control Software.	Agilent MSD type SL with an atmospheric pressure electrospray interface.
Voltage	5 kV	3 kV	4.5 kV	4 kV
Isocratic mobile phase	Not mentioned	Methanol/H_2O (1/1) with 5 mM ammonium acetate	Not mentioned	MeOH/H_2O with 0.1 % of acetic acid
Flow rate	0.2 L/min	4 µL/min	0.06 mL/min	0.25 mL.min
Sheathing gaz	Nitrogen at 415 kPa	Nitrogen at 21 kPa	Not mentioned	Nitrogen at 207 kPa
Heated capillary	200 °C	200 °C	300 ° C	350 °C

Table 1.5: Conditions used to analyse poly(alkyl acrylate)s by ESI-MS in the literature.

	Literature [53]	**Literature [58]**	**Literature [59]**	**Literature [60]**
Acrylate	Poly(n-butyl acrylate)	Poly(alkyl acrylates)*	Poly(n-butyl acrylate)	Poly(methyl acrylate)
Sample	0.4 g L^{-1} in THF/MeOH (5/3 v/v)	0.01 g L^{-1} in THF/MeOH (5/3 v/v)	0.4 g L^{-1} in DCM/MeOH (3/1 v/v)	THF/MeOH (5/3 v/v) and DCM/MeOH (75/25 v/v)
System	Thermo Finnigan LCQ Deca quadrupole ion-trap mass spectrometer (Thermo Finnigan, San Jose, CA)	LTQ Orbitrap Velos Pro mass spectrometer (ThermoFischer Scientific)	Thermo Finnigan LCQ Deca quadrupole ion-trap mass spectrometer (Thermo Finnigan, San Jose, CA)	Thermo Finnigan LCQ Deca ion trap mass spectrometer (Thermo Finnigan, San Jose, CA)
Voltage	5 kV	5 kV	5 kV	4.5 kV
Isocratic mobile phase	Not mentioned	Not mentioned	Not mentioned	Not mentionned
Flow rate	Not mentioned	3 (units not mentioned)	5 (units not mentioned)	4 µL/min
Sheathing gaz	Nitrogen gas	Nitrogen gas	Nitrogen gas	Nitrogen gas
Heated capillary	275 °C	275 °C	275 °C	275 °C

*Poly(*n*-butyl acrylate), Poly(*t*-butyl acrylates) and P2EHA.

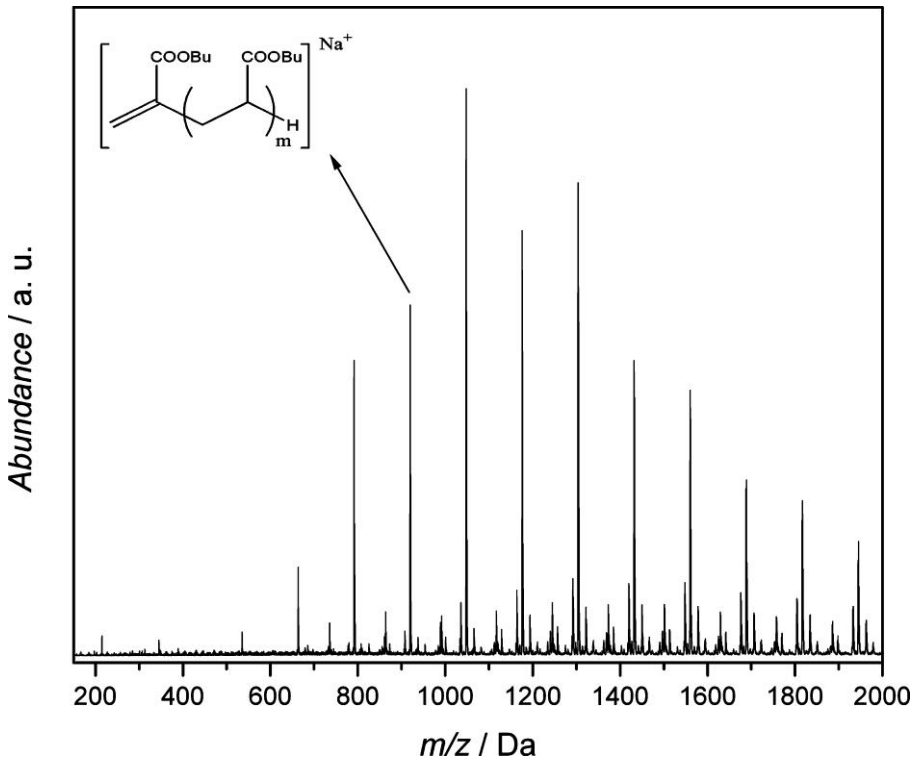

Figure 1.5: Typical ESI-MS spectrum of polymer obtained from bulk polymerization of butyl acrylate at 100 °C in the presence of 1-octanethiol initiated AIBN. Reprinted with permission from [53]. Copyright 2009 American Chemical Society.

1.5.2 Size exclusion chromatography

Size exclusion chromatography (SEC) is a type of liquid phase chromatography used to separate macromolecules according to their hydrodynamic volume. It allows determination of the distribution of hydrodynamic volumes in polymers. It has also been termed gel permeation chromatography (GPC). The stationary phase is generally a porous cross-linked gel swollen by the mobile phase. The mobile phase is either an organic solvent or an aqueous solution. The gel is made of spherical beads whose size distribution should correspond to the size distribution of the sample under investigation. If the distribution of polymer sizes is broad, then one must use either a series of columns of different but narrow pore sizes, or else one should use a column with a broad distribution of pore sizes.

In 1967, Benoit et al. demonstrated that, in an SEC column, particles are separated according to their hydrodynamic volume and not their molecular weight [61]. In other words, under ideal circumstances the separation is by entropic factors alone: according only to its size, the

molecule can enter the porous volume or be excluded. If there are also enthalpic factors, then SEC is more complicated and difficult.

Where size is the only factor, a universal calibration curve – see Figure 5 – is used to characterize polymers. If a plot of log $M[\eta]$ (where M is peak average molecular weight and $[\eta]$ the intrinsic viscosity) against elution volume (V_e) is drawn, the line will be the same regardless of the nature of the polymer. This method is based on the hydrodynamic volume, which depends on both molecular weight and intrinsic viscosity ($V_h=[\eta]M$).

According to the Mark-Houwink-Sakurada relation (Equation 21), $[\eta]$ depends on M. So if the intrinsic viscosity is measured, it is possible to rely on Mark-Houwink parameters (K and α) to determine the molecular weight.

$$[\eta] = KM^{\alpha} \tag{1.21}$$

However, this approach is neither fast nor accurate. Even though this relation can be used for an extended range of polymers, it is not a universal relation and it is not proven that Eq. (1.21) would work for branched polymers. The universal calibration curve provides more reliable results. Details are given by Figure 1.6 and Eq. (1.22).

$$[\eta]_{sample}M_{sample} = [\eta]_{standard}M_{standard} \tag{1.22}$$

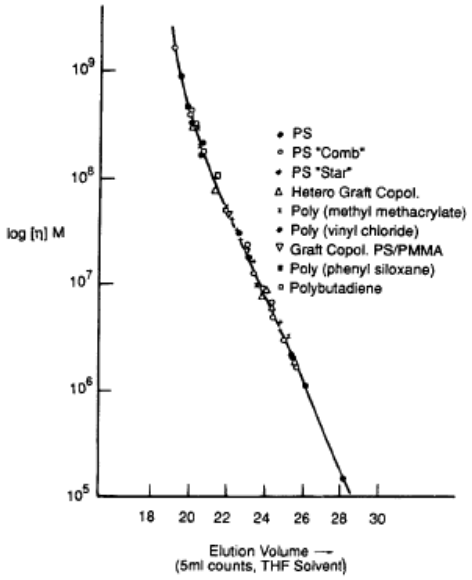

Figure 1.6: Universal calibration curve for size exclusion chromatography. Figure reprinted from [61]. Copyright permission has been requested.

As particles are separated according to their hydrodynamic volume, the presence of branching induces errors in the molecular weight determination. It may lead to coelution of polymer with different molecular weight, i.e., a linear sample of a lower *M* with a branched sample of a higher *M*, both having the same hydrodynamic volume.

To overcome this problem, multiple detection has been tested. The true molecular weight is determined by two independent methods: light scattering and viscometry.

Light scattering detectors yield absolute molecular weight and radius of gyration using the Rayleigh equation [62]:

$$\frac{Kc}{\Delta R_\theta} = \frac{1}{M_W} + \frac{16\pi^2 n_0^2}{3\lambda_0^2}\frac{\langle R_g^2\rangle}{M_W} sin^2\left(\frac{\theta}{2}\right) \quad (1.22)$$

$$K = \frac{4\pi^2 n^2 \left(\frac{dn}{dc}\right)^2}{N_A \lambda_0^4} \quad (1.23)$$

Here c is the concentration of analyte in the solution, λ_0 is the wavelength of the light source, n_0 is the refractive index of the solvent, M_W is the weight-average molar mass, ΔR_θ is the Rayleigh ratio, dn/dc is the change in refractive index in the solution with the change in concentration (also called refractive index increment) and R_g is the radius of gyration. R_g and M_W are accessible using low angle laser light scattering (LALLS), right angle laser light scattering (RALLS) or multi angle laser light scattering (MALLS), via a "Zimm plot", ($Kc/\Delta R_\theta$ against $\sin^2(\theta/2)$ [62].

Viscometry (relying on universal calibration) allows determination of the local number average molecular and hydrodynamic radius (See Eq. (1.24)) [63].

$$V_H = \frac{2[\eta]M_n}{5N_A} \quad (1.24)$$

The difference between the local M_W and the local M_n determined by SEC assesses the accuracy of the determined molar mass [10] and provides an indirect assessment of the heterogeneity of branching. Branched polymers can be separated into two categories: regularly branched polymer (star-polymer, dendrimer…) and complex branched polymer (with a distribution of number of branches, size of branches, and position of branches).

If the local M_W is far greater than the local M_n (e.g. the local dispersity close to 2) , the branching is heterogeneous: this corresponds to complex branched polymers with a low level of LCB. Incomplete separation in terms of molar mass would be expected. If the local M_W and the local

M_n are close to each other (e.g. the local dispersity equal or slightly superior to the unity), either polymer chains are linear or the branching is homogeneous. This is observed in the case of regularly branched polymers and in complex branched polymers with a high level of LCBs. In this case, complete separation in terms of molar mass should be observed.

To sum up, several disadvantages of SEC can be stressed:

- It relies on the validity of the MHS relation, which is not valid for low molecular weight, high molecular weight, and branched polymers.
- Light scattering can lead to other types of artefacts related to the signal-to-noise ratio [64].
- Band broadening is significant [65].
- The size exclusion mechanism leading to universal calibration might not be dominant and anomalous elution can occur [64].
- Separation in terms of molecular weight can be incomplete due to the presence of LCBs. This has been observed in the case of PAA [3] and poly(alkyl acrylate)s [66].

Even though some methods of analysis were developed to reduce these issues, such as the Goldwasser method [67] to determine M_n from the viscosity, it is useful to consider the potential of other methods of characterization.

1.5.3 Capillary electrophoresis

Capillary electrophoresis (CE) is a method used to separate chemicals according to their charges and friction forces (charge to friction ratio). CE is considered as the method of choice to separate natural polymers like DNA and proteins. Species are separated according to their electrophoretic mobilities, μ_{ep}, defined by Eq. (1.25) [68]:

$$\mu_{ep} = \frac{lL}{V}\left(\frac{1}{t_M} - \frac{1}{t_{eo}}\right) \tag{1.25}$$

Here L is the total length of the capillary, l is the effective length (from the inlet to the detection window), t_M is the migration time of the species, t_{eo} is the electroosmotic flow (EOF) and V is the applied voltage.

The migration time depends on both EOF and $\mu_{ep.}$ The EOF depends itself on numerous factors that also influence the migration time. Figure 1.7 represents the separation of species in a capillary electrophoresis experiment.

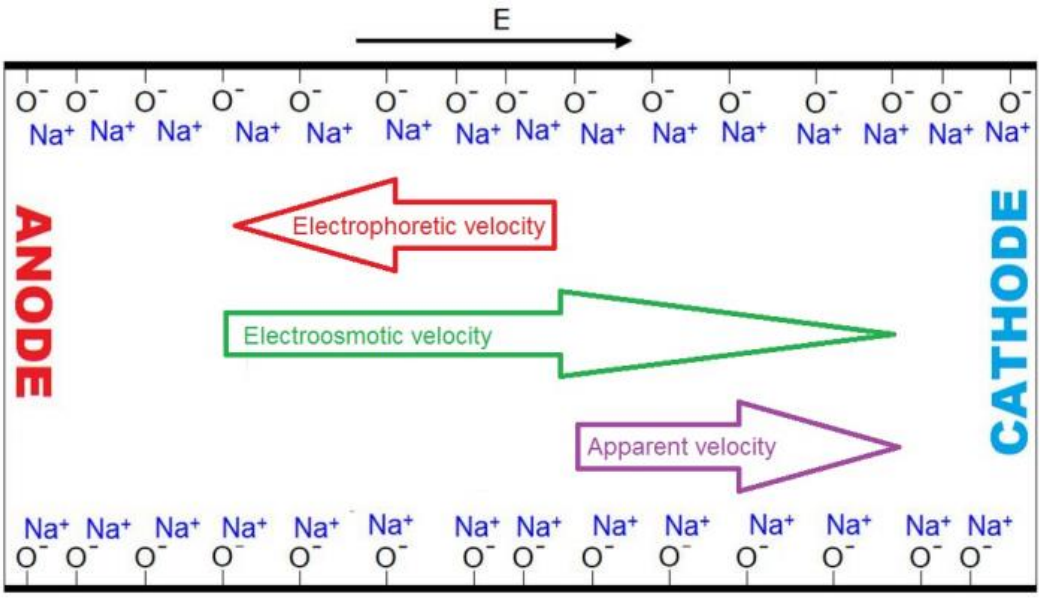

Figure 1.7: Fused-silica capillary filled with buffer, with vectors representing the electroosmotic flow (EOF) and the electrophoretic mobility in which the electrophoretic velocity combined with the electroosmotic velocity results in the apparent velocity. Reprinted with permission from [11]. Copyright © 2013, Springer-Verlag Berlin Heidelberg.

In 2010, Gaborieau *et al.* applied this method with ESI-MS detection to separate oligoacrylates according to their molecular weight and tacticity [55]. The separation was obtained with a much higher resolution than with SEC. The higher the degree of polymerization, the higher the electrophoretic mobility. Isobaric peaks observed were found to correspond to the tacticity. Nevertheless, it is not possible at this stage to identify the tacticity with ESI-MS or UV detectors.

However, this separation of polyelectrolytes (according to the molecular weight) is not possible when the degree of polymerization is above approximately 10, which corresponds to the critical conditions.

The critical conditions do not refer to a separation mode but to the conditions sought in liquid chromatography in which polymers are not separated according to their molar mass [69]. In 2013, Maniego *et al* demonstrated the potential of free solution capillary electrophoresis in the

critical conditions (CE-CC) for separating poly(sodium acrylate) (PNaA) according to its branching topology, using sodium borate buffer at pH = 9.2 as background electrolyte (BGE) [11] with no influence of the molar mass. Figure 1.8 shows the output from such a separation. This separation tendency is likely due to the complexation (more important for branched polymer chains) between polyaqcrylate and sodium ions, leading to a decrease of effective charge. Recently, Thevarajah et *al*. proposed a model to use the CE-CC to provide a direct assessment of the heterogeneity of branching [6]. By heterogeneity, is meant that different macromolecules within the same sample can differ by their branching, namely the number of branches per macromolecule, but also the position of the respective branching points along the polymer chain, the distribution of molar masses of the branches, etc. CE-CC was used to determine the dispersity of the electrophoretic mobility distributions. As different branching topologies lead to different electrophoretic mobilities in the case of PNaA, the obtained values of dispersity are representative of the heterogeneity of branching.

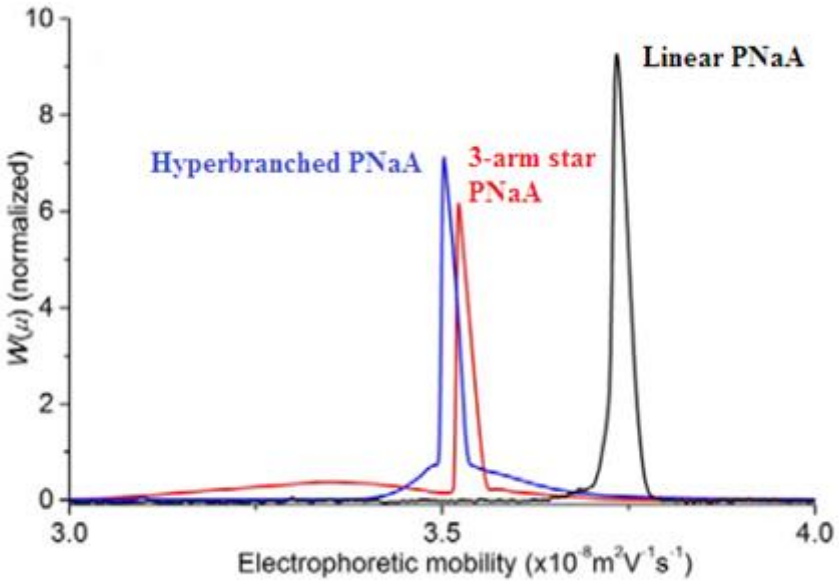

Figure 1.8: Electrophoretic mobility distributions of PNaA samples. PNaAs with different topologies: linear (black), 3-arm star (red) and hyperbranched (blue). Reprinted with permission from [6]. Copyright 2016 American Chemical Society.

1.5.4 ^{13}C NMR spectroscopy

NMR spectroscopy is a technique that uses the magnetic properties of some atomic nuclei. It allows detection and identification atoms in organic molecules (mostly hydrogens and carbons). The molecules are placed into a magnetic field and are subject to electromagnetic radiation as pulse. Atomic nuclei can absorb energy and then "relax". The energy involved over the process corresponds to a very precise frequency that depends on the magnetic field and other factors, such as the molecular environment. Only nuclei with a spin can be detected. As ^{12}C has a zero net spin, ^{13}C isotopes are detected in ^{13}C NMR spectroscopy. This method can be either analytical or quantitative.

Over the last decade, the branching of polyacrylates has been detected and quantified using ^{13}C NMR spectroscopy. *DB* is determined from the integration of the signal of the quaternary carbons (C_q) characteristic of a branched polymer and of a signal of a carbon whose characteristics remain unchanged in the branched and unbranched monomer units. This method has been utilized several times in order to determine *DB* in PAA [5, 31, 32] and poly(alkyl acrylate)s [4, 70-74]. Both resolution and sensitivity are required for reliable quantification of *DB*. Various NMR methods (solution-state, solid-state and melt-state) were previously compared for poly(*n*-alkyl acrylate)s [4]. However, optimal analyses were obtained by melt-state NMR spectroscopy at 150 °C above the glass transition temperature (T_g) [4]. As the T_g of PAA is relatively high (between 90 and 150 °C) and PAAs degrade between 250 and 400 °C [75], solution state is the method of choice to study the branching in PAA. Melt-state MAS-NMR can be used to study the branching in poly(alkyl acrylate)s as the degradation temperature is over 150 °C above the T_g. Tables 1.6 and 1.7 summarize the conditions used in previous work to detect or quantify the branching in PAA and poly(alkyl acrylate)s using ^{13}C NMR spectroscopy.

Table 1.6: Conditions for ^{13}C NMR analyses of branching in PAA and PNaA in the literature.

Ref.	[11]	[11]	[11]	[31]	[32]	[5]
Type of study	Detection of branching	Detection of branching	Detection of branching	Quantifi-cation of branching	Quantifi-cation of branching	Quantifi-cation of branching
Larmor frequency	75 MHz	75 MHz	75 MHz	100.6 MHz	125.7 MHz	Not given
Pulse angle	90°	90°	90°	70°	20°	Not given
Repetition delay	20 s	20 s	20 s	4.5 s	20 s	Not given
Temp-erature	RT*	RT	RT	60 °C	RT	Not given
Concen-tration	150 g L^{-1}	50 g L^{-1}	50 g L^{-1}	30 % (w/w)	Not given	Not given
Solvent	D_2O	1,4-Dioxane-d_8	D_2O with 428 nM NaOH	D_2O	D_2O	D_2O
Sample	Linear PNaA	Hyperbranched PNaA	3-arm star PNaA (synthesized by NMP, trifonctional initiator)	PNaAs synthesized by RAFT	PNaAs synthesized by NMP	PAAs produced by batch radical polymerization

Table 1.7: Conditions for ^{13}C NMR analyses of branching in poly(alkyl acrylate)s in the literature.

Ref.	[70]	[71]	[4]	[4]	[72]	[74]	[73]	[36]
Type of study	Quantification of branching	Quantification of branching	Quantification of branching	Quantification of branching	Quantification of branching	Quantification of branching	Quantification of branching	Quantification of branching
Larmor frequency	75.47 MHz	125.8 MHz	125.26 MHz	75.47 MHz	125.77 MHz	2.3 kHz	125.8 MHz	125.8 MHz
Pulse angle	90°	45°	90°	90°	90°	90°	45°	45°
Repetition delay	10 s	10.5 s	10 s	10 s	10 s	10 s	10.5 s	10.5 s
Temp-erature	80-100 °C (Tg+150 °C)	Not mentioned	29-33 °C	T_g + 150 °C*	25 °C	T_g + 150 °C	Not mentioned	Not mentioned
Concen-tration	-	100 g L^{-1}	300 g L^{-1}	-	200 g L^{-1}	-	100 g L^{-1}	100 g L^{-1}
NMR method	Melt-State	Solution-state (in $CDCl_3$)	Solution-state (in $CDCl_3$)	Melt-State	Solution-state (in $CDCl_3$)	Melt-State	Solution-state (in $CDCl_3$)	Solution-state (in $CDCl_3$)
Sample	Poly(***n***-butyl acrylate)	Poly(***n***-butyl acrylate)	Different poly(alkyl acrylates)	Different poly(alkyl acrylates)	Poly(n-butyl acrylates)	Poly(n-butyl acrylates)	Poly(n-butyl acrylates)	P2EHA

*Poly(methyl acrylate) and poly(ethyl acrylate) were analysed at T_g + 100 °C and the resolution was low.

Previous studies have proven that *DB* increases with temperature due to a rise of the frequency of reactions leading to branches (inter and intramolecular chain transfer) in both poly(acrylic acid) and poly(alkyl acrylate)s [5, 70, 72]. However the presence of a CTA considerably reduced the *DB* of poly(alkyl acrylate)s. This was attributed either to a "patching effect" (a transfer of hydrogen radical from the CTA to the MCR, as illustrated in Scheme 1.5) [70] or a reduction in the number of backbiting events in the presence of CTA, as the polymerization occurs for a shorter time [72]. The last hypothesis could also explain the reduction of *DB* due to the use of controlled radical polymerization, as observed for poly(alkyl acrylate)s [73], since SG1 and RAFT agents also shorten the polymerization time. Another explanation could be polymer entanglement: poly(alkyl acrylate) prepared with CTA (thiols, RAFT agents, SG1) are shorter and so less entangled, meaning there is less contact with other players and thus less long-chain branching [71]. Of course such an effect could only be relevant if a significant contribution to *DB* is made by LCBs, which is unlikely.

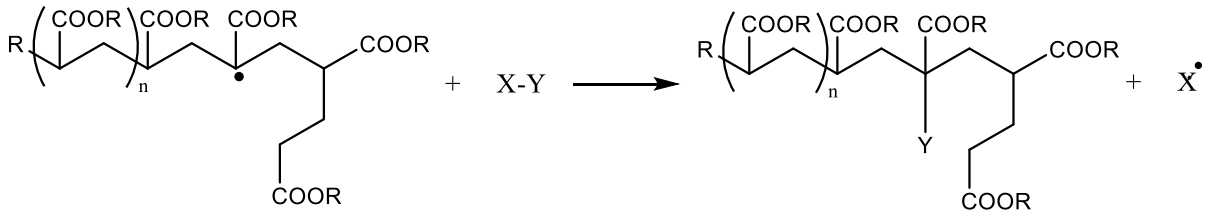

Scheme 1.5: Patching of a MCR by a chain transfer agent.

In some cases, carbon centres adjacent to long branches and short branches could be distinguished by ^{13}C NMR spectroscopy analyses due to the change of molecular environment with the proximity of the end group. This has confirmed the presence of both LCB and SCB. The effect is illustrated in Figure 1.9 and quantified by Eq. (1.26) and (1.27) [31].

$$\int C_a + C_b = SB + LB \tag{1.26}$$

$$\int S_1 = 3LB + 2\,SB \tag{1.27}$$

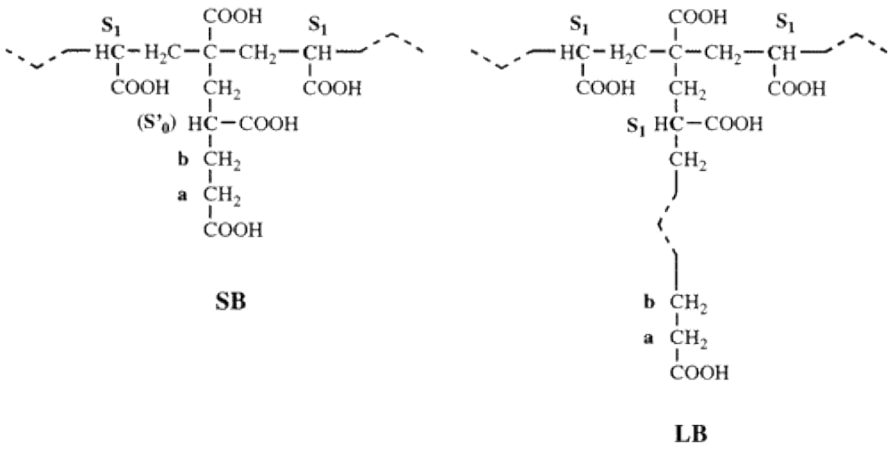

Figure 1.9: Representation of branches obtained by transfer to polymer and specific resonance areas chosen for quantification. Reprinted with permission from [31]. Copyright 2003 American Chemical Society

However, it is interesting to note that (i) some studies may indicate that the *DB* obtained for PAAs synthesized by controlled radical polymerization are higher than those of PAAs synthesized by conventional radical polymerization [5, 31] even though the opposite is observed for the poly(alkyl acrylates) [73], and (ii) in the case of PAA, the effect of the presence of CTA like commercial mercaptans on *DB* was never tested before the start of the research for this thesis.

1.6 Objectives of this Ph.D. project

This Ph.D. is divided into 4 distinct parts, outlined below.

1.6.1 Investigating the influence of temperature, initial monomer concentration and the presence of a CTA on the branching of PAA

Inter- and intramolecular chain transfer occur during the polymerization of acrylic acid. The effect of the presence of CTA on *DB* has not been tested in the case of PAA and to do so will bring new insight. Even though a few studies have been done to test the effect of temperature and initial monomer concentration on the branching of PAA, further investigations would be useful to provide a bigger picture. Some information on k_{bb} can be extracted from *DB*. The use of Equation 20 as well as the possibility to extrapolate Equation 19 at high conversion will be

tested. The most innovative part will be the investigation of the heterogeneity of branching (using CE-CC) in PAAs synthesized by conventional radical polymerization. Some studies were carried out for PAAs synthesized by RAFT [6, 76]. Results are compared to the ones obtained in this study for PAAs obtained by radical polymerization. This work is presented in chapter 2.

1.6.2 Further characterization of branching in water soluble polyacrylates using CE-CC

CE-CC is an excellent method for characterizing branched PNaA as (i) it is much cheaper than SEC, (ii) results are more reproducible, and (iii) it allows a direct assessment of the heterogeneity of branching, which is not the case with SEC. Even though the potential of CE-CC in the separation of branched PNaA has been proven [6, 11], the mechanism of separation is not fully understood. For instance, branched PNaA exhibits a bimodal distribution of electrophoretic mobilities whilst it is unimodal for linear PNaA. The relation between the electrophoretic mobility and the structure can be determined using the so-called "slope plot" [77]. This method will be applied to provide a deep and full understanding of the mechanism of separation in the case of water-soluble PNaA. Some factors – namely buffer concentration and addition of metal – will be tested to learn whether or not they impact the separation's selectivity. Finally, the optimal conditions to separate PNaA using CE-CC will be presented. This work is presented in chapter 3.

1.6.3 Effect of transfer agent and temperature on branching and β-scission in radical polymerization of 2-ethylhexyl acrylate

Some studies of the *DB* of poly(alkyl acrylate)s synthesized at different temperatures, both with and without CTA, have already been published. The aim of this research project is to extend the existing study to synthesis of P2EHA with and without commercial mercaptans and using redox initiators. This will give a broader picture of the variation of *DB* with temperature and also the possibility to observe transfer to thiol at temperatures between 0 and 30 °C. Comparing the results for P2EHA with those from other poly(alkyl acrylate)s should provide insight to learn how k_{bb} is affected by pendant group size. Since batch polymerizations will be

carried out in this work, it is important to use Equation 20 rather than Equation 19, and in this way Equation 20 will be tested. This work is presented in chapter 4.

1.6.4 Further size-based characterization of poly(acrylic acid) using alternative methods to size exclusion chromatography

Even though the main focus on this Ph.D is the characterization of PAA by branching and its impact on the kinetics of radical polymerization, knowing the size of polymer is also essential to fully understand the mechanism of polymer formation. As typically 100 % error occurs in the size of PAA determined by SEC (likely due to the presence of LCB), two other methods of characterization will be tested.

The first is the fraction of chain-end using ^{1}H NMR spectroscopy (for CTA-containing PAA). This allows estimation of M_n. From that, the influence of the temperature of synthesis on C_T can be evaluated and information on the kinetics of transfer to CTA can be provided.

The second alternative method is Taylor Dispersion Analysis, which will be tested to estimate the diffusion coefficient of different PAA (analysed as PNaAs). This method has been successfully applied to different polymers [78]. More details about these methods will be given at a later stage in this thesis in chapter 6.

1.7 References

[1] P.M. Wood-Adams, J.M. Dealy, A.W. deGroot, O.D. Redwine, Effect of molecular structure on the linear viscoelastic behavior of polyethylene, Macromolecules, 33 (2000) 7489-7499.

[2] M. Gaborieau, R.G. Gilbert, A. Gray-Weale, J.M. Hernandez, P. Castignolles, Theory of multiple detection size exclusion chromatography of complex branched polymers, Macromolecular Theory and Simulations, 16 (2007) 13-28.

[3] I. Lacík, M. Stach, P. Kasák, V. Semak, L. Uhelská, A. Chovancová, G. Reinhold, P. Kilz, G. Delaittre, B. Charleux, I. Chaduc, F. D'Agosto, M. Lansalot, M. Gaborieau, P. Castignolles, R.G. Gilbert, Z. Szablan, C. Barner-Kowollik, P. Hesse, M. Buback, SEC analysis of poly(acrylic acid) and poly(methacrylic acid), Macromolecular Chemistry and Physics, 216 (2015) 23-37.

[4] P. Castignolles, R. Graf, M. Parkinson, M. Wilhelm, M. Gaborieau, Detection and quantification of branching in polyacrylates by size-exclusion chromatography (SEC) and melt-state 13C NMR spectroscopy, Polymer, 50 (2009) 2373-2383.
[5] N.F.G. Wittenberg, C. Preusser, H. Kattner, M. Stach, I. Lacík, R.A. Hutchinson, M. Buback, Modeling acrylic acid radical polymerization in aqueous solution, Macromolecular Reaction Engineering, 10 (2016) 95-107.
[6] J.J. Thevarajah, A.T. Sutton, A.R. Maniego, E.G. Whitty, S. Harrisson, H. Cottet, P. Castignolles, M. Gaborieau, Quantifying the heterogeneity of chemical structures in complex charged polymers through the dispersity of their distributions of electrophoretic mobilities or of compositions, Analytical Chemistry, 88 (2016) 1674-1681.
[7] O.F. Olaj, I. Bitai, F. Hinkelmann, The laser-flash-initiated polymerization as a tool of evaluating individual kinetic constants of free-radical polymerization .2. The direct determination of the rate-constant of chain propagation, Makromolekulare Chemie-Macromolecular Chemistry and Physics, 188 (1987) 1689-1702.
[8] G.T. Russell, Kinetics of Radical Polymerization, in: Encyclopedia of Polymer Science and Technology, John Wiley & Sons, Inc., 2002.
[9] E. Sato, T. Emoto, P.B. Zetterlund, B. Yamada, Influence of mid-chain radicals on acrylate free radical polymerization: Effect of ester alkyl group, Macromolecular Chemistry and Physics, 205 (2004) 1829-1839.
[10] P. Castignolles, Transfer to polymer and long-chain branching in PLP-SEC of acrylates, Macromolecular Rapid Communications, 30 (2009) 1995-2001.
[11] A.R. Maniego, D. Ang, Y. Guillaneuf, C. Lefay, D. Gigmes, J.R. Aldrich-Wright, M. Gaborieau, P. Castignolles, Separation of poly(acrylic acid) salts according to topology using capillary electrophoresis in the critical conditions, Analytical and Bioanalytical Chemistry, 405 (2013) 9009-9020.
[12] A.D. Wallace, A. Al-Hamzah, C.P. East, W.O.S. Doherty, C.M. Fellows, Effect of poly(acrylic acid) end-group functionality on inhibition of calcium oxalate crystal growth, Journal of Applied Polymer Science, 116 (2010) 1165-1171.
[13] A.B. Lopez, J.C. de la Cal, J.M. Asua, Highly Hydrophobic Coatings from Waterborne Latexes, Langmuir, 32 (2016) 7459-7466.
[14] A.J. DeFusco, K.C. Sehgal, D.R. Bassett, Overview of uses of polymer latexes, in: J.M. Asua (Ed.) Polymeric Dispersions: Principles and Applications, 1997, pp. 379-396.
[15] H.D. Iler, A. Brown, A. Landis, G. Schimke, G. Peters, Free Radical Addition Polymerization Kinetics without Steady-State Approximations: A Numerical Analysis for the

Polymer, Physical, or Advanced Organic Chemistry Course, Journal of Chemical Education, 91 (2014) 374-379.
[16] I. Lacik, S. Beuermann, M. Buback, Aqueous phase size-exclusion-chromatography used for PLP-SEC studies into free-radical propagation rate of acrylic acid in aqueous solution, Macromolecules, 34 (2001) 6224-6228.
[17] S. Beuermann, M. Buback, P. Hesse, S. Kukuckova, I. Lacik, Propagation rate coefficient of non-ionized methacrylic acid radical polymerization in aqueous solution. The effect of monomer conversion, Macromolecular Symposia, 248 (2007) 41-49.
[18] M. Buback, P. Hesse, I. Lacik, Propagation rate coefficient and fraction of mid-chain radicals for acrylic acid polymerization in aqueous solution, Macromolecular Rapid Communications, 28 (2007) 2049-2054.
[19] A.N. Nikitin, R.A. Hutchinson, The effect of intramolecular transfer to polymer on stationary free radical polymerization of alkyl acrylates, Macromolecules, 38 (2005) 1581-1590.
[20] N.M. Ahmad, D. Britton, F. Heatley, P.A. Lovell, Chain transfer to polymer in emulsion polymerization, Macromolecular Symposia, 143 (1999) 231-241.
[21] C. Barner-Kowollik, S. Beuermann, M. Buback, P. Castignolles, B. Charleux, M.L. Coote, R.A. Hutchinson, T. Junkers, I. Lacik, G.T. Russell, M. Stach, A.M. van Herk, Critically evaluated rate coefficients in radical polymerization - 7. Secondary-radical propagation rate coefficients for methyl acrylate in the bulk, Polymer Chemistry, 5 (2013) 204-212.
[22] M.S. Hussain, B. Adamu, A review of chain transfer catalysis and catalytic homopolymerization of acrylates and styrene, Arabian Journal for Science and Engineering, 24 (1999) 3-26.
[23] R.A. Gregg, D.M. Alderman, F.R. Mayo, Chain transfer in the polymerization of styrene .5. Polymerization of styrene in the presence of mercaptans, Journal of the American Chemical Society, 70 (1948) 3740-3743.
[24] J.L. O'brian, F. Gornick, Chain Transfer in the polymerization of methyl methacrylate .1. Transfer with monomer and thiols - The mechanism of the termination reaction at 60-degrees, Journal of the American Chemical Society, 77 (1955) 4757-4763.
[25] C. Loubat, B. Boutevin, Telomerization of acrylic acid with thioglycolic acid - Effect of the solvent on the C-T value, Polymer Bulletin, 44 (2000) 569-576.
[26] J.P.A. Heuts, T.P. Davis, G.T. Russell, Comparison of the Mayo and chain length distribution procedures for the measurement of chain transfer constants, Macromolecules, 32 (1999) 6019-6030.

[27] X.H. Xu, B. Bai, C.X. Ding, H.L. Wang, Y.R. Suo, Synthesis and properties of an ecofriendly superabsorbent composite by grafting the poly(acrylic acid) onto the surface of dopamine-coated sea buckthorn branches, Industrial & Engineering Chemistry Research, 54 (2015) 3268-3278.
[28] B. Bolto, J. Gregory, Organic polyelectrolytes in water treatment, Water Research, 41 (2007) 2301-2324.
[29] S.F. Duan, S. Cai, Y.M. Xie, T. Bagby, S.Q. Ren, M.L. Forrest, Synthesis and characterization of a multiarm poly(acrylic acid) star polymer for application in sustained delivery of cisplatin and a nitric oxide prodrug, Journal of Polymer Science Part A -Polymer Chemistry, 50 (2012) 2715-2724.
[30] L.A. Connal, Q. Li, J.F. Quinn, E. Tjipto, F. Caruso, G.G. Qiao, PH-responsive poly(acrylic acid) core cross-linked star polymers: Morphology transitions in solution and multilayer thin films, Macromolecules, 41 (2008) 2620-2626.
[31] J. Loiseau, N. Doerr, J.M. Suau, J.B. Egraz, M.F. Llauro, C. Ladaviere, Synthesis and characterization of poly(acrylic acid) produced by RAFT polymerization. Application as a very efficient dispersant of CaCO3, kaolin, and TiO2, Macromolecules, 36 (2003) 3066-3077.
[32] L. Couvreur, C. Lefay, J. Belleney, B. Charleux, O. Guerret, S. Magnet, First nitroxide-mediated controlled free-radical polymerization of acrylic acid, Macromolecules, 36 (2003) 8260-8267.
[33] C. Plessis, G. Arzamendi, J.M. Alberdi, M. Agnely, J.R. Leiza, J.M. Asua, Intramolecular chain transfer to polymer in the emulsion polymerization of 2-ethylhexyl acrylate, Macromolecules, 34 (2001) 6138-6143.
[34] D.J. Haloi, N.K. Singha, Synthesis of Poly(2-ethylhexyl acrylate)/Clay Nanocomposite by In Situ Living Radical Polymerization, Journal of Polymer Science Part a-Polymer Chemistry, 49 (2011) 1564-1571.
[35] T. Junkers, M. Schneider-Baumann, S.P.S. Koo, P. Castignolles, C. Barner-Kowollik, Determination of Propagation Rate Coefficients for Methyl and 2-Ethylhexyl Acrylate via High Frequency PLP-SEC under Consideration of the Impact of Chain Branching, Macromolecules, 43 (2010) 10427-10434.
[36] F. Heatley, P.A. Lovell, T. Yamashita, Chain transfer to polymer in free-radical solution polymerization of 2-ethylhexyl acrylate studied by NMR spectroscopy, Macromolecules, 34 (2001) 7636-7641.
[37] B. Dervaux, T. Junkers, M. Schneider-Baumann, F.E. Du Prez, C. Barner-Kowollik, Propagation Rate Coefficients of Isobornyl Acrylate, tert-Butyl Acrylate and 1-Ethoxyethyl

Acrylate: A High Frequency PLP-SEC Study, Journal of Polymer Science Part a-Polymer Chemistry, 47 (2009) 6641-6654.
[38] A.N. Nikitin, P. Castignolles, B. Charleux, J.P. Vairon, Determination of propagation rate coefficient of acrylates by pulsed-laser polymerization in the presence of intramolecular chain transfer to polymer, Macromolecular Rapid Communications, 24 (2003) 778-782.
[39] T. Junkers, M. Schneider-Baumann, S.S.P. Koo, P. Castignolles, C. Barner-Kowollik, Determination of Propagation Rate Coefficients for Methyl and 2-Ethylhexyl Acrylate via High Frequency PLP−SEC under Consideration of the Impact of Chain Branching, Macromolecules, 43 (2010) 10427-10434.
[40] L. Couvreur, G. Piteau, P. Castignolles, M. Tonge, B. Coutin, B. Charleux, J.P. Vairon, Pulsed-laser radical polymerization and propagation kinetic parameters of some alkyl acrylates, Macromolecular Symposia, 174 (2001) 197-207.
[41] S. Beuermann, M. Buback, P. Hesse, T. Junkers, I. Lacik, Free-radical polymerization kinetics of 2-acrylamido-2-methylpropanesulfonic acid in aqueous solution, Macromolecules, 39 (2006) 509-516.
[42] M. Buback, H. Hippler, J. Schweer, H.P. Vogele, Time-resolved study of laser-induced high-pressure ethylene polymerization, Makromolekulare Chemie-Rapid Communications, 7 (1986) 261-265.
[43] M. Buback, C. Kowollik, Termination kinetics in free-radical bulk copolymerization: The systems dodecyl acrylate dodecyl methacrylate and dodecyl acrylate methyl acrylate, Macromolecules, 32 (1999) 1445-1452.
[44] G.S. Timmins, M.J. Davies, B.C. Gilbert, H. Caldararu, EPR spin-labeling and spin-trapping study of proteins in reverse micelles, Journal of the Chemical Society-Faraday Transactions, 90 (1994) 2643-2648.
[45] C. Plessis, G. Arzamendi, J.M. Alberdi, A.M. van Herk, J.R. Leiza, J.M. Asua, Evidence of branching in poly(butyl acrylate) produced in pulsed-laser polymerization experiments, Macromolecular Rapid Communications, 24 (2003) 173-177.
[46] A.N. Nikitin, R.A. Hutchinson, M. Buback, P. Hesse, Determination of intramolecular chain transfer and midchain radical propagation rate coefficients for butyl acrylate by pulsed laser polymerization, Macromolecules, 40 (2007) 8631-8641.
[47] J. Barth, W. Meiser, M. Buback, SP-PLP-EPR study into termination and transfer kinetics of non-ionized acrylic acid polymerized in aqueous solution, Macromolecules, 45 (2012) 1339-1345.

[48] A.N. Nikitin, R.A. Hutchinson, G.A. Kalfas, J.R. Richards, C. Bruni, The Effect of Intramolecular Transfer to Polymer on Stationary Free-Radical Polymerization of Alkyl Acrylates, 3-Consideration of Solution Polymerization up to High Conversions, Macromolecular Theory and Simulations, 18 (2009) 247-258.

[49] H. Kattner, M. Buback, Termination, Propagation and Transfer Kinetics of Midchain Radicals in Methyl, Acrylate and Dodecyl Acrylate Homopolymerization, Macromolecules, (2017).

[50] J. Barth, M. Buback, P. Hesse, T. Sergeeva, Termination and Transfer Kinetics of Butyl Acrylate Radical Polymerization Studied via SP-PLP-EPR, Macromolecules, 43 (2010) 4023-4031.

[51] C. Barner-Kowollik, T.P. Davis, M.H. Stenzel, Probing mechanistic features of conventional, catalytic and living free radical polymerizations using soft ionization mass spectrometric techniques, Polymer, 45 (2004) 7791-7805.

[52] T. Junkers, S.P.S. Koo, T.P. Davis, M.H. Stenzel, C. Barner-Kowollik, Mapping poly(butyl acrylate) product distributions by mass spectrometry in a wide temperature range: Suppression of midchain radical side reactions, Macromolecules, 40 (2007) 8906-8912.

[53] S.P.S. Koo, T. Junkers, C. Barner-Kowollik, Quantitative product spectrum analysis of poly(butyl acrylate) via electrospray ionization mass spectrometry, Macromolecules, 42 (2009) 62-69.

[54] C.J. Ferguson, R.J. Hughes, D. Nguyen, B.T.T. Pham, R.G. Gilbert, A.K. Serelis, C.H. Such, B.S. Hawkett, Ab initio emulsion polymerization by RAFT-controlled self-assembly, Macromolecules, 38 (2005) 2191-2204.

[55] M. Gaborieau, T.J. Causon, Y. Guillaneuf, E.F. Hilder, P. Castignolles, Molecular weight and tacticty of oligoacrylates by capillary electrophoresis - mass spectrometry, Australian Journal of Chemistry, 63 (2010) 1219-1226.

[56] M. Siauw, B.S. Hawkett, S. Perrier, Short Chain Amphiphilic Diblock Co-Oligomers via RAFT Polymerization, Journal of Polymer Science Part a-Polymer Chemistry, 50 (2012) 187-198.

[57] L. S.J.K, Particle formation in RAFT-mediated emulsion

polymerization, Ph.D. thesis, (2007).

[58] J. Vandenbergh, T. Junkers, Synthesis of Macromonomers from High-Temperature Activation of Nitroxide Mediated Polymerization (NMP)-made Polyacrylates, Macromolecules, 46 (2013) 3324-3331.

[59] F. Gunzler, T. Junkers, C. Barner-Kowollik, Studying the Mechanism of Thioketone-Mediated Polymerization via Electrospray Ionization Mass Spectrometry, Journal of Polymer Science Part a-Polymer Chemistry, 47 (2009) 1864-1876.
[60] G. Hart-Smith, H. Chaffey-Millar, C. Barner-Kowollik, Living star polymer formation: Detailed assessment of poly(acrylate) radical reaction pathways via ESI-MS, Macromolecules, 41 (2008) 3023-3041.
[61] Z. Grubisic, P. Rempp, H. Benoit, A universal calibration for gel permeation chromatography, Journal of Polymer Science Part B Polymer Letters, 5 (1967) 753-759.
[62] C. Kim, J. Sainte Beuve, S. Guilbert, F. Bonfils, Study of chain branching in natural rubber using size-exclusion chromatography coupled with a multi-angle light scattering detector (SEC-MALS), European Polymer Journal, 45 (2009) 2249-2259.
[63] J.M. Hernández, M. Gaborieau, P. Castignolles, M.J. Gidley, A.M. Myers, R.G. Gilbert, Mechanistic investigation of a starch branching enzyme using hydrodynamic volume SEC analysis, Biomacromolecules, 9 (2008) 954-965.
[64] T.H. Mourey, SEC molecular-weight-sensitive detection, International Journal of Polymer Analysis and Characterization, 9 (2004) 97-135.
[65] A. Wolpers, G.T. Russell, P. Vana, The Impact of Band Broadening on Molar-Mass Determination of Narrow-Distribution Polymer by Size-Exclusion Chromatography, Macromolecular Theory and Simulations, 20 (2011) 667-674.
[66] M. Gaborieau, J. Nicolas, M. Save, B. Charleux, J.P. Vairon, R.G. Gilbert, P. Castignolles, Separation of complex branched polymers by size-exclusion chromatography probed with multiple detection, Journal of Chromatography A, 1190 (2008) 215-223.
[67] P. Castignolles, M. Gaborieau, Viscosimetric detection in size-exclusion chromatography (SEC/GPC): the Goldwasser method and beyond, Journal of Separation Science, 33 (2010) 3564–3570.
[68] P. Castignolles, M. Gaborieau, E.F. Hilder, E. Sprong, C.J. Ferguson, R.G. Gilbert, High-resolution separation of oligo(acrylic acid) by capillary zone electrophoresis, Macromolecular Rapid Communications, 27 (2006) 42-46.
[69] J.J. Thevarajah, M. Gaborieau, P. Castignolles, Separation and characterization of synthetic polyelectrolytes and polysaccharides with capillary electrophoresis, Advances in Chemistry, 2014 (2014) Article ID 798503.
[70] M. Gaborieau, S.P.S. Koo, P. Castignolles, T. Junkers, C. Barner-Kowollik, Reducing the degree of branching in polyacrylates via midchain radical patching: A quantitative melt-state NMR study, Macromolecules, 43 (2010) 5492-5495.

[71] N.M. Ahmad, F. Heatley, P.A. Lovell, Chain transfer to polymer in free-radical solution polymerization of n-butyl acrylate studied by NMR spectroscopy, Macromolecules, 31 (1998) 2822-2827.
[72] N. Ballard, J.C. de la Cal, J.M. Asua, The role of chain transfer agent in reducing branching content in radical polymerization of acrylates, Macromolecules, 48 (2015) 987-993.
[73] N.M. Ahmad, B. Charleux, C. Farcet, C.J. Ferguson, S.G. Gaynor, B.S. Hawkett, F. Heatley, B. Klumperman, D. Konkolewicz, P.A. Lovell, K. Matyjaszewski, R. Venkatesh, Chain transfer to polymer and branching in controlled radical polymerizations of n-butyl acrylate, Macromolecular Rapid Communications, 30 (2009) 2002-2021.
[74] B. Wenn, G. Reekmans, P. Adriaensens, T. Junkers, Photoinduced acrylate polymerization: Unexpected reduction in chain branching, Macromolecular Rapid Communications, 36 (2015) 1479-1485.
[75] T. Caykara, O. Guven, Effect of preparation methods on thermal properties of poly(acrylic acid) silica composites, Journal of Applied Polymer Science, 70 (1998) 891-895.
[76] A.R. Maniego, A.T. Sutton, Y. Guillaneuf, C. Lefay, M. Destarac, C.M. Fellows, P. Castignolles, M. Gaborieau, Characterization of branching in poly(acrylic acid) prepared by controlled and conventional radical polymerization.
[77] A. Ibrahim, S.A. Allison, H. Cottet, Extracting Information from the Ionic Strength Dependence of Electrophoretic Mobility by Use of the Slope Plot, Analytical Chemistry, 84 (2012) 9422-9430.
[78] H. Cottet, J.P. Biron, M. Martin, Taylor dispersion Analysis of mixtures, Analytical Chemistry, 79 (2007) 9066-9073.

Chapter 2

Effect of temperature, initial monomer concentration, and presence of a chain transfer agent on branching in poly(acrylic acid)

This work has been published in: J.-B. Lena, A.K. Goroncy, J.J. Thevarajah, A.R. Maniego, G.T. Russell, P. Castignolles, M. Gaborieau, Effect of transfer agent, temperature and initial monomer concentration on branching in poly(acrylic acid): A study by ^{13}C NMR spectroscopy and capillary electrophoresis, *Polymer*, 114 (2017) 209-220.

2.1 Introduction

Poly(acrylic acid) (PAA) is a hydrophilic polymer with a wide range of applications (as mentioned in Chapter 1) Even if it is not always acknowledged, PAA is branched when produced by radical polymerization [1-3]. The branching strongly influences the properties of the polymer. One consequence of the branching can be inaccurate determination of the propagation rate coefficient, k_p, by pulse-laser polymerization (PLP) coupled with size exclusion chromatography (SEC)[4]. Long-chain branching (LCB) was detected even at low conversion and it was shown that it can decrease the accuracy of the molar mass determined by SEC, and hence the k_p obtained is less accurate (up to 100 % error) [5]. The molar masses of PAAs determined by SEC showed low accuracy [6] potentially due to long-chain branching. In terms of kinetics, LCB results from intermolecular chain transfer to polymer (or random intramolecular transfer to polymer) and short-chain branching (SCB) results from intramolecular transfer to polymer such as backbiting [7]. In both cases, the secondary propagating radical (SPR) is transformed into a mid-chain radical (MCR) (see Figure 2.1). The MCR can propagate but with a rate coefficient, k_p^{tert}, much lower than k_p. Intramolecular transfer to polymer thus influences the polymerization rate and can lead to inaccurate k_p values determined by PLP if not at low enough polymerization temperature [4, 8, 9] or high enough pulse frequency[10]. Studying the branching in PAA obtained by radical polymerization thus gives important information regarding its kinetics.

As mentioned in Chapter 1, the only method to determine the average degree of branching (*DB*) in PAA is quantitative ^{13}C NMR spectroscopy. Both resolution and sensitivity are required for reliable quantification of *DB*. Various NMR methods (solution-state, solid-state and melt-state) were previously compared for poly(n-alkyl acrylate)s [11]. However, optimal analyses were by melt-state NMR spectroscopy obtained at 150 °C above the glass transition temperature (T_g) [11]. As the T_g of PAA is relatively high (between 90 and 150 °C) and PAAs degrade between 250 and 400 °C [12], there is not always stability of the polymer at T_g + 150 °C. Consequently, the branching in PAA was determined in this work by solution-state NMR spectroscopy.

In 2010, Gaborieau *et al.* studied the influence of the polymerization temperature and presence of 1-octanethiol on the branching in poly(*n*-butyl acrylate) [13]. They confirmed that *DB* increases with temperature and showed that *DB* is considerably reduced when 1-octanethiol (as a chain transfer agent, CTA) is present amongst the reactants. The temperature increases the frequency of the reaction which leads to formation of MCRs. MCR species can then take 4

different pathways: propagation of the tertiary radical, which leads to a branched polymer; *β*-scission, which does not lead to a branched polymer (at least not directly); a "patching" reaction, in which a hydrogen radical is transferred from the 1-octanethiol to an MCR; and radical-radical termination (Figure 2.1). *DB* is measurably reduced when 1-octanethiol is present; this has been attributed to "patching". Ballard *et al.* [14] showed that there is another possible explanation for the decrease of *DB*. The presence of CTA may reduce the number of backbiting events in comparison to the number of propagation events as the macroradical polymerizes for a shorter time when the reaction is carried out with a CTA and the chains formed after only a few propagation events are too short to undergo backbiting. This is expected to apply to very low molar mass polymer chain (not long enough to allow the six-membered transition state to be formed)

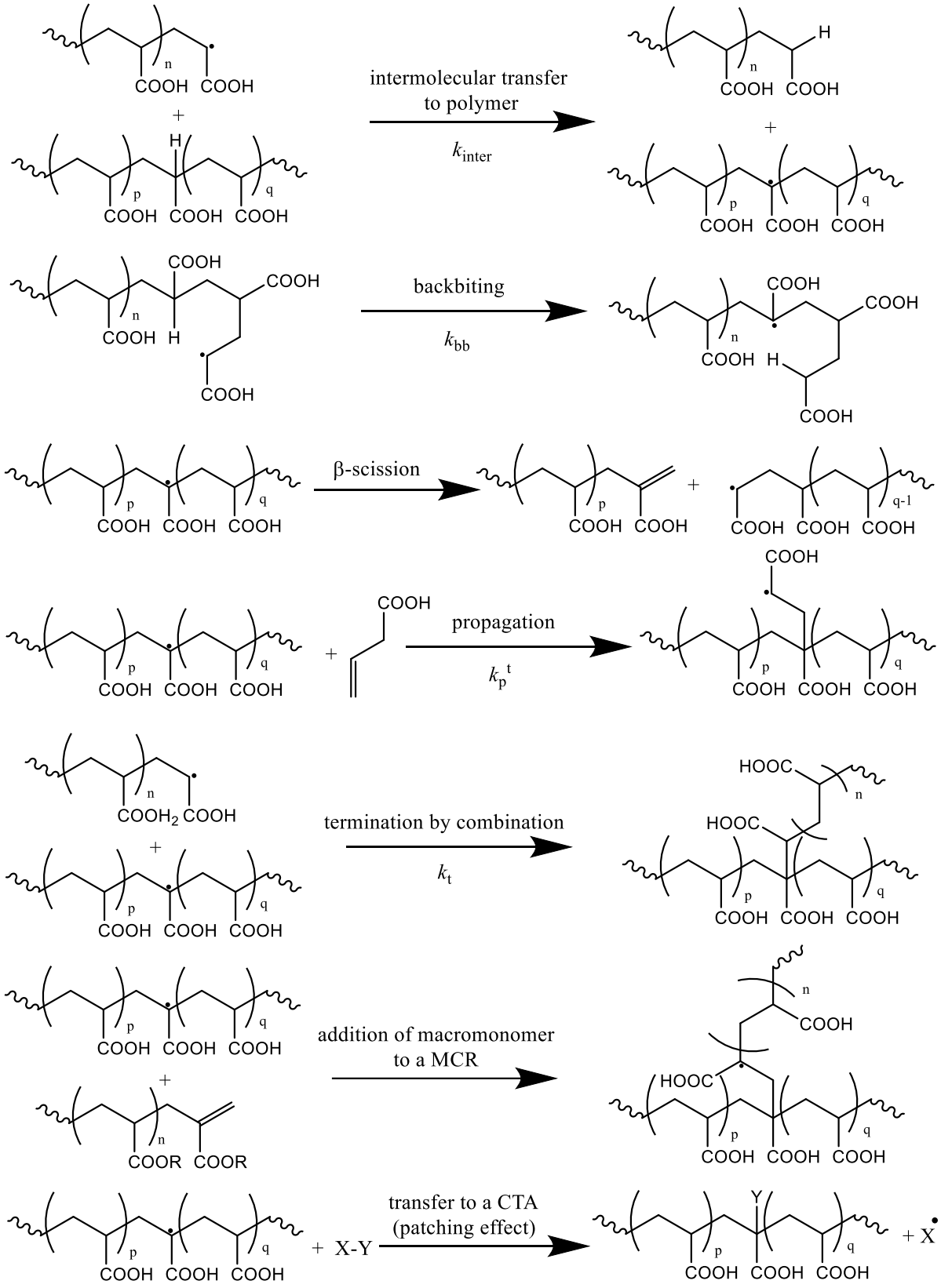

Figure 2.1: Various pathways for obtaining and consuming a MCR

As explained in Chapter 1, the development of electrospray-ionization mass spectrometry (ESI-MS) has allowed important characterization of polymer and to obtained information related to their chain length and end groups. However, linear and branched species cannot be distinguished by ESI-MS, which gives molar masses but no information related to branching. It is however challenging to obtain consistent ionization of different macromolecules within a sample. Different end-groups [15] or molar masses [16] can for example affect the ionization efficiency. This can thus limit the accuracy of the average molar mass values and of molar mass distributions determined by MS. ESI-MS analysis gives complementary information to other methods of analysis, such as SEC and NMR spectroscopy. SEC is the most widely used method to determine molar mass [17]. It separates polymers according to their hydrodynamic volume, V_h [18, 19], which depends on both molar mass and branching [20]. This may lead to incomplete SEC separation in terms of molar mass due to branching [21-23]. Multiple-detection SEC can be used to detect LCBs [11]. This method allows determination of the local number- and weight-average molar mass as well as the local dispersity of molar mass at each elution volume $Đ(V_h)$ [20]. The local dispersity assesses the accuracy of the determined molar mass [5] but it provides only an indirect assessment of the heterogeneity of the macromolecular structure due to branching. In the case of PAA, aqueous and organic SEC provide different molar mass values [6] due to the presence of branches.

In further work, poly(sodium acrylate)s (PNaAs) were separated by free-solution capillary electrophoresis in the critical conditions (CE-CC) according to their branching topology with limited influence of the molar mass [2]. The electrophoretic mobility increases as *DB* decreases [2, 24]. Capillary electrophoresis in the critical conditions (CE-CC) can thus separate polyelectrolytes according to their microstructure and allow characterization of the heterogeneity of branching. CE-CC was used in this work to determine the dispersity of the electrophoretic mobility distributions. As different branching topologies lead to different electrophoretic mobilities in the case of poly(sodium acrylate), the obtained values of dispersity are representative of the heterogeneity of branching [24].

The aim of this study was to characterize the structure of PAA (synthesized by conventional radical polymerization) by ESI-MS, solution-state NMR spectroscopy and CE-CC. From these three methods, the influence of different parameters – temperature, initial monomer concentration and presence of CTA – on the chemical structure of PAA was determined in order to better understand the mechanism and kinetics of polymerization.

2.2 Materials and methods

2.2.1 Materials

Acrylic acid (AA, 99%), 4,4'-azobis(4-cyanovaleric acid) (75%+) and thioglycolic acid (98%) were supplied by Sigma-Aldrich. Deuterium oxide (99.9% D), NaOD (40% in D_2O) and DCl (35% in D_2O) were supplied by Cambridge Isotope Laboratory Inc. Traces of PAA were found in the deuterium oxide at the last stage of the experimental work. The effect of the contamination on this study was tested and results are available in the supplementary data (Figures A6 and A7). Methanol (analytical grade) was supplied by Merck. Tetrahydrofuran (THF, HPLC grade) was passed through a solvent purification system [25]. Acetonitrile and methanoic acid (analytical grade) were provided by Fluka. Water was of Milli-Q quality. Boric acid (≥ 98%) was purchased from BDH AnalaR, Merck Pty Ltd. Sodium hydroxide pellets and dimethyl sulfoxide, DMSO, were supplied by Sigma Chemical Company. One PAA sample was received from Sigma-Aldrich (catalog number: 026C; lot number: 100416003). The linear PNaA was obtained from PSS (Mainz, Germany), as described in [2].

4,4'-azobis(4-cyanovaleric acid) was used as received. Thioglycolic acid and acrylic acid were distilled under reduced pressure.

2.2.2 Synthetic methods

Into a 50 mL Schlenk round-bottom flask were added 12.4 mg of 4,4'-azobis(4-cyanovaleric acid) (to give a concentration of 2.00×10^{-3} mol L^{-1} for polymerization), 3.00 mL of acrylic acid (1.99 mol L^{-1} for polymerization), 0.0 or 0.3 mL of thioglycolic acid (0.0 or 0.2 mol L^{-1} for polymerization) and 22 mL of solvent (H_2O/THF 8/2 v/v). This solvent mixture was chosen because it has been found to be efficient for chain transfer to thioglycolic acid [26]. The amount of CTA was chosen in order to obtain a DP_n close to 10, and thus facilitate analysis of these (short) polymers by ESI-MS. The Schlenk round bottom flask was degassed by bubbling nitrogen through the solution for 30 min. The mixture was left under stirring at 50, 70 or 90 °C for 24 h, 6 h or 1 h, respectively. After these reactions times, the samples were quenched in ice water. THF was evaporated using a rotary evaporator and the remaining aqueous solution was freeze-dried for 48 h. Then, a white powder was collected. Polymerization at 90 °C without CTA was repeated with different amounts of solvent (14.6 mL and 44 mL, corresponding to 3.00 mol L^{-1} and 0.99 mol L^{-1}, respectively, of acrylic acid) in order to study the influence of

the initial monomer concentration on the structure of the polymer. Reaction times were chosen to give high conversion (see Table A.2.1). The monomer conversions were shown to be higher than 88 % by both ^{1}H NMR spectroscopy and CE (see Figure A.2.1 and Table A.2.2).

2.2.3 Mass spectrometry

These experiments were carried out by Alexander Goroncy (operator a) and Marie Squire (operator b)

Two different operators performed the ESI MS analyses: one run the PAA samples synthesized at 70 and 90 °C (operator a) and the second one the PAA sample synthesized at 50 °C (operator b).

The samples for ESI-MS analysis were prepared as follows: 1 mg of PAA was dissolved in 1 mL of water/methanol (1/1 v/v). The samples were injected into a Thermo Fisher Scientific Dionex UltiMate 3000 liquid chromatography (LC) system (without a column) comprised of an Ultimate 3000 RS Pump, 3000 RS Autosampler, 3000 RS Column Compartment, 3000 Diode Array Detector. The LC system was attached to a Bruker maXis 3G Ultra High Resolution Time of Flight tandem mass spectrometer (Bruker Daltonics). The isocratic mobile phase comprised 0.1% (v/v) formic acid and 50% (v/v) acetonitrile in water at a flow rate of 300 µL min^{-1} (operator a) and 200 µL min^{-1} (operator b). Ions were generated by electrospray ionization (ESI) and cleaned of solvent by a nitrogen flow of 8.0 L min^{-1}, temperature of 200 °C, nebulizer at 1 bar, end plate offset at 500 V, capillary voltage at 4000 V, and analysis in positive-ion mode. The intensity of positive ions was recorded in the range of 30–2414 m/z (operator a) and 100-3000 m/z (operator b), at a rate of 2 s^{-1} and analysed using Bruker Compass HyStar 3.2 – SR 2 (Build 44). The voltage peak to peak was 3000 Vpp (operator a) and 1200 Vpp (operator b).

2.2.4 NMR spectroscopy

2.2.4.1 Conditions of analyses

The PAA provided by Sigma-Aldrich was analysed by ^{13}C NMR spectroscopy by Alison R. Maniego (Ph.D. candidate, Western Sydney University, Australia) but data were analysed at UC.

Spectra of PAAs synthesized by conventional radical polymerization with and without CTA were acquired in D_2O at 26 °C (^1H NMR spectra) or 49 °C (^{13}C NMR spectra) on an Agilent 400 MR with Varian 7600-AS auto-sampler, equipped with a OneNMR probe and variable temperature capabilities, operating at Larmor frequencies of 399.84 MHz for ^1H and 100.55 MHz for ^{13}C. The presence of thioglycolic acid during the synthesis is expected to influence the chain length and *DB*. The solubility of the PAAs in D_2O and the signal to noise ratios (*SNRs)* of the peak of the quaternary carbon thus vary, and so some conditions of analysis (number of scans, concentration of PAA in D_2O) were adjusted for each sample. The polymer concentrations for ^{13}C NMR analyses are given in Table 2.1.

Table 2.1: [PAA] in D2O for each ^{13}C NMR experiment

Samples	Concentration in D_2O
PAA synthesized at 50 °C with CTA at $[AA]_0 = 2$ M	750 mg mL^{-1}
PAA synthesized at 50 °C without CTA at $[AA]_0 = 2$ M	100 mg mL^{-1}
PAA synthesized at 70 °C with CTA at $[AA]_0 = 2$ M	750 mg mL^{-1}
PAA synthesized at 70 °C without CTA at $[AA]_0 = 2$ M	190 mg mL^{-1}
PAA synthesized at 90 °C with CTA at $[AA]_0 = 2$ M	750 mg mL^{-1}
PAA synthesized at 90 °C without CTA at $[AA]_0 = 2$ M	190 mg mL^{-1}
PAA synthesized at 90 °C without CTA at $[AA]_0 = 1$ M	190 mg mL^{-1}
PAA synthesized at 90 °C without CTA at $[AA]_0 = 3$ M	190 mg mL^{-1}
PAA supplied by Sigma-Aldrich	27 mg mL^{-1}

For the ^1H NMR analyses, a few mg of PAA were dissolved in a few tenths of mL of D_2O. The volume of D_2O was measured with a plastic syringe. One-dimensional ^1H NMR spectra were acquired with 16,384 data points, 128 scans, 16 ppm spectral width (6,410.3 Hz), 40 s relaxation delay, 2.556 s acquisition time and a 90° flip angle. One-dimensional ^{13}C NMR spectra were recorded with 32,768 data points, 16,500 to 19,000 scans, 246.8 ppm spectral width (25,000 Hz), 10.0 s relaxation delay and a 90° flip angle with inverse-gated decoupling.

The PAA from Sigma Aldrich was analyzed at room temperature on a Bruker DRX300 spectrometer (Bruker, Biospin Ltd, Sydney) equipped with a 5 mm dual $^{1}H/^{13}C$ probe at Larmor frequencies of 300.13 MHz for ^{1}H and 75 MHz for ^{13}C NMR. The PAA provided by Sigma-Aldrich was dissolved at 27 g L^{-1} in D_2O (with 1 mol equivalent of NaOD to the carboxylic acid unit and 0.5 mol equivalent of DCl to the carboxylic acid unit). A one-dimensional ^{1}H NMR spectrum was acquired with 8 scans, 5.0 s acquisition time + relaxation delay, and 30° flip angle. A one-dimensional ^{13}C NMR spectrum was recorded with 27,411 scans, 5.8 s relaxation delay, 0.2 s acquisition time and a 90° flip angle, with inverse-gated decoupling.

2.2.4.2 Signals assignment

The chemical shift scales were calibrated for ^{1}H and ^{13}C NMR spectra by measuring spectra of acrylic acid with methanol in D_2O. NMR spectra are shown in Figure 2.2 to 2.5, A.2.3 and A.2.8, and the ^{1}H and ^{13}C NMR signal assignments are provided in Tables 2.2 and 2.3. In order to assign each peak, 2D COSY and HSQC NMR experiments were carried out (see Figure A.2.2).

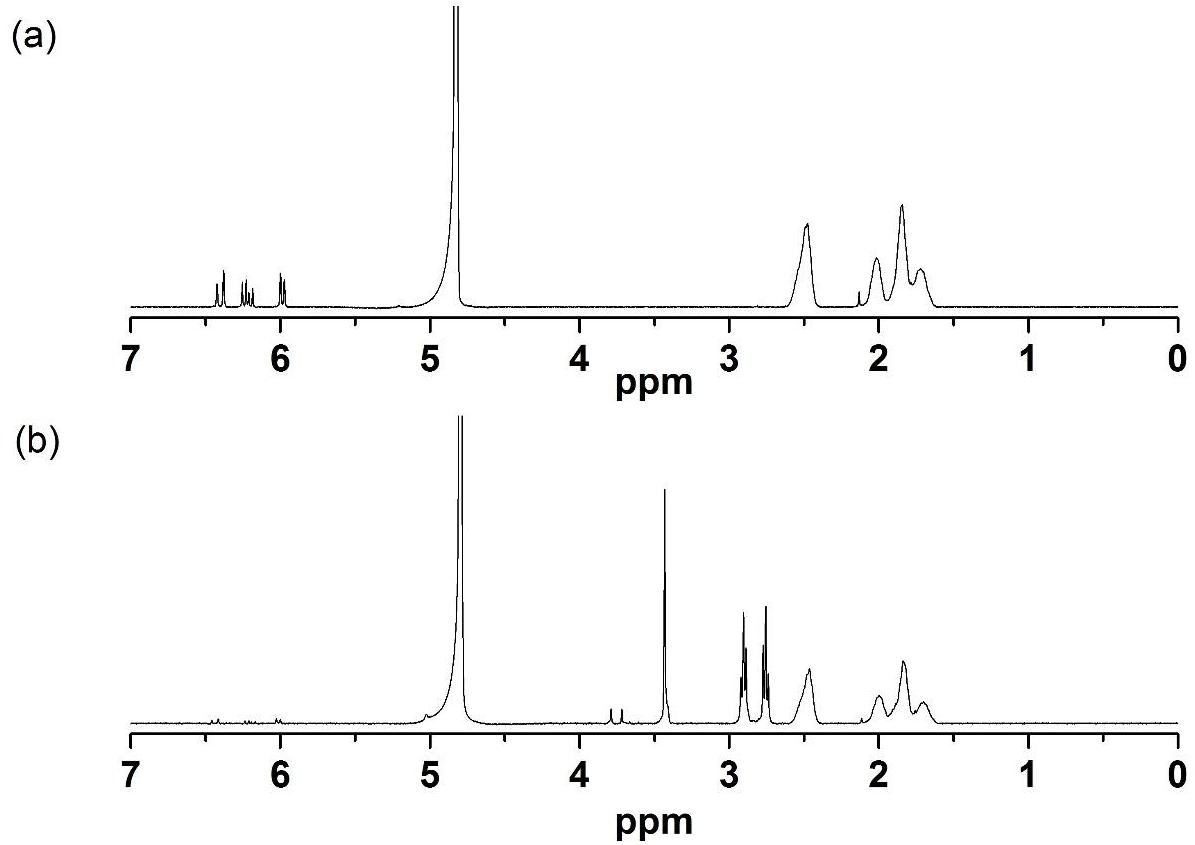

Figure 2.2: Full ^{1}H solution-state NMR spectra in D_2O at 26 °C of PAA synthesized at 90 °C (a) without CTA and (b) with CTA.

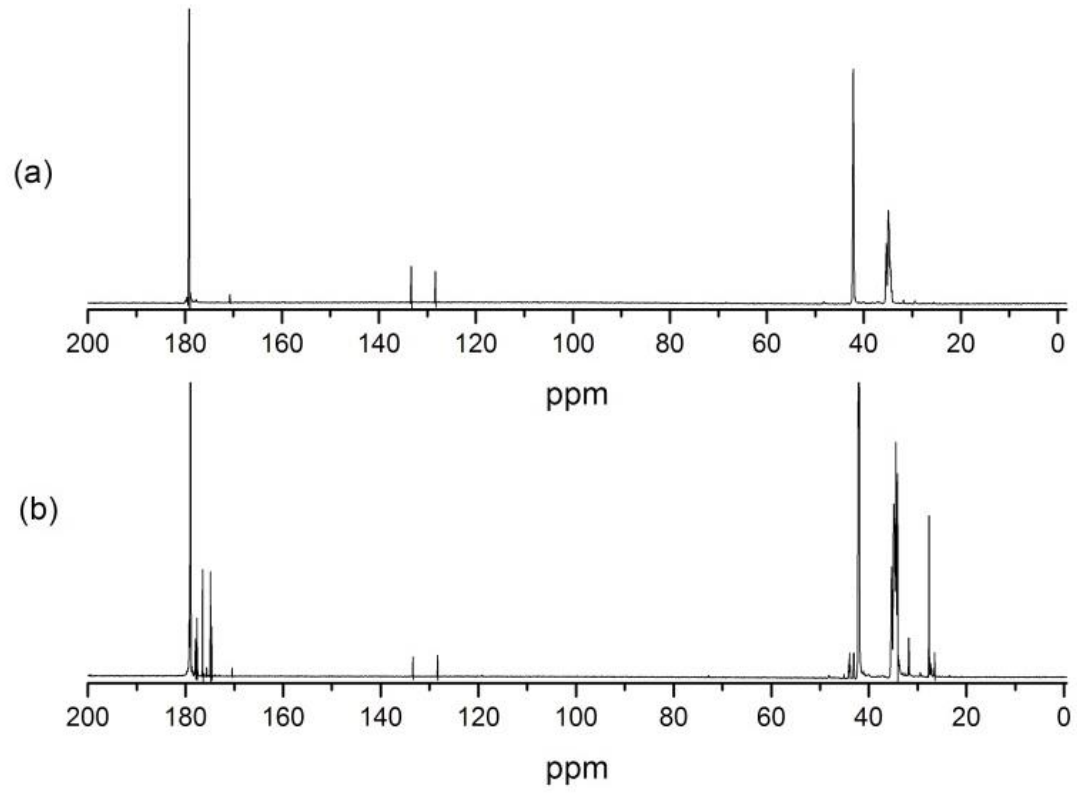

Figure 2.3: Full ^{13}C solution-state NMR spectra in D_2O at 49 °C of PAA synthesized at 90 °C (a) without CTA and (b) with CTA.

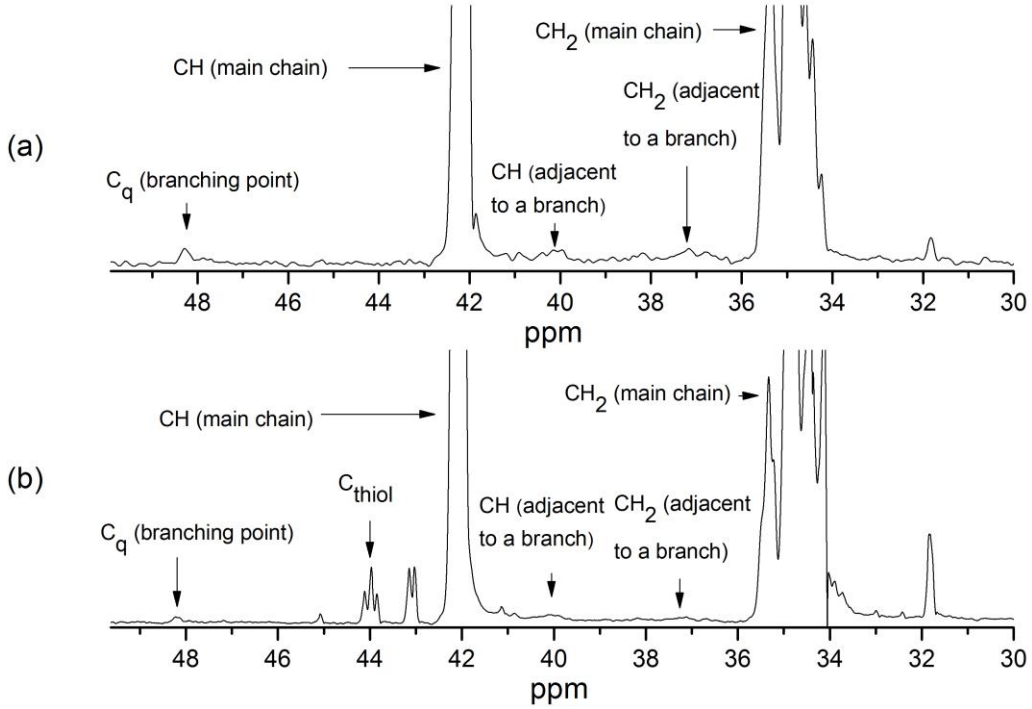

Figure 2.4: Partial ^{13}C solution-state NMR spectra in D_2O at 49 °C of PAA synthesized at 90 °C (a) without CTA and (b) with CTA.

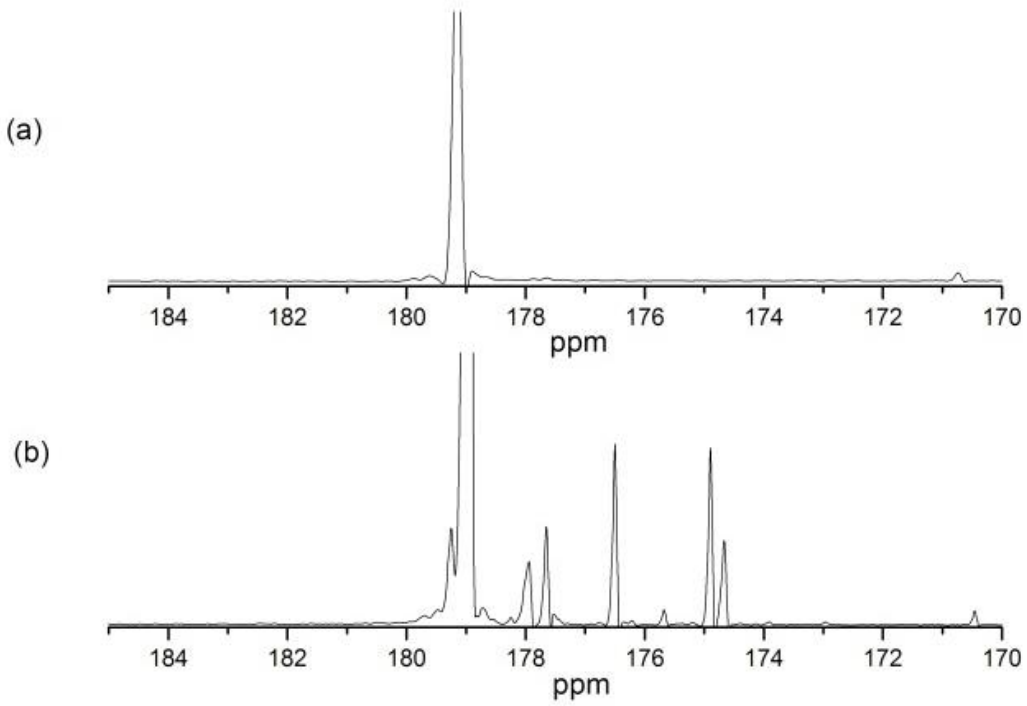

Figure 2.5: Partial ^{13}C solution-state NMR spectra in D_2O at 49 °C of PAA synthesized at 90 °C (a) without CTA and (b) with CTA.

Table 2.2: Signal assignment for ^{1}H NMR spectra of PAA in D_2O at 26 °C

δ (ppm) for thiol-containing PAA	δ (ppm) for non thiol-containing PAA	δ (ppm) Literature **[2]** (analyses done in D_2O with NaOH at RT)	δ (ppm) Literature **[1]** (analyses done in D_2O at 60 °C)	δ (ppm) Literature **[27]** (analyses done in dioxane-d_8 at RT)	δ (ppm) ChemNMR calculations and solvent table**[28]** in the case of residual water	Assignment
1.65-1.95	1.65-1.95	1.3-1.8	1.3-1.8	1.0-1.8	1.75	CH_2 (main chain)
2.3-2.5	2.3-2.5	2-2.3	1.9-2.3	1.8-2.3	2.35	CH (main chain)
2.75		-	-	2.60	2.33	CH_2-CH_2-COOH (end group)
2.88		-	-	2.87	1.79	CH_2-CH_2-COOH (end group)
3.4	-	-	-	-	3.38	S-CH_2-COOH (end group)
4.76	4.7	-	4.7	-	4.79	Residual solvent
6	6	5.8-5.9	-	-	5.75	monomer (H in cis to COOH)
6.2	6.2	5.9-6	-	-	6.22	monomer (H on same C as COOH)
6.4	6.4	6.7	-	-	6.50	monomer (H in trans to COOH)

Table 2.3: Signal assignment for ^{13}C NMR spectra of PAA in D_2O at 49 °C

δ (ppm) for thiol-containing PAA	δ (ppm) for non thiol-containing PAA	δ (ppm) Literature **[2]** (analyses done in D_2O with NaOH at RT)	δ (ppm) Literature **[1]** (analyses done in D_2O at 60 °C)	δ (ppm) Literature **[27]** (analyses done in dioxane-d_8 at RT)	δ (ppm) ChemNMR calculations	assignment
27.5	-	-	-	-	27.4, 29.6	CH_2-CH_2-COOH, CH_2-CH_2-COOH(end group)
31.8	-	-	-	-	30.9	CH_2-S-CH_2-COOH (end-group)
34-36	34-36	36-39	30.5-33	35-40	26-27.5	CH_2 (main chain)
36.5-37.5	36-37	-	38-39	-	-	CH_2 adjacent to a branch
39.6-40.4	39.8-40.8	-	41.8-43.4	-	-	CH adjacent to a branch
41-42.5	41-43	45-47	43.6-48	44.5-48.5	40-41	CH (main chain)
43	-	-	-	-	43.6	COOH-CH_2-S-CH_2-CH
44	-	-	-	-	44.5	COOH-CH_2-S (end group)
48.2	48.3	50.4	48.5-50	-	-	quaternary carbon (branching point)
128.3	128.3	127	-	-	127.5	HC(sp^2) unreacted monomer
133.4	133.4	135	-	-	134.1	H_2C(sp^2) unreacted monomer
170.5	170.5	-	-	-	170.4	COOH unreacted monomer
174.9	-	-	-	-	174.6	S-CH_2-COOH (end group)
176.5	-	-	-	-	-	not identified
178	-	-	-	-	178.3	COOH-CH-CH_2-S
179-179.5	179-179.5	-	-	183-187	182.9	COOH main chain

2.2.4.3 Inversion recovery experiment

2.2.4.3.1 Estimating accurately the longitudinal relaxation time T_1

In order to obtain quantitative results, it is necessary to have an estimation of the longitudinal relaxation time, T_1, of each signal that will be quantified.

The most common experiment used to determine T_1 is a so-called inversion recovery experiment [29].

This experiment consists of a 2-pulse sequence. In a first step, the spin population is inverted through the application of a 180° pulse. The magnetization vector will first shrink back toward the X-Y plane and then make a full recovery along the Z-axis at a rate dictated by the relaxation time T_1. As the magnetization along the Z-axis is not observable, the vector will be placed back in the X-Y plane with a 90° pulse after a suitable waiting time τ.

For a short τ, the magnetization vector will be located along the negative Y axis, and a negative signal will be observed. For a long τ, the magnetization vector will be recovered and a positive signal will be observed.

The intensity of the detected magnetization M_τ follows Eq. (2.1):

$$M_\tau = M_0\left(1 - 2e^{-\tau/T_1}\right) \quad (2.1)$$

So the experiment is repeated for several values of τ, and when extinction of the signal is observed, the waiting time corresponds to:

$$\tau_{\text{null}} = T_1\, ln2 \quad (2.2)$$

2.2.4.3.2 Estimating roughly the longitudinal relaxation time T_1

The branching was observable with a *SNR* > 5 only after 53 h (except for the PAA synthesized at 50 °C without CTA). So, it would unpractical and very expensive to perform a full inversion recovery experiment with many values of τ. However, it is possible to check if the repetition time between 2 pulses (acquisition time + relaxation delay) used when the branching was detected is greater than $5T_1$. In that case, these parameters are valid for quantitative NMR spectroscopy analysis.

The spectra were recorded with 10 s relaxation delay and 1.311 s acquisition time. So, if 11.311 s > 5T_1, i.e., if τ_{null} < 1.568 s for C_q and main-chain CH signals, the analysis is quantitative. An inversion recovery experiment with τ = 1.568 s was completed. It was found that the C_q signal and the signals of the main chain CH and the CH adjacent to a branch are positive (see Figure 2.6). Consequently, the condition for quantitative analysis is fulfilled.

Another experiment was performed to check if a relaxation delay of 6.5 s with an acquisition time of 1.311 s was enough to be quantitative (which means if τ_{null} < 1.082 s). However, Figure 2.7 shows that the quaternary carbon signal is in its extinction zone (not observable in the spectrum). It may be exactly absent, slightly positive, or slightly negative (below the noise level). Thus it is unsure if a ^{13}C NMR signal recorded with the corresponding repetition time is quantitative.

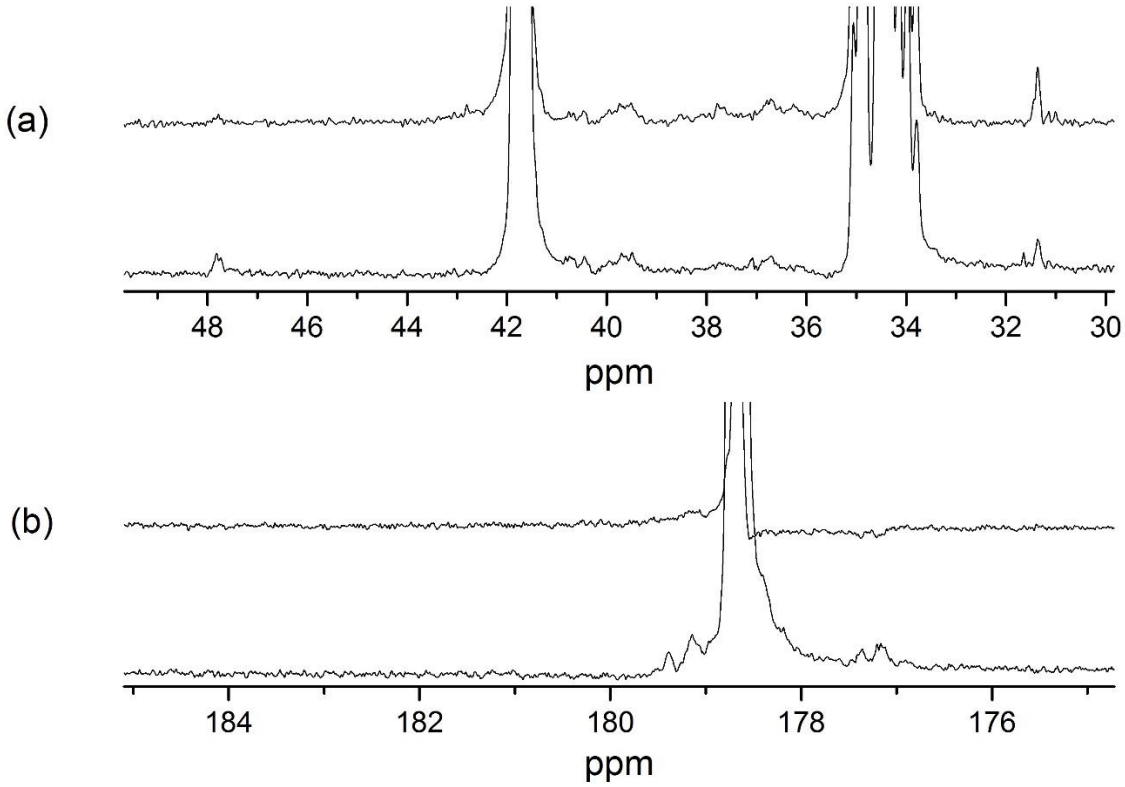

Figure 2.6: Partial ^{13}C NMR spectra of PAA synthesized at 70 °C without CTA: top – obtained from an inversion recovery experiment with τ = 1.568 s; bottom – regular conditions.

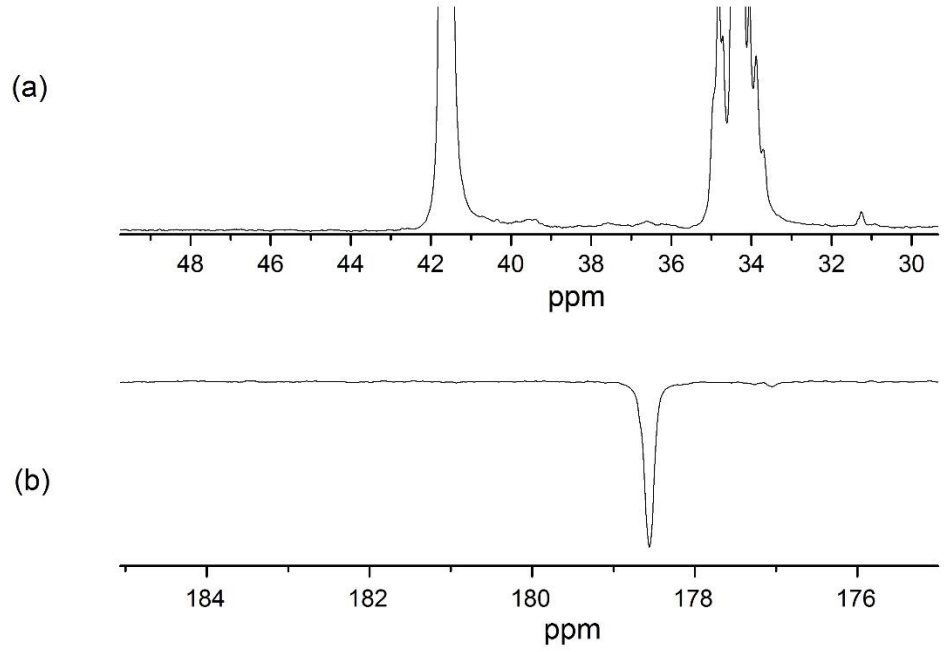

Figure 2.7: Partial ^{13}C NMR spectrum of PAA synthesized at 70 °C without CTA obtained from an inversion recovery experiment with τ = 1.082 s.

For the PNaA provided by Sigma-Aldrich, one-dimensional T_1-relaxation time experiments have determined that a relaxation delay of 5.8 s with an acquisition time of 0.2 s would be sufficient to ensure quantitative results (acquisition time + relaxation delay > 5 T_1)

2.2.4.4 Calculation of *DB*

DB was quantified in percentage of monomer units by comparing the integrals, *I*, of C_q at 48 ppm and of the main chain CH at 39-42 ppm as follows:

$$DB(\%) = \frac{100 \cdot I(\mathrm{C_q})}{I(\mathrm{C_q}) + I(\mathrm{CH})} \tag{2.3}$$

For thiol-containing PAA, the carbon called C_{thiol}, meaning the carbon of the CH adjacent to the thioglycolic acid end group-residue (i.e. adjacent to the sulfur atom), exhibited a signal at 44 ppm. This is overlapping with the main-chain CH signal (see Figure A.2.3). An over- and underestimation of *DB* were calculated as follows for thiol-containing PAA. For the overestimation, the integral of the CH signal excluded the contribution of the overlapping C_{thiol}

signal by setting the left integration limit to the valley between the C_{thiol} and CH signals (Eq. (2.4)). For the underestimation, the integral of the CH signal included the contribution of the overlapping C_{thiol} signal by setting the left integration limit to the left of the C_{thiol} signal (Eq. (2.5)).

$$DB_{overestimate}(\%) = \frac{100 \cdot I(\mathrm{C_q})}{I(\mathrm{C_q}) + I(\mathrm{CH})_{\text{excluding overlapping } \mathrm{C_{thiol}}}} \tag{2.4}$$

$$DB_{underestimate}(\%) = \frac{100 \cdot I(\mathrm{C_q})}{I(\mathrm{C_q}) + I(\mathrm{CH})_{\text{including overlapping } \mathrm{C_{thiol}}}} \tag{2.5}$$

The signal of C_q of in the ^{13}C NMR spectrum of PAA synthesized at 50 °C without CTA was observed with a *SNR* < 3, which is the limit of detection (LOD). To have an estimate of a "potential" maximum degree of branching, the *SNR* of the main chain CH signal and the one of the C_q signal were compared (see Eq. (A.2.1) and (A.2.2)).

For the PNaA provided by Sigma-Aldrich, the signal of the main-chain CH was overlapping with the signal of the main-chain CH_2 (see Figure A.2.4). Consequently, *DB* was calculated by comparing the integral of the signal of quaternary carbon to that of the carboxylic acid group, as follows:

$$DB(\%) = \frac{100 \cdot I(C_q)}{I(COOH)} \tag{2.6}$$

This equation was also used to obtain another estimate of *DB* for all samples of this work (Table A.2.3).

The relative standard deviation (*RSD*) of *DB* (in percent of *DB* values) was calculated from the signal-to-noise ratio (*SNR*) of the quaternary carbon C_q using Eq. (2.7), which was established for branching measurements in polyethylene by combination of both derivation from calculation error and empirical results [30] and assessed to be accurate also for branching measurements in hydrophobic polyacrylates [11].

$$RSD = \frac{238}{SNR^{1.28}} \tag{2.7}$$

2.2.5 Capillary Electrophoresis

The instrument and conditions were as in [2]. The preparation of a 110 mM sodium borate buffer at pH 9.2 was as in [2]. For each sample, 10 mg of PAA were dissolved in 1.5 mL of Milli-Q water with a small volume of sodium hydroxide solution (15 μL, 1 mol L^{-1} in Milli-Q water). 500 μL of dissolved PNaA were mixed with 10 μL of 10 wt. % aqueous DMSO (added as an electroosmotic flow marker). Each sample was diluted several times with Milli-Q water until repeatable normalized electrophoretic mobility distributions at two successive concentrations were obtained (see Table A.2.6 as well as Figures A.2.9 and A.2.10). The separations were performed with a high sensitivity, 50 μm internal diameter fused-silica capillary (Agilent, Australia) with a total length of 62.2 cm and an effective length of 53.7 cm at 30 kV and 25 °C. The electrophoretic mobility distributions and their dispersities were calculated from the raw electropherograms, as in [24] (see also Eq. (A.2.8) to (A.2.11)). Electrophoretic mobility is preferred to migration time because it is more repeatable and it characterizes the topology of polymers [31]. The pH of each PNaA sample before injection was measured to be between 4 and 5 (using a pH meter). In order to check if incomplete dissolution due to low pH influences the electropherograms, the samples were titrated until pH > 8 and CE experiments were repeated in similar conditions. Electrophoretic mobility distributions of PNaA dissolved at acidic and basic pH are reproducible in terms of shape and electrophoretic mobility (Figure A.2.11).

However, an effect on the peak area of the electropherogram exists. This issue will not be discussed at this stage. Data was treated with the Origin 9.0 software. The pH meter was a SevenCompact™ pH/Ion meter S220 (Mettler Toledo), calibrated with internal standards with pH values of 4, 7 and 9.2 or 4, 7 and 10.

2.3 Results and discussions

The PAAs synthesized in the presence and in the absence of thiol were characterized in terms of end groups, chain length and branching. They were compared to other PAAs (or PNaAs). Table 2.4 summarizes all polymers used to carry out this study and how they were synthesized.

Table 2.4: Summary of all polymerizations used to carry out this study

Polymer	**Synthesis method**	**Reactants (Initiator/CTA/monomer/ solvent)**	**Conversion**	M_n
PAAs specifically synthesized for this study (without CTA)	Conventional radical polymerization	ACVA/No CTA/Acrylic acid/water THF (v/v 8/2)	> 94 %*	unknown
PAAs specifically synthesized for this study (with CTA)	Conventional radical polymerization	ACVA/thioglycolic acid/Acrylic acid/water THF (v/v 8/2)	> 88 %*	Unknown (but the DP_ns are expected to be close to 10 at 65 °C)
PAA provided by sigma Aldrich	unknown	unknown	unknown	240,000 $g.mol^{-1}$ #
Linear PNaA**[2]**	Anionic polymerization	*t*-butyl acrylate	unknown	39,300 $g.mol^{-1}$ **
Hyperbranched PAA**[2]**	Nitroxide mediated polymerization	Alkoxyamine/SG1/acrylic acid/1,4-dioxane	50 %	12,300 $g.mol^{-1}$ **

*: the monomer conversion of AA was estimated using ^{1}H NMR spectroscopy and CE (See Table A.2.2 and Figure A.2.1.

**: The M_n was determined by SEC.

#: from the supplier, determination method not given.

2.3.1 End groups by ESI-MS

Figure 2.8 shows the mass spectra of PAAs synthesized with thiol at 50, 70 and 90 °C. When synthesized without CTA, no peaks were observed, as high molar mass components tend to ionize poorly [32]. When the PAA is synthesized at 70 °C with CTA, the number-average degree of polymerization, DP_n, is expected to be about 10 [26] (i.e. number-average molar mass, M_n, of about 813 g.mol^{-1}, this being the molar mass of 10 acrylic acid units inserted into a thioglycolic acid molecule).

According to the ESI-MS spectra, the majority of the species have the same end groups (HOOC-CH_2-S of CTA at one end and H at the other). The different families of peaks observed for the PAA obtained at 50, 70 and 90 °C correspond to different adducts. The main observed adducts are HOOC-CH_2-S-$(AA)_n$-H H^+, HOOC-CH_2-S-$(AA)_n$-H NH_4^+, and HOOC-CH_2-S-$(AA)_n$-H Na^+. Doubly charged adducts were observed in the spectrum of thiol-containing PAA synthesized at 70 °C and 90 °C. Tables 2.5, 2.6 and 2.7 detail the different adducts and compare their observed *m*/*z* with the theoretical value calculated with the mMass software (version 3.1.0). [33] The average size of the polymer is, of course, reduced by transfer from propagating radicals to a CTA. No terminal double bond was detected in the polymers obtained at any of the three polymerization temperatures, which is a similar trend to the the results of Junkers *et al.*, who found that the presence of a CTA reduces the amount of *β*-scission in poly(alkyl acrylates) [34]. This should also apply to PAA.

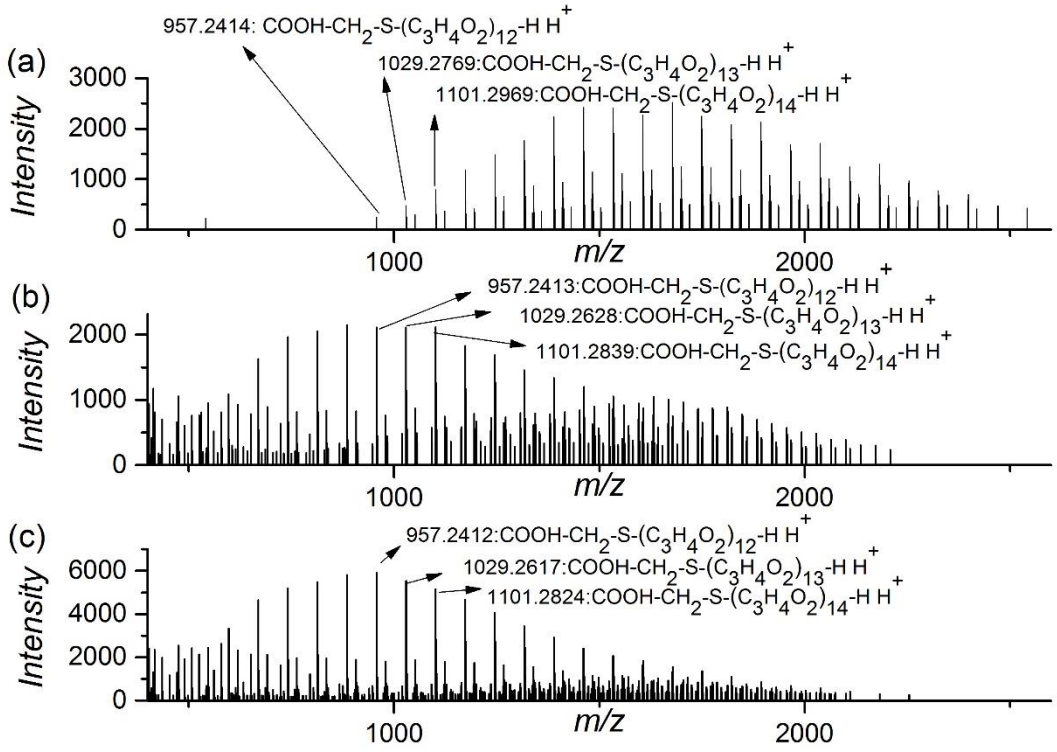

Figure 2.8: ESI mass spectra of thiol-containing PAAs synthesized at (a) 50 °C, (b) 70 °C, and (c) 90 °C.

Table 2.5: Species detected by ESI-MS for PAA synthesized at 50 °C with CTA

Formula	M_{exp} (amu)	M_{th} (amu)	h_{peak} (arbitrary units)
$C_2H_3O_2S(C_3H_4O_2)_{15}H$ H^+	1173.3175	1173.3174	1067
$C_2H_3O_2S(C_3H_4O_2)_{15}H$ Na^+	1195.2949	1195.2994	298

Table 2.6: Species detected by ESI-MS for PAA synthesized at 70 °C with CTA

Formula	M_{exp} (amu)	M_{th} (amu)	h_{peak} (arbitrary units)
$C_2H_3O_2S(C_3H_4O_2)_7H$ H^+	1173.3048	1173.3174	1828
$C_2H_3O_2S(C_3H_4O_2)_7H$ Na^+	1195.2858	1195.2994	782
$C_2H_3O_2S(C_3H_4O_2)_{32}H$ 2 H^+	1199.3287	1199.3419	564
$C_2H_3O_2S(C_3H_4O_2)_{32}H$ Na^+ H^+	1210.3189	1210.3329	358
$C_2H_3O_2S(C_3H_4O_2)_{32}H$ 2 Na^+	1221.3129	1221.3239	281

Table 2.7: Species detected by ESI-MS for PAA synthesized at 90 °C with CTA

Formula	M_{exp} (amu)	M_{th} (amu)	h_{peak} (arbitrary units)
$C_2H_3O_2S(C_3H_4O_2)_7H$ H^+	1173.3038	1173.3174	4680
$C_2H_3O_2S(C_3H_4O_2)_7H$ NH_4^+	1190.3295	1190.3440	324
$C_2H_3O_2S(C_3H_4O_2)_7H$ Na^+	1195.2846	1195.2994	1754
$C_2H_3O_2S(C_3H_4O_2)_{32}H$ 2 H^+	1199.328	1199.3419	690
$C_2H_3O_2S(C_3H_4O_2)_{32}H$ Na^+ NH_4^+	1246.83	1218.8462	479
$C_2H_3O_2S(C_3H_4O_2)_{32}H$ 2 Na^+	1221.309	1221.3239	361

M_{exp} is the experimental molar mass obtained for an adduct, M_{th} is the theoretical molar mass of the same adduct calculated with the mMass software, and h_{peak} is the peak height.

2.3.2 Average degree of branching

2.3.2.1 Determination of the average degree of branching

2.3.2.1.1 Influence of temperature and pH on the longitudinal relaxation time T_1

As the PAAs synthesized by conventional radical polymerization and the PAA provided by Sigma were analyzed in different conditions (temperature and pH), the influence of these physical parameters on the required time for precise, quantitative measurement of *DB* by ^{13}C NMR spectroscopy was studied.

The temperature and magnetic field of the NMR spectroscopy analysis, as well as the electronic configuration of the analyzed molecule – the PAA provided by Sigma was analyzed as PNaA – influence the relaxation delay, T_1, of its nuclei. When the molecule is charged and the temperature is lower, T_1 decreases. A repetition delay of 6 s was sufficient to have quantitative results when PAA was analyzed at room temperature and with NaOD, whilst a repetition delay of 7.811 s was insufficient to obtain a quantitative ^{13}C NMR spectrum of PAA when analyzed at 49 °C in D_2O without NaOD. At room temperature and with 27,411 scans, a higher *SNR* is observed than at 49 °C with 17,500 scans, but the resolution is lower (see Figures 2.9 and 2.10). Table 2.8 sums up these results.

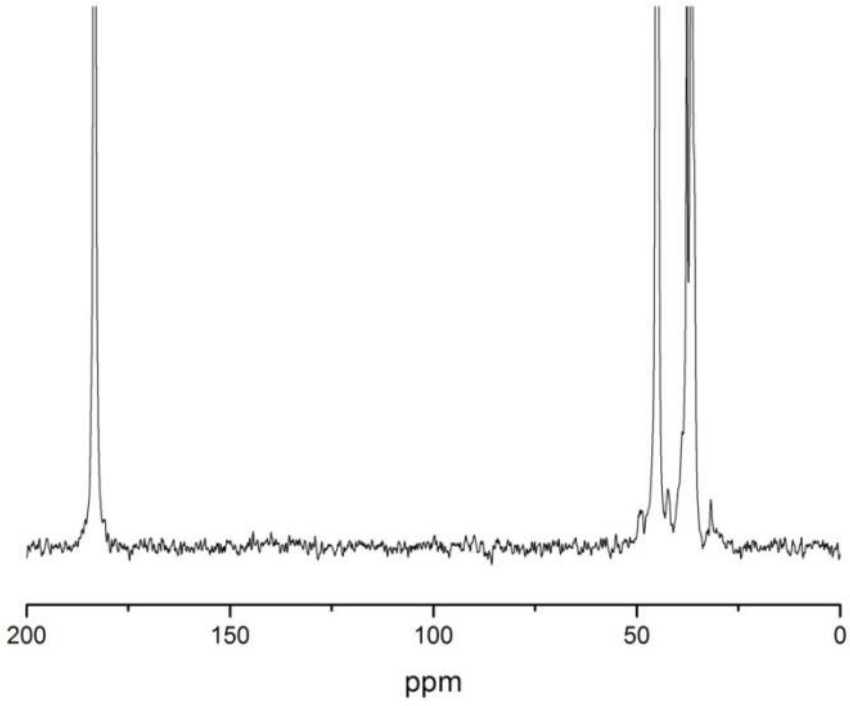

Figure 2.9: ^{13}C NMR spectrum of PAA provided by Sigma-Aldrich, analyzed at 27 g L^{-1} in D2O (with 1 mol eq. of NaOD and 0.5 mol eq. of DCl) at room temperature.

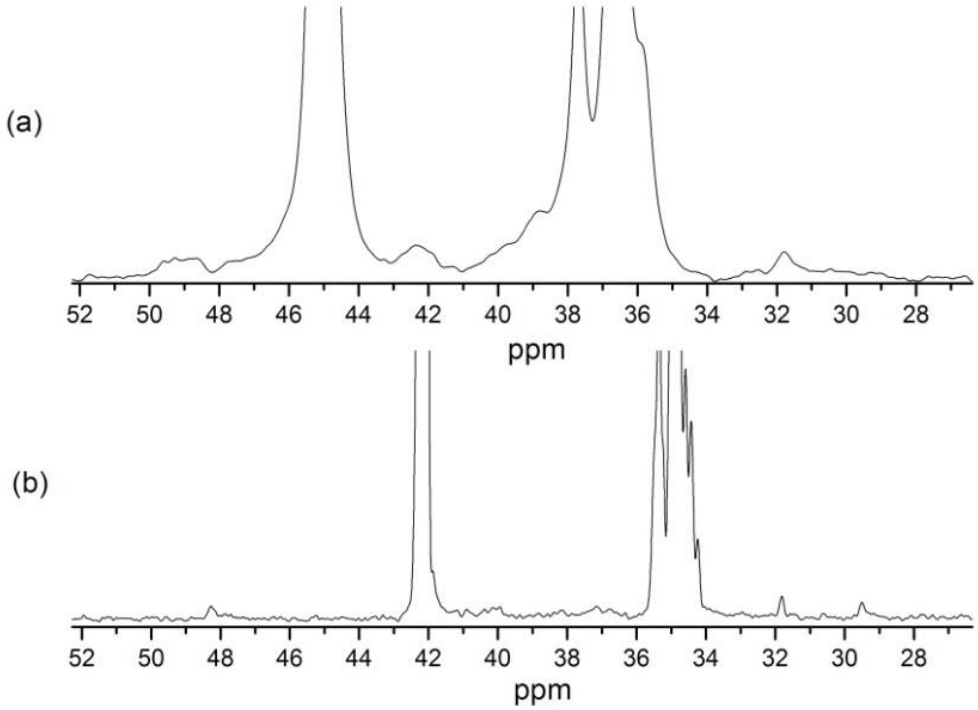

Figure 2.10: Partial ^{13}C NMR spectra of (a) PAA supplied by Sigma-Aldrich, analyzed at room temperature at 27 g L^{-1} in D_2O (with 1 mol eq. of NaOD and 0.5 mol eq. of DCl) with 27,411 scans, and (b) PAA synthesized at 90 °C without CTA, analyzed at 190 g L^{-1} in D_2O.

Table 2.8: Estimated values of the longitudinal relaxation time T_1 measured for the signals of interest for *DB* quantification of PAA in different conditions.

Samples	**Conditions of NMR analyses**	**T_1 of signals of interest for *DB* quantification**
PAAs synthesized in this work	D_2O, 49 °C	1.56 s < T_1 < 2.26 s for the C_q signal T_1 < 1.56 s for CH and CH_2 signals (main chain) 1.56 s < T_1 < 2.26 s for COOH signal (main chain)
PAA from Sigma	D_2O/NaOD, RT	T_1 < 1.2 s the C_q signal, T_1 < 1.2 s for the CH and CH_2 signals (main chain) T_1 < 1.2 s for COOH signal (main chain)

Table 1.6 in the introduction sums up all the conditions for analyses of branching in PAA or PNaA by ^{13}C NMR spectroscopy that have been reported in the literature. The *SNR* of the C_q peak is never given in the literature and the time of analysis is not always mentioned. Moreover,

even when it is claimed that the analyses are quantitative, the T_1 measurement experiment is not always mentioned, while it is the only way to know whether or not the conditions for quantitative analysis are met. Consequently, it was not possible to determine the optimal conditions of analyses based on literature.

2.3.2.1.2 Accuracy of the determination of the average degree of branching

The different values obtained for *DB* (with Eq. (2.3), (2.4), (2.5) and (2.6)) in section 2.2.4 are similar (and in the same range if the *RSD* is taken into account). This confirms that the analyses were quantitative.

The dissolution of polymers is a process whose complexity is regularly underestimated.[35, 36] For example in the case of starch, transparent liquids resisting to centrifugation were shown by NMR spectroscopy to still be incompletely dissolved.[37] Some inaccuracies of *DB* measurement could be due to incomplete dissolution of PAA in D_2O (especially for the CTA-containing PAAs due to the sulphur-containing end groups). The solubility of PAA in D_2O was tested by comparing the ^{13}C NMR spectra of different PAAs using the normalized peak area to noise ratio, defined as follows.

The "peak area to noise ratio" (*PNR*) of a NMR signal is defined as the absolute peak area divided by the noise. The peak area and the "signal" (peak height) are measured with the Origin 9.0 software package while the *SNR* is obtained from ACD Lab software package.

It is relevant to study the dissolution of a sample in the deuterated solvent as the peak area is used as the quantity proportional to the amount of sample and the noise as the scaling factor to put all spectra on the same scale. The normalized *PNR* corresponds to the *PNR* of a signal divided by the PAA label concentration used for the NMR measurement and by the square root of the number of scans (Eq. (2.8) was used).

$$Normalized\ PNR = \frac{PNR}{[analyte]\sqrt{number\ of\ scans}} \tag{2.8}$$

Both main chain CH and COOH signals were used in this instance. The normalized *PNR* of COOH and CH signals in all PAAs synthesized by conventional radical polymerization were compared to the normalized *PNR* of the same signals in the linear PNaA (which is assumed to be fully soluble in D_2O). Results are presented in Figure 2.11. Similar calculations were carried

out using the *SNR* instead of the *PNR*. Results are presented in Figure A.2.7. However, *PNR* is preferred to *SNR* as it is not demonstrated that the height of the signal is proportional to the amount of sample.

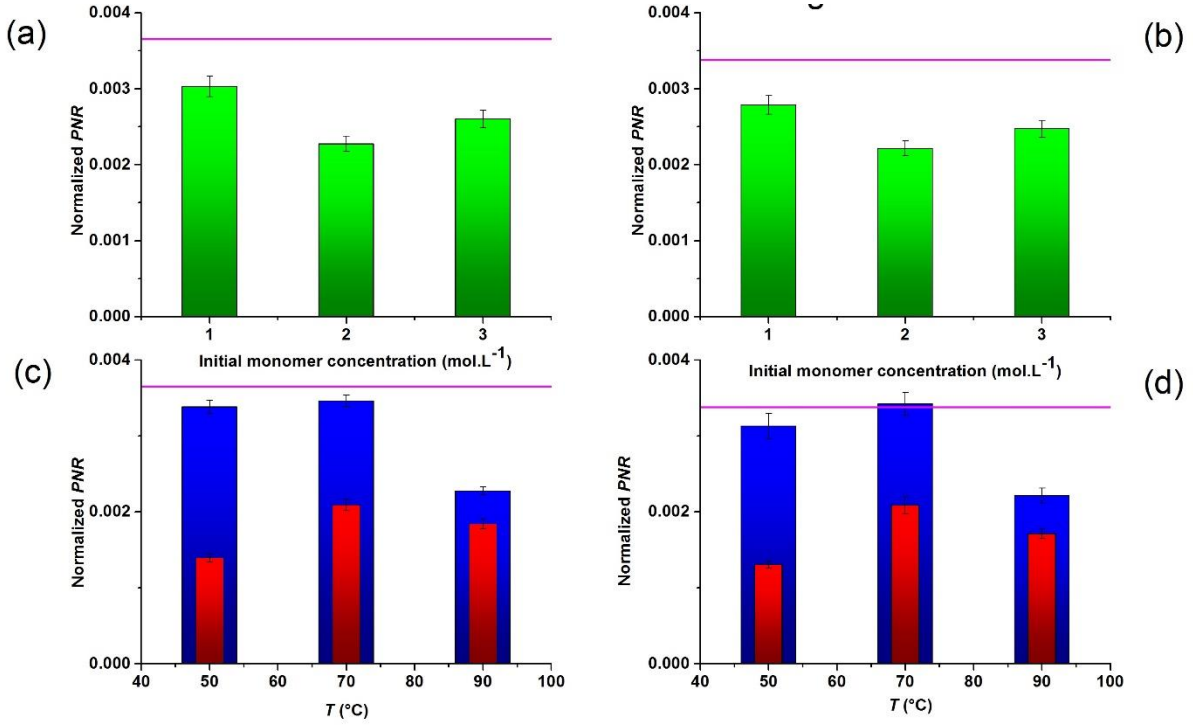

Figure 2.11: Normalized PNR of the different PAAs synthesized by conventional radical polymerization. Green bars represents the PAAs synthesized at 90 °C without CTA at different initial minomer concentrations, red and blue bars represent the PAAs synthesized at $[AA]_0$=2 M at different temperatures, with and without CTA, respectively. Graphs a and b represents the results obtained with the backbone COOH signal, c and d graphs represents the results obtained with the backbone CH signal. Magenta lines represent the SNR values obtained for the linear PNaA.

In the case of PAAs synthesized with CTA, a significantly lower normalized *PNR* than in the case of the linear PNaA is observed for both COOH and CH backbone signals, which suggests that they are less dissolved in D_2O. This could be due to the presence of sulfur in the end group. Consequently, *DB* values obtained for these two samples may be less accurate than the ones measured in the other PAAs.

2.3.2.2 Values of average degree of branching

*DB*s obtained for CTA-containing polymers are significantly lower than the ones obtained in conventional systems at 70 °C and 90 °C (Figure 2.12b). Thus the CTA reduces not only the average chain length of the polymer but also *DB*. Of course reduction of average chain length also reduces the number of branches per chain, as observed in PLP [34]. However, *DB* is expressed per monomer unit and not per chain, and so the reduction of *DB* is a different phenomenon, as conventional transfer to CTA does not change the macroradical concentration and consequently should not change the frequency of transfer to polymer reactions. One likely explanation is the patching effect of tertiary MCRs by CTA, as postulated for poly(*n*-butyl acrylates) [13]. Another possible explanation for the reduction of *DB* due to the presence of a CTA is the lowering of the number of backbiting events in comparison to propagation of SPRs [14, 38], since the time of polymerization is shorter for the PAA synthesized in the presence of the CTA. It conflates the formation of very short chains in which a six membered ring transition state is impossible. This difference might also be exacerbated by unintended temperature increase. Although in laboratory experiments like these one strives to maintain constant temperature, the polymerizations were performed in round-bottom flasks with magnetic stirring and the fast rates of acrylate polymerizations sometimes give rise to an exotherm, even in relatively dilute solution. In the absence of CTA, chains will be longer, and hence solutions more viscous. This makes heat transfer more difficult, and hence exotherm effects more likely. Such would give an enhancement of *DB*, as observed.

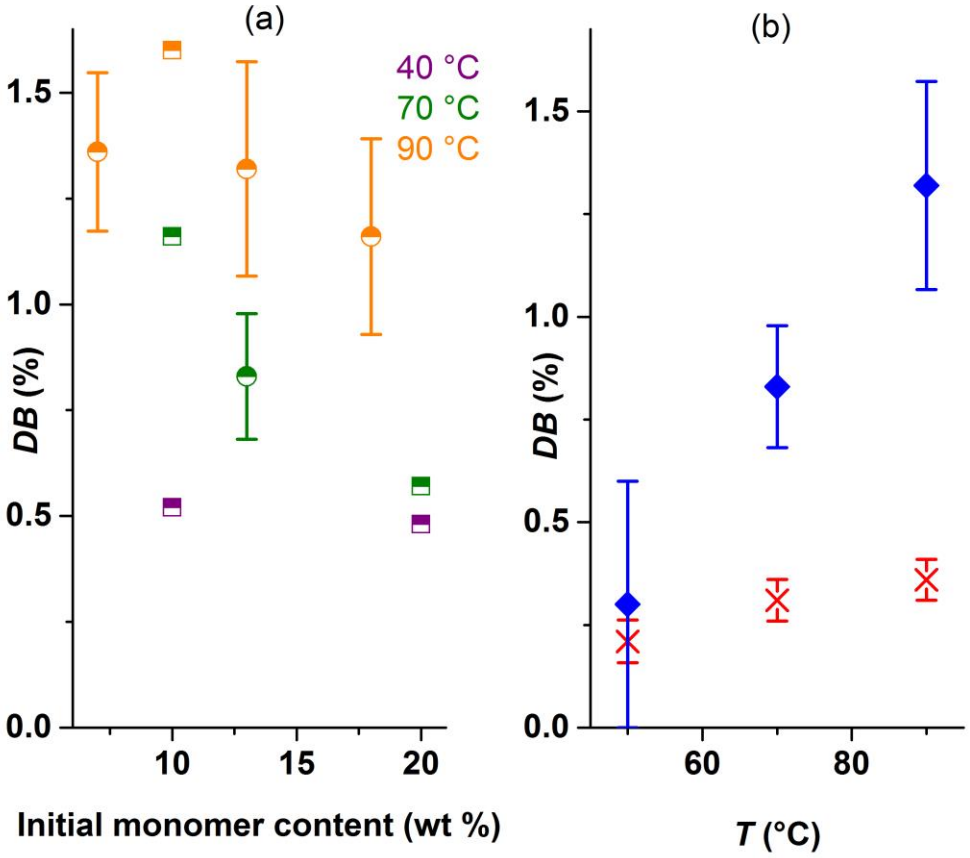

Figure 2.12: Average degree of branching, DB, in percent of monomer units, as a function of: (a) initial monomer concentration: results from Wittenberg [39] are represented by semi-filled squares and results from this study by semi-filled circles; and (b) synthesis temperature for PAA synthesized in solution without (blue diamonds) or with (red crosses) 0.2 mol L^{-1} CTA. DBs of CTA-containing polymers presented in this graph were calculated with Eq. (2.4). *DB*s of non-CTA containing PAAs were calculated with Eq. (2.3) (except for the PAA synthesized at 50 °C without CTA, where Eq. (A.2.2) was used).

DB increases with the temperature. This can be explained by the increase of frequencies of the reactions that lead to MCRs, viz. inter- and intramolecular (chain) transfer. Typical activation energies of these transfer reactions are between 20 and 25 kJ mol^{-1} higher than that of chain-end (as opposed to mid-chain) propagation in the case of alkyl acrylates [7]. Wittenberg *et al.* tabulated the activation energy of backbiting and chain-end propagation steps for polymerization of non-ionized acrylic acid as being 38 and 13 kJ mol^{-1} respectively [39]. These values were calculated for batch radical polymerization of 5 to 40% non-ionized acrylic acid in aqueous solution between 40 °C and 90 °C. In this study, the temperatures and monomer

concentration are within the same range but acrylic acid was polymerized in water/THF (8/2 v/v)), also in batch. Thus conditions were essentially the same, apart from having 20% THF as solvent rather than 100% water.

Figure 2.12b shows that as temperature is increased, the effect of CTA on *DB* becomes stronger, i.e. there is a bigger gap between *DB* with and without CTA: at 50 °C there is no difference within the limit of detection, but at 90 °C the value with 0.2 mol L^{-1} CTA is about one third of what it is without. An obvious explanation for this is that the patching reaction becomes more prominent as the temperature increases.

Wittenberg *et al.* [39] also quantified *DB* of PAA produced by radical polymerization in water without CTA at high conversion (> 95 %) in a similar range of temperatures (40 °C to 90 °C). Their results (*DB* from 0.48 % to 1.60 %) are close to the ones in this study (and are in the same range taking the error bars into account). Figure 2.13 provides a comparison between *DB* obtained for PAA synthesized without CTA in this study and in the study by Wittenberg *et al*. The *DB*s are of the same magnitude between both sets of work, for polymer obtained under similar conditions and analysed with the same solvent, D_2O, in ^{13}C NMR. It is important to note that, although Wittenberg *et al.* carried out AA polymerizations in the presence of 2-mercaptoethanol, they do not appear to have measured *DB* in such experiments, rather just the molar mass distributions (by size exclusion chromatography) and conversion as a function of time (by infrared spectroscopy). Nevertheless, the fact that our *DB*s from PAAs synthesized without CTA are in such good agreement gives confidence that *DB*s given by Wittenberg *et al*. are obtained without CTA.

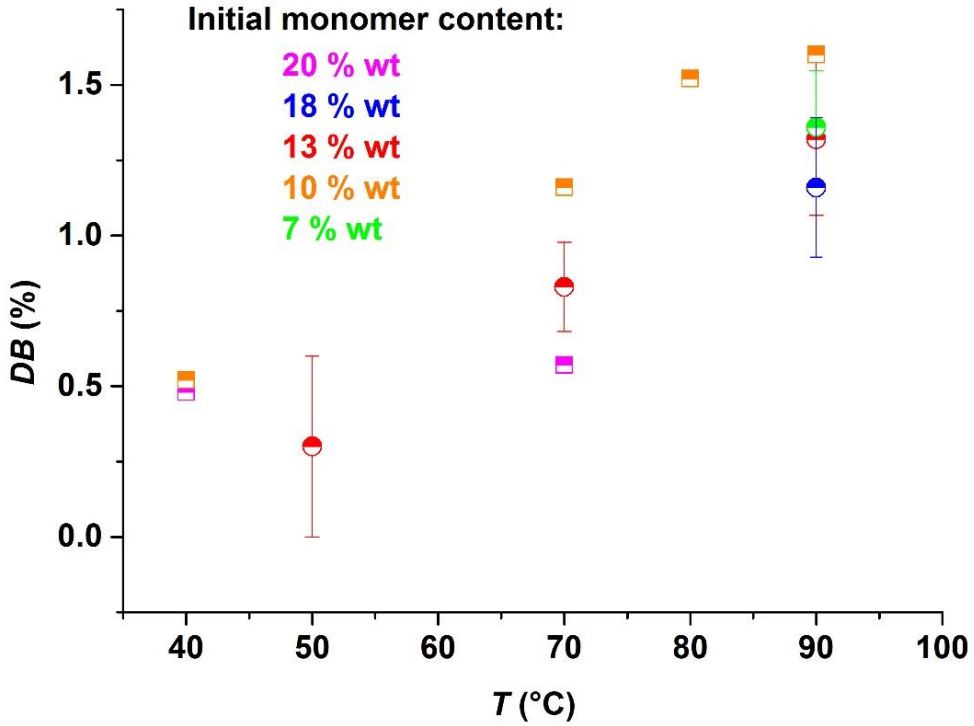

Figure 2.13: *DB* of PAAs synthesized by conventional radical polymerization in aqueous solution without CTA: comparison between the results obtained in this study (semi-filled circles) and results obtained by Wittenberg et al. (semi-filled squares) [18]. In both studies *DB* is from the whole polymer present near the end of a batch polymerization.

Turning again to Figure 2.12b, at 50 °C the results are different to 70 °C and 90 °C: the presence of the CTA does not reduce *DB* as at the other temperatures (within experimental error). At 50 °C, poly(acrylic acid) radicals might not transfer as efficiently to thioglycolic acid. The lower likelihood of exotherm effects at 50 °C, where the polymerization is slower than at 70 and 90 °C, could also be playing a role (see earlier discussion).

The present *DB*s – for PAA synthesized in water/THF (8/2 v/v) – are lower than for poly(*n*-butyl acrylate) (PnBA) synthesized in bulk by Gaborieau *et al.* between 60 and 140 °C. To be precise, these PnBAs have *DB*s of 2 to 5 % when synthesized without CTA and 0.7 to 2 % when synthesized with CTA.[13] Both these minimum values are lower than those obtained at 90 °C in this work (see Figure 2.12 b). This could possibly be explained by a lower rate of intermolecular chain transfer when polymers are in dilute solution: polymers do not overlap and consequently *DB* is reduced. Dilution by water also favors the propagation through an

entropic effect: the strong hydrogen bonding between the water and the propagating radicals creates disorder (thus lowering the pre-exponential factor of the propagation rate coefficient) [40]. The propagation rate coefficient of AA was observed both experimentally and theoretically to strongly increase with dilution by water. Dilution and H-bonding may also reduce the formation of branching points (by intramolecular transfer to polymer). As water forms H-bonding with the carboxylic group of the acrylic acid unit, the dilution by water could explain the discrepancy between this work and results from Gaborieau et *al*.. However, the most likely explanation for the lower *DB* is simply that backbiting relative to propagation is slower in AA than in *n*-butyl acrylate.

The initial monomer concentration does not seem to have any influence on *DB* (Figure 2.12a). Indeed, *DB*s at initial [AA] = 1 mol L^{-1}, 2 mol L^{-1} and 3 mol L^{-1} (which correspond to 7.3 to 18.1 wt.%) are comparable. The monomer conversion could also play a role here, as the rates of polymerization and of branch formation depend on the monomer conversion: the cumulative *DB* is expected to increase significantly when above 90 % monomer conversion[39, 41]. The syntheses at initial monomer concentrations of 1, 2 and 3 mol L^{-1} may not have led to exactly the same monomer conversion. According to Wittenberg et al.'s simulations, even a small difference of conversion above 90 °C would lead to different *DB*s. As the syntheses of PAAs at 3 different monomer concentrations were carried out using the same reaction time, this is quite possible. Another issue that could lead to these results is an exotherm. As explained previously, this issue becomes more important in viscous solutions, and could explain the results observed at different monomer concentrations (the increase in monomer content leads to more viscous solutions). Another explanation can be based on observations by Lovell *et al.* at high conversion (on *n*-butyl acrylate) [42] and Loiseau *et al.* for the RAFT polymerization of acrylic acid [1]: branches can result from intermolecular chain transfer to polymer reactions, whose rate does not depend on the initial monomer concentration as soon as the polymer concentration is above the critical overlapping concentration, *c**. Since all the syntheses of PAA without CTA have been done mostly above *c**, there is thus the possibility of intermolecular chain transfer, leading to *DB* roughly independent of initial monomer concentration. Of course backbiting is assumed to dominate in most cases, especially in PLP (even if LCB was detected for poly(alkyl acrylates) obtained by PLP [5]). It cannot be affirmed that the branching is mostly due to intermolecular transfer to polymer. Finally, as the relative standard deviation of *DB* of PAAs synthesized at 90 °C without CTA is quite large (up to 20

%), the precision of these results is relatively limited. Some variations of *DB*, lower than 20%, may exist.

Wittenberg *et al.* observed potentially different results. When the polymerization occurs at 40 °C and 70 °C, a potential decrease in *DB* is observed when the initial monomer concentration is increased from 10 to 20 wt.% [39]. This is in line with expectation: as monomer concentration is increased, the frequency of propagation (a bimolecular process) is increased whereas the frequency of backbiting (a unimolecular process) remains unchanged, and thus the fraction of branches decreases. This has been observed in most other works, and thus doubt is cast on the present results for *DB* as a function of initial [AA]. However, as the standard deviation is not given by Wittenberg *at al.*, it is impossible to know whether or not their observed differences are significant. Moreover, it is not proven that their ^{13}C NMR analyses are quantitative (it was not shown that the repetition delay was greater than $5T_1$). The presence of a non-soluble fraction, whose branching would not be detected and quantified by solution-state NMR, could also play a role.

The present results were compared with *DB* of a PAA provided by Sigma Aldrich. This PAA has an expected number average molar mass M_n = 240 000 g mol^{-1} (it is however to be noted that determination of PAA molar mass suffers from a poor accuracy [6, 17]). A *DB* was measured in this work as 1.13 ± 0.07 %. This value is in the same range as *DB*s of PAAs synthesized by conventional radical polymerization without CTA, which suggests that it may have been synthesized using similar experimental conditions.

2.3.3 Backbiting rate coefficients

Assuming, reasonably, that the loss of MCRs by transfer (in the absence of transfer agent), β-scission and termination by disproportionation is negligible, then every backbiting event leads to a branching point, and thus the fraction of branching points is given by the ratio of the rate of backbiting to the rate of propagation. Moreover, as the consumption of monomer by a MCR is assumed to be negligible, *DB* can be expressed using Eq. (2.9).

$$DB\ (\%) = \frac{100 \times k_{bb}}{k_p[M]} \tag{2.9}$$

This equation is valid for an instantaneous *DB*, obtained at low monomer conversion (when branching due to intermolecular transfer is supposed to be negligible). The possibility to extrapolate this equation at high monomer conversion was tested. However, Figure 2.14 shows that there is no proportionality between *DB* and $1/[M]_0$.

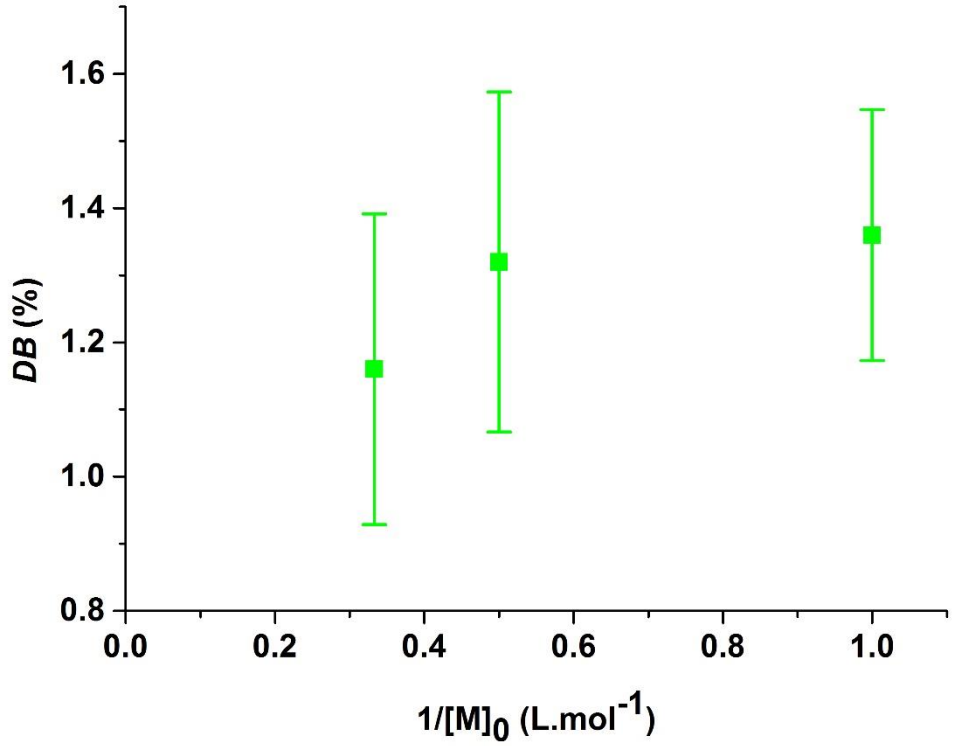

Figure 2.14: Average *DB* as a function of the inverse of the initial monomer concentration, where all experiments were at 90 °C and without CTA.

The rate of propagation is not constant during a polymerization but Nikitin et al. were able to link the *DB* to the ratio of the backbiting to the propagation rate coefficients as in Eq. (2.10), taking into account the presence of LCB:

$$DB\ (\%) = \frac{k_{\mathrm{bb}}\ 100\ \left(\frac{\ln([\mathrm{M}]_0)}{([\mathrm{M}]_\mathrm{e})}\right)}{k_\mathrm{p}\ ([\mathrm{M}]_0 - ([\mathrm{M}]_\mathrm{e})} \qquad (2.10)$$

Where $[M]_0$ is the initial monomer concentration and $[M]_e$ is the final monomer concentration (values are given in table A.2.2). Thus from a measurement of *DB* one can very easily obtain k_{bb}/k_p, where this k_p refers to chain-end (secondary-radical) propagation. Wittenberg *et al.* [39]

were able to use an even simpler expression since they used low-conversion conditions in their particular experiments to determine k_{bb}/k_p from *DB*. In the present case, our results are from batch polymerization in which conversion traversed from 0 % to nearly 100 % and Eq. (2.6) is thus used instead. If one uses *DB* values of similar precision and accuracy, then Wittenberg et al.'s expression should lead to more accurate values since it is not impacted by the uncertainty on the determination of the conversion.

To obtain individual values of k_{bb}, the value of k_p was needed. This was calculated using an expression of k_p depending on the weight fraction of acrylic acid given in [39] as well as in table 1.2 in Chapter 1, which is re-estimated from an earlier PLP-SEC study on non-ionized AA [43]. Values of k_{bb} and k_p are in table A.2.4.

Figure 2.15 is an Arrhenius plot for k_{bb} obtained in both the presence and absence of CTA in water/THF (8/2 v/v) compared with the Arrhenius equation tabulated by Wittenberg *et al.* [39] and Barth *et al.*[44]. Wittenberg *et al.*'s equation was obtained by combining their k_{bb} from a handful of low-conversion *DB* (from polymerization in pure water) with a larger data set from Barth *et al.* [44], who used single pulse - pulsed laser polymerization - electron paramagnetic resonance (SP-PLP-EPR) spectroscopy experiments to determine k_{bb}, also at low-conversion conditions. These experiments involve monitoring of EPR signals on a microsecond timescale over which the conversion of chain-end radicals into MCRs can be observed. Eqs. (2.11), (2.12) and (A.2.6) represent, respectively, the Arrhenius fits for k_{bb} calculated from *DB*s of this study in both the absence and presence of CTA; and from Wittenberg *et al.* at low conversion [44]. The linear fits parameters are presented in table A.2.4. The linear fit for the PAA obtained in this work in the absence of CTA gave a Pearson's R^2 coefficient of 0.56 only with the point for the polymerization at 90 °C and 1 M monomer concentration looking like an outlier. This point was removed and the Pearson's R^2 coefficient increased to 0.996. The parameters for both fits are given in Table A.2.4, but only the fit excluding 1 M monomer concentration is given on figure 15. The *RSD* of ln k_{bb} was calculated based on the *RSD* of *DB*, according to Eq. (A.2.7), which assumes that the error on k_{bb} only depends on the error on *DB*. The error is not visible on the graph as it is negligible (between 4×10^{-7} and 4×10^{-4}). This high precision is distinct from the accuracy of these measurements, which is likely lower than in previous works due to the high monomer conversion.

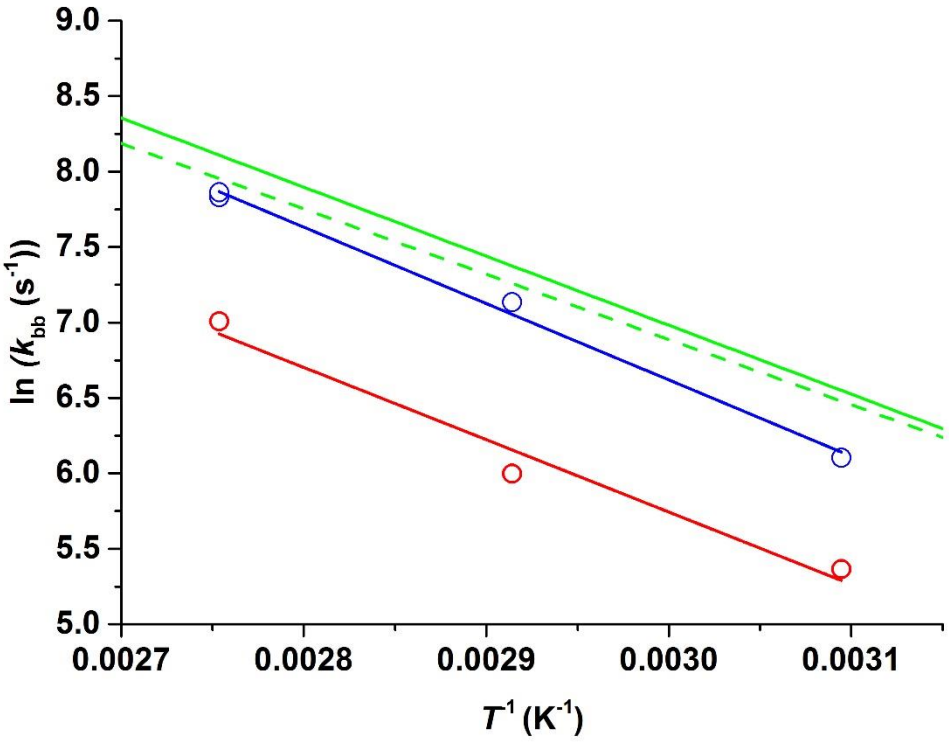

Figure 2.15: Arrhenius plot of k_{bb} in absence of CTA (blue line and points), presence of CTA (red line and points) and from Wittenberg et al. [18] (full green line) and Barth et al [54] (dashed green line).

$$k_{bb}\,(s^{-1}) = 2.99 \times 10^{9}\,(s^{-1})\,e^{-\frac{5066}{T/K}} \tag{2.11}$$

$$k_{bb}\,(s^{-1}) = 5.20 \times 10^{8}(s^{-1})\;e^{-\frac{4777}{T/K}} \tag{2.12}$$

In Figure 2.15 the (apparent) activation energy of k_{bb} is similar in the presence of CTA. The pre-exponential factor is, however, lower in the presence of CTA. As previously explained, the presence of CTA might reduce the number of backbiting steps as the macroradical polymerizes for a shorter time [14]. Another hypothesis is the invalidity of Eq. (2.10) in the presence of CTA. Given that a patching effect is possible some MCRs could not lead to a branched chain, thus *DB* would not be directly related to k_{bb}. In effect this is a breakdown of the assumption that all MCRs undergo propagation rather than any other reaction (see above).

The k_{bb} values observed in this study in the absence of CTA are a bit more than 170 % lower than the ones determined using Eq. A.2.6) (obtained by Wittenberg *et al.*). Details are given in table A.2.4. Several explanations are possible. First, the observed differences could just be due

to different systematic error (for example due to incomplete dissolution in some cases). Second, the high conversion in this work leads to a lower accuracy of the determined k_{bb} values for at least three potential reasons: (i) the uncertainty on the value of the monomer conversion, (ii) the non-validity of the assumption that k_p is constant, (iii) intermolecular chain transfer to polymer may not be negligible, (iv) potential occurrence of β-scission whose resulting macromonomer would be consummed. In the case of Wittenberg *et al.*, the conditions to obtain quantitative *DB* values were not checked and the *RSD* of *DB* was not provided at all.

2.3.4 Heterogeneity of branching

While the average *DB* has been determined for PAAs obtained in a number of different polymerization conditions in this work and in the literature, the variation of *DB* from macromolecule to macromolecule within a given sample has not been examined. CE-CC provides important information related to the heterogeneity of branching. This heterogeneity is not just due to different *DB*s within a sample but also different positions of the branching points or a distribution of molar masses of the branches. As polymers are separated according to their topology and not according to their size in CE-CC, the dispersity of the distribution of electrophoretic mobilities is related to the heterogeneity of branching [24]. It is in contrast with SEC with which polymers are separated according to their hydrodynamic volume [18] (which depends on both the molar mass and the branching). Multiple-detection SEC allows measurement of local weight- and local number-average molar mass as well as their ratio $Đ(V_h)$. Values of the local dispersity $Đ(V_h)$ (of the local molar mass distribution) primarily inform the accuracy of the determined molar mass but also provide indirect information on the heterogeneity of branching. In the case of poly(alkyl acrylates), the most heterogeneous samples (in terms of branching) were shown to be obtained for low *DB*s [5, 11]. Multiple-detection SEC is however not only an indirect characterization method for the branching, but also a tedious method. Free-solution CE allows much higher throughput and simple characterization of the branching [2, 31]. The dispersity of the electrophoretic mobility distributions was calculated in this work as a standard deviation [45], and as a ratio of four moments of the mobility distribution [24]. The dispersities of the distributions of electrophoretic mobilities $D(W(\mu),1,0)$, $D(W(\mu),2,0)$, $D(W(\mu),3,0)$ and D_σ were calculated according to Eq. (A.2.8) to (A-2-11) [24]. $D(W(\mu),1,0)$ is calculated as the ratio of the first and zeroth order moments divided by the ratio of the zeroth and -1st order moments. It is in analogy

with M_w/M_n where M_w is the weight-average molar mass. $D(W(\mu),2,0)$ is calculated as the ratio of the second and first order moments divided by the ratio of the first and zeroth order moments. It is in analogy with M_z/M_w where M_z is the z-average molar mass. $D(W(\mu),3,0)$ is calculated as the ratio of the third and second order moments divided by the ratio of the second and first order moments. The last dispersity D_σ is calculated as a standard deviation of the weight distribution of electrophoretic mobilities. The weight-average electrophoretic mobility μ_W is the equivalent of the weight-average molar mass in term of electrophoretic mobility. μ_W is determined as the ratio of the first and zeroth order moments of the mobility distributions and is given by Eq. (A.11) [24]. The values of the different dispersities and of the μ_W of the different PNaAs are given in Table A.2.7.

The electrophoretic mobility distributions of branched PNaA exhibit two peaks (see Figure 2.16) that are not resolved. This is not the case for the linear PNaA, whose electropherogram exhibits only one peak. The bimodal shape of branched PNaA was already observed in previous work [2, 24]. The relation between the polymer structure and it electrophoretic mobility can be undertaken using a "slope plot"[46]. This method was used to identify both peaks and it is detailed in Chapter 3. The dispersities of electrophoretic mobility distributions were calculated on the whole distributions of electrophoretic mobilities in order to assess the heterogeneity due to branching in each individual PNaA sample. As a DP_n around 10 is expected for the PAAs synthesized at 50 °C, 70 °C and 90 °C with CTA [26], their separation and analysis by capillary electrophoresis are not expected to be in the critical conditions and are thus not considered in this study of the heterogeneity of branching (the distributions are broader in the case of CTA-containing polymers than non-CTA containing polymer, as observed in Figures A.2.9 and A.2.10 due to the combined influences of molar mass and branching).

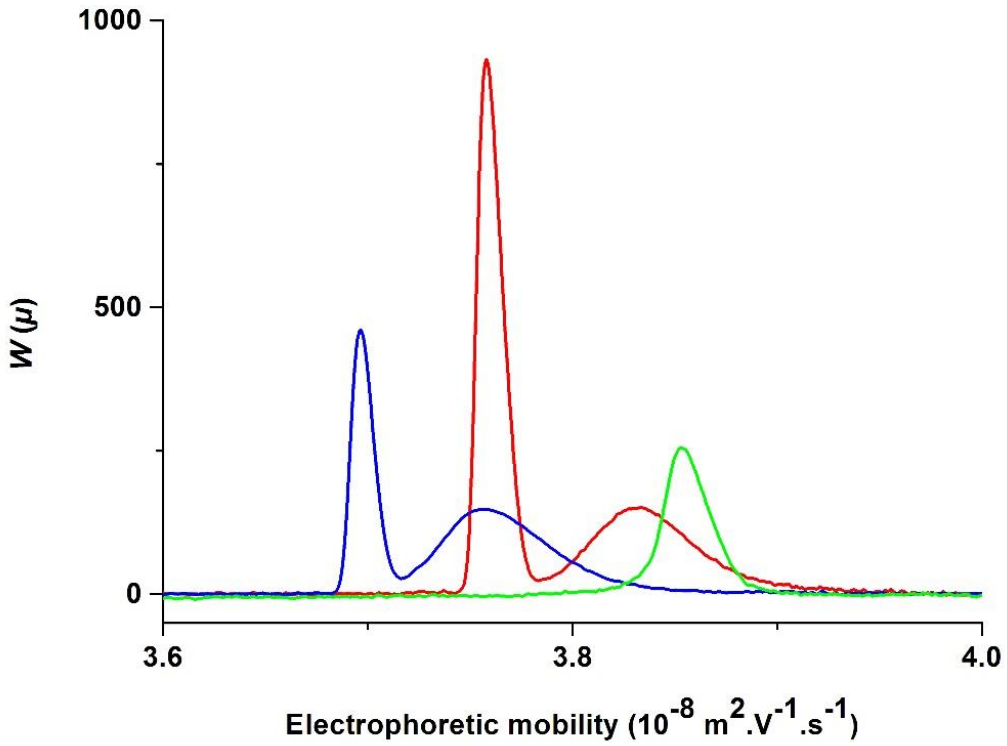

Figure 2.16: Electropherograms of PAAs synthesized without CTA at 70 °C (red line,) 90 °C (blue line) and a linear PNaA (green line). All samples are analyzed as PNaAs at high pH.

Figure 2.17 shows that neither the temperature nor the initial monomer concentration influences significantly the heterogeneity of branching of the 3 PNaAs obtained by conventional radical polymerization at different temperatures and monomer concentrations. When the PNaA is synthesized without CTA, high enough *DB*s may be obtained for the branching to be relatively homogeneous which would explain the similar heterogeneity of branching with the temperature and the initial monomer concentration.

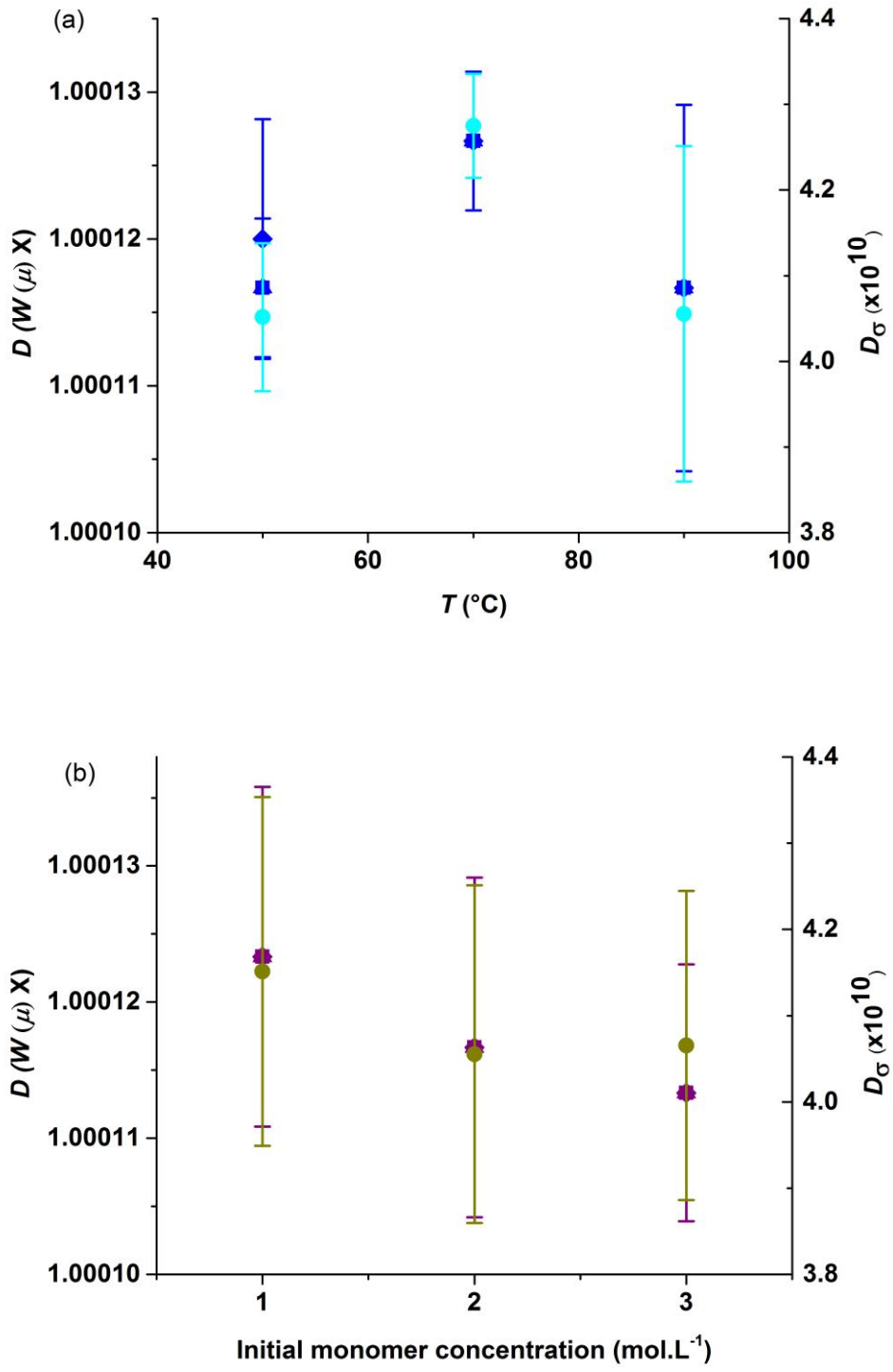

Figure 2.17: Dispersities $D(W(\mu), x, 0)$ of electrophoretic mobility distributions of PNaAs as a function of (a) synthesis temperature (all PAAs synthesized without CTA at $[M]_0$ = 2 mol L^{-1}), (b) initial monomer concentration (all PAAs synthesized at 90 °C). x = 1: ■; x = 2: ▲; x = 3: ◆; D_σ: ●.

The evolution of the dispersity of electrophoretic mobility distributions with *DB* is shown on Figure 2.18. The dispersity of electrophoretic mobility distributions of the PNaAs produced by conventional radical polymerization is compared with those of the linear PNaA and of a hyperbranched PNaA [24] produced by nitroxide-mediated polymerization in the presence of an alkoxyamine inimer, leading to a *DB* estimated at 3.9 ± 0.1 %. The synthesis of the hyperbranched PNaA is described elsewhere in detail [2]. The linear PNaA has the lowest heterogeneity of branching as all chains are unbranched (the dispersity should be equal to unity, the lowest value possible, as no heterogeneity from branching is expected). The heterogeneity of branching of the hyperbranched PNaA (produced by controlled polymerization and with a *DB* of 3.9 ± 0.1 %) is higher than the ones observed for the PNaAs produced by conventional radical polymerization. When PNaAs are produced by conventional radical polymerization, branching results only from inter and intramolecular (chain) transfer to polymer. Only LCB and SCB are expected. Branching initiated by the inimer is also expected in the case of the hyperbranched PNaA, which may explain the higher heterogeneity. A higher $Đ(V_h)$ was also observed for poly(alkyl acrylates) produced by controlled radical polymerization than by conventional radical polymerization [23]. The dispersities determined in this work should relate to the local dispersities $Đ(V_h)$ which could also be determined by multiple-detection SEC but have not been reported in the literature for PAA or PNaA. The lowest dispersity of the electrophoretic mobility distribution should correspond to the lowest $Đ(V_h)$ and thus the most accurate determined molar mass. The higher dispersities observed for PNaAs produced by radical polymerization can be explained by branching and is one likely cause of the low accuracy of the molar mass of PNaA (or PAA, or equivalent) determined by SEC [6]. Figure 19 shows the evolution of the dispersity with μ_w, and confirms that the more a polyelectrolyte is branched, the lower the mobility is. The same phenomenon as in Figure 2.19 is observed. The hyperbranched PNaA produced by controlled radical polymerization has the highest dispersity of the electrophoretic mobility distributions and, as the highest *DB*, the lowest mobility and the linear PNaA which has no branches has the highest mobility (as expected).

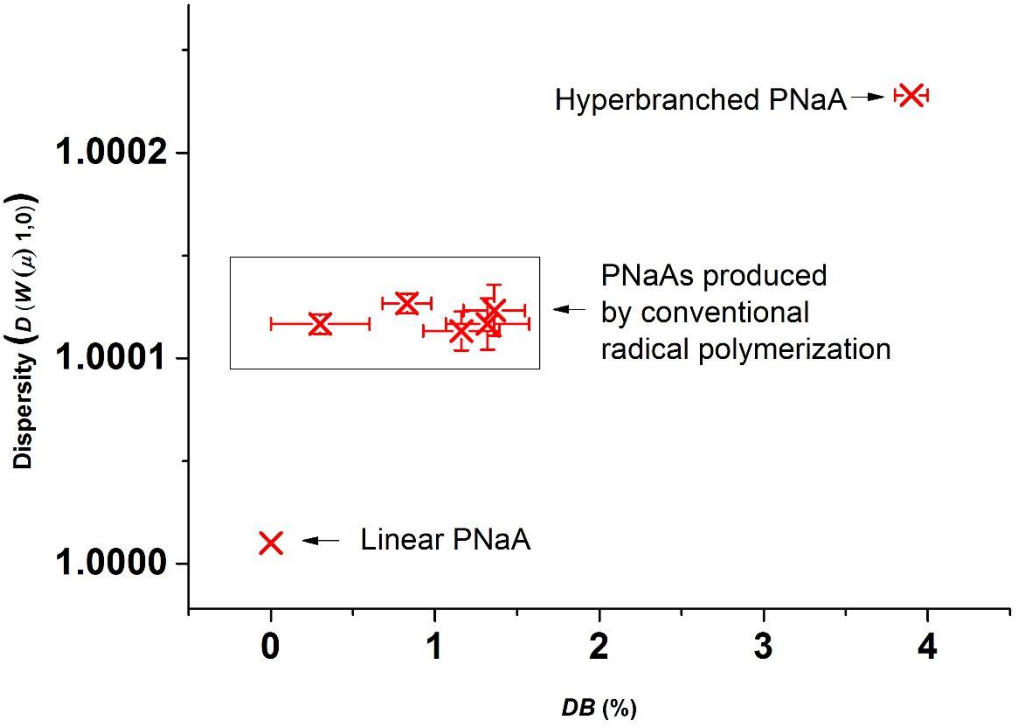

Figure 2.18: Dispersity $D(W(\mu),1,0)$ of the electrophoretic mobility distributions of PNaAs as a function of their average *DB*.

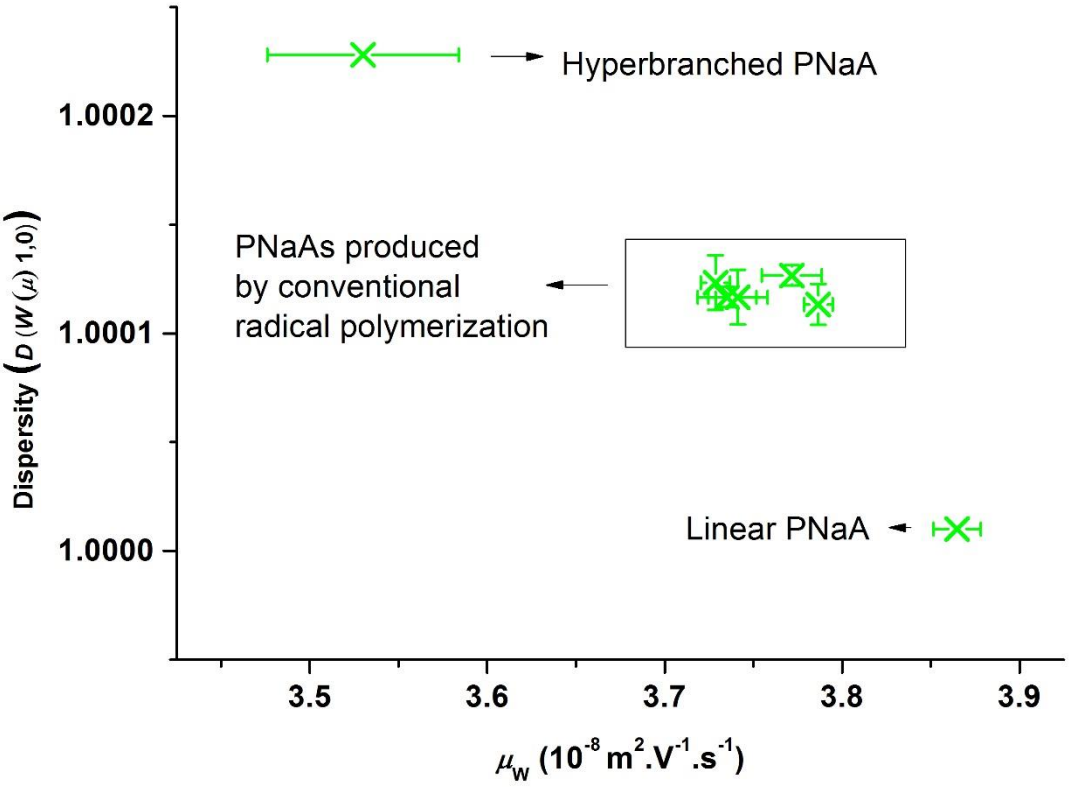

Figure 2.19: Dispersity $D(W(\mu),1,0)$ of the electrophoretic mobility distributions of PNaAs as a function of the weight-average electrophoretic mobility μ_W.

2.4 Conclusion

DB was measured with quantitative ^{13}C solution-state NMR spectroscopy and the heterogeneity of branching was measured by CE-CC. These were both done for PAA synthesized in both the presence and absence of thioglycolic acid at various temperatures and initial monomer concentrations. The presence of thiol decreases *DB*, the so-called "patching effect" is observed for PAA, exactly as it has been for other acrylic monomers. However, the reduction in *DB* may also be due to a decrease of the number of backbiting steps in comparison to propagation steps. *DB* was observed to increase with the temperature. This is due to an acceleration of the reactions which lead to the formation of branching points (transfer to polymer). When PAA is synthesized at 90 °C without a CTA, the initial monomer concentration (1, 2 and 3 mol L^{-1}) does not appear to influence the degree or the heterogeneity of branching, although this observation for *DB* is not commensurate with other observations, both in this work and in the literature. This might be due to unintended temperature increase

over the polymerization process, slight differences in monomer conversion, or the limited precision of the analyses. PAA produced by conventional radical polymerization is not only branched, but different macromolecules within a sample are branched differently. The heterogeneity of branching observed for a linear PNaA is negligible, as it should, and lower than the one of the PNaAs synthesized by conventional radical polymerization, which is in turn lower than the one of the hyperbranched PNaA (synthesized by nitroxide-mediated polymerization). The heterogeneity increases with the diversity of branching structures. Moreover, it is confirmed that the electrophoretic mobility decreases with the increase of branching. This work provides relevant information for a systematic variation of reaction conditions that can be used for future kinetic and mechanistic studies, which will help to optimize conditions for poly(acrylic acid) synthesis in numerous applications.

2.5 References

[1] J. Loiseau, N. Doerr, J.M. Suau, J.B. Egraz, M.F. Llauro, C. Ladaviere, Synthesis and characterization of poly(acrylic acid) produced by RAFT polymerization. Application as a very efficient dispersant of CaCO3, kaolin, and TiO2, Macromolecules, 36 (2003) 3066-3077.

[2] A.R. Maniego, D. Ang, Y. Guillaneuf, C. Lefay, D. Gigmes, J.R. Aldrich-Wright, M. Gaborieau, P. Castignolles, Separation of poly(acrylic acid) salts according to topology using capillary electrophoresis in the critical conditions, Analytical and Bioanalytical Chemistry, 405 (2013) 9009-9020.

[3] L. Couvreur, C. Lefay, J. Belleney, B. Charleux, O. Guerret, S. Magnet, First nitroxide-mediated controlled free-radical polymerization of acrylic acid, Macromolecules, 36 (2003) 8260-8267.

[4] C. Barner-Kowollik, S. Beuermann, M. Buback, P. Castignolles, B. Charleux, M.L. Coote, R.A. Hutchinson, T. Junkers, I. Lacik, G.T. Russell, M. Stach, A.M. van Herk, Critically evaluated rate coefficients in radical polymerization - 7. Secondary-radical propagation rate coefficients for methyl acrylate in the bulk, Polymer Chemistry, 5 (2013) 204-212.

[5] P. Castignolles, Transfer to polymer and long-chain branching in PLP-SEC of acrylates, Macromolecular Rapid Communications, 30 (2009) 1995-2001.

[6] I. Lacík, M. Stach, P. Kasák, V. Semak, L. Uhelská, A. Chovancová, G. Reinhold, P. Kilz, G. Delaittre, B. Charleux, I. Chaduc, F. D'Agosto, M. Lansalot, M. Gaborieau, P. Castignolles, R.G. Gilbert, Z. Szablan, C. Barner-Kowollik, P. Hesse, M. Buback, SEC analysis of

poly(acrylic acid) and poly(methacrylic acid), Macromolecular Chemistry and Physics, 216 (2015) 23-37.
[7] T. Junkers, C. Barner-Kowollik, The role of mid-chain radicals in acrylate free radical polymerization: Branching and scission, Journal of Polymer Science Part A - Polymer Chemistry, 46 (2008) 7585-7605.
[8] A.N. Nikitin, P. Castignolles, B. Charleux, J.P. Vairon, Determination of propagation rate coefficient of acrylates by pulsed-laser polymerization in the presence of intramolecular chain transfer to polymer, Macromolecular Rapid Communications, 24 (2003) 778-782.
[9] M. Buback, P. Hesse, I. Lacik, Propagation rate coefficient and fraction of mid-chain radicals for acrylic acid polymerization in aqueous solution, Macromolecular Rapid Communications, 28 (2007) 2049-2054.
[10] K.B. Kockler, A.P. Haehnel, T. Junkers, C. Barner-Kowollik, Determining Free-Radical Propagation Rate Coefficients with High-Frequency Lasers: Current Status and Future Perspectives, Macromolecular Rapid Communications, 37 (2016) 123-134.
[11] P. Castignolles, R. Graf, M. Parkinson, M. Wilhelm, M. Gaborieau, Detection and quantification of branching in polyacrylates by size-exclusion chromatography (SEC) and melt-state 13C NMR spectroscopy, Polymer, 50 (2009) 2373-2383.
[12] T. Caykara, O. Guven, Effect of preparation methods on thermal properties of poly(acrylic acid) silica composites, Journal of Applied Polymer Science, 70 (1998) 891-895.
[13] M. Gaborieau, S.P.S. Koo, P. Castignolles, T. Junkers, C. Barner-Kowollik, Reducing the degree of branching in polyacrylates via midchain radical patching: A quantitative melt-state NMR study, Macromolecules, 43 (2010) 5492-5495.
[14] N. Ballard, J.C. de la Cal, J.M. Asua, The role of chain transfer agent in reducing branching content in radical polymerization of acrylates, Macromolecules, 48 (2015) 987-993.
[15] M. Gaborieau, T.J. Causon, Y. Guillaneuf, E.F. Hilder, P. Castignolles, Molecular weight and tacticty of oligoacrylates by capillary electrophoresis - mass spectrometry, Australian Journal of Chemistry, 63 (2010) 1219-1226.
[16] C.M. Guttman, K.M. Flynn, W.E. Wallace, A.J. Kearsley, Quantitative mass spectrometry and polydisperse materials: Creation of an absolute molecular mass distribution polymer standard, Macromolecules, 42 (2009) 1695-1702.
[17] D. Berek, Size exclusion chromatography - A blessing and a curse of science and technology of synthetic polymers, Journal of Separation Science, 33 (2010) 315-335.
[18] Z. Grubisic, P. Rempp, H. Benoit, A universal calibration for gel permeation chromatography, Journal of Polymer Science Part B Polymer Letters, 5 (1967) 753-759.

[19] Z. Grubisic, P. Rempp, H. Benoit, A universal calibration for gel permeation chromatography (Reprinted from Polymer Letters, vol 5, pg 753-759, 1967), Journal of Polymer Science Part B Polymer Physics, 34 (1996) 1707-1713.
[20] M. Gaborieau, P. Castignolles, Size-exclusion chromatography (SEC) of branched polymers and polysaccharides, Analytical and Bioanalytical Chemistry, 399 (2011) 1413-1423.
[21] L.K. Kostanski, D.M. Keller, A.E. Hamielec, Size-exclusion chromatography - a review of calibration methodologies, Journal of Biochemical and Biophysical Methods, 58 (2004) 159-186.
[22] M. Gaborieau, R.G. Gilbert, A. Gray-Weale, J.M. Hernandez, P. Castignolles, Theory of multiple detection size exclusion chromatography of complex branched polymers, Macromolecular Theory and Simulations, 16 (2007) 13-28.
[23] M. Gaborieau, J. Nicolas, M. Save, B. Charleux, J.P. Vairon, R.G. Gilbert, P. Castignolles, Separation of complex branched polymers by size-exclusion chromatography probed with multiple detection, Journal of Chromatography A, 1190 (2008) 215-223.
[24] J.J. Thevarajah, A.T. Sutton, A.R. Maniego, E.G. Whitty, S. Harrisson, H. Cottet, P. Castignolles, M. Gaborieau, Quantifying the heterogeneity of chemical structures in complex charged polymers through the dispersity of their distributions of electrophoretic mobilities or of compositions, Analytical Chemistry, 88 (2016) 1674-1681.
[25] A.B. Pangborn, M.A. Giardello, R.H. Grubbs, R.K. Rosen, F.J. Timmers, Safe and convenient procedure for solvent purification, Organometallics, 15 (1996) 1518-1520.
[26] C. Loubat, B. Boutevin, Telomerization of acrylic acid with thioglycolic acid - Effect of the solvent on the C-T value, Polymer Bulletin, 44 (2000) 569-576.
[27] M.F. Llauro, J. Loiseau, F. Boisson, F. Delolme, C. Ladaviere, J. Claverie, Unexpected end-groups of poly(acrylic acid) prepared by RAFT polymerization, Journal of Polymer Science Part a-Polymer Chemistry, 42 (2004) 5439-5462.
[28] H.E. Gottlieb, V. Kotlyar, A. Nudelman, NMR chemical shifts of common laboratory solvents as trace impurities, Journal of Organic Chemistry, 62 (1997) 7512-7515.
[29] T.D.W. Claridge, High-resolution NMR techniques in organic chemistry, 2nd ed., Elsevier Science, Amsterdam, 2009.
[30] K. Klimke, M. Parkinson, C. Piel, W. Kaminsky, H.W. Spiess, M. Wilhelm, Optimisation and application of polyolefin branch quantification by melt-state 13C NMR spectroscopy, Macromolecular Chemistry and Physics, 207 (2006) 382-395.

[31] J.J. Thevarajah, M. Gaborieau, P. Castignolles, Separation and characterization of synthetic polyelectrolytes and polysaccharides with capillary electrophoresis, Advances in Chemistry, 2014 (2014) Article ID 798503.
[32] J.A. Leenheer, C.E. Rostad, P.M. Gates, E.T. Furlong, I. Ferrer, Molecular resolution and fragmentation of fulvic acid by electrospray ionization/multistage tandem mass spectrometry, Analytical Chemistry, 73 (2001) 1461-1471.
[33] M. Strohalm, "mMass - Open Source Mass Spectrometry Tool", in.
[34] T. Junkers, S.P.S. Koo, T.P. Davis, M.H. Stenzel, C. Barner-Kowollik, Mapping poly(butyl acrylate) product distributions by mass spectrometry in a wide temperature range: Suppression of midchain radical side reactions, Macromolecules, 40 (2007) 8906-8912.
[35] B.A. Miller-Chou, J.L. Koenig, A review of polymer dissolution, Progress in Polymer Science, 28 (2003) 1223-1270.
[36] J.J. Thevarajah, J.C. Bulanadi, M. Wagner, M. Gaborieau, P. Castignolles, Towards a less biased dissolution of chitosan, Analytica Chimica Acta, 935 (2016) 258-268.
[37] S. Schmitz, A.C. Dona, P. Castignolles, R.G. Gilbert, M. Gaborieau, Assessment of the extent of starch dissolution in dimethyl sulfoxide by 1H NMR spectroscopy, Macromolecular Bioscience, 9 (2009) 506-514.
[38] N. Ballard, J. Ignacio Santos, J.M. Asua, Reevaluation of the formation and reactivity of midchain radicals in nitroxide-mediated polymerization of acrylic monomers, Macromolecules, 48 (2015) 2909-2915.
[39] N.F.G. Wittenberg, C. Preusser, H. Kattner, M. Stach, I. Lacík, R.A. Hutchinson, M. Buback, Modeling acrylic acid radical polymerization in aqueous solution, Macromolecular Reaction Engineering, 10 (2016) 95-107.
[40] I. Degirmenci, T.F. Ozaltin, O. Karahan, V. Van Speybroeck, M. Waroquier, V. Aviyente, Origins of the solvent effect on the propagation kinetics of acrylic acid and methacrylic acid, Journal of Polymer Science Part A -Polymer Chemistry, 51 (2013) 2024-2034.
[41] A.N. Nikitin, R.A. Hutchinson, G.A. Kalfas, J.R. Richards, C. Bruni, The Effect of Intramolecular Transfer to Polymer on Stationary Free-Radical Polymerization of Alkyl Acrylates, 3-Consideration of Solution Polymerization up to High Conversions, Macromolecular Theory and Simulations, 18 (2009) 247-258.
[42] N.M. Ahmad, F. Heatley, P.A. Lovell, Chain transfer to polymer in free-radical solution polymerization of n-butyl acrylate studied by NMR spectroscopy, Macromolecules, 31 (1998) 2822-2827.

[43] I. Lacik, S. Beuermann, M. Buback, Aqueous phase size-exclusion-chromatography used for PLP-SEC studies into free-radical propagation rate of acrylic acid in aqueous solution, Macromolecules, 34 (2001) 6224-6228.
[44] J. Barth, W. Meiser, M. Buback, SP-PLP-EPR study into termination and transfer kinetics of non-ionized acrylic acid polymerized in aqueous solution, Macromolecules, 45 (2012) 1339-1345.
[45] J. Chamieh, M. Martin, H. Cottet, Quantitative analysis in capillary electrophoresis: Transformation of raw electropherograms into continuous distributions, Analytical Chemistry, 87 (2015) 1050-1057.
[46] A. Ibrahim, S.A. Allison, H. Cottet, Extracting Information from the Ionic Strength Dependence of Electrophoretic Mobility by Use of the Slope Plot, Analytical Chemistry, 84 (2012) 9422-9430.

Chapter 3

Further characterization of the branching in hydrophilic poly(acrylates) using capillary electrophoresis

3.1 Introduction

As branching strongly influences the properties of the polymer – short branches influence physical properties such as density, melting point and glass transition temperature, while long branches influence rheological properties [1] – it is important to characterize branching and be able to separate PAAs and PNaAs according to their branching structure. As mentioned previously, two different methods have been used for this separation over recent decades, namely size exclusion chromatography (SEC) and free solution capillary electrophoresis in the critical conditions (CE-CC) [2-4]. In the case of hydrophobic poly(acrylates), errors of up to 100 % were reported in the determined molar mass using multiple detection SEC [5, 6] due to the presence of long chain branching (LCB). Aqueous and organic SEC analyses of PAA lead to different apparent molar mass due to the presence of LCB[7], demonstrating the limitations of this method. Moreover, SEC allows the local number- and weight-average molar mass to be determined as well as the local dispersity of molar mass [$Đ(V_h)$], which assesses the accuracy of the determined molar masss [8] but provides only an indirect assessment of the heterogeneity of the macromolecular structure due to branching.

CE-CC has been applied to separate PNaAs according to their branching topology with limited influence of molar mass [2, 4, 9]. In previous analyses of PNaA by CE-CC it has been observed that the electrophoretic mobility, μ_{ep}, of PNaA decreases whilst *DB* increases [2, 4], which demonstrated the potential of CE-CC to separate water-soluble polyelectrolytes according to their branching. Moreover, the dispersity of electrophoretic mobility, which is directly related to the heterogeneity of branching was determined for different PNaAs synthesized by conventional and controlled radical polymerization.

When branched PNaAs were characterized using CE-CC with sodium borate as the background electrolyte (BGE), two peaks were observed in the electropherogram with incomplete resolution, while the electropherogram of linear PNaA was unimodal [2, 4, 9]. These peaks were not formally identified but were thought to correspond to different branching populations. It is known that μ_{ep} varies with ionic strength. Generally, a decrease of μ_{ep} is expected when the ionic strength increases. However, due to a higher Joule heating effect, increasing the ionic strength also leads to a rise of temperature inside the capillary [10] which leads to a lower viscosity and thus an increase of μ_{ep}, as observed in the case of proteins [11]. Sometimes, the later effect may cancel or even overwhelm the mentioned decrease of μ_{ep}. Some studies of the effect of ionic strength on the μ_{ep} have been carried out for polyelectrolytes [12-

14]. In 2012, Ibrahim *et al*. developed a simple model to study the phenomenological dependence of μ_{ep} on the ionic strength called "slope plot" [15]. This has allowed further understanding of the relationship between μ_{ep} and structure of the analyte, taking into account the logarithmic dependence of μ_{ep} with the ionic strength [16]. This model was applied to small ions, polyelectrolytes, nanoparticles [15], and proteins [17]. Ionic strength is expected to play a role in the selectivity of separation of electrolyte, as has been observed in the case of carbohydrates [18]. The addition of metal is also expected to affect the selectivity of separation in the case of PNaA. The complexation between metals and PNaA without precipitation may lead to different structures according to the branching topology of PNaA [19]. Consequently, the separation of the two branching populations (corresponding to the two unresolved peaks observed on the electropherograms of branched PNaA) is expected to be improved by changing the buffer concentration or adding metal to the buffer. Identifying both peaks, testing the effects of both buffer concentration and addition of metal on the separation of PNaA by CE is the main focus of this current study. Moreover, in order to fully determine the optimal condition for PNaA separation, the potential adsorption of PNaA on the capillary [20] was tested in different BGE concentrations using a pressure mobilization experiment. This adsorption could be due to incomplete dissolution of the polyelectrolyte, as already observed for chitosan [20] and biases CE results by influencing the CE separation. Pressure mobilization involves gathering a solute in a capillary by applying pressure. It has been proven that CE equipment can be used to carry out this experiment and to detect the solute [21-23]. Adsorption of species is detected by the presence of a broad peak beside a Gaussian-shaped peak in the pressure mobilization elugram [24].

Once the selectivity of separation in PNaA by CE-CC was improved and understood (the sharp and broad peaks identified and completely resolved), it became possible to characterize the two peaks separately. Previously, CE-CC was used to separate polyelectrolytes according to their microstructure and has allowed characterization of the heterogeneity of branching [4, 9]. By heterogeneity, we mean that different macromolecules within the same sample can differ by their branching, namely number of branches per macromolecule, but also position of the respective branching points along the polymer chain, distribution of molar masses of the branches etc. CE-CC was used in this work to determine the dispersity of the μ_{ep} distributions. As different branching topologies lead to different electrophoretic mobilities in the case of PNaA, the obtained values of dispersity are representative of the heterogeneity of branching [4, 9]. Nevertheless, with the improvement in separation of branching populations, the

dispersity of μ_{ep} distribution can be studied separately for different chain branching populations in a single sample of PNaA.

3.2 Materials and methods

3.2.1 Materials

Milli-Q water was used. Boric acid (≥ 98 %) was purchased from BDH AnalaR, Merck Pty Limited. Sodium hydroxide pellets, dimethyl sulfoxide (DMSO) and silver nitrate (≥ 99 %) were provided by Sigma Aldrich. Ammonium acetate (98%) was obtained from Sharlau. *N*-cyclohexyl-3-aminopropanesulfonic acid (CAPS) (≥ 98%) was provided by Sigma Aldrich. The linear, hyperbranched and 3-arm star PNaAs were obtained from PSS (Mainz, Germany), as described in [2]. Acrylic acid (AA, 99%) and 4,4'-azobis(4-cyanovaleric acid) (75%+) were supplied by Sigma-Aldrich.

3.2.2 Synthetic methods

Linear, 3-arm star and hyperbranched PAA were synthesized as described in [2]. The synthesis of PAA by conventional radical polymerization is described in [4].

3.2.3 Free-solution Capillary electrophoresis

The instrument and experimental conditions were as in [2]. The PNaAs were analyzed with sodium borate buffer at pH = 9.2 and at different buffer concentrations ([NB25], [NB50], [NB75], [NB110], [NB150], [NB200], [NB250], [NB300], X mmol L^{-1} = [NBX]). Sodium borate buffer was prepared as described in [2] in the absence of silver. In the presence of silver, the buffer was prepared from a solution of Milli-Q water and 1 M NaOH with silver nitrate at 1×10^{-6} mol L^{-1}, 2×10^{-6} mol L^{-1} and 100×10^{-6} mol L^{-1}. Other buffers were also tested in this study. Ammonium acetate buffer at pH = 9.2 was prepared as described in [25]. CAPS buffer (500 nM) at pH = 9.4 was prepared by dissolving 1.1 g of CAPS in 7 mL of Milli-Q water. The solution was then titrated with 1 M NaOH until pH = 9.4 was achieved. Extra Milli-Q water was added to obtain 10 mL of buffer. The buffer was then diluted to the desired concentration. For each sample, 10 mg of PAA was dissolved in 1.5 ml of Milli-Q water with a small volume of sodium hydroxide (15 µL, 1 mol L^{-1}). 500 µL of dissolved PNaA was mixed

with 10 µL of 10 wt% aqueous DMSO (added as an electroosmotic flow marker). Each PNaA sample was diluted several times until repeatable, normalized μ_{ep} distributions at two different concentrations were achieved. For these linear, 3-arm star and hyperbranched PNaAs, the concentration was approximately 1.4 g L^{-1}. The separation experiments were performed using a fused-silica capillary with a total length of 62.2 cm and an effective length of 53.7 cm. μ_{ep} was calculated as in [25]. μ_{ep} is preferred to migration time because it is more reproducible and it characterizes the topology of a polymer [26]. Data obtained by UV detection (at a wavelength of 195 nm) were treated with the Origin 9.0 software package. The pH meter was a SevenCompact™ pH/Ion meter S220 (Mettler Toledo), calibrated using internal standards with pH values of 4, 7 and 9.2 or 4, 7 and 10.

3.2.4 Pressure mobilization

Pressure mobilization (PM) was carried out using the same equipment as for the CE. PM was undertaken at a pressure of 100 mbar, without electric field. The sample was mixed with the BGE with the electric field. This involves increasing the voltage up to 30 kV, then down to -30 kV and back up to 0 kV over the first 4 min of separation. The mixing of the PNaA with the mobile phase is due to the electroneutrality of the solution (which needs to be maintained all over the PM experiment, including during the mixing with electric field). More details are given in [20]. The mobile phase comprised sodium borate at different concentrations and at pH = 9.2. Linear and hyperbranched PNaA as well as PNaAs synthesized by conventional radical polymerization were analyzed as follows. Two different capillaries were used. Both were polyimide coated fused silica high sensitivity capillaries (50 µm internal diameter) from Agilent, as for the free solution CE experiments. However, their sizes were different. The Linear PNaA was analyzed with a capillary of 62.5 cm total length and 54 cm effective length, whilst the hyperbranched PNaA and the PNaAs synthesized by conventional radical polymerization were analyzed with a capillary of 62.3 cm total length and 53.8 cm effective length. The capillary was pretreated prior to use and after each run by flushing for 5 min with the mobile phase. Data were treated with the Origin 9.0 software package.

3.3 Results and discussion

The influence of the buffer concentration and the presence of silver in the buffer on μ_{ep} and selectivity was studied. In order to conduct this study, three PNaAs with different structures were used, namely: a linear PNaA, synthesized as poly(*n*-butyl acrylate) by ionic polymerization and hydrolyzed; a 3-arm star and hyperbranched PNaA synthesized by nitroxide mediated polymerization (NMP) using an inimer. Table 3.1 summarizes all polymers used to carry out this study and how they were synthesized.

In order to calculate the normalized mobilities and the different selectivities (defined below), μ_{ep} was measured at the maximum of each peak. As broad and sharp peaks overlap when the BGE has a concentration between 110 mmol L^{-1} and 250 mmol L^{-1}, it was not possible to use the weight average μ_{ep} as in the literature [13].

Table 3.1: Summary of all polymerizations used to carry out this study

Polymer	Synthesis method	Reactants (initiator/CTA/monomer/solvent)	Conversion	M_n
Linear PNaA [2]	Anionic polymerization	t-butyl acrylate	unknown	39,300 g mol^{-1}
3-arm star PNaA [2]	Nitroxide mediated polymerization	Alkoxyamine/SG1/acrylic acid/1,4-dioxane	65 %	8,500 g mol^{-1} #
Hyperbranched PNaA [2]	Nitroxide mediated polymerization	Alkoxyamine/SG1/acrylic acid/1,4-dioxane	50 %	12,300 g mol^{-1} #
Other branched PNaA [4]	Conventional radical polymerization	ACVA/No CTA/Acrylic acid/water THF (v/v 8/2)	>94 %	unknown

#: This does not correspond to the true molar mass, but the molar mass of the linear polystyrene equivalent [27].

3.3.1 Joule heating effect

It is known that Joule heating effect can affect the electrophoretic mobility as the passage of electrical current through the buffer (which has a resistance) in the capillary leads to a temperature increase. This will reduce the viscosity of the buffer and thus increase the electrophoretic mobility [10]. The effect of temperature increase was tested using Eq. (3.1) to (3.4). Details are in Table 3.2

ΔT_{Radial}, defined as the radial temperature difference across the capillary inside the electrolyte is calculated using Eq. (3.1).

$$\Delta T_{Radial} = \frac{1}{4\pi\lambda}\frac{P}{l} \tag{3.1}$$

Where P is the power, l is the capillary length, and λ is the thermal conductivity of the background electrolyte (BGE). For diluted aqueous electrolyte, such as sodium borate and ammonium acetate and CAPS basic buffer, $\lambda \approx 0.605$ W m^{-1} K^{-1}.

ΔT_{Wall}, defined as the temperature difference across the capillary wall is calculated using Eq. (3.2).

$$\Delta T_{Wall} = \frac{1}{2\pi\lambda_{Wall}} ln\left(\frac{d_o}{d_i}\right)\frac{P}{l} \tag{3.2}$$

Where d_o and d_i are the outer and inner diameters of the capillary and λ_{Wall} is the thermal conductivity of the wall.

As fused silica capillaries used in this study are coated with polyimide, Eq. (3.2) need to be adjusted. The temperature difference across the fused silica wall (ΔT_{FS}) and the polyimide coating (ΔT_{PI}) have to be calculated separately (see Eq. (3.3) and (3.4)).

$$\Delta T_{Wall,\ FS} = \frac{1}{2\pi\lambda_{FS}} ln\left(\frac{d_{o,FS}}{d_{i,FS}}\right)\frac{P}{l} \tag{3.3}$$

$$\Delta T_{Wall,\ PI} = \frac{1}{2\pi\lambda_{PI}} ln\left(\frac{d_{o,PI}}{d_{i,FI}}\right)\frac{P}{l} \tag{3.4}$$

λ_{FS}=1.40 W m^{-1} K^{-1} and λ_{PI}=0.155 W m^{-1} K^{-1}.

The total temperature increase is the sum of ΔT_{Radial}, $\Delta T_{\text{Wall, FS}}$, and $\Delta T_{\text{Wall, PI}}$.

Table 3.2: Temperature increase for injections using sodium borate buffers at pH=9.2 and from 110 mmol L^{-1} to 300 mmol L^{-1}

Buffers	Current (µA)	Temperature increase (°C)
NB110	34-35	0.76-0.79
NB150	37-39	0.88-0.90
NB200	60-66	1.35-1.46
NB250	64-68	1.48-1.58
NB300	92-123	2.07-2.76

A temperature increase superior to 2 °C can induce a non-negligible effect on the variation of $\mu_{ep.}$ Consequently, the μ_{ep} obtained when PNaAs are injected using NB300 might be biased. However, the potential effect of temperature increasing due to Joule heating was neglected in this study.

3.3.2 Adsorption of PNaA on the capillary

To determine the reliability of the CE-CC analyses of PNaA in different buffers, pressure mobilization experiments were carried out using sodium borate buffers at different concentrations to test whether PNaA can potentially adsorb on the capillary. The adsorption could be due to the low solubility of PNaA in Milli-Q water. First, the linear PNaA was analyzed. Adsorption on the capillary was observed when using a sodium borate concentration below 110 mM. This is consistent with observations in the literature where adsorption of PNaA on a capillary has already been observed at low buffer concentration [28]. As the linear PNaA is expected to be the most soluble [4], it is assumed that branched PNaAs also adsorb on the capillary if injected using sodium borate below 110 mM as the mobile phase [4]. Consequently, pressure mobilization of branched PNaA was carried out using only sodium borate at 110 nM and above. Figure 3.1, Figure A.3.1 and Table A.3.1 prove that when the mobile phase corresponds to a concentration equal to or greater than 110 mM, no adsorption of PNaA on the capillary is observed. Indeed, Gaussian fits have a correlation coefficient close to unity. Moreover, it is observed that the correlation coefficients R^2 of Gaussian fits become closer to 1 when the buffer concentration increases. Increasing the ionic strength helps to dissolve PNaA in Milli-Q water as it increases the interactions between the solvent and the analyte. Consequently, using a high buffer concentration allows optimal analyses. The decrease of analyte-capillary wall interactions at high buffer concentration was already observed in proteins [29-32]. This also applies for polyelectrolytes.

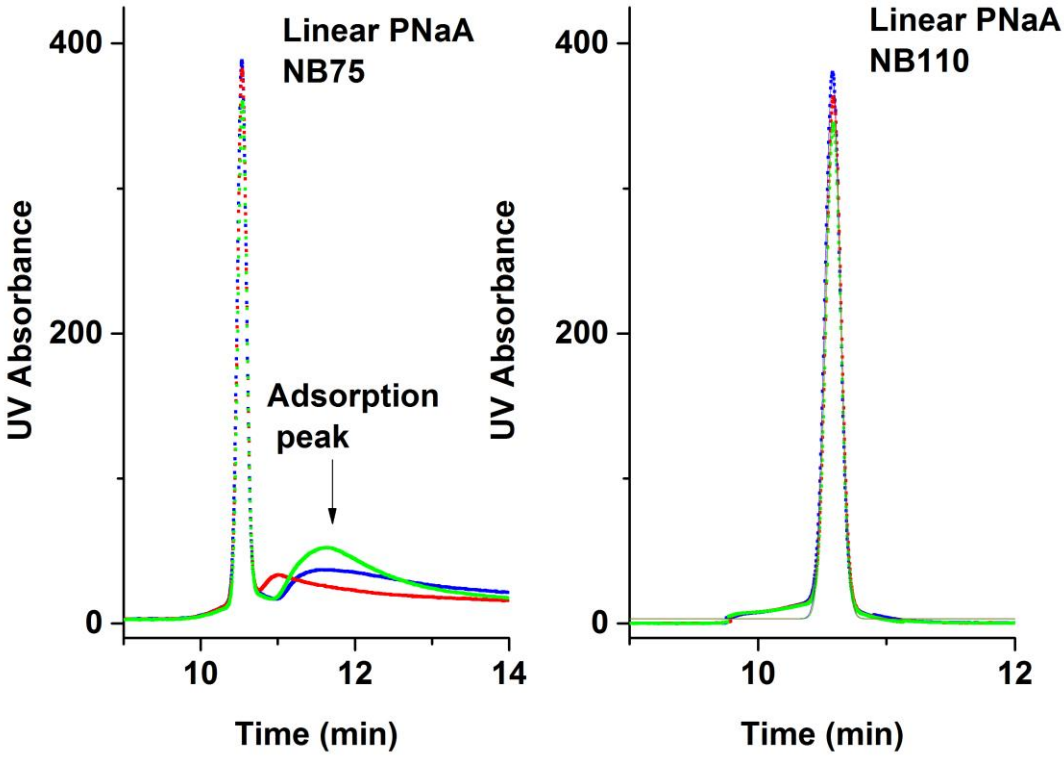
Linear PNaA
NB75
Adsorption
peak
UV Absorbance
Time (min)
Linear PNaA
NB110
UV Absorbance
Time (min)

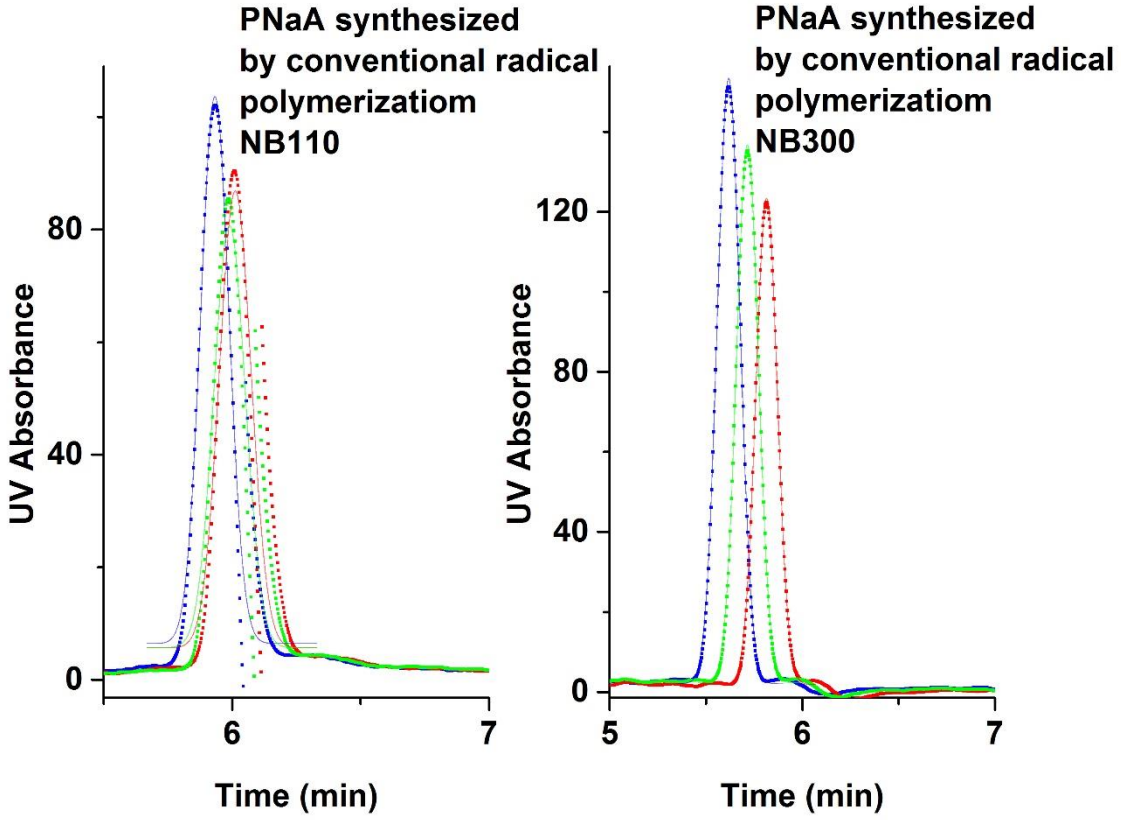
PNaA synthesized
by conventional radical
polymerizatiom
NB110
UV Absorbance
Time (min)
PNaA synthesized
by conventional radical
polymerizatiom
NB300
UV Absorbance
Time (min)

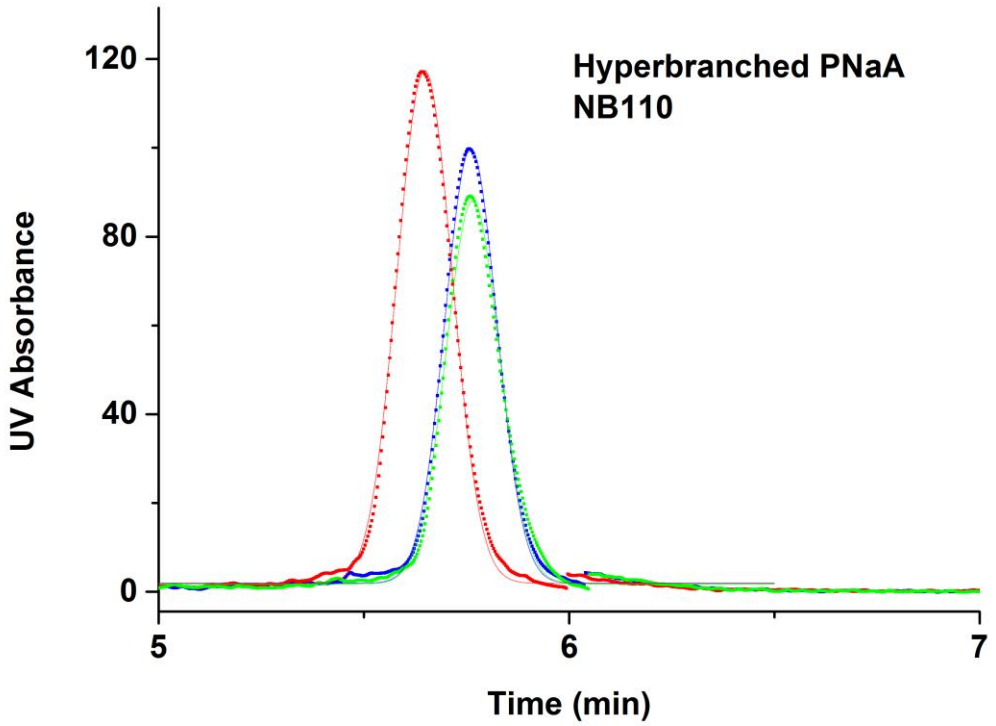

Figure 3.1: Elugrams from pressure mobilization experiments for linear, (conventionally) branched (i.e., synthesized by conventional radical polymerization) and hyperbranched PNaA in different buffers. Dash lines represent the elugrams and strenght lines represents the Gaussian fits. Results for Linear PNaAs are obtained using a different capillary to that for the Hyperbranched PNaA and PNaAs synthesized by conventional radical polymerization. Samples were injected in triplicate. Each colour represent one injection.

3.3.3 Peak identification – Effect of buffer concentration

3.3.3.1 Influence of buffer concentration on peak area

Preliminary studies were carried out in order to check that the variation of the buffer concentration did not influence the peak area. Some oligoacrylates synthesized by RAFT and separated by CE previously were injected in sodium borate at different concentration. The areas of three peaks of oligoacrylates (corresponding to the oligoacrylates with 1 unit (AA1), 1 unit with the RAFT agent (AA1 RAFT) and two units with the RAFT agent (AA2 RAFT) were compared in order to demonstrate the independence of the optimal PNaA concentration (when no overloading occurs) with the buffer concentration. Higher peak area values are observed

when [NB25] is used as buffer: this is likely due to adsorption of PNaA on the capillary. Results are presented in Figure 3.2 and in Table A.3.2 in the Appendix 2.

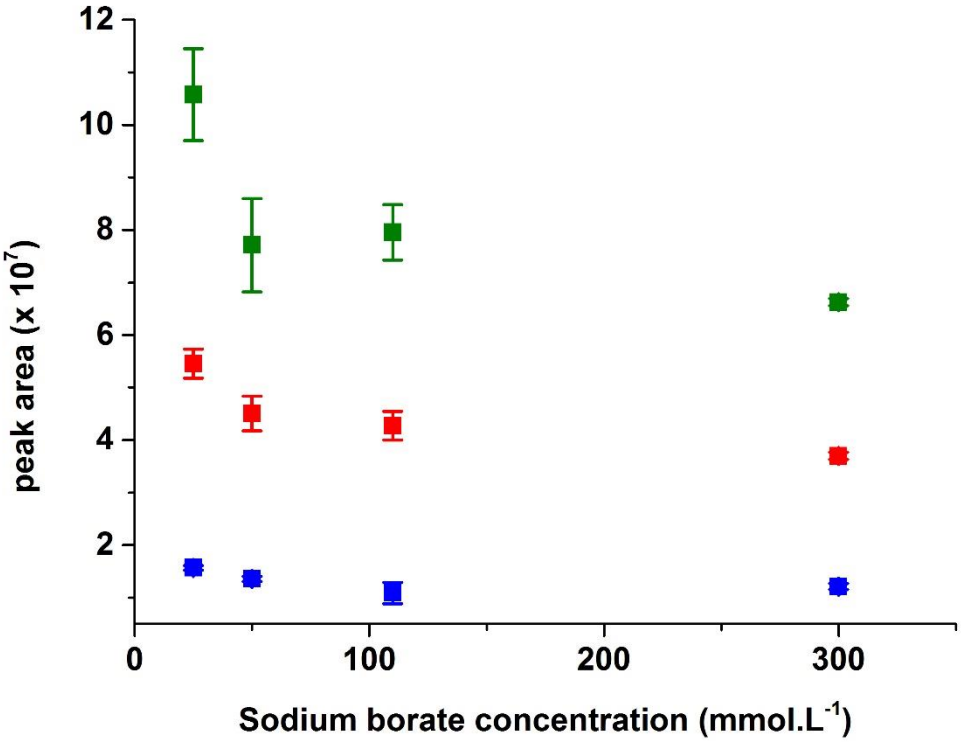

Figure 3.2: Peak areas of oligo acrylates as a function of sodium borate concentration. blue squares represent the AA1, red squares the AA1 RAFT and green squares the AA2 RAFT.

3.3.3.2 Peak identification

Electropherograms of branched PNaAs exhibit two peaks with occasional overlap. One of the peaks is broad and the other one is sharp (as can be seen in Figure 3.3). Linear, hyperbranched and 3-arm star PNaA were separated using sodium borate at different concentrations (Figure 3.3). As explained previously, a dependence of μ_{ep} on the ionic strength was already observed [15, 17]. If the BGE contains only a single buffer and both buffer and counter ions are singly charged, the ionic strength I is equal to the buffer concentration. Its dependence on the electrophoretic mobility has been investigated with Eq. (3.5), which takes into account the expected logarithmic dependence:

$$\mu_{ep,normalized} = -S\log(I) + Q \quad (3.5)$$

where the slope (S) represents the relative μ_{ep} decrease by log of ionic strength and Q is a constant for a given solute [15].

The normalized electrophoretic mobility here refers to μ_{ep} divided by μ_{ep} at a ionic strength of 110 mmol L^{-1} (see Eq. (3.6)). The standard deviation was calculated using Eq. (A.3.1).

$$\mu_{ep,normalized} = \frac{\mu_{ep}}{\mu_{ep}{}^{110mM}} \quad (3.6)$$

Figure 3.3 shows the electropherograms of the 3-arm star and hyperbranched PNaAs injected at different buffer concentrations. It is clearly observed that the μ_{ep} of the sharp and broad peaks behave differently if the buffer concentration is modified. Figure 3.4 presents the variation of the normalized μ_{ep} with log I for the broad and sharp peaks for (a) hyperbranched PNaA and (b) 3-arm star PNaAs compared with the linear PNaAs. Figure 3.5 presents a "slope plot" for these PNaAs [13]. Detailed results are presented in Tables A.3.3 and A.3.4 (Appendix 2). The standard deviation (SD) of the normalized mobility is given by Eq. (A.3.1). The linear fits do not include the injections in NB300 as it makes the correlation coefficients significantly lower (from around 0.8 to 0.2). This could be due to an increase of μ_{ep} due to the Joule heating effect being more important in NB300. At this buffer concentration, an increase superior to two degrees is expected. Detailed results are in the Appendix (Table A.3.4 and Figure A.3.2). It is important to note that the correlation coefficient is negative for the linear fit of the sharp peaks. This is likely due to the high standard deviation of the point, which prevent to obtain a good estimation of the fits parameters. Even though it is clearly observed that the variation of μ_{ep} with log I are lower for the sharp peaks than for the broad ones and the linear PNaA peak, the measurements are not accurate enough to obtain a linear model following the trend of the data. The linear best fits calculated with Origin 9.0 software package are not, in the case of the variation of the sharp peak position with the ionic strength, an average trend of the data. In these cases, the correlation coefficient cannot be interpreted.

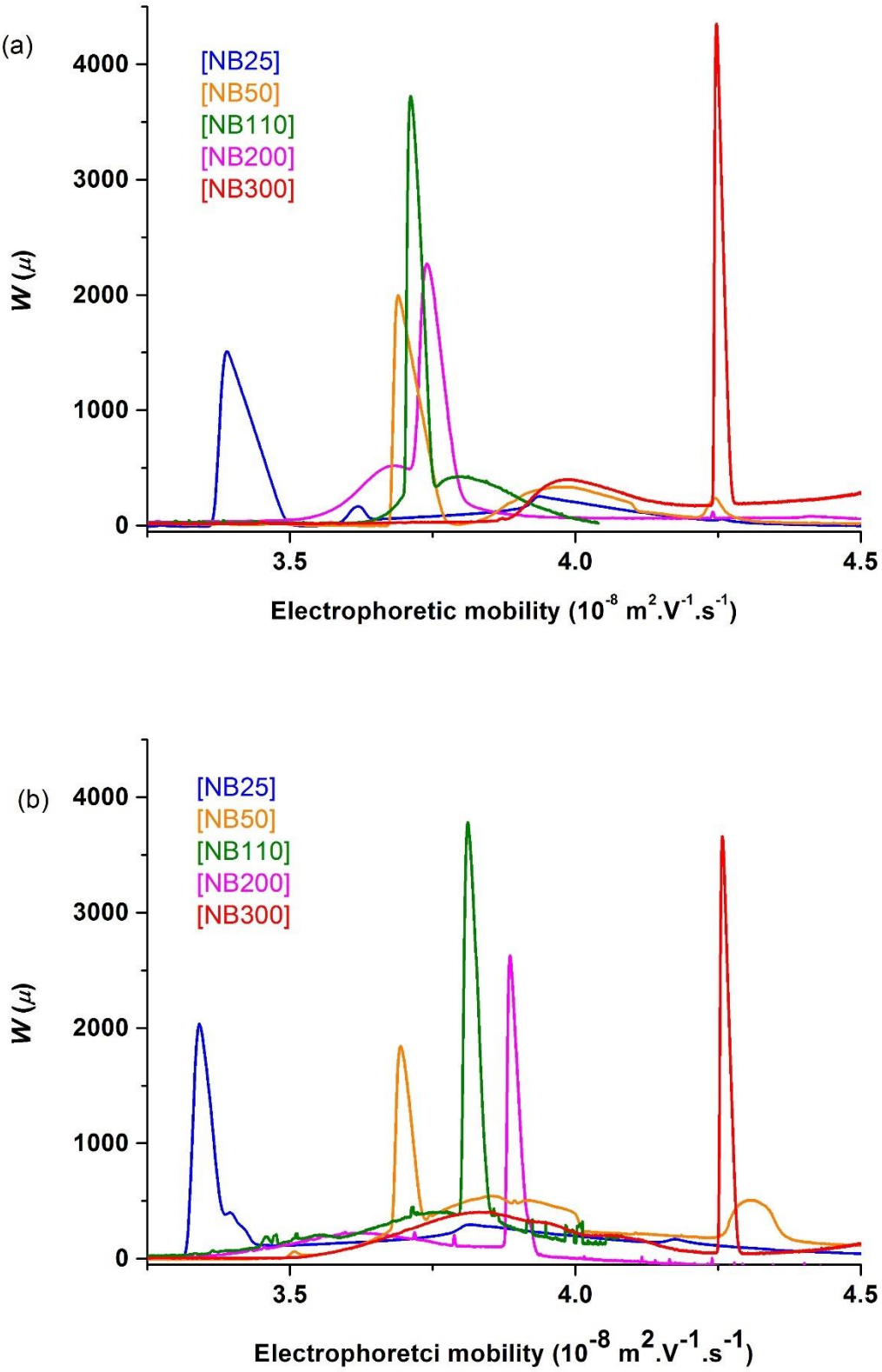

Figure 3.3: Electropherogram of (a) hyperbranched PNaA and (b) 3-arm star PNaA injected with different sodium borate buffer concentration.

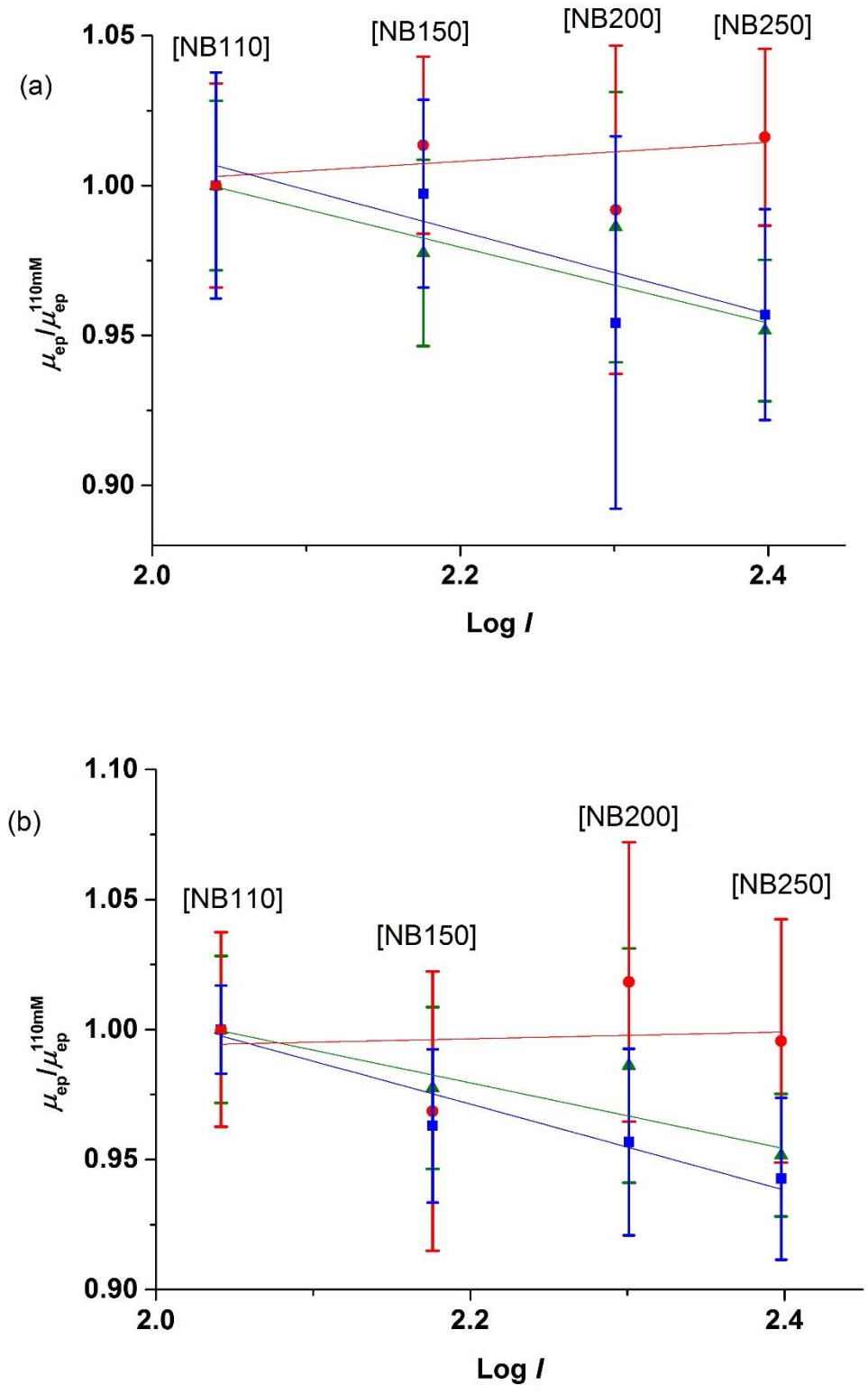

Figure 3.4: Logarithmic dependence of the μ_{ep} with the ionic strength for (a) hyperbranched PNaA and (b) 3-arm star PNaA. Red circles represent the sharp peak, blue squares the broad peaks, and green triangles the linear PNaA. Fits were drawn by excluding the injections in [NB300].

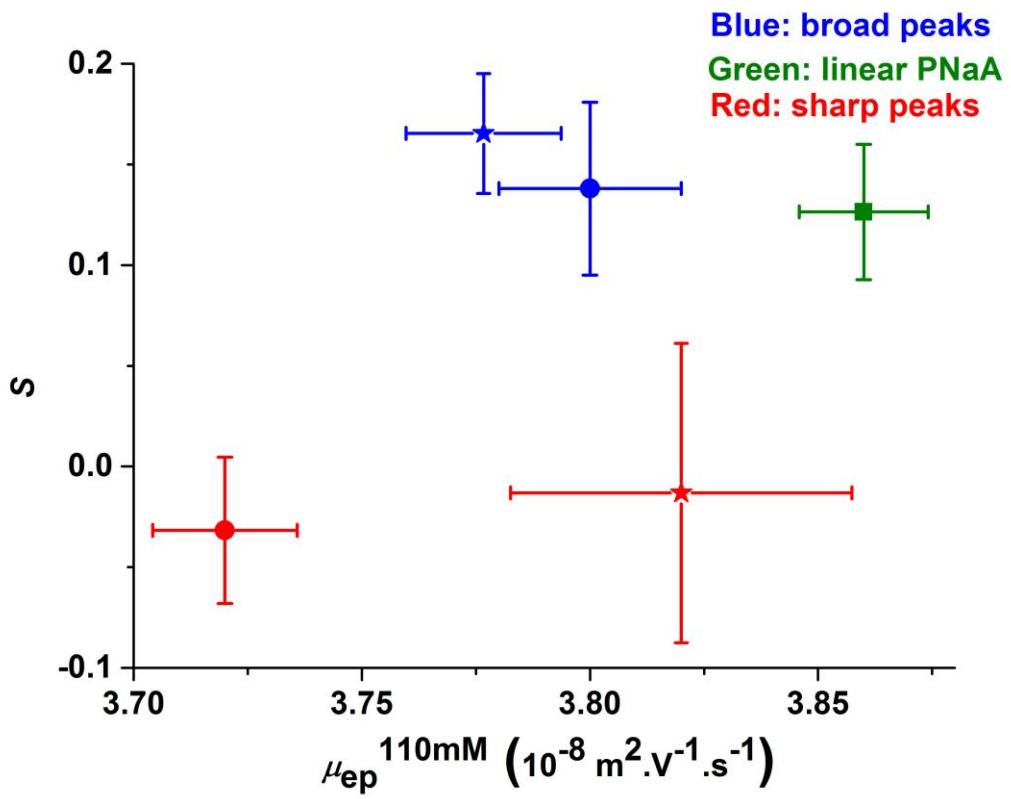

Figure 3.5: Slope plot: *S* values as a function of μ_{ep}^{110mM} for different PNaA: Hyperbranched PNaA (circles), 3-arm star PNaA (stars), and linear PNaA (square). *SD* (S) was calculated with the Origin 9.0 software package. The values are in Table A.3.4.

It can be observed in Figures 3.3, 3.4 and 3.5 that the μ_{ep} of the broad peak (for both 3-arm star and hyperbranched PNaAs) behaves relatively similarly to that for the linear PNaA with ionic strength. First, it is important to remember that Maniego *et al.* demonstrated in 2013 that when PNaAs are separated by CE-CC in [NB110], the lowest mobility was observed for the most branched PNaAs [2]. They also observed that electropherograms of PNaAs obtained using this buffer exhibit a lower μ_{ep} for the sharp peak than for the broad peak [2]. These results were confirmed by our previous study on PNaAs synthesized by conventional radical polymerization [4]. This mechanism is inverted at high buffer concentration as observed in Figure 3.3 (in [NB300], the sharp peak exhibits a higher μ_{ep} than the broad peak) and in Figure 3.6, in which the μ_{ep} is seen to increase with the degree of branching [2, 4].

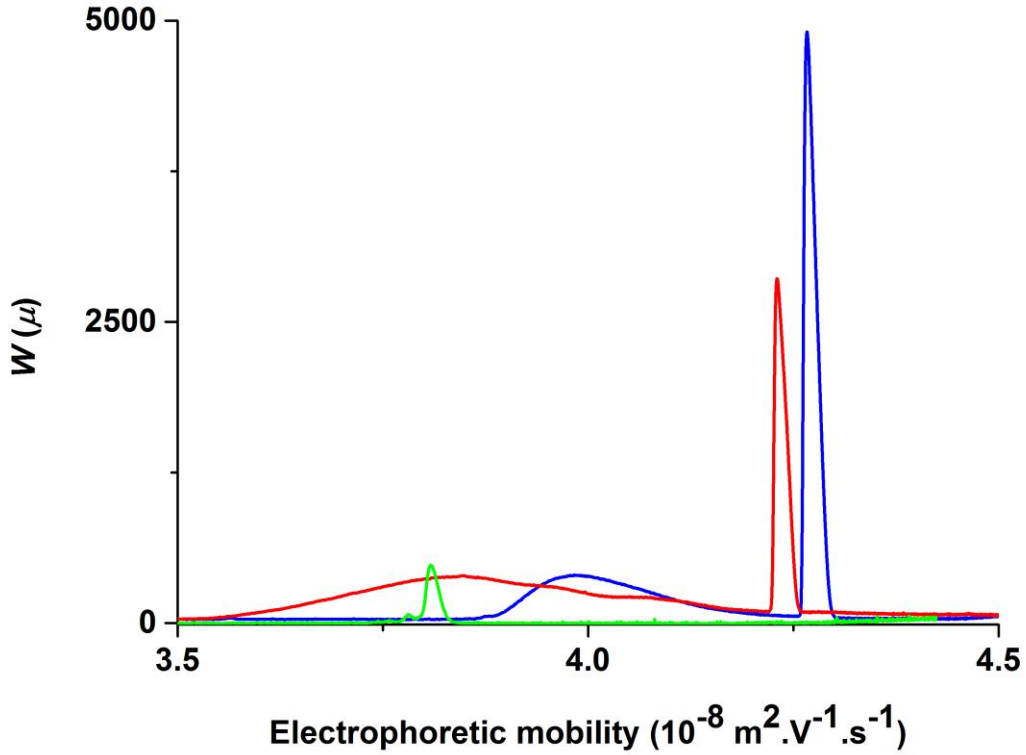

Figure 3.6: Electropherograms of linear (green line), 3-arm star (red line) and hyperbranched (blue line) PNaA injected in [NB300]

To understand this phenomenon, it is useful to remember that μ_{ep} is proportional to the absolute value of the charge of the analyte divided by the friction. Moreover, it can be expected that the more branched the polyelectrolyte, the denser the structure. This higher density facilitates the complexation between a poly(acrylate) and a Lewis acid. As poly(acrylate)s and sodium ions (from NaOH; used in dissolution of PAAs and sodium borate buffer) have negative and positive charges respectively, increasing the number of sodium ions complexing with the poly(acrylate) chain will reduce the charge of the chain, and so μ_{ep}. At very high sodium borate concentration, poly(acrylate) chains might complex more with borate (which is negatively charged) than with sodium. The absolute charge and thus the μ_{ep} of the complex would be increased by the number of borates ions complexed by a single poly(acrylate) chain. Some CE-CC experiments using CAPS as basic buffer at different concentrations confirm this hypothesis. CAPS cannot complex with poly(acrylate), and increasing the concentration of CAPS from 25 to 300 mmol L^{-1} does not invert the relative positions of the broad and sharp peaks in the electropherogram (see Figure 3.7). Another possible explanation could be the densities of the analyte, which depend on the ionic strength. The structure of PNaA are more compact at high buffer

concentration. The smaller the spheres, the lower the friction and thus the higher the mobilities. This is likely to apply to a bigger extent to the sharp peak, which corresponds to denser polymer chains.

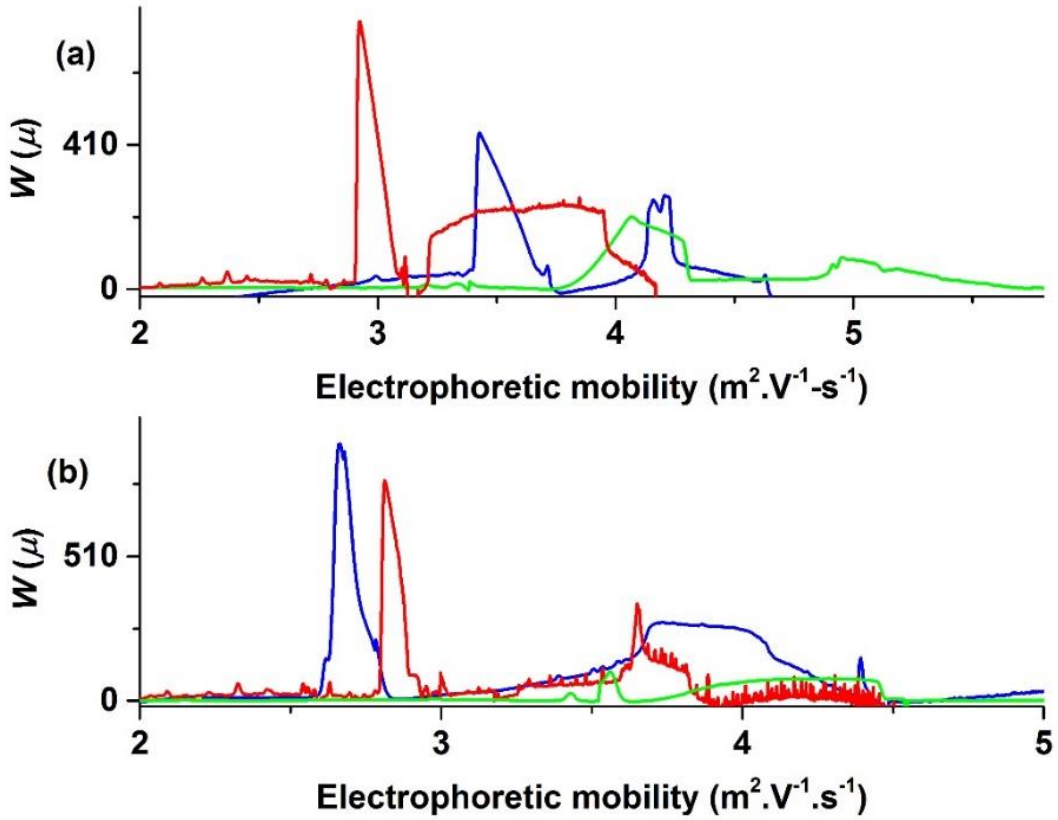

Figure 3.7: (a) Hyperbranched and (b) 3-arm star PNaAs injected in CAPS at 25 mmol L^{-1} (green line), 110 mmol L^{-1} (blue line) and 300 mmol L^{-1} (red line). The broad peak always has a higher electrophoretic mobility than the sharp peak.

Another explanation could be due to the effect of adsorption. As the solubility is expected to decrease with an increase in branching, the chain population exhibiting the sharp peak may adsorb onto the capillary more than the broad peak, and thus the migration time of the sharp peak would be overestimated at low buffer concentration. However, what is observed is the reverse phenomenon with the migration time of the sharp peak increasing with the buffer concentration.

Consequently, the former hypothesis leads us to deduce that on electropherograms of branched PNaA, the broad peak could be identified as a population of very slightly branched PNaA and the sharp peak as a population of PNaA with more branching (which would correspond to a denser structure). This hypothesis is confirmed by an observation in Figure 4 that the broad peaks of hyperbranched and 3-arm star PNaA behave similarly to the linear PNaAs in comparison to the sharp peaks. The CE-CC technique not only allows separation of different samples of PNaA according to their branching topology, but also allows observation of different branching structures in a single sample [33]. However, it is important to note that the results observed in this study are quite different from the ones observed by Ibrahim *et al.* in 2012 on polyelectrolytes [15] and by Bekri *et al*. in 2016 on proteins [17]. They observed an important linear decrease of μ_{ep} with log *I* for poly(acrylamide-*stat*-2-acrylamido-2-methylpropanesulfonate) (PAMAMPS), using sodium borate buffer at pH = 9.2 from 5 to 100 mM. The slope observed was negative, i.e., μ_{ep} decreased with the logarithm of ionic strength. This decrease was less pronounced for dense structures. In this study, the electrophoretic mobility of the broad peaks of branched PNaAs and of the single peak of the linear PNaA either decrease slightly or remain steady (if the error on the normalized μ_{ep} is taken into account), whilst the μ_{ep} of the sharp peak increase significantly from low to high buffer concentration. Figure 4 shows the different behavior but not the significant increases as the lowest buffer concentrations (25 to 75 mmol L^{-1}) were not taken into account due to the potential adsorption of PNaA on the capillary and the injections at the highest buffer concentration (300 mmol L^{-1}) as it did not fit, likely due to the Joule heating effect. This discrepancy is explained by the nature of the predominant phenomenon. In both case, a decrease of *S* value is observed when the charge density of the polyelectrolyte increases. This is likely due to the change of friction. Increasing the buffer concentration would increase of friction between buffer and analytes less significantly for dense analytes. However, in the case of PNaA, the complexation of borate by carboxylate groups may also play a role. Increasing the buffer concentration favors this complexation more significantly for dense structures and thus lead to the observed results: the expected decrease of μ_{ep} is reduced, cancelled or even overwhelmed by an increase of the absolute value of the overall charge due to the borate complexation. This might also explain the unexpected increase of μ_{ep} in [NB300], highly concentrated buffer is likely to be dominant.

Other hypotheses were considered. The sharp peak could have been identified as PNaA produced by autopolymerization, as it fits with a peak present in an acrylic acid sample (see Figure 3.8). However, it is difficult to make a firm conclusion, as the mechanism of

autopolymerization of acrylic acid is not well known at this stage. Even though this hypothesis is not the most likely, it cannot be discarded.

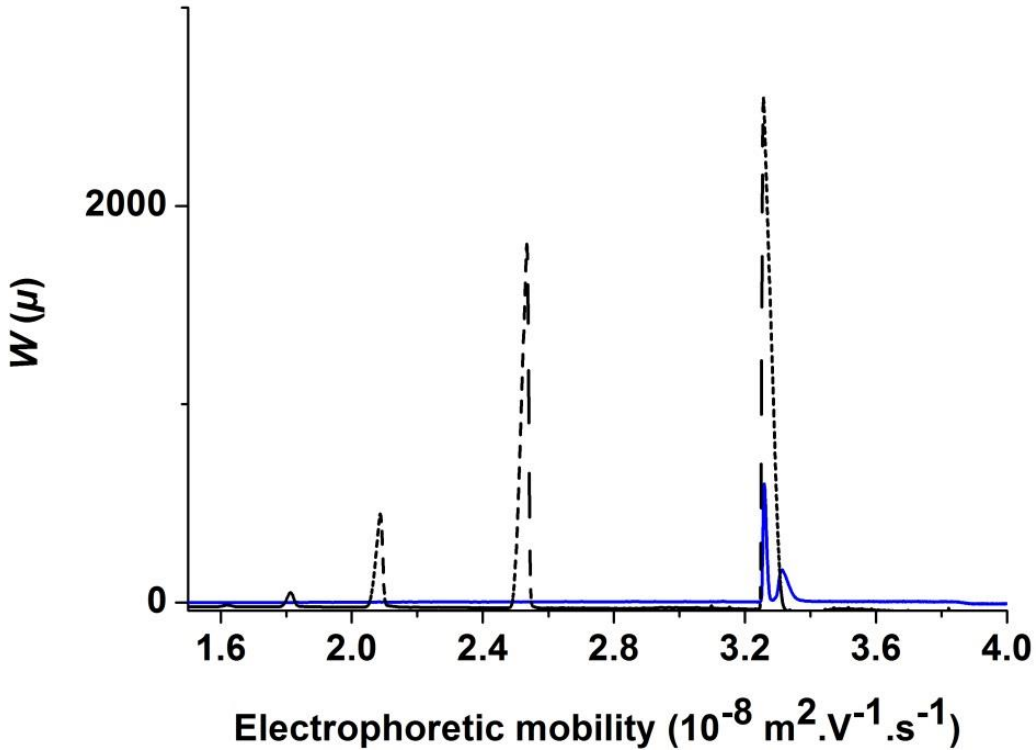

Figure 3.8: Overlay of injections of acrylic acid and PAA. The injection of acrylic acid is in dash line and the injection of PNaA synthesized at 90 °C without CTA is in blue line. The polymer resulting from autopolymerization fits with the sharp peak of the injection.

The sharp peak could also have corresponded to a peak of a complex between sodium borate and PNaA, but injections with ammonium acetate (which cannot complex with PNaA) as buffer also give two peaks (see Figure 3.9), which provides strong evidence that this hypothesis is wrong.

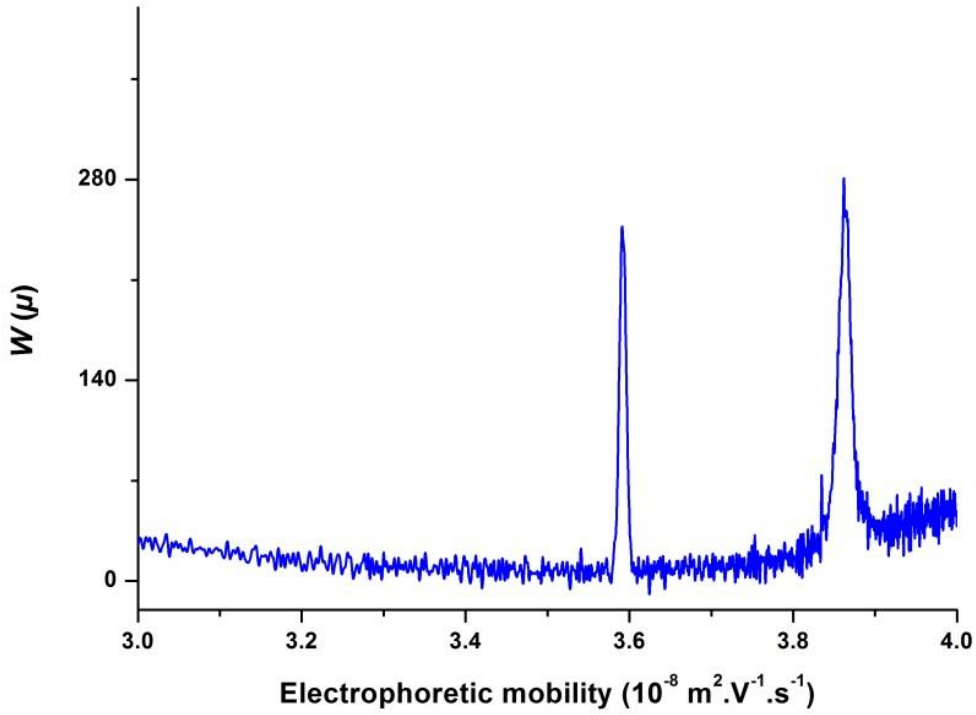

Figure 3.9: Injection of PAA (synthesized at 70 °C without CTA) with ammonium acetate as buffer: both peaks are present.

In conclusion, (i) both peak are identified as different branched chain population with different densities, (ii) both the complexation between PNaA and borate and the reduction of friction at high buffer concentration could play an important role in the separation.

3.3.4 Increase of selectivity

3.3.4.1 Effect of buffer concentration

As observed in Figure 3.3, the relative position of the sharp and broad peaks is different according to the buffer concentration. Consequently, the separation of the two peaks observed on electropherograms of branched PNaA can be improved by changing the buffer concentration. In the present study, the inverse of the difference of mobility (*IDM*), defined and calculated according to Eq. (3.7), was measured for the injections of 3-arm star and hyperbranched PNaAs using different sodium borate buffer concentrations. The inverse of the difference of the two maxima is preferred to the absolute difference of the two maxima in order to look at the relative difference and reduce the scale effect [33, 34]. The lower the *IDM*, the higher the selectivity, the better the separation. Figure 3.10 summarizes the results. The

standard deviation was calculated according to Eq. (A.3.2). The values of the selectivity are given in Table (A.3.5) in the Appendix 2.

$$IDM\ (sharp\ and\ broad\ peak) = \frac{1}{\left|\mu_{ep}(broad\ peak) - \mu_{ep}(sharp\ peak)\right|} \tag{3.7}$$

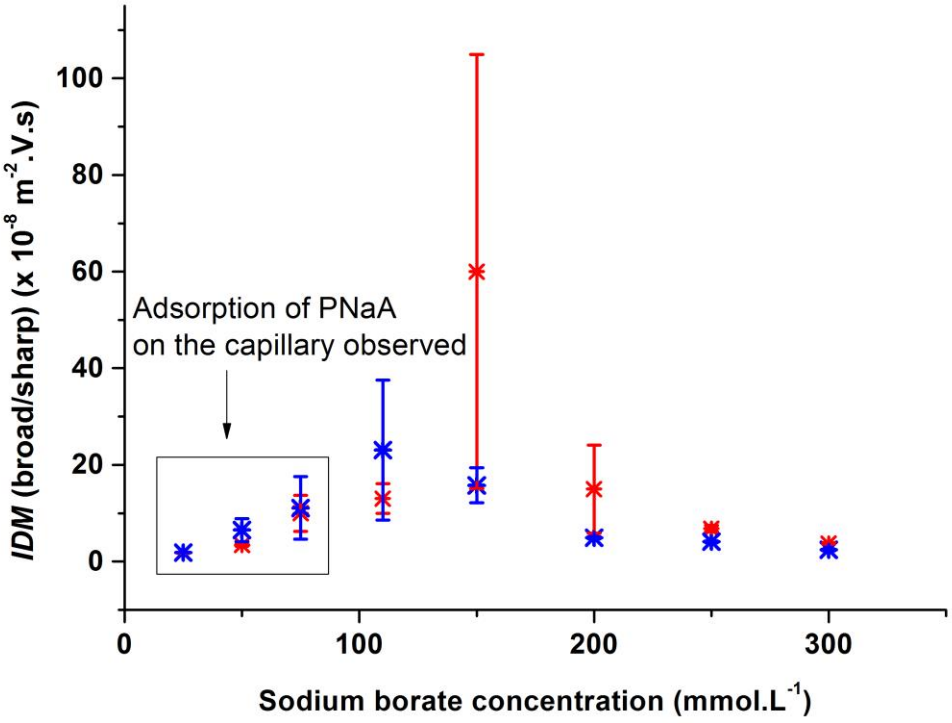

Figure 3.10: Selectivity (sharp peak/broad peak) of the hyperbranched PNaA (red stars) and 3-arm star PNaA (blue stars)

As the μ_{ep} of the sharp peak increases with ionic strength faster than that of the broad peak, the relative position of the two different peaks varies. At low sodium borate concentration, the μ_{ep} of the sharp peak is lower than that of the broad peak. At an intermediate concentration, both maxima are close to each other and the selectivity is low (the *IDM* is high). At a high concentration, the μ_{ep} of the sharp peak becomes higher than that of the broad peak, and consequently the selectivity increases (the *IDM* decreases). Variations of selectivity with the ionic strength and reversal zones at high buffer concentration have already been observed [35, 36].

The best separation of the broad and sharp peaks is achieved when the PNaAs are separated using [NB25] and [NB300], as observed in Figures 3.3 and 3.10. At low sodium borate

concentration, the migration time needed to observe the PNaA peaks is lower than at high sodium borate concentration. For optimal separation of polyelectrolytes, both resolution and time for the measurement leading to this resolution need to be taken into account. T_{Res}, defined as the time to achieve a given resolution, is given by Eq. (3.8) and should be as low as possible [34].

$$T_{\mathrm{Res}} = \frac{V_s t}{P} \tag{3.8}$$

V_s is the height of the valley (defined as the minimum between the two apexes) between two peaks, P is the height of the lowest peak and t is the migration time at the valley. More details are given in Figure 1c of [34]. In the present case, T_{Res} is lowest in NB25.

Some pressure mobilization experiments have showed that at low buffer concentration, PNaA adsorbs on the capillary and results are biased (see Figures 3.1 and A.3.1). Consequently, optimal analyses of branched PNaAs by CE-CC are obtained at high buffer concentrations. Here, both peaks are completely resolved and results are not biased by adsorption of PNaA on the capillary. If measurements with BGE in which adsorption occurs are discounted, occasional overlapping occurs except in [NB300] (as observed in Figure 3 and A.3.3). Even though they allow a T_{Res} shorter than in [NB300], basic sodium borate at concentrations from 110 mmoL L^{-1} to 250 mmol L^{-1} are not ideal to analyze branched PNaA.

3.3.4.2 Effect of addition of silver

At concentrations below 5 mmol L^{-1}, silver nitrate is expected to complex PNaA without precipitation [19]. Therefore the effect of the addition of silver nitrate on the selectivity was tested. PNaAs were injected in [NB110] with and without silver nitrate. Three different silver nitrate concentrations were tested (1, 2 and 100 mM) and the normalized μ_{ep} were calculated (with Eq. (3.9)). The standard deviation was calculated from Eq. (A.3.1). Results are presented in Figure 3.11 and 3.12. The values of normalized μ_{ep} are given in Table A.3.6 (Appendix 2).

$$\mu_{ep,\,normalized} = \frac{\mu_{ep}}{\mu_{ep}(PNaA\ in\ sodium\ borate\ without\ silver)} \tag{3.9}$$

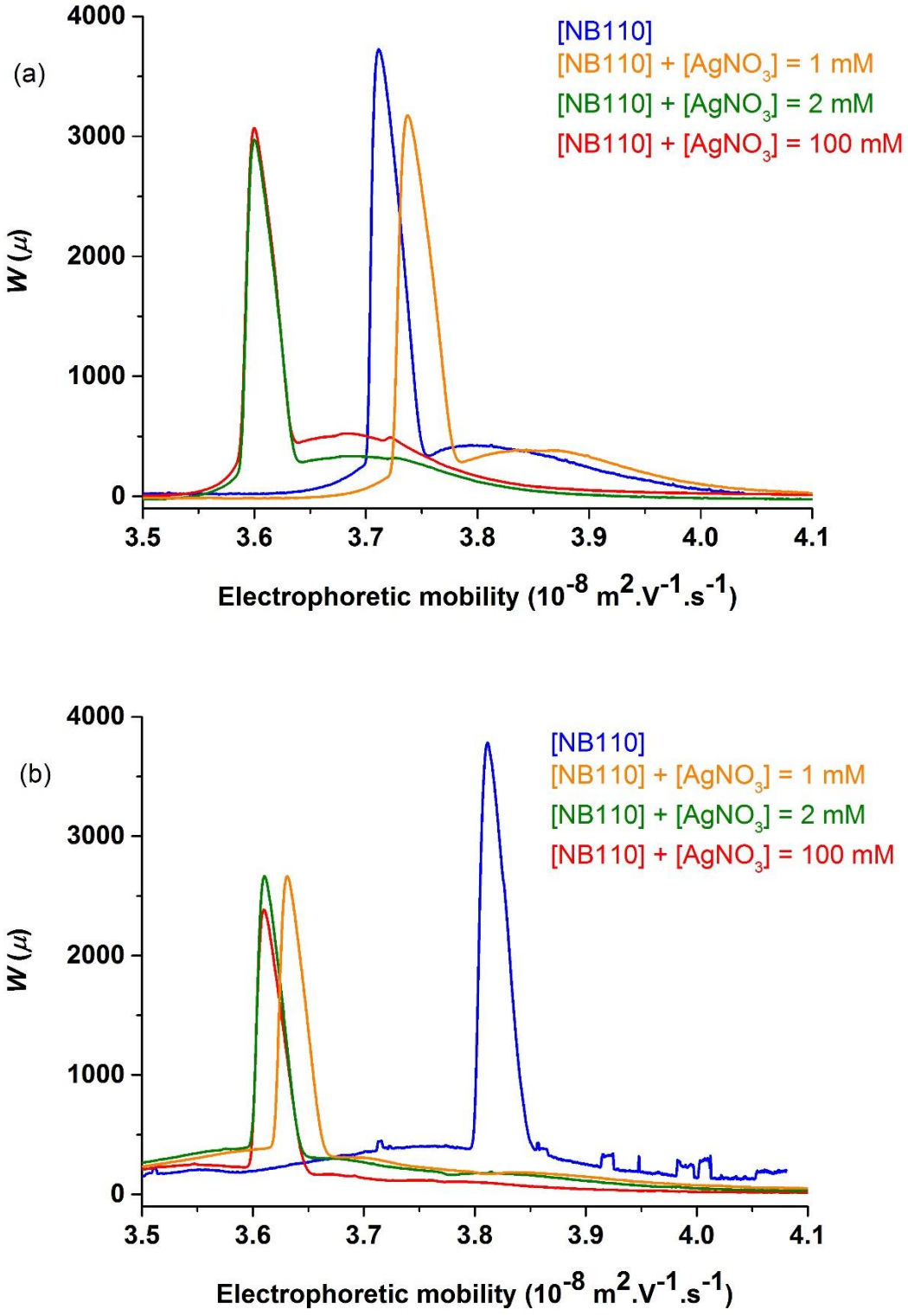

Figure 3.11: Electropherogram of (a) Hyperbranched PNaA and (b) 3-arm star PNaA injected in [NB110] with and without silver nitrate.

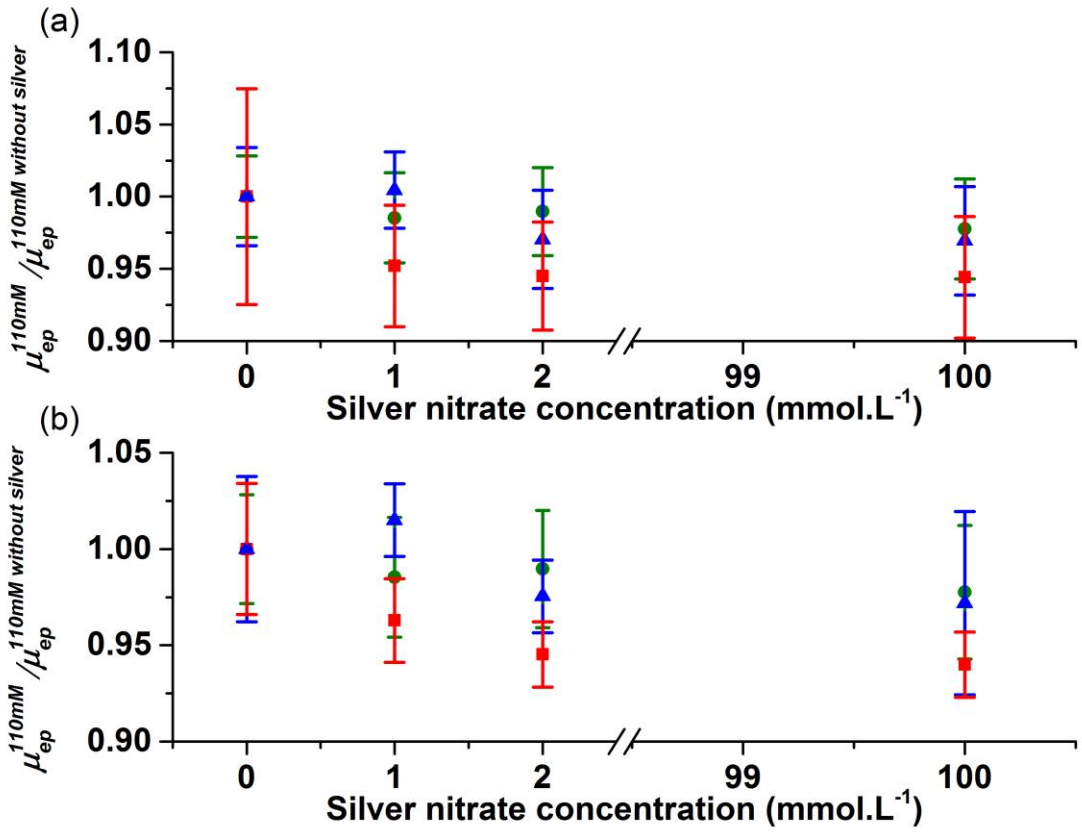

Figure 3.12: Evolution of the normalized mobility of linear PNaA (green circles), hyperbranched (blue triangles), and 3-arm star PNaA (red squares) with silver nitrate concentration for (a) the sharp peak and (b) the broad peak of electropherograms.

The addition of silver nitrate to the sodium borate does not have the expected effect; rather, μ_{ep} remains in the same range when the silver nitrate concentration is varied from 0 to 100 mmol L^{-1} (see Figure 3.11). The addition of silver in the BGE shows that borate is likely stronger at complexing PNaA than silver. The movement of the species in the capillary due to the electric field might also prevent the interactions between silver and PNaA.

Another possible hypothesis is the precipitation of silver with PNaA, which is not expected to occur at [$AgNO_3$] = 1 or 2 mmol L^{-1} but should occur at [$AgNO_3$] = 100 mmol L^{-1}. As PNaAs separated by CE are detected by UV and the absorbance is proportional to the concentration, comparing the peak areas of PNaAs injected with and without silver can provide information on the relative amount of PNaA, and thus on its eventual precipitation with silver. The peak

areas of each PNaA injected in [NB110] with and without silver were calculated by integrating the peak in the electropherogram. The values are given in Table A.3.6 and presented in Figure 3.13, which does not show significant diminution of the peak area when the silver concentration increases. Consequently, the present hypothesis looks incorrect. Therefore, the complexation between silver and boric acid (or borate) that is observed at high buffer concentrations is likely the correct reason. Another possibility is the increase of density with the raise of ionic strength due to the addition of silver. This would reduce the friction and compensate the decrease of charge due to complexation between PNaA and silver.

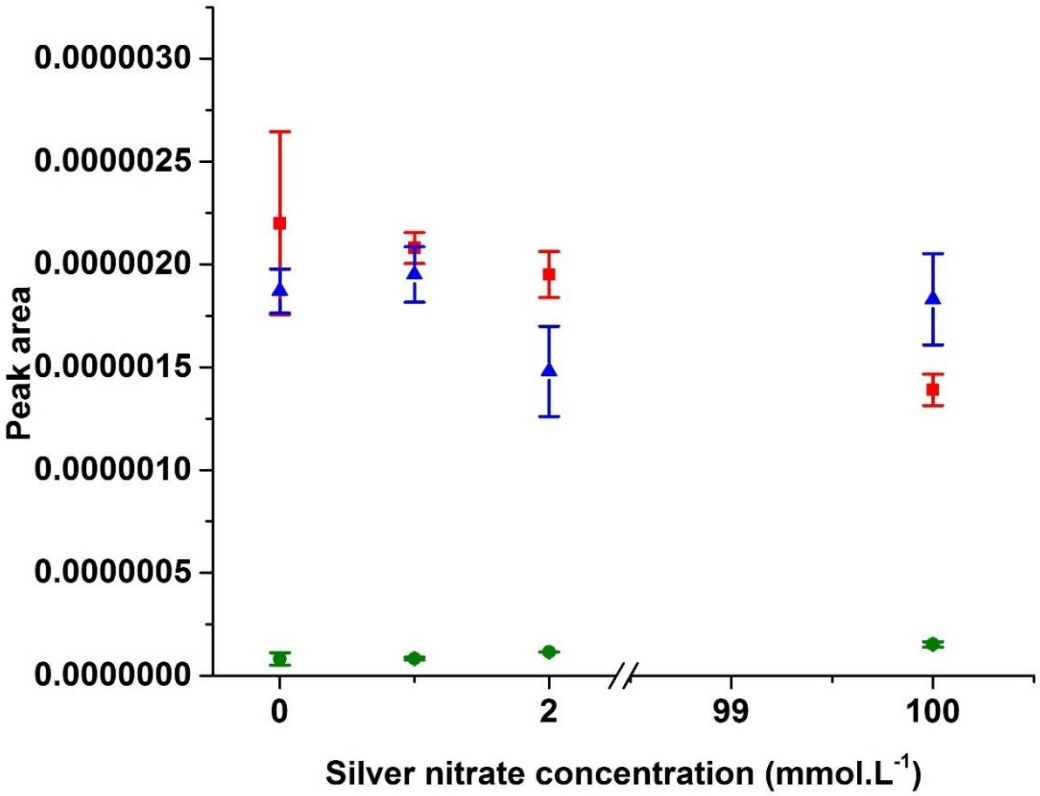

Figure 3.13: Variation of the electropherogram peak area of the linear (green circles), hyperbranched (blue triangles) and 3-arm star (red squares) PNaAs with the silver nitrate concentration.

From this section, it can be concluded that the addition of silver in the background electrolyte does not affect the separation's selectivity of PNaA by CE-CC. The selectivity can be improved only by using sodium borate at higher concentration.

3.3.5 Dispersity of branching population in PNaA

As explained in chapter 2, CE-CC provides important information related to the heterogeneity of branching. This heterogeneity is not just due to different degrees of branching (*DB*) within a sample but also different positions of the branching points or a distribution of LCB or SCB. As polymers are separated in CE-CC according to their topology and not according to their size, the dispersity of the distribution of μ_{ep} is related to the heterogeneity of branching [9]. As previously, the dispersity of the μ_{ep} distributions was calculated in this work as a standard deviation [37] and as a ratio of four moments [9]. Details are given in the Appendix 2 (Eq. A.1.8 to A.1.12) and in Chapter 2.

3.3.5.1 Effect of buffer concentration on the dispersity

In this work, $D(W(\mu),1,0)$ was measured for the linear, 3-arm star and hyperbranched PNaAs at different sodium borate buffer concentration. The results are presented in Figure 3.14. Detailed results are in Table A.3.8 in the Appendix 2.

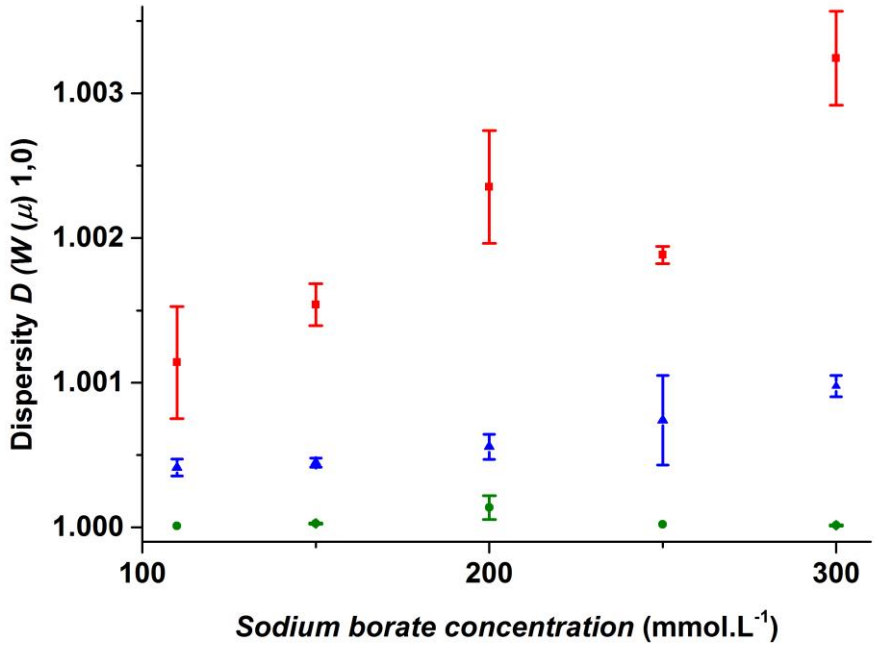

Figure 3.14: Dispersity $D(W(\mu),1,0)$ of μ_{ep} measured for linear PNaA (green circles), 3-arm star PNaA (red squares) and hyperbranched PNaA (blue triangles) using different sodium borate concentrations.

An effect of buffer concentration on the dispersity of μ_{ep} distribution is observed. It appears to increase with the buffer concentration. This is likely due to the complexation of borate and PNaA at high buffer concentration, which could broaden the peak.

3.3.5.2 Heterogeneity of branching of the broad and sharp peaks in branched PNaA

The heterogeneity of branching of PNaAs produced by radical polymerization at different temperatures (from 50 to 90 °C) and initial monomer concentrations (from 1 to 3 mol L^{-1}) without CTA has been measured in NB110 previously [4]. This is also the case for the hyperbranched, 3-arm star and linear PNaA [9]. However, the two peaks were not resolved. In the present work, the same analyses were carried out using NB300 buffer, in which both peaks are well separated (see Figure A.3.4), allowing separate characterization of the heterogeneity of branching of the broad and the sharp peaks. Moreover, the contribution of each peak to the total quantity of PNaA can be studied as the area of both peaks can be calculated. Results are presented in Figure 3.15, Figure 3.16, Table 3.3 and Table A.3.9.

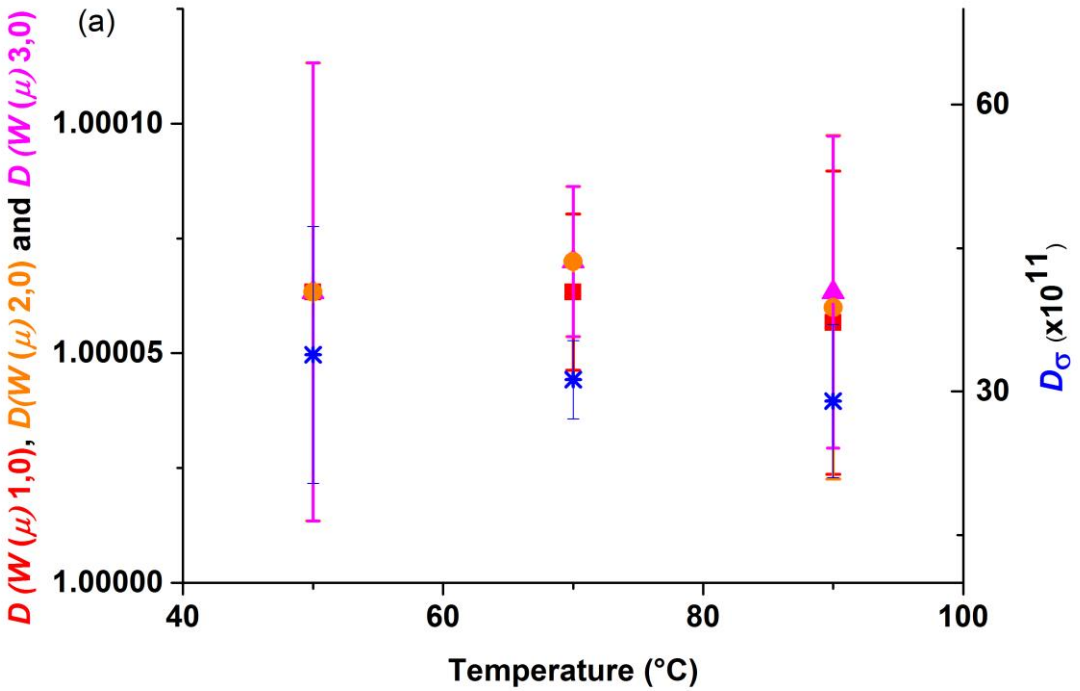

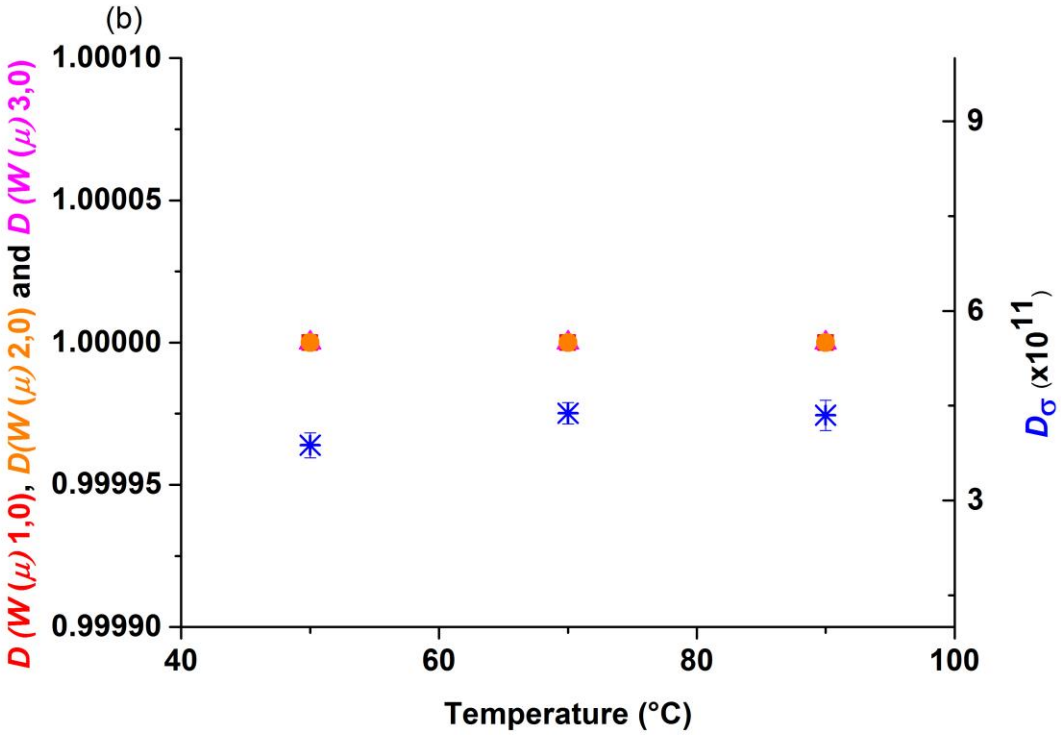

Figure 3.15: Dispersity of μ_{ep} distribution as a function of polymerization temperature for (a) the broad peak and (b) the sharp peak. $D(W(\mu),1,0)$, $D(W(\mu),2,0)$ and $D(W(\mu),3,0)$ are represented by red squares, orange circles, and pink triangles, respectively, while D_σ is represented by blue stars.

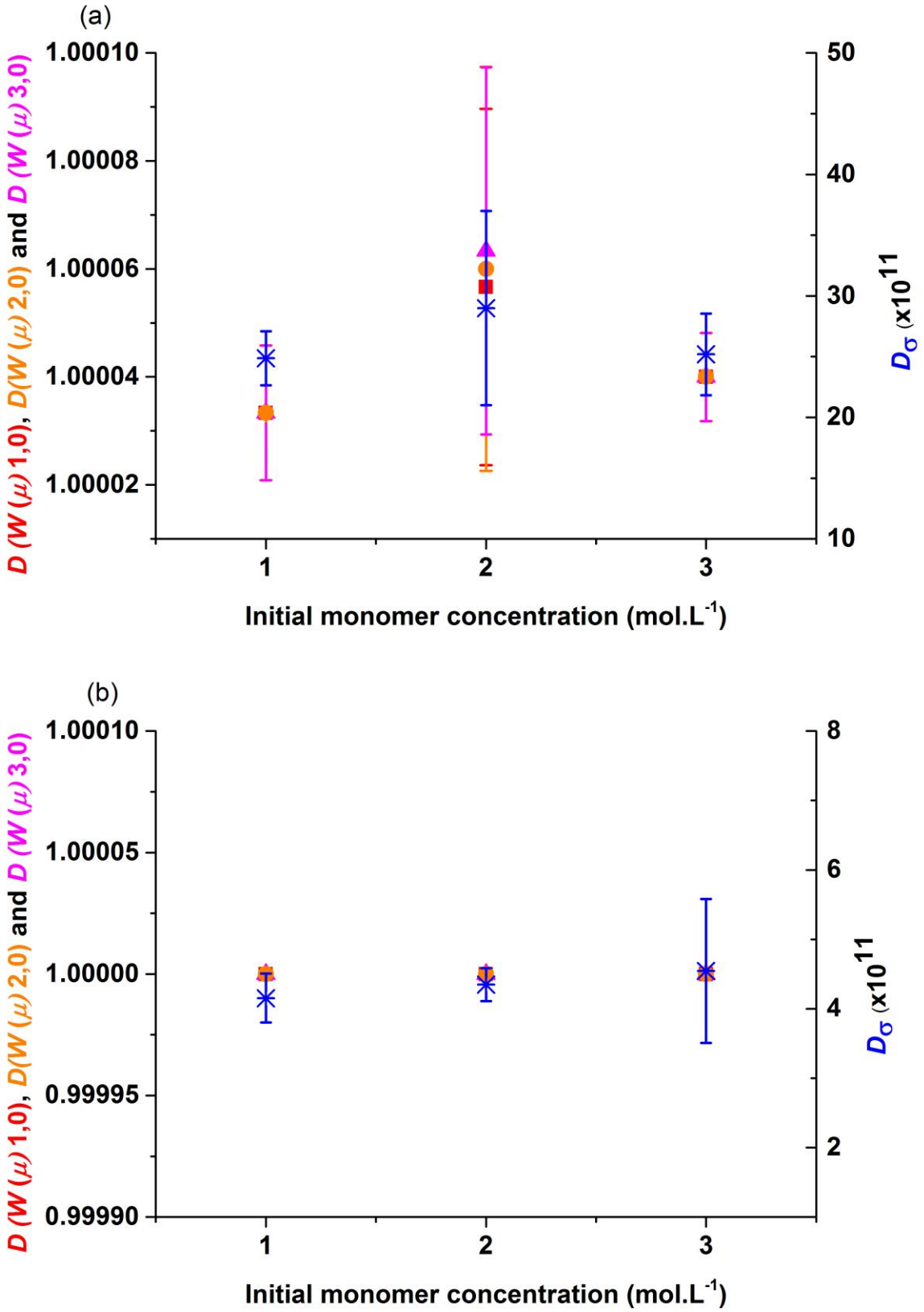

Figure 3.16: Dispersity of μ_{ep} as a function of initial monomer concentration for (a) the broad peak and (b) the sharp peak. $D(W(\mu),1,0)$, $D(W(\mu),2,0)$ and $D(W(\mu),3,0)$ are represented by red squares, orange circles and pink triangles, respectively, while D_σ is represented by blue stars.

Table 3.3: Dispersity of μ_{ep} distribution of linear, 3-arm star and hyperbranched PNaAs in NB300.

Dispersities and *SD*	3 arm star PNaA (broad peak)	3 arm star PNaA (sharp peak)	Hyperbranched PNaA (broad peak)	Hyperbranched PNaA (sharp peak)	Linear PNaA
$\boldsymbol{D(W(\mu),1,0)}$	1.00166	1	1.00042	1.000003	1.00001
SD	9.56847×10^{-5}	0	5.35×10^{-5}	4.71×10^{-6}	0
$\boldsymbol{D(W(\mu),2,0)}$	1.00166	1	1.000423	1.000003	1.00001
SD	9.10×10^{-5}	0	5.73×10^{-5}	4.71×10^{-6}	0
$\boldsymbol{D(W(\mu),3,0)}$	1.00165	1	1.000423	1.000003	1.00001
SD	8.64×10^{-5}	0	5.73×10^{-5}	4.71×10^{-6}	0
$\boldsymbol{D_\sigma}$	1.59×10^{-9}	8.85×10^{-11}	7.59×10^{-10}	8.81×10^{-11}	1.17×10^{-10}
SD	4.99×10^{-11}	5.17×10^{-12}	1.45×10^{-10}	9.14×10^{-12}	8.17×10^{-13}

For PNaAs synthesized by conventional radical polymerization, the evolution of the dispersity values of both peaks with polymerization temperature and initial monomer concentration is similar to what was observed in chapter 2 (when PNaAs were separated using [NB110] as buffer). Neither the temperature nor the initial monomer concentration significantly influences the heterogeneity of branching. When PNaA is synthesized without CTA, sufficiently high *DB* is obtained for the branching to be homogeneous, which explains the stability of the dispersities of electrophoretic mobility when the temperature and the initial monomer concentration vary. The main new information obtained from the improved selectivity of separation is the difference of dispersity between the broad peak and the sharp peak. The difference in dispersity of μ_{ep} distribution between the hyperbranched and the 3-arm star PNaAs is consistent with the previous research results from Thevarajah *et al* [9]. The hyperbranched PNaA has more homogeneous branching than the 3-arm star PNaA due to the relatively high degree of branching of 3.9 ± 0.1 % [38].

In all cases the sharp peak exhibits much lower dispersities of electrophoretic mobility distribution than the broad peak. This result was expected, as the sharp peak corresponds to a chain population whose amount of branching is large enough to be homogeneous. This applies to PNaAs synthesized by conventional radical polymerization as well as to the hyperbranched and 3-arm star PNaAs.

3.3.5.3 Contribution of broad and sharp peaks in branched PNaA

To study the contribution of each peak to the quantity of overall sample, the areas of broad and sharp peaks were calculated by integration. Results are presented in Figure 3.17 and Table A.3.10 for PNaAs produced by conventional radical polymerization, and in Table 3.4 for hyperbranched and 3-arm star PNaAs.

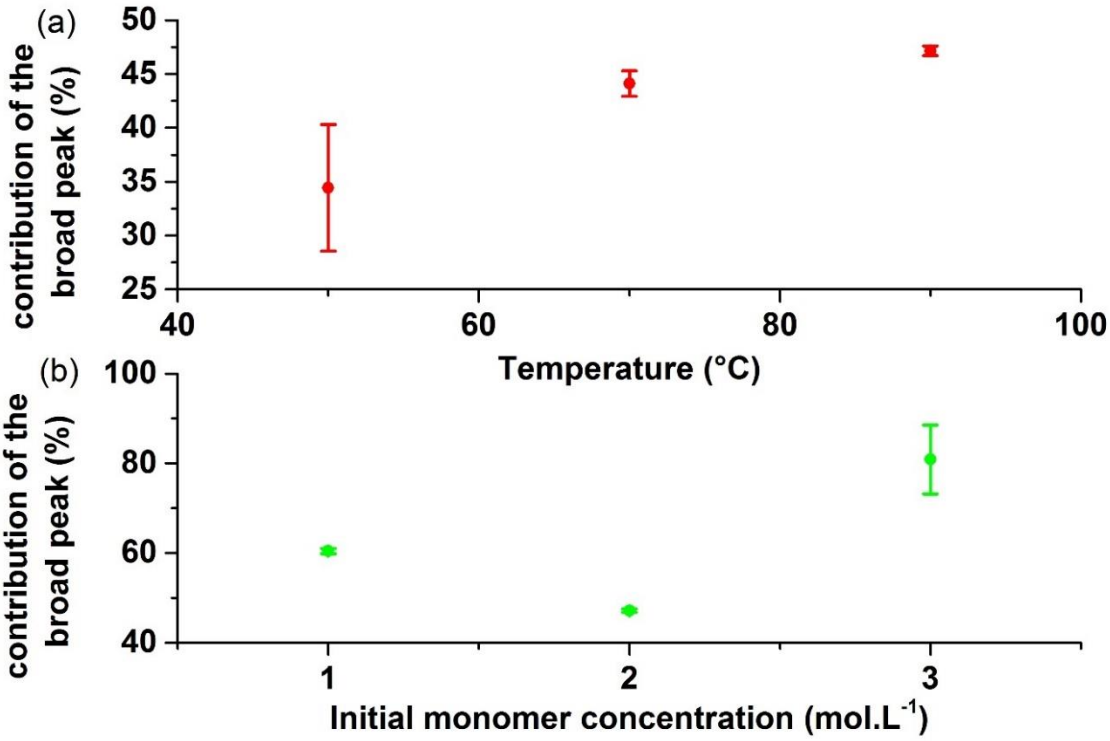

Figure 3.17: Contribution of the broad peak to the total peak area for PNaAs synthesized by conventional radical polymerization as a function of (a) polymerization temperature and (b) initial monomer concentration.

Table 3.4: Contribution of the broad peak to the total area for hyperbranched and 3-arm star PNaAs.

	3-arm star PNaA	Hyperbranched PNaA
Contribution of broad peak	71.8 %	41.8 %
Standard deviation	1.18 %	0.47 %

Table 3.4 shows that the sharp peak contributes more for the hyperbranched than for the 3-arm star PNaA. As the *DB* of the hyperbranched PNaA is greater than that of the 3-arm star PNaA [9, 38], this confirms the previous hypothesis from peak identification that the sharp peak is more likely from a highly branched population.

Figure 3.16 shows that the contribution of the broad peak increases with the temperature of synthesis. This means that if the synthesis of PNaA is carried out at high temperature, the proportion of slightly branched chains will increase. This result can be interpreted using the kinetics of the formation of branches. Two paths are possible, intermolecular chain transfer to polymer (or random intramolecular transfer to polymer) leading to LCB, and intramolecular chain transfer to polymer (also called backbiting) leading to SCB [39]. As more initiator is decomposed at high temperature, more chains are expected to be formed, and less entanglement should occur, because the chains are shorter. The high activation energy of backbiting might mean that SCB has a higher relative occurrence than LCB at high temperature.

There should be more LCB at higher initial monomer concentration simply because the polymer concentration will ultimately be higher [40, 41]. Moreover, these polymers were obtained with a conversion > 90 % (see table A.2.2 in the Appendix 2). Thus the contribution of the broad peak is expected to diminish while increasing the initial monomer concentration. This is observed in Figure 10 between 1 and 2 mmol L^{-1}. However the point at 3 mmol L^{-1} is unexpected. The experiment was repeated several times and the presence and size of the sharp peak was not repeatable. The most likely explanation is that as the branching decreases the solubility, the sharp peak might be in the non-soluble fraction of PNaA, and thus not always detected by UV absorbance. Because of this, the results cannot be used to confirm any hypothesis.

3.4 Conclusions

This work has allowed better understanding of the mechanism of separation of water soluble polyelectrolytes using CE-CC. The separation of PNaAs by branching in sodium borate, which was observed previously is confirmed. However, μ_{ep} does not always decrease when the degree of branching increases. This depends on the buffer concentration. In [NB110], the mobility of branched PNaA is lower than that of the unbranched PNaA. This is due either to a reduction of the overall charge, as a branched PNaA (negatively charged) can easily complex with a positively charged counter ion (sodium in this case), or to an overestimation of the migration

time of the broad peak due to adsorption. At higher sodium borate concentrations, the polyelectrolyte might complex with the borate rather than with the sodium. As a result, the overall charge might be increased, and then μ_{ep} is higher than for the unbranched species, which may not complex the borate as effectively. Based on these results, the selectivity of separation was improved. Branched PNaAs exhibit two peaks in the electropherogram. Both were identified. The sharp peak corresponds to a highly branched chain population and the broad peak to a slightly branched chain population. In [NB110], occasional overlapping between the two peaks occurs. The conditions to overcome this issue (full resolution of these peaks), high sodium borate buffer concentration is recommended (around 300 mM). Moreover, biased results due to adsorption of PNaA on the capillary are avoided. Based on these results, the heterogeneity of branching in polymers synthesized by conventional radical polymerization and by NMP were determined in optimal conditions. The sharp peak has a more homogenous branching than the sharp peak.

3.5 References

[1] P.M. Wood-Adams, J.M. Dealy, A.W. deGroot, O.D. Redwine, Effect of molecular structure on the linear viscoelastic behavior of polyethylene, Macromolecules, 33 (2000) 7489-7499.

[2] A.R. Maniego, D. Ang, Y. Guillaneuf, C. Lefay, D. Gigmes, J.R. Aldrich-Wright, M. Gaborieau, P. Castignolles, Separation of poly(acrylic acid) salts according to topology using capillary electrophoresis in the critical conditions, Analytical and Bioanalytical Chemistry, 405 (2013) 9009-9020.

[3] M. Gaborieau, P. Castignolles, Size-exclusion chromatography (SEC) of branched polymers and polysaccharides, Analytical and Bioanalytical Chemistry, 399 (2011) 1413-1423.

[4] J. Lena, A.K. Goroncy, J.J. Thevarajah, A.R. Maniego, G.T. Russell, P. Castignolles, M. Gaborieau, Effect of transfer agent, temperature and initial monomer concentration on branching in poly(acrylic acid): a study by 13C NMR spectroscopy and capillary electrophoresis Polymer, (2016, in press).

[5] T. Junkers, M. Schneider-Baumann, S.P.S. Koo, P. Castignolles, C. Barner-Kowollik, Determination of propagation rate coefficients for methyl and 2-ethylhexyl acrylate via high frequency PLP-SEC under consideration of the Impact of chain branching, Macromolecules, 43 (2010) 10427-10434.

[6] P. Castignolles, Transfer to polymer and long-chain branching in PLP-SEC of acrylates, Macromolecular Rapid Communications, 30 (2009) 1995-2001.
[7] I. Lacik, M. Stach, P. Kasak, V. Semak, L. Uhelska, A. Chovancova, G. Reinhold, P. Kilz, G. Delaittre, B. Charleux, I. Chaduc, F. D'Agosto, M. Lansalot, M. Gaborieau, P. Castignolles, R.G. Gilbert, Z. Szablan, C. Barner-Kowollik, P. Hesse, M. Buback, SEC analysis of poly(acrylic acid) and poly(methacrylic acid), Macromolecular Chemistry and Physics, 216 (2015) 23-37.
[8] P. Castignolles, R. Graf, M. Parkinson, M. Wilhelm, M. Gaborieau, Detection and quantification of branching in polyacrylates by size-exclusion chromatography (SEC) and melt-state C-13 NMR spectroscopy, Polymer, 50 (2009) 2373-2383.
[9] J.J. Thevarajah, A.T. Sutton, A.R. Maniego, E.G. Whitty, S. Harrisson, HervéCottet, P. Castignolles, M. Gaborieau, Quantifying the heterogeneity of chemical structures in complex charged polymers through the dispersity of their distributions of electrophoretic mobilities or of oompositions, Analytical Chemistry, 88 (2016) 1674-1681.
[10] C.J. Evenhuis, R.M. Guijt, M. Macka, P.J. Marriott, P.R. Haddad, Temperature profiles and heat dissipation in capillary electrophoresis, Analytical Chemistry, 78 (2006) 2684-2693.
[11] R. Plasson, H. Cottet, Determination of homopolypeptide conformational changes by the modeling of electrophoretic mobilities, Analytical Chemistry, 77 (2005) 6047-6054.
[12] C. Walldal, S. Wall, D. Biddle, A study of the interactions between cationic polymers and colloidal silicic acid, Colloids and Surfaces a-Physicochemical and Engineering Aspects, 131 (1998) 203-213.
[13] H. Cottet, P. Gareil, O. Theodoly, C.E. Williams, A semi-empirical approach to the modeling of the electrophoretic mobility in free solution: Application to polystyrenesulfonates of various sulfonation rates, Electrophoresis, 21 (2000) 3529-3540.
[14] D.A. Hoagland, E. Arvanitidou, C. Welch, Capillary electrophoresis measurements of the free solution mobility for several model polyelectrolyte systems, Macromolecules, 32 (1999) 6180-6190.
[15] A. Ibrahim, S.A. Allison, H. Cottet, Extracting information from the ionic strength dependence of electrophoretic mobility by use of the slope plot, Analytical Chemistry, 84 (2012) 9422-9430.
[16] C. Desruisseaux, D. Long, G. Drouin, G.W. Slater, Electrophoresis of composite molecular objects. 1. Relation between friction, charge, and ionic strength in free solution, Macromolecules, 34 (2001) 44-52.

[17] S. Bekri, L. Leclercq, H. Cottet, Influence of the ionic strength of acidic background electrolytes on the separation of proteins by capillary electrophoresis, Journal of Chromatography A, 1432 (2016) 145-151.
[18] Y. Mechref, G.K. Ostrander, Z. El Rassi, Capillary electrophoresis of carboxylated carbohydrates - IV. Adjusting the separation selectivity of derivatized carboxylated carbohydrates by controlling the electrolyte ionic strength at subambient temperature and in the absence of electroosmotic flow, Journal of Chromatography A, 792 (1997) 75-82.
[19] A. Ezhova, K. Huber, Specific interactions of Ag+ ions with anionic polyacrylate chains in dilute solution, Macromolecules, 47 (2014) 8002-8011.
[20] J.J. Thevarajah, J.C. Bulanadi, M. Wagner, M. Gaborieau, P. Castignolles, Towards a less biased dissolution of chitosan, Analytica Chemica Acta, 935 (2016) 258-268.
[21] J.D. Oliver, M. Gaborieau, P. Castignolles, Ethanol determination using pressure mobilization and free solution capillary electrophoresis by photo-oxidation assisted ultraviolet detection, Journal of Chromatography A, 1348 (2014) 150-157.
[22] T. Le Saux, H. Cottet, Size-based characterization by the coupling of capillary electrophoresis to Taylor dispersion analysis, Analytical Chemistry, 80 (2008) 1829-1832.
[23] J. Ostergaard, H. Jensen, Simultaneous evaluation of ligand binding properties and protein size by electrophoresis and Taylor dispersion in capillaries, Analytical Chemistry, 81 (2009) 8644-8648.
[24] L.T. Cherney, A.P. Petrov, S.N. Krylov, One-dimensional approach to study kinetics of reversible binding of protein on capillary walls, Analytical Chemistry, 87 (2015) 1219-1225.
[25] P. Castignolles, M. Gaborieau, E.F. Hilder, E. Sprong, C.J. Ferguson, R.G. Gilbert, High-resolution separation of oligo(acrylic acid) by capillary zone electrophoresis, Macromolecular Rapid Communications, 27 (2006) 42-46.
[26] J.J. Thevarajah, M. Gaborieau, P. Castignolles, Separation and Characterization of Synthetic Polyelectrolytes and Polysaccharides with Capillary Electrophoresis, Advances in Chemistry, (2014) Article ID 798503.
[27] A.R. Maniego, D. Ang, Y. Guillaneuf, C. Lefay, D. Gigmes, J.R. Aldrich-Wright, M. Gaborieau, P. Castignolles, Separation of poly(acrylic acid) salts according to topology using capillary electrophoresis in the critical conditions, Analytical and Bioanalytical Chemistry, 405 (2013) 9009-9020.
[28] E.G. Whitty, A.R. Maniego, S.A. Bentwitch, Y. Guillaneuf, M.R. Jones, M. Gaborieau, P. Castignolles, Cellular response to linear and branched poly(acrylic acid), Macromolecular Bioscience, 15 (2015) 1724-1734.

[29] I. Recio, E. Molina, M. Ramos, M. Defrutos, Quantitative-analysis of major whey proteins by capillary electrophoresis using uncoated capillaries, Electrophoresis, 16 (1995) 654-658.
[30] J.P. Landers, R.P. Oda, T.C. Spelsberg, J.A. Nolan, K.J. Ulfelder, Capillary electrophoresis - A powerful microanalytical technique for bIiologically-active molecules, Biotechniques, 14 (1993) 98-&.
[31] J.S. Green, J.W. Jorgenson, Minimizing adsorption of proteins on fused-silica in capillary zone electrophoresis by the addition of alkali-metal salts to the buffers, Journal of Chromatography, 478 (1989) 63-70.
[32] M.M. Bushey, J.W. Jorgenson, Capillary electrophoresis of proteins in buffers containing high-concentrations of zwitterionic salts, Journal of Chromatography, 480 (1989) 301-310.
[33] M.R. Toutounji, M.P. Van Leeuwen, J.D. Oliver, A.K. Shrestha, P. Castignolles, M. Gaborieau, Quantification of sugars in breakfast cereals using capillary electrophoresis, Carbohydrate Research, 408 (2015) 134-141.
[34] J.D. Oliver, A.T. Sutton, N. Karu, M. Phillips, J. Markham, P. Peiris, E.F. Hilder, P. Castignolles, Simple and robust monitoring of ethanol fermentations by capillary electrophoresis, Biotechnology and Applied Biochemistry, 62 (2015) 329-342.
[35] J.C. Reijenga, T. Verheggen, J. Martens, F.M. Everaerts, Buffer capacity, ionic strength and heat dissipation in capillary electrophoresis, Journal of Chromatography A, 744 (1996) 147-153.
[36] W. Friedl, J.C. Reijenga, E. Kenndler, Ionic-strength and charge number correction for mobilities of multivalent organic-anions in capillary electrophoresis, Journal of Chromatography A, 709 (1995) 163-170.
[37] J. Chamieh, M. Martin, H. Cottet, Quantitative analysis in capillary electrophoresis: Transformation of raw electropherograms into continuous distributions, Analytical Chemistry, 87 (2015) 1050-1057.
[38] A.R. Maniego, A.T. Sutton, Y. Guillaneuf, C. Lefay, M. Destarac, C.M. Fellows, P. Castignolles, M. Gaborieau, Characterization of branching in poly(acrylic acid) prepared by controlled and conventional radical polymerization, Manuscript in preparation.
[39] T. Junkers, C. Barner-Kowollik, The role of mid-chain radicals in acrylate free radical bolymerization: Branching and scission, Journal of Polymer Science Part A-Polymer Chemistry, 46 (2008) 7585-7605.
[40] J. Loiseau, N. Doerr, J.M. Suau, J.B. Egraz, M.F. Llauro, C. Ladaviere, Synthesis and characterization of poly(acrylic acid) produced by RAFT polymerization. Application as a very efficient dispersant of CaCO3, kaolin, and TiO2, Macromolecules, 36 (2003) 3066-3077.

[41] N.M. Ahmad, D. Britton, F. Heatley, P.A. Lovell, Chain transfer to polymer in emulsion polymerization, Macromol. Symp., 143 (1999) 231-241.

Chapter 4

Effect of transfer agent and temperature on branching and *β*-scission in radical polymerization of 2-ethylhexyl acrylate

This work has been accepted as: J.-B. Lena, M. Deschamps, S.L. Masters, M.A. Squire, G.T. Russell, Effect of transfer agent and temperature on branching and *β*-scission in radical polymerization of 2-ethylhexyl acrylate, *Macromolecular Chemistry & Physics*, (macp.201700579).

4.1 Introduction

Poly(2-ethylhexyl acrylate) (P2EHA) is a hydrophobic polymer. The long ester sidegroup strongly influences properties such as viscosity and glass transition temperature, T_g, which is far below room temperature. A high number of applications of P2EHA have been reported in the literature. The main ones are waterborne coatings [1], pressure sensitive adhesives [2] – thanks to its low T_g – and nanocomposites [3]. As stated in chapter 1, P2EHA is branched.LCB and SCB have been detected in P2EHA [4]. In term of kinetics, SCB arises from intramolecular transfer, also known as backbiting, of rate coefficient k_{bb}, while LCB arises either from random intramolecular transfer or from intermolecular transfer to polymer. All three of these reactions transform a secondary propagating radical (SPR) into a mid-chain radical (MCR). MCRs can undergo several reactions.. Most of these reactions are presented in Scheme 2.1 in Chapter 2.

It is important to note that a study on P2EHA by electrospray-ionization (ESI) MS has demonstrated that the radical on an MCR can migrate along the chain, which could lead either to different branch lengths (if propagation and termination occur) or different sizes of unsaturated dead chain, due to β-scission [5]. For a more detailled overview on this melting pot of reactions, the reader is referred to a recent review on "Radical polymerization of acrylic monomers". Of course it is well known that branching primarly influences the properties of a polymer: short branches influence physical properties such as density, melting point and glass transition temperature, while long branches primarly influence rheological properties, as already mentionned in Chapter 2 [6].

^{13}C NMR spectroscopy is by far the superior method for quantification of branching in polymers. At a branching point there is a quaternary carbon, denoted C_q, that exhibits a signal around 48 ppm [4, 7, 8]. Details on the calculation of the average degree of branching are already given in Chapter 1 and 2. Various NMR methods – solid-state, solution-state and melt-state – have been tested for the study of branching [9]. Melt state appears to provide the highest resolution [9]. For optimal analyses, melt-state ^{13}C NMR spectroscopy is best performed at T_g + 150 °C [9]. As the T_g of P2EHA is quite low and P2EHA is expected to degrade above 300 °C, this method can be applied to quantify the branching in P2EHA [9].

Both ^{13}C solution- and melt-state NMR spectroscopy were previously used to quantify the branching in P2EHA synthesized in solution and emulsion [4, 7-9]. Similar studies were carried

out for other poly(alkyl acrylate)s [4, 10-14] and poly(acrylic acid) (PAA) [15-18]. In 2001, Heatley *et al.* quantified the branching in P2EHA produced in solution by ^{13}C solution-state NMR spectroscopy. Their results indicated that transfer to polymer: (i) Increases with conversion, which would be expected due to rising [P] (if intermolecular in nature) and/or decreasing [M] (if intramolecular); (ii) Increases as the initial monomer concentration decreases, which is most likely explained by a decreasing frequency of SPR propagation. Another effect they observed was (iii) *DB* of P2EHA is higher than *DB* of poly(*n*-butyl acrylate) (P*n*BA) prepared under the same conditions. They concluded that "changes in k_{bb}/k_p must account for the observed differences in the extent of chain transfer to polymer" [7], i.e., that this rate coefficient ratio must be larger for 2EHA. Certainly this is in accord with the recent results of Kattner and Buback, who found that the fraction of MCR sites increases as side-group length increases [19]. One would expect this to result from higher preexponential factor rather than altered activation energy [7, 19].

Theoretically, branches could be formed in 2EHA polymerization on the ester side group as it contains a tertiary CH, which is a potential site for hydrogen abstraction. This would lead to a quaternary carbon whose ^{13}C NMR signal is predicted to be ~45 ppm. However, this signal has never been observed. Furthermore, it is now widely accepted that transfer to polymer in acrylates occurs at tertiary CH sites in the polymer backbone, as these are "activated" by the adjacent carbonyl group.

In 2001, Plessis *et al.* demonstrated that in emulsion polymerization of 2EHA, *DB* increases with the initiator concentration and decreases with the monomer concentration, which suggests that most branches are formed by backbiting [8]. Even if intramolecular transfer is dominant, the occurrence of some LCB due to intermolecular transfer was also suggested by gel formation [8]. In 2004, Sato *et al.* studied the polymerization in benzene of 2EHA and tert-butyl acrylate (*t*BA). Using electron paramagnetic resonance (EPR) spectroscopy, the presence of both LCB and SCB was demonstrated. Also, the MCR concentration in 2EHA polymerization was shown to be higher than that in *t*BA polymerization [4], and their studies of branching by ^{13}C NMR spectroscopy confirmed a higher *DB* for P2EHA than for P*t*BA. However, they suggested that this could be due to a faster termination process in the case of *t*BA polymerization. ^{1}H NMR spectra showed the presence of unsaturated groups, providing evidence for the occurrence of *β*-scission. They showed that if the polymerization is carried out at 25 °C, the presence of MCRs is important but neither branching nor *β*-scission can be detected by NMR spectroscopy

[4]. This suggests that both fragmentation and propagation of MCRs are negligible at such a low temperature.

Studies on PAA and P*n*BA show that *DB* increases with the temperature, which is likely due to an increase in k_{bb}/k_p due to backbiting having a higher activaiton energy. Furthermore, *DB* is considerably reduced by the presence of a CTA among the reactants [20]. Two explanations were suggested: either a reduction in backbiting as the polymerization occurs for a shorter time, or transfer from a CTA to the MCR, known as the "patching effect" [11, 15, 21].

The development of ESI-MS has enabled determination of the product spectrum of a polymer sample and its changes within the chain length distribution [20, 22]. Polymer chains can be sorted precisely according to their end groups and chain length. The influence of temperature and of CTA concentration on the structure of P*n*BA has been studied by ESI-MS [23, 24]. The amount of *β*-scission increased with temperature and decreased with CTA concentration. However, it is challenging to obtain consistent ionization of different macromolecules within a sample: it is well known that different end-groups [25] or molar masses [26] can affect the ionization efficiency. This limits the accuracy of the average molar mass values and molar mass distributions determined by MS. In 2013, Vandenbergh *et al.* detected the *β*-scission products (without specific quantification) of P2EHA synthesized by controlled radical polymerization as well as the chain length selectivity [5].

LCB was detected in P2EHA produced by PLP using multiple-detection size-exclusion chromatography (SEC), even at low temperature (down to –34 °C) [27] and at low conversion.[28] The local dispersities, $Đ(V_h)$, obtained can reach values close to 2. This means that the error in molar mass determination using SEC can reach 100 % [27-29]. The occurrence of LCB, leading to inaccurate molar mass determination by SEC, is more important for P2EHA than for acrylates with shorter side groups, like P*n*BA and poly(methyl acrylate). It was suggested that the bulky ester group of 2EHA does not favour the formation of a six-membered ring, and thus more random intramolecular transfer would occur [29]. One consequence of the presence of LCB is inaccurate k_p determination using the technique of pulsed laser polymerization coupled with SEC (PLP-SEC). Even though there have been several attempts to determine k_p in 2EHA polymerization, it is suspected that the obtained values suffer from relatively low accuracy due to LCB. For example, the error in PLP-SEC values for P2EHA was estimated to be between 30 – 100 % for –34 °C < T < 22 °C [27].

Although – as outlined above – there is a reasonably sized body of work on branching in acrylates, including some attention to 2EHA in particular, there are several motivations for the present investigation: (1) As is evident, there is some conflict in the literature: whether branching is present in P2EHA synthesized at low temperature, how the *DB* of P2EHA compares with that for other acrylates (with the different literature trends giving rise to contrasting mechanistic explanations), and so on; (2) Literature studies have not always been as systematic as one would prefer; (3) Advances in NMR instruments and in understanding of how best to use NMR for branching investigations mean that more accurate data may now be obtained; and (4) It is aimed to build on the preceding study of PAA (detailed in Chapter 2) [15], in particular with a view to establishng the effect of sidegroup size on *DB*. For these reasons, the aim of this work was to synthesize P2EHA in bulk at various temperatures (from 4 °C to 140 °C) both with and without CTA. The end-groups of CTA-containing P2EHA were characterized using ESI-MS, and the *DB* as well as the degree of *β*-scission, *DβS*, of all P2EHA samples were determined by ^{13}C melt-state NMR spectroscopy, where *DβS* is defined here as the number of unsaturated end groups produced by *β*-scission per monomer unit, i.e., in analogy with *DB*.

4.2 Materials and methods

4.2.1 Materials

2,2'-azobisisobutyronitrile (AIBN) was purchased from Akzo Nobel. Aluminium oxide, activated basic, Brockmann I, standard grade was provided by Sigma-Aldrich. Iron (II) sulphate 7-hydrate (ferrous sulphate) was purchased from BDH laboratories. *Tert*-butyl hydroperoxide (*t*-BuOOH) (5.5 mol L^{-1} in decane) was purchased from Fluka. 1-dodecanethiol ($\geq$ 98%) and 2-ethylhexyl acrylate (2EHA) (98%) were purchased from Aldrich Chemistry. Chloroform-d_3 ($\geq$ 99.75%) was provided by Acros Organics. Acetonitrile and methanoic acid (analytical grade) were provided by Fluka. Dichloromethane (DCM; HPLC grade) and methanol (MeOH; HPLC grade) were passed through a solvent purification system [30].

AIBN was recrystallized twice in methanol. 2EHA was passed through a column of activated basic alumina to remove the inhibitor. 1-dodecanethiol, iron (II) sulfate and *t*-BuOOH were used as received.

4.2.2 Synthetic methods

4.2.2.1 Synthesis with a thermal initiator

Into a Schlenk round bottom flask, 6.5 mL of 2EHA (3.1×10^{-2} mol), 0 or 0.62 mL of 1-dodecanethiol (0 or 2.6×10^{-3} mol) and 5.5 mg of AIBN (3.3×10^{-5} mol) were added. The Schlenk round bottom flask was degassed by bubbling nitrogen through the solution for 30 min. The mixture was left under stirring at 65 °C, 100 °C or 140 °C for 24 hr, 40 min and 20 min respectively. After these reactions times, the samples were quenched in ice water. Excess unreacted thiol compound and residual monomer were removed under vacuum on a Schlenk line at ambient temperature for 5 days. Conversion was determined by gravimetry and ^{13}C NMR spectroscopy. Detailed results are in Table A.4.1.

4.2.2.2 Synthesis with a redox initiator

Into a Schlenk round bottom flask, 3.5 g of 2EHA (1.9×10^{-2} mol), 0 or 417 µL of 1-dodecanethiol (1.7×10^{-3} mol) were added. The Schlenk round bottom flask was degassed by bubbling nitrogen through the solution for 30 min, then 2.22 g of iron (II) sulfate (7.9×10^{-3} mol) and 200 µL of *t*-BuOOH (2.1×10^{-3} mol) were added. Samples were then left under stirring at room temperature for 24 hours, or in the fridge at 4 °C for 4 days or 9 days for synthesis with and without CTA respectively. The samples were quenched by opening the flask. Excess unreacted thiol compound and residual monomer were removed under vacuum on a Schlenk line at ambient temperature for 5 days. Conversions were measured by ^{1}H solution-state NMR spectroscopy. Details about the conversion measurement are given in the Supporting Appendix 2 (Figures A.4.1 to A.4.3).

1-dodecanethiol (DDM) was chosen as CTA because it is known to function well for polymerization of alkyl (meth)acrylates in bulk [31, 32].

4.2.2.3 Summary

Table 4.1 summarises all reactions conditions together with resulting conversion and number-average degree of polymerization, DP_n. The latter were determined by comparing the (NMR) signals of terminal CH_2 to main chain CH. End groups corresponding to dead chains formed by combination were too low to detect by ^{13}C NMR spectroscopy. Consequently, the number of end groups is underestimated and so DP_n values are overestimated. Of course this analysis is only possible where chain lengths are relatively short, as promoted by higher temperature and the presence of CTA.

Table 4.1: Temperatures, reactants and conversions of 2EHA polymerizations.

Sample	Initiator/CTA	Reaction temperature	Reaction time	Final conversion	DP_n (with error*)
P2EHA-1	AIBN/DDM	140 °C	20 min	81 %	8.1 ± 1.5%
P2EHA-2	AIBN/none	140 °C	20 min	89 %	33.7 ± 10%
P2EHA-3	AIBN/DDM	100 °C	40 min	79 %	7.4 ± 16%
P2EHA-4	AIBN/none	100 °C	40 min	87 %	26.2 ± 12%
P2EHA-5	AIBN/DDM	65 °C	24 h	59 %	14.6 ± 9.2%
P2EHA-6	AIBN/none	65 °C	24 h	93 %	–
P2EHA-7	Fe^{2+} + *t*-BuOOH/DDM	25 °C	24 h	87 %	14.5 ± 5.6%
P2EHA-8	Fe^{2+} + *t*-BuOOH/none	25 °C	24 h	80 %	–
P2EHA-9	Fe^{2+} + *t*-BuOOH/DDM	4 °C	4 days	91 %	–
P2EHA-10	Fe^{2+} + *t*-BuOOH/none	4 °C	9 days	70 %	–

* Obtained by considering the error in the area of each NMR signal used to determine DP_n.

4.2.3 Electrospray ionization-mass spectrometry

Analyses were carried out by Marie Squire (University of Canterbury)

The samples for ESI-MS analysis were prepared as follows: 1 mg of P2EHA was dissolved in 1 mL of DCM/MeOH (7/3 v/v). The samples were injected into a Thermo Fisher Scientific Dionex UltiMate 3000 liquid chromatography (LC) system (without a column) comprised of an Ultimate 3000 RS Pump, 3000 RS Autosampler, 3000 RS Column Compartment and a 3000 Diode Array Detector. The LC system was attached to a Bruker maXis 3G Ultra High

Resolution -Qq- Time of Flight tandem mass spectrometer (Bruker Daltonik GmbH, Bremen, Germany). The isocratic mobile phase comprised 0.1% (v/v) formic acid and 50% (v/v) acetonitrile in water at a flow rate of 200 μL min^{-1}. Ions were generated by electrospray ionization (ESI) and cleansed of solvent by a nitrogen flow of 8.0 L min^{-1} with temperature of 200 °C, nebulizer at 1 bar, end plate offset at 500 V, capillary voltage at 4000 V; analysis was in positive-ion mode. The intensity of positive ions was recorded in the range of 100–3000 *m*/*z*, at a rate of 2 s^{-1} and analysed using Bruker Compass HyStar 3.2 – SR 2 (Build 44). ESI-L Low Concentration Tuning Mix (Agilent Technologies) was injected after each sample as a calibrant.

4.2.4 Thermal analyses

4.2.4.1 Differential scanning calorimetry

Analyses were carried out by Dr. Hank de Bruyn and Dr. Natasha Sciortino (University of Sydney, Australia).

P2EHAs were analysed with a Mettler 823E DSC instrument. Samples were accurately weighed into 40 μL aluminium crucibles and crimped shut with a pierced lid. A similar empty crucible with a crimped pierced lid was used as a reference. The samples were cycled in a heat-cool-heat sequence between –150 °C and 150°C at rate of 10 °C min^{-1} under a high purity nitrogen gas flow of 50 mL min^{-1}. Some sample measurements included an additional 'cooling-heating' step. The first heating and cooling steps are used to erase the thermal history of the samples and detect evaporation of small molecules trapped in the samples. Data analyses for determining T_g values were carried out using the last heating cycle thermogram. Results are presented in Figure A.4.4 of the Appendix 2.

4.2.4.2 Thermogravimetric analysis

Some analyses were carried out by Dr. Hank de Bruyn and Dr. Natasha Sciortino (University of Sydney, Australia)

Thermogravimetric analyses on samples P2EHA-1 to -4 were performed using a TA Instruments Discovery TGA. Samples (5–15 mg) were weighted into tared platinum TGA pans

and heated to 900 °C at 10 °C min^{-1} under a flow of N_2. Samples P2EHA-5 to -10 (5–15 mg) were analysed on a Texas instrument Q-600 thermogravimetric analyser. Again, TGA was carried out under nitrogen atmosphere with the temperature increased from room temperature to 900 °C at 10 °C min^{-1}. The degradation temperature was determined from a significant mass loss step in the mass versus temperature curve. In some cases a smaller mass loss step was observed at around 100 °C due to loss of hydration water (previously absorbed by the sample). Results are presented in Figure A.4.5 to A.4.7 of the Appendix 2.

4.2.5 NMR Spectroscopy

4.2.5.1 Solution-state NMR spectroscopy

4.2.5.1.1 Conditions of analyses

^{1}H NMR spectra of P2EHAs synthesized at 25 °C and 4 °C were acquired in $CDCl_3$ at 25 °C on an Agilent 400 MHz NMR with Varian 7600-AS auto-sampler, equipped with a oneNMR probe and variable temperature capabilities, operating at a Larmor frequency of 399.84 MHz. A few mg of P2EHA were dissolved in a few mL of $CDCl_3$. ^{1}H NMR spectra were acquired with 16,384 data points, 8 scans, 16 ppm spectral width (6410.3 Hz), 40 s relaxation delay, 2.556 s acquisition time and 90° flip angle. As the peaks were not assigned using solution-state NMR, the scale was not calibrated for these spectra, which were used only for the measurement of conversion.

4.2.5.1.2 Measurement of the longitudinal relaxation time T_1

Prior to this an inversion recovery experiment was carried out to measure the longitudinal relaxation time, T_1, of the residual monomer signals as well as the CH and CH_2 main-chain signals. Theinversion recovery experiment was carried out with 32 values of τ. Results are given below;

Table 4.2: T_1 values for the main chain CH and residual monomer signals. These measurements were carried out with the P2EHA synthesized at 25 °C without CTA, and were injected into $CDCl_3$ at room temperature at a few mg per mL.

Signal	Chemical shift (ppm)	T_1 (s)
Main chain CH	2.3	0.07
Residual monomer	5.7-6.5	6.3

4.2.5.2 Melt-state NMR spectroscopy

4.2.5.2.1 Conditions of analyses

These experiments were carried out by Prof. Michael Deschamps (CNRS, CEMHTI, Orleans, France)

^{13}C magic angle spinning (MAS) NMR experiments on samples P2EHA-1 to -6 were carried out on a Bruker Avance 850 MNR spectrometer operating at a Larmor frequency of 213.8 MHz for ^{13}C using a double resonance ^{1}H-^{13}C MAS 4 mm probe. The chemical shift was referenced to TMS at 0 ppm. The spinning frequency was set to 10 000 Hz to reduce the intensities of the first two spinning side bands.

^{13}C magic angle spinning (MAS) NMR experiments of samples P2EHA-7 and -8 were carried out on a Bruker Avance 400 MNR spectrometer operating at a Larmor frequency of 100.5 MHz for ^{13}C using a KelF (PTCFE) liquid insert inside a ZrO_2 rotor with KelF caps. The spinning frequency was set to 6 kHz to reduce the number of spinning side bands.

Quantitative ^{13}C NMR spectra were recorded at 50 °C with single-pulse excitation under magic-angle spinning (SPE-MAS) using 1.4 μs at high field and 4.3 μs at low field, corresponding to 25° pulse (Ernst angle), and a 10 s relaxation delay, accumulating 20 000 to 40 000 transients corresponding to two to five days of experimental time, with inverse gated spinal 64 dipolar decoupling (12.5 kHz during 82 ms acquisition time). Recording spectra with 10 and 20 s relaxation delays led to the same relative peak intensities for the C_q and backbone signals, while some peaks were not relaxed properly for shorter delays.

Full spectra of CTA-containing P2EHA and of non-CTA-containing P2EHAare in the below (figure 4.1) and in the Appendix 2 (figures A.4.9, A.4.12 and A.4.13).

4.2.5.2.2 Signals assignment

Figure 4.1 gives full ^{13}C NMR spectra for P2EHA. Figure 4.2 and 4.3 show portions of ^{13}C NMR spectra of P2EHAs synthesized at 140 °C with and without CTA. Quantitative spectra with good sensitivity were obtained with 10 s repetition delay at 50 °C, which is about 120 – 130 °C above T_g. Schemes 4.1 to 4.5 present the different structures observed by ^{13}C NMR spectroscopy. Table 4.3 provides the signal attribution.

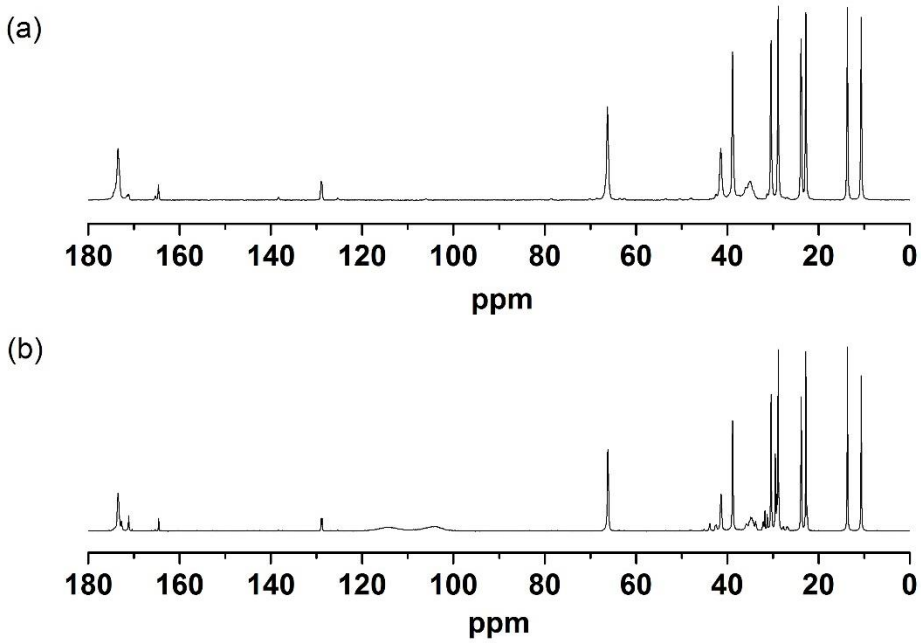

Figure 4.1: ^{13}C NMR spectra of P2EHA synthesized at 140 °C (a) without CTA and (b) with CTA.

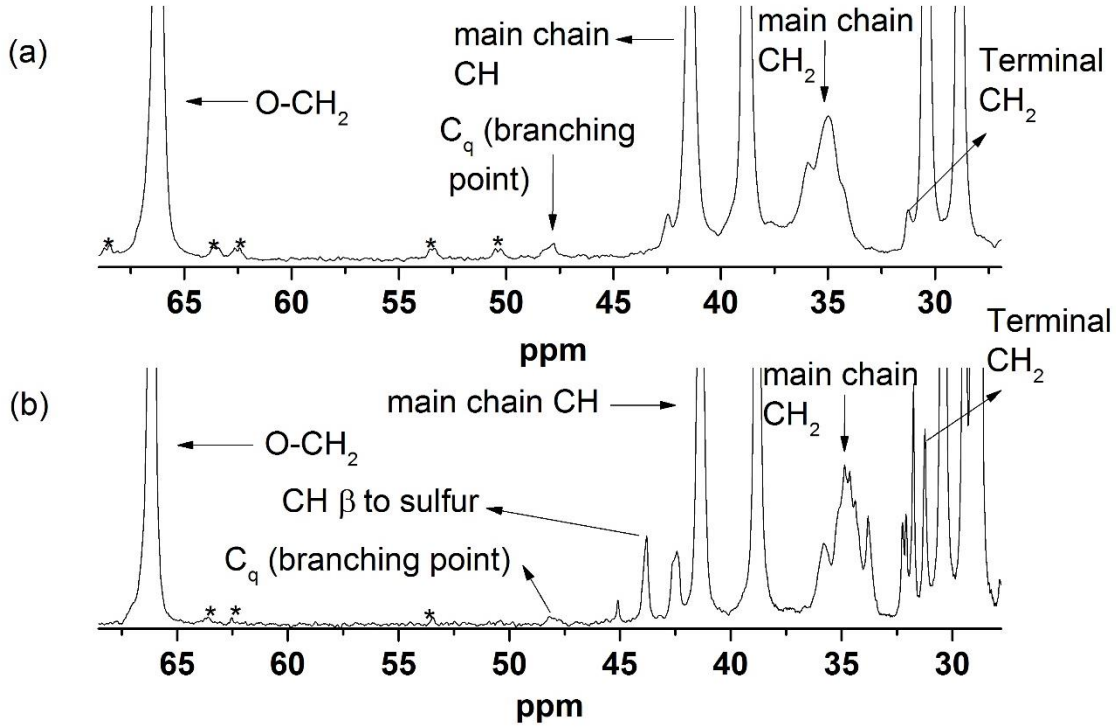

Figure 4.2: Partial ^{13}C melt-state NMR spectra (27 – 70 ppm) at 50 °C of P2EHA synthesized at 140 °C (a) without and (b) with CTA, where * denotes signals from side spinning bands.

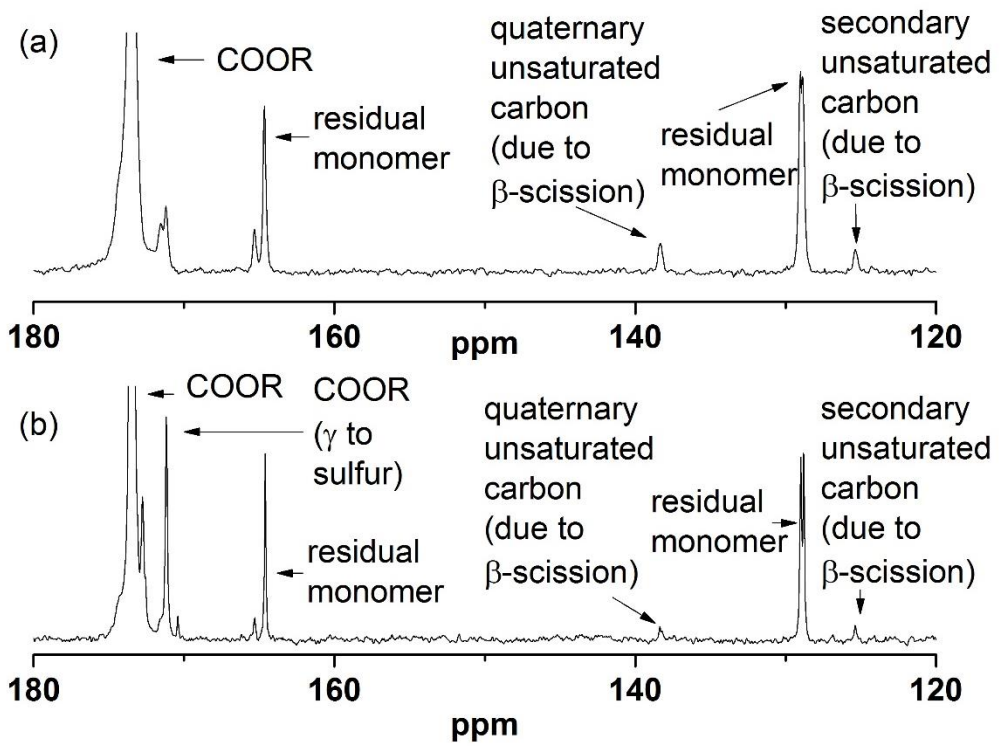

Figure 4.3: Partial ^{13}C melt-state NMR spectra (120 – 180 ppm) at 50 °C of P2EHA synthesized at 140 °C (a) without and (b) with CTA.

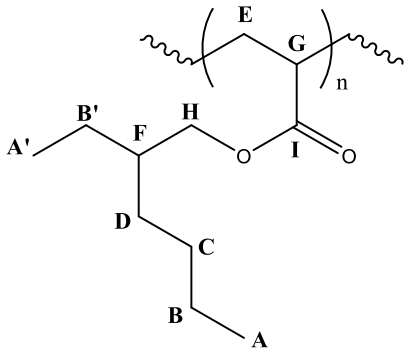

Scheme 4.1: Structure of P2EHA

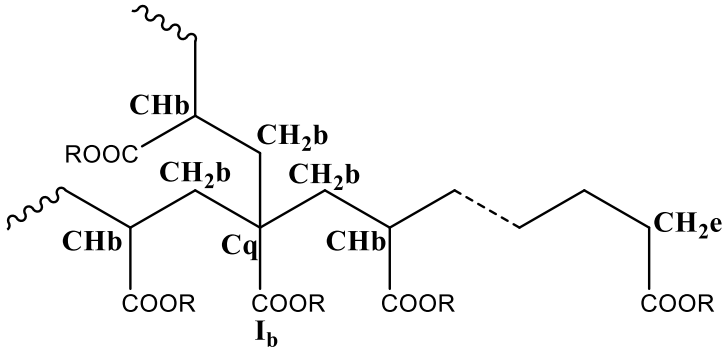

Scheme 4.2: Structure of P2EHA around a branch

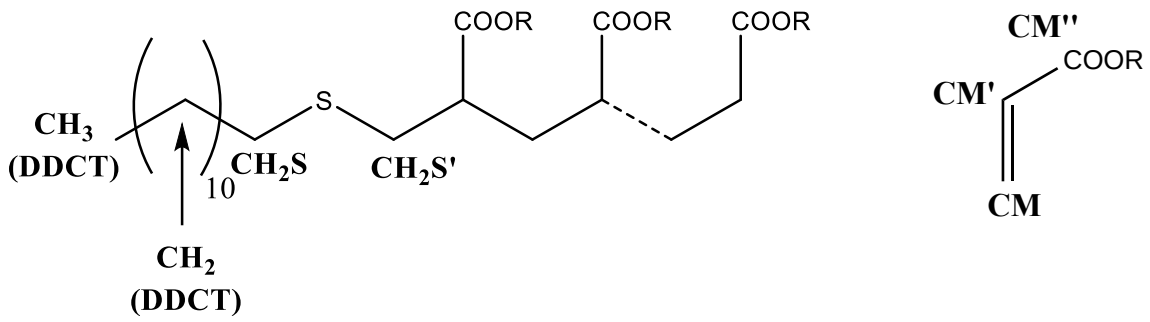

Scheme 4.3: Structure of DDM-containing P2EHA **Scheme 4.4:** Structure 2EHA

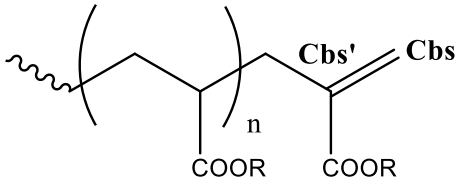

Scheme 4.5: Structure of an unsaturated P2EHA produced by *β*-scission

Table 4.3: Signal assignment for ^{13}C NMR spectra of P2EHA.

Signal	δ (ppm) (CTA-containing P2EHA)	δ (ppm) (non CTA-containing P2EHA)	δ (ppm) (literature) [8] (analysed in $CDCl_3$ at RT)	δ (ppm) (literature) [7] (analysed in $CDCl_3$ at RT)	δ (ppm) (literature) **[4]** (analysed in $CDCl_3$)
A	10.6	10.6	10.3	10.7	-
A’	13.7	13.7	13.4	14.0	-
CH_3 (DDCT)	13.7	-	-	-	-
CH_2 (DDCT) adjacent to a CH_3	22.5	-	-	-	-
B	22.8	22.8	22.6	23.0	-
B’	23.8	23.8	23.4	23.5	-
C	28.8	28.9	28.6	28.9	-
D	30.4	30.4	30.1	30.1	-
CH_2e	31.2	31.2	-	31.7	31.6
Other CH_2 (DDCT)	26-33	-	-	-	-
E	33.3-36.4	33.3-36.7	34.8-35.6	33.5-37.3	33.5-37.0
CH_2b	-	-	-	37.5-38.7	39.5
F	38.8	38.8	38.5	38.5	-
CHb	-	-	-	39.5	-
G	41.4	41.4	41.2	41.5	41.4
CH (S)	43.8	-	-	-	-
Cq	47.3-48.6	47.2-48.6	48.0	47.2-48.4	48.1
H	66.2	66.2	66.0	66.9	-
Cbs	125.4	125.3	-	125	-
CM	128.8	128.8	-	-	-
CM’	129.0	129.0	-	-	-
Cbs’	138.4	138.3	-	138	-
CM’’	164.6	164.6	-	-	-
Ib	171.2	171.2	171.2	-	-
I (S)	171.2	-	-	-	-
I	173.5	173.5	173.5	174.3	-

4.2.5.2.3 Measurement of average degree of branching and average degree of β-scission

The degree of branching, *DB*, was quantified in percentage of monomer units by comparing the integrals, *I*, of C_q at 48 ppm and of the main chain CH at 40–43 ppm as follows:

$$DB\ (\%) = \frac{100\ .\ I(C_q)}{I(C_q) + I(CH)} \qquad (4.1)$$

As ^{13}C NMR spectra showed that even after 5 days of drying in a Schlenk line, a non-negligible amount of residual monomer was still present, it was not possible to use the signals of the carbons in the ester side groups to quantify *DB*.

DB was also calculated by comparing the integrals of the quaternary carbon to that of the carboxylic ester group, as follows:

$$DB\ (\%) = \frac{100\ .\ I(C_q)}{I(COOR)} \qquad (4.2)$$

The degree of β-scission, *DβS*, was also calculated in percentage of monomer units by comparing the integrals of the quaternary unsaturated carbon produced by β-scission at 138 ppm (Cbs') and of the main chain CH at 40-43 ppm:

$$D\beta S\ (\%) = \frac{100\ .\ I(Cbs')}{I(Cbs') + I(CH)} \qquad (4.3)$$

The quaternary unsaturated carbon Cbs' was chosen rather than the secondary unsaturated carbon Cbs as the latter gives a lower signal due to potential spinning side bands.

The DMfit software package [33] was used to analyse and fit the data. It allows reconstitution of the NMR spectra by fitting the different signals as Gaussian and Lorentzian functions. The integration and relative standard deviations (*RSD)* of *DB* and *DβS* (in percent of *DB* and *DβS* values) were calculated with this software, based on the error on the amplitude of each fitted signal (more details are given below table A.4.4). The values of DB and *DβS* as well as an example of a fit are given in the Appendix 2 (Table A.4.4 and Figure A.4.8).

4.3 Results and discussions

4.3.1 Polymerization

In experiments with AIBN, final conversion was higher in the absence of CTA (see Table 4.1). This is consistent with termination being faster in the presence of DDM, which is a well known consequence of chain-length-dependent termination [34, 35]. On the other hand, CTA-containing-P2EHAs synthesized with a redox initiator have a higher conversion than the non-CTA ones, opposite to what is expected. This could be caused by a higher rate of initiation for redox systems in the presence of mercaptans, which can be oxidized to form disulfide, thus additionally stimulating peroxide reduction to generate radicals. We simply wish to note this as an observation – i.e., higher polymerization rate for redox-initiated systems in the presence of DDM – rather than investigate it in detail.

4.3.2 Thermal analyses

By DSC it was found that T_g values for our P2EHA samples were between –90 and –70 °C. This establishes that 50 °C is an acceptable temperature for melt-state NMR measurement, which should be done around T_g + 150 °C. By TGA it was shown that our polymer samples do not degrade until the temperature is above 300 °C. This confirms that the polymer still has its integrity in NMR experiments at 50 °C.

4.3.3 End groups by ^{13}C NMR spectroscopy

Number-average degree of polymerization, DP_n, was estimated by integration of ^{13}C NMR signals of main-chain CH and terminal CH_2. Where values could be obtained (i.e., chain length less than 100), they are reported in Table 4.1. They show that addition of CTA reduces DP_n, as it should, and that increasing temperature also reduces DP_n, as also would be expected (on the basis of increasing rate of initiation). As this was entirely the point of this NMR analysis, no further scrutiny of the DP_n values is carried out.

4.3.4 End groups by ESI-MS

All P2EHA samples were analysed by ESI-MS in order to deduce the end-groups. Figures 4.4 and 4.5 show partial ESI-MS spectra of P2EHA synthesized at 140, 100, 65, 25 and 4 °C.

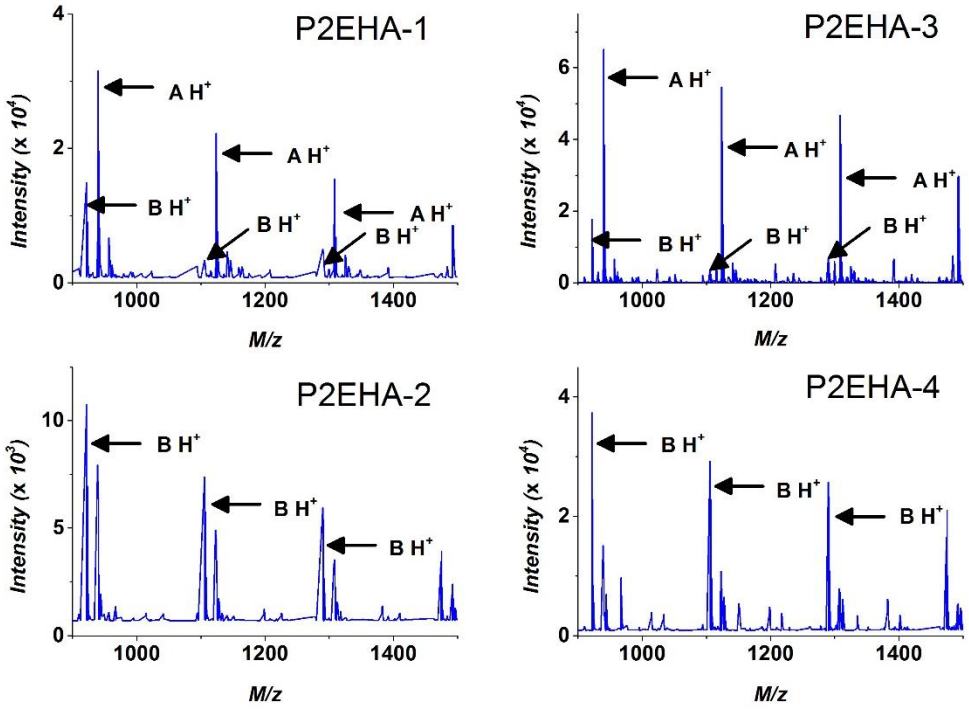

Figure 4.4: Partial ESI-MS spectra: P2EHA-1 and -2 were synthesized at 140 °C in presence and absence, respectively, of CTA; analogous for P2EHA-3 and -4 but at 100 °C. Letters refer to species in Schemes 4.6 and 4.7.

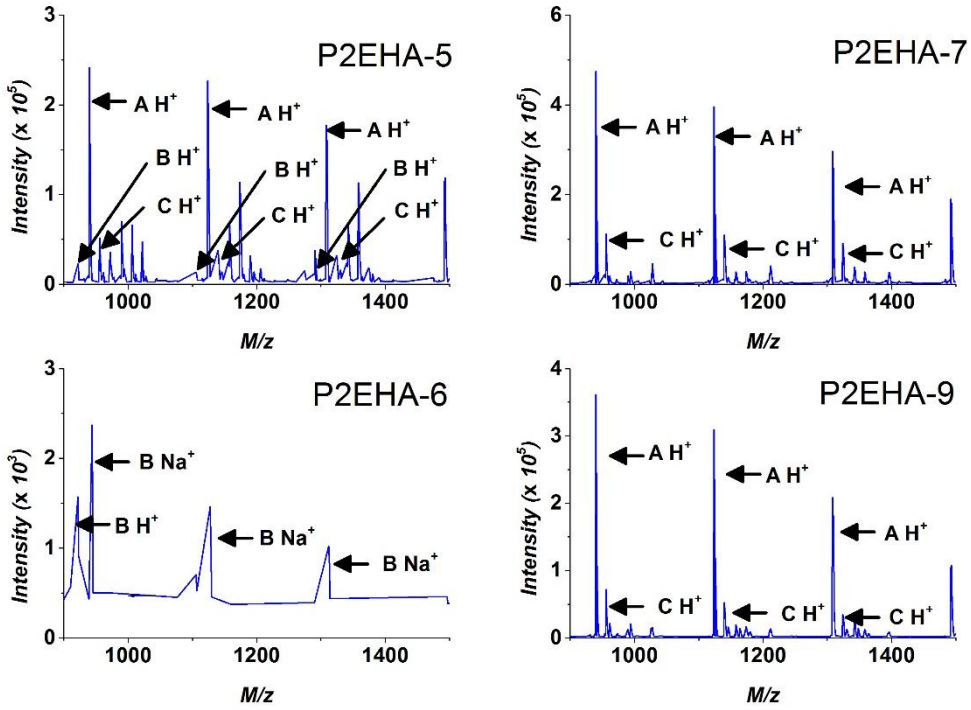

Figure 4.5: Partial ESI-MS spectra: P2EHA-5 and -6 were synthesized at 65 °C in presence and absence, respectively, of CTA; P2EHA-7 and -9 were synthesized at 25 and 4 °C, respectively, in presence of CTA. Letters refer to species in Schemes 4.6 and 4.7.

Note that P2EHA-8 and -10 were analysed by ESI-MS but only noisy spectra were obtained (figure A.4.14). These are the samples from the lowest two temperatures without CTA. Thus the polymer chains were relatively long, making ionization difficult. Furthermore, these syntheses used Fe^{2+} for initiation, and the samples were solid. Under such circumstances it is believed that iron aggregates are incorporated with the polymer, which makes ESI-MS analysis difficult. On the other hand, samples P2EHA-7 and -9 (made with CTA) were oily, with the residual iron on the bottom of the flask, and thus it did not affect the ESI-MS process.

A striking conclusion from Figures 4.4 and 4.5 is the strong presence of polymer with neither cyanoisopropyl ($(CH_3)_2(CN)C$–, from AIBN) nor $C_{12}H_{25}S$– (from DDM) as endgroups. Such polymer can only arise from *β*-scission. Thus it is established that *β*-scission occurred to a significant extent in our syntheses. We denote polymer formed from *β*-scission with a 'B'. Figures 1 and 2 also show polymer with $C_{12}H_{25}S$– and –H as endgroups. These species we denote with an 'A'; they arise from polymer started (hence $C_{12}H_{25}S$–) and terminated (–H) by transfer to CTA. They are present in samples P2EHA-1, -3, -5, -7 and -9, all the syntheses with CTA, thereby evidencing the importance of transfer to CTA in these systems, even right down

to 4 °C. This is consistent with the finding of Hutchinson *et al* [32]. that the tansfer constant for DDM has a low activation energy. Finally, polymer with $C_{12}H_{25}S$– at both ends is found in systems with CTA at and below 65 °C. Such polymer can only arise from combination – hence the 'C' label – of two macroradicals started by chain transfer. All this labelling is presented visually in the top half of Scheme 4.6.

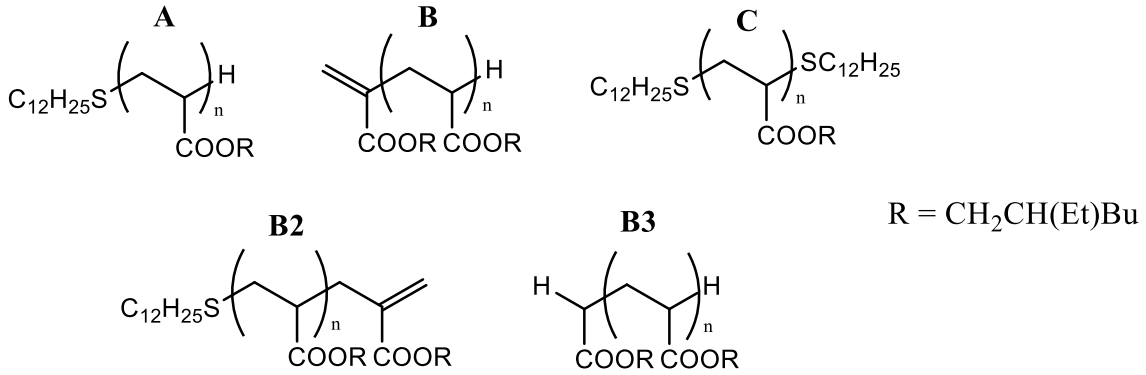

Scheme 4.6: Structure of P2EHA species detected by ESI-MS (see text)

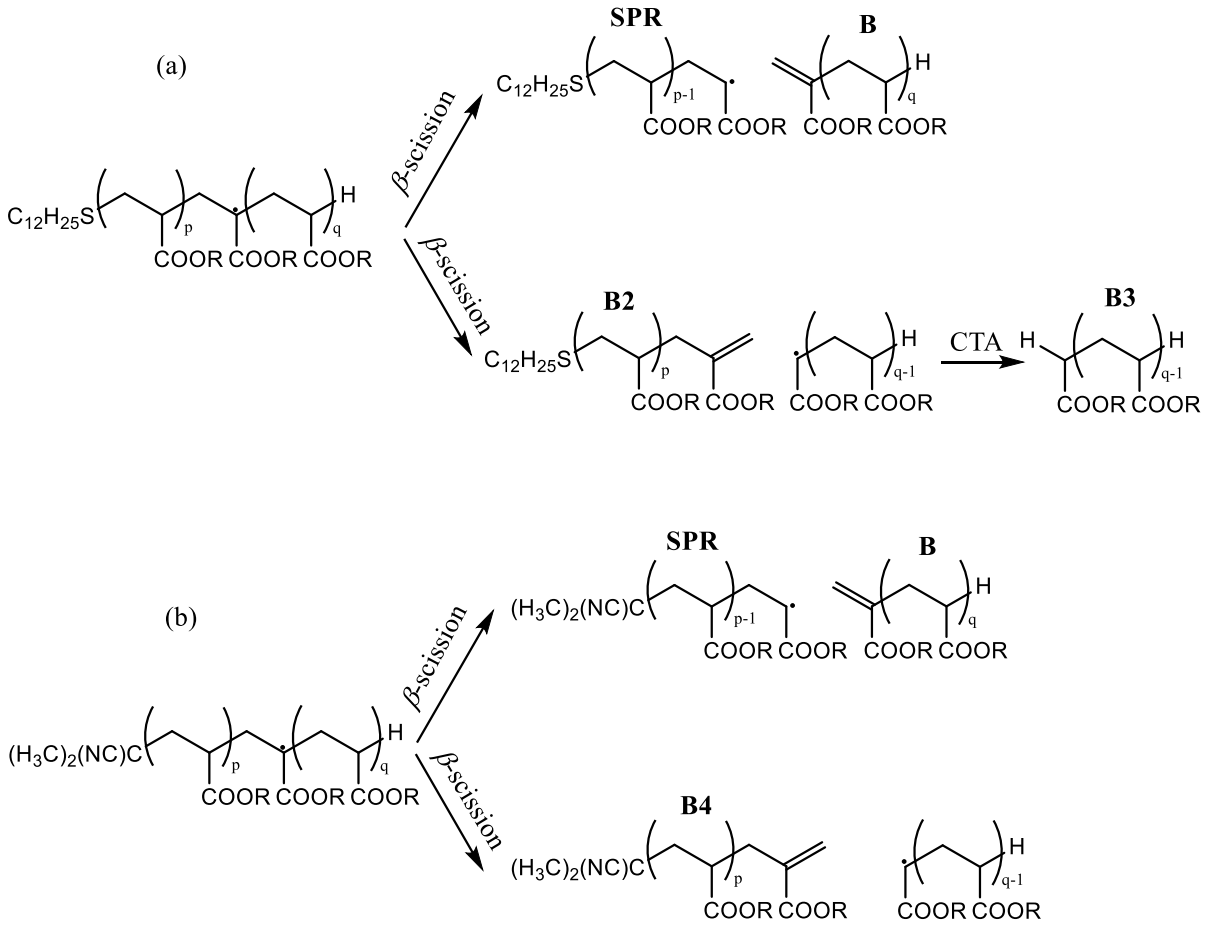

Scheme 4.7: The different *β*-scission products obtained (a) in the presence of CTA, and (b) in the absence of CTA. This scheme is adapted from Koo et al [24].

Although *β*-scission is a relatively simple reaction, it ultimately gives rise to a multitude of products, as shown in Scheme 4.7. This is because an MCR from a thiol-generated polymer can split into either an H-ended or $C_{12}H_{25}S$-ended radical, as shown in the top half of Scheme 4.6. Furthermore, there is also the possibility of chains started from AIBN undergoing all these reactions, as shown in the bottom half of Scheme 3. As it turns out, in this work we only detect products from thiol-generated polymer, viz. B, B2 and B3, as summarized in the bottom half of Scheme 4.6, and as signified in Figures 4.4, 4.5 and 4.6. Note that it is necessary to go to high resolution (e.g. Figure 4.6) in order to see species B2 and B3.

The other matter to deal with is the nature of the adduct ion in ESI-MS. Predominantly it is H^+ in this work, as indicated in the figures (A H^+, B H^+, etc.). There are also many minor peaks. These we could always assign to the species identified above but either with different adduct ions (NH_4^+, Na^+, *n* H_2O H^+, CH_3-CH_2-NH_2 H^+ ,[36] CH_3OH H^+, CH_3OH H_2O H^+, $(CH_3CN)_2$ H^+) or two adduct ions. We therefore believe that only polymers A, B, B2, B3 and C were

obtained in this work. Tables 4.4 to 4.11 detail the different adducts and compare their observed *m*/*z* with theoretical values, as calculated with the mMass software (version 3.1.0) [37].

β-scission is detected in P2EHA synthesized at all temperatures. This does not correspond to what was observed previously by NMR spectroscopy, and *β*-scission was not expected below 80 °C [38]. *β*-scission was not observed in P2EHA synthesized in solution at 60 °C [7] and in emulsion at 75 °C [8] but it was observed at 140 °C in bulk[39] and solution [5]. However, Koo *et al.* observed by ESI-MS a significant amount of *β*-scission even at 60 °C for P*n*BA in both presence and absence of 1-octanethiol [24]. This is likely due to the sensitivity of ESI-MS, which is higher than in NMR spectroscopy. As well as extending the P*n*BA finding to P2EHA, the presence of species B in P2EHA made at 25 °C and 4 °C is a new discovery in this study. The presence of MCRs in P2EHA made at 25 °C was detected by EPR spectroscopy[4] and at -34 °C by SEC [27]. While this does not corroborate the occurrence of *β*-scission at these low temperatures, it at least establishes it as a possibility.

A noticeable result is that polymerization of 2EHA at elevated temperature (100 and 140 °C) predominantly produces pure macromonomer – see the ESI-MS spectra for P2EHA-2 and -4. This is consistent with previous findings for P*n*BA [40]. However, when CTA is introduced this situation changes: there is a higher proportion of A species. Again, this is consistent with results in the literature: Junkers *et al.* found that the presence of a CTA reduces the amount of *β*-scission in P*n*BA [23]. A simple explanation for this is that the frequency of transfer to CTA exceeds that of *β*-scission, which should be (relatively) unaffected by the presence of CTA. There may also be a boost to the level of A species from the so-called patching effect. However, this is not essential to explain the fundamental observation.

The other observation about B species is that they diminish as temperature decreases. This is an expected result because it is well known that backbiting has a relatively high activation energy, and thus the MCR fraction decreases as temperature is lowered. We observed that C species – from combination of transfer-started radicals – are evident in samples P2EHA-5, -7 and -9, being of relatively equal amount to B species at 65 °C and largely replacing them at the two lower temperatures, consistent with the known low activation energy of acrylate termination [41, 42]. That said, Figure 4.6 suggests that B species are still present at 25 and 4 °C, but at very low amount.

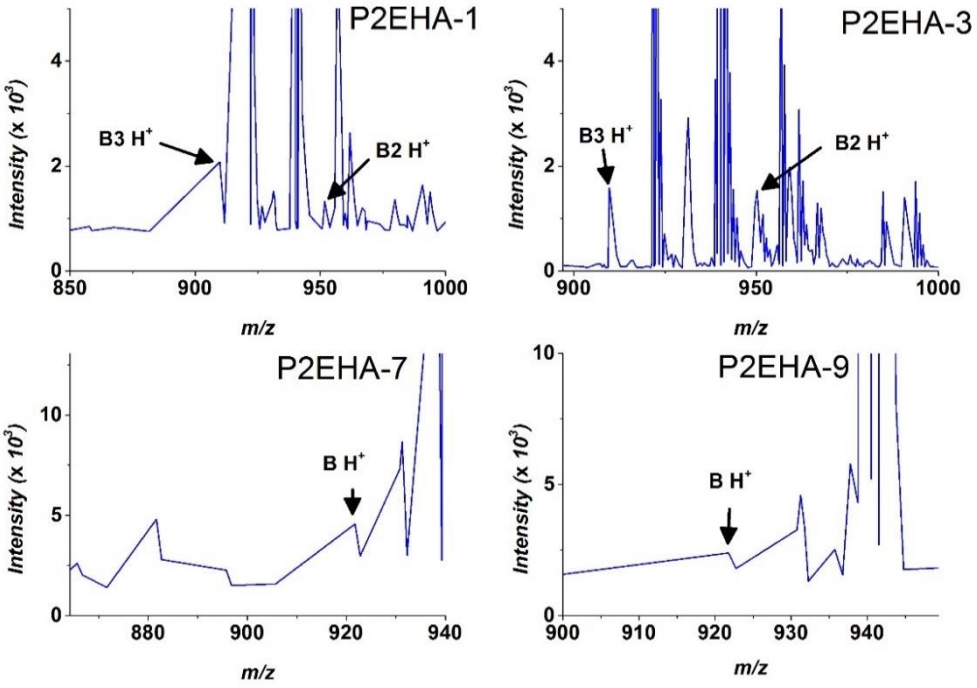

Figure 4.6: Close-ups of ESI-MS spectra of CTA-containing P2EHAs synthesized at 140 °C (P2EHA-1), 100 °C (P2EHA-3), 25 °C (P2EHA-7) and 4 °C (P2EHA-9).

Of course C species may not form in the absence of CTA. This means that dead chains must form either by *β*-scission or by termination of radicals from initiator. As already mentioned, the latter species are not observed in this work. Accordingly, only B species are observed for P2EHA-6 (65 °C without CTA), but their relative amount is very low, because the chain-length distribution is relatively long.

Some further points to note about our ESI-MS results now follow. Species B2 and B3 are observed in the CTA-containing P2EHAs obtained at 140 °C and 100 °C but the intensity of their peaks is less than 10 % of the intensity of the peaks of species B. This was also observed in the case of P*n*BA [24] and explained by a complex set of equilibria between the scission products and the MCRs, as *β*-scission is a reversible reaction [43]. Species B4 is never observed in this study although it was present (in low abundance) in the work of Koo *et al.* on P*n*BA [24].

Table 4.4: Species detected by ESI-MS for P2EHA synthesized at 4 °C with CTA.

Formula	M_{exp} (amu)	M_{th} (amu)	h_{peak} (arbitrary units)
$(C_{11}H_{20}O_2)_5\ H^+$	921.7422	921.7389	2382
$C_{12}H_{25}S(C_{11}H_{20}O_2)_4H\ H^+$	939.7715	939.7681	361407
$C_{12}H_{25}S(C_{11}H_{20}O_2)_3C_{12}H_{21}O_2\ H^+$	951.7578	951.7681	1852
$C_{12}H_{25}S(C_{11}H_{20}O_2)_3C_{12}H_{25}S\ H^+$	955.7654	955.7817	71885
$C_{12}H_{25}S(C_{11}H_{20}O_2)_4H\ Na^+$	961.7526	961.7501	21222
$C_{12}H_{25}S(C_{11}H_{20}O_2)_4H\ (H_2O)_3\ H^+$	993.7804	993.7998	21015

Table 4.5: Species detected by ESI-MS for P2EHA synthesized at 25 °C with CTA.

Formula	M_{exp} (amu)	M_{th} (amu)	h_{peak} (arbitrary units)
$(C_{11}H_{20}O_2)_5\ H^+$	921.7438	921.7389	4562
$C_{12}H_{25}S(C_{11}H_{20}O_2)_4H\ H^+$	939.7731	939.7681	474470
$C_{12}H_{25}S(C_{11}H_{20}O_2)_3C_{12}H_{25}S\ H^+$	955.7677	955.7817	112353
$C_{12}H_{25}S(C_{11}H_{20}O_2)_4H\ Na^+$	961.7545	961.7501	18150
$C_{12}H_{25}S(C_{11}H_{20}O_2)_4H\ (H_2O)_3\ H^+$	993.7824	993.7998	21015
$C_{12}H_{25}S(C_{11}H_{20}O_2)_3C_{12}H_{25}S\ (H2O)_4\ H^+$	1027.8247	1027.8239	46534

Table 4.6: Species detected by ESI-MS for P2EHA synthesized at 65 °C with CTA.

Formula	M_{exp} (amu)	M_{th} (amu)	h_{peak} (arbitrary units)
$(C_{11}H_{20}O_2)_5\ H^+$	921.7384	921.7389	23097
$C_{12}H_{25}S(C_{11}H_{20}O_2)_4H\ H^+$	939.7682	939.7681	241628
$C_{12}H_{25}S(C_{11}H_{20}O_2)_3C_{12}H_{25}S\ H^+$	955.7628	955.7817	51647
$C_{12}H_{25}S(C_{11}H_{20}O_2)_4H\ CH_3OH\ H^+$	971.7571	971.7943	36095
$C_{12}H_{25}S(C_{11}H_{20}O_2)_4H\ CH_3OH\ H_2O\ H^+$	989.7861	989.8049	70298
$C_{12}H_{25}S(C_{11}H_{20}O_2)_3C_{12}H_{25}S\ CH_3OH\ H_2O\ H^+$	1005.782	1005.8184	66409
$C_{12}H_{25}S(C_{11}H_{20}O_2)_4H\ (CH_3CN)_2\ H^+$	1021.777	1021.8212	47205

Table 4.7: Species detected by ESI-MS for P2EHA synthesized at 65 °C without CTA.

Formula	M_{exp} (amu)	M_{th} (amu)	h_{peak} (arbitrary units)
$(C_{11}H_{20}O_2)_5\ H^+$	921.7446	921.7389	1569
$(C_{11}H_{20}O_2)_5\ NH_4^+$	938.7685	938.7655	434
$C_{11}H_{20}O_2)_5\ Na^+$	943.7264	943.7209	2371

Table 4.8: Species detected by ESI-MS for P2EHA synthesized at 100 °C with CTA.

Formula	M_{exp} (amu)	M_{th} (amu)	h_{peak} (arbitrary units)
$C_{10}H_{19}O_2(C_{11}H_{20}O_2)_4H\ H^+$	909.7	909.7389	1586
$(C_{11}H_{20}O_2)_5\ H^+$	921.7	921.7389	17753
$C_{12}H_{25}S(C_{11}H_{20}O_2)_9H\ 2H^+$	930.8	930.7535	2195
$(C_{11}H_{20}O_2)_5\ NH_4^+$	938.8	938.7655	3650
$C_{12}H_{25}S(C_{11}H_{20}O_2)_4H\ H^+$	939.8	939.7681	65158

$C_{12}H_{25}S(C_{11}H_{20}O_2)_3C_{12}H_{21}O_2\ H^+$	951.8	951.7681	1076
$C_{12}H_{25}S(C_{11}H_{20}O_2)_4H\ NH_4^+$	956.8	956.7947	6585
$C_{12}H_{25}S(C_{11}H_{20}O_2)_4H\ Na^+$	961.8	961.7501	3075
$C_{12}H_{25}S(C_{11}H_{20}O_2)_{10}H\ 2H^+$	1022.8	1022.827	2658

Table 4.9: Species detected by ESI-MS for P2EHA synthesized at 100 °C without CTA.

Formula	M_{exp} (amu)	M_{th} (amu)	h_{peak} (arbitrary units)
$(C_{11}H_{20}O_2)_5\ H^+$	921.7467	921.7389	37303
$(C_{11}H_{20}O_2)_5\ NH_4^+$	938.7734	938.7655	3650
$(C_{11}H_{20}O_2)_5\ Na^+$	943.7286	943.7209	6930
$(C_{11}H_{20}O_2)_5\ CH_3CH_2NH_2\ H^+$	966.8042	966.7966	9696
$(C_{11}H_{20}O_2)_{11}\ 2H^+$	1013.8208	1013.8121	2969

Table 4.10: Species detected by ESI-MS for P2EHA synthesized at 140 °C with CTA.

Formula	M_{exp} (amu)	M_{th} (amu)	h_{peak} (arbitrary units)
$C_{10}H_{19}O_2(C_{11}H_{20}O_2)_4H\ H^+$	909.7416	909.7389	2078
$(C_{11}H_{20}O_2)_5\ H^+$	921.7422	921.7389	14904
$(C_{11}H_{20}O_2)_5\ NH_4^+$	938.768	938.7655	6165
$C_{12}H_{25}S(C_{11}H_{20}O_2)_4H\ H^+$	939.7713	939.7681	31551
$(C_{11}H_{20}O_2)_5\ Na^+$	943.7266	943.7209	2223
$C_{12}H_{25}S(C_{11}H_{20}O_2)_3C_{12}H_{21}O_2\ H^+$	951.769	951.7681	1330
$C_{12}H_{25}S(C_{11}H_{20}O_2)_4H\ NH_4^+$	956.7965	956.7947	6665
$C_{12}H_{25}S(C_{11}H_{20}O_2)_4H\ Na^+$	961.753	961.7501	2635

Table 4.11: Species detected by ESI-MS for P2EHA synthesized at 140 °C without CTA.

Formula	M_{exp} (amu)	M_{th} (amu)	h_{peak} (arbitrary units)
$(C_{11}H_{20}O_2)_5\ H^+$	921.7459	921.7389	10750
$(C_{11}H_{20}O_2)_5\ NH_4^+$	938.7725	938.7655	7938
$(C_{11}H_{20}O_2)_5\ Na^+$	943.7273	943.7209	1937

M_{exp} is the experimental molar mass obtained for an adduct, M_{th} is the theoretical molar mass of the same adduct and h_{peak} is the peak height.

4.3.5 Average degree of branching and average degree of *β*-scission

Samples P2EHA-1 to -8 were analysed by ^{13}C solid-state NMR spectroscopy. *DB* and *DβS* were quantified. P2EHA-9 and -10 were not analysed by ^{13}C NMR spectroscopy as the detection of the quaternary carbon would take over one week on a 400 MHz equipment. Furthermore, as we were not able to measure *DB* and *DβS* from NMR of our 25 °C samples (see below), it follows that they would also not be measureable for the samples from 4 °C.

The different values obtained for *DB* (with Eq. (1) and (2)) are similar in magnitude if the residual standard deviation (*RSD*) is considered. Results are presented in Figure 4.7. At 25 °C, neither branching nor *β*-scission products were observed by ^{13}C NMR spectroscopy. This confirms the findings of Sato *et al*. [4] but is different to the results of Castignolles *et al.* [27] and Couvreur *et al.* [28], who both divined the presence of LCB in P2EHA synthesized by PLP in bulk at –34 °C and low conversion. This was done using SEC, analysing the shape of the chromatogram. As a tool for probing kinetics there can be no doubt that ^{13}C NMR is far more sensitive than SEC, however It is possible that SEC can detect the rheological effects of LCB (e.g. one such branch per long chain) even when it is negligible as a kinetic event.

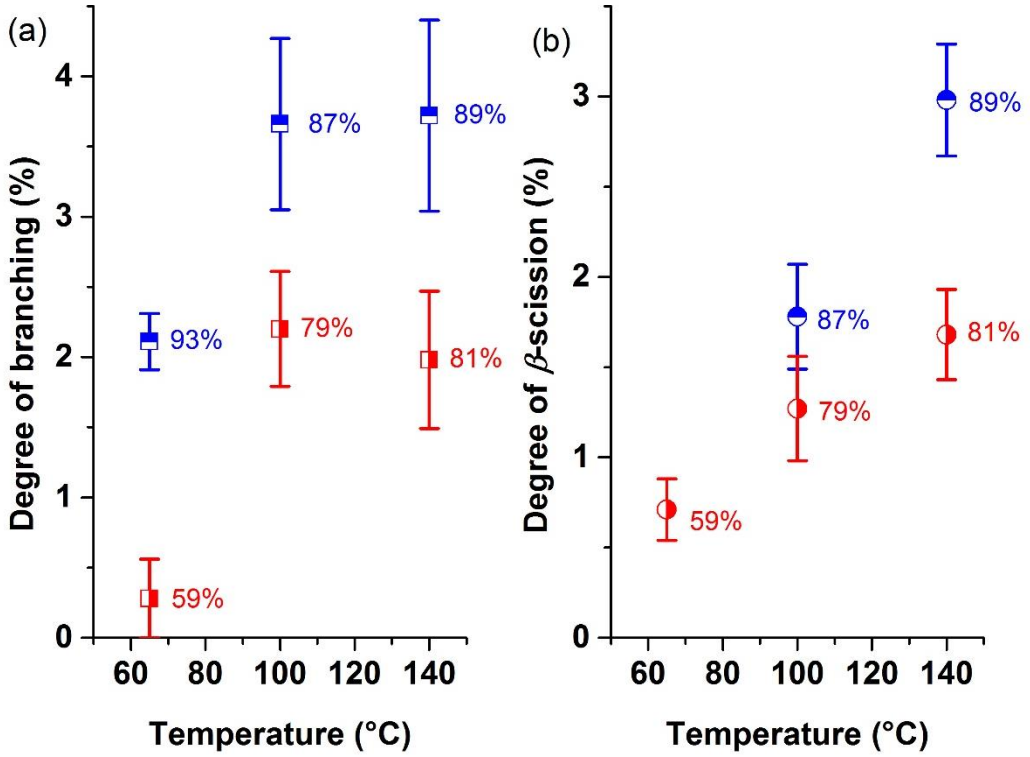

Figure 4.7: (a) Average degree of branching (*DB*; squares; from Equation 1) and (b) average degree of *β*-scission (*DβS*; circles; from Equation 3) of CTA-containing (red points with vertical division) and non-CTA-containing (blue, horizontal) P2EHAs synthesized in bulk at different temperatures. The monomer conversion from the synthesis is given as a written value next to each point.

Firstly, Figure 4.7(b) is consistent with the ESI-MS results obtained by Junkers *et al*.[23] and by Koo *et al*. [24]: for both these previous investigations of *n*BA and the present study of 2EHA

it is found that the amount of *β*-scission is reduced by the presence of a CTA and increases with temperature. The most obvious explanation for the lower *DβS* in the presence of CTA is the patching effect – some MCRs react with thiol before they have a chance to undergo *β*-scission or propagation. In this context we note that we were unable to measure *DβS* for the sample made at 65 °C but without CTA (i.e., the absent blue point in Figure 4.7(b)). Moreover, we did observe *β*-scission product in the ESI-MS of P2EHA-6 (see above) with very low intensity, whereas B species in P2EHA-5 were present in higher intensity. This is likely due to the conversion. The CTA-containing P2EHA made at 65 °C was obtained with 59 % of monomer conversion whilst 96 % for the one made without CTA. This low conversion is confirmed by the low T_g observed for this polymer in comparison to others (see Figure A.4.4 in Appendix 2). It has been observed previously that the kinetic rate coefficient of *β*-scission is lower at high conversion. This was explained by the potential consumption of macroradicals at high monomer conversion, biasing the results [4].

Secondly, in Figure 4.7(a) it is observed that *DB* is considerably reduced by the presence of CTA and increases with temperature up to 100 °C before remaining the same at 140 °C. The reduction of *DB* with addition of CTA is by now well known, having already been observed for P*n*BA [11, 21, 23, 24] and by ourselves with PAA [15]. Again, the most likely reason is the occurrence of a "patching effect", i.e., a transfer of hydrogen atom between DDM and an MCR. Other contributing factors are also possible. These include: (1) Reduction of the amount of backbiting as, in the presence of CTA, the lifetime of an SPR is shorter [11]; (2) Due to chain-length-dependent propagation [44], shorter chains – as formed in the presence of CTA – must have a lower *DB*, as the average time between propagation events is lower, (3) When the polymerization temperature is between 65 °C and 140 °C, the conversion is higher for non-CTA-containing P2EHA. It is known that *DB* increases with conversion, and has been observed experimentally in the case of P2EHA [7] and by simulation in the case of PAA [16]. This is simply an effect of lower monomer concentration and therefore lower frequency of propagation (cf. backbiting, which is a unimolecular process); (4) Another possible explanation is an unintended temperature increase, as the fast rate of polymerization of alkyl acrylates can give rise to an exotherm, particularly in bulk polymerization. In the absence of a CTA, chains are longer and so viscosity is higher, meaning that heat is more difficult to remove. If there is an exotherm, then *DB* would increase. In this context it may seem strange that *DB* does not continue to rise to 140 °C. However this is simply explained by *β*-scission becoming predominant, meaning the effect of an increasing MCR fraction is not immediately reflected in

DB. It will be shown below that our data does in fact evidence that the backbiting rate coefficient increases from 100 to 140 °C.

It is worthwhile to compare the results obtained in this study with ones from the literature. This is done in Figure 4.8. Firstly, in Figure 4.8(a) we have gathered *DB* results from polymer made with CTA and at a similar temperature, viz. 60–70 °C. This temperature is chosen because it is high enough to give measurable *DB* but low enough that *β*-scission plays only a minor role. It is clear that our 65 °C value for *DB* is consistent with those from the literature. It is also clear that there is a decrease of *DB* with initial monomer concentration (noting that whereas our data point is from bulk polymerizaiton, all the literature values are from experiments in solution). For conditions of constant monomer concentration, [M], it is well known that $DB \sim [M]^{-1}$ [16, 45]. The data of Figure 4.8(a) shows this trend, which provides a vote of confidence in our data.

In contrast to Figure 4.8(a), Figure 4.8(b) examines the effect of temperature. The results obtained in this study are compared with those from Gaborieau *et al*.[21] for P*n*BA. In both studies the polymerizations were carried out in bulk and with the same initiator at approximately the same concentration (about 40% different). Furthermore, the same ratio of CTA to monomer was used, the only difference in this regard being 1-octanethiol in the previous work versus DDM presently, which should make negligible difference. In summary, conditions in both sets of experiments were almost identical, apart from *n*BA versus 2EHA. Considering this it must be said that the results of Figure 4.8(b) are in excellent agreement. The only differences are in the no-CTA systems at 100 and 140 °C, and even these are within experimental error to all intents and purposes. In this context it should be noted that in the P*n*BA work there was no measurement of *DβS*, so it is possible that the P*n*BA *DP* at 140 °C somehow includes a contribution from *β*-scission, and so is an overestimate. Then again, it has been observed that P2EHA is more affected by *β*-scission than P*n*BA [4].

Having said this above, in the literature it has been found that the P2EHA is more branched than P*n*BA when synthesized in solvent at 60 °C [4] and 70 °C [7]. This was explained by a higher accessibility of the tertiary CH-bond in P2EHA, which would lead to the formation of more MCRs.[7] Kattner and Buback have recently confirmed that as the pendant alkyl group of an acrylate increases in size, the fraction of MCRs increases [19], which – in the absence of *β*-scission – would mean higher *DB*. This is left as an open issue, although it is noted that there are only 3 points in the P*n*BA study and that this was a method-establishment work [21].

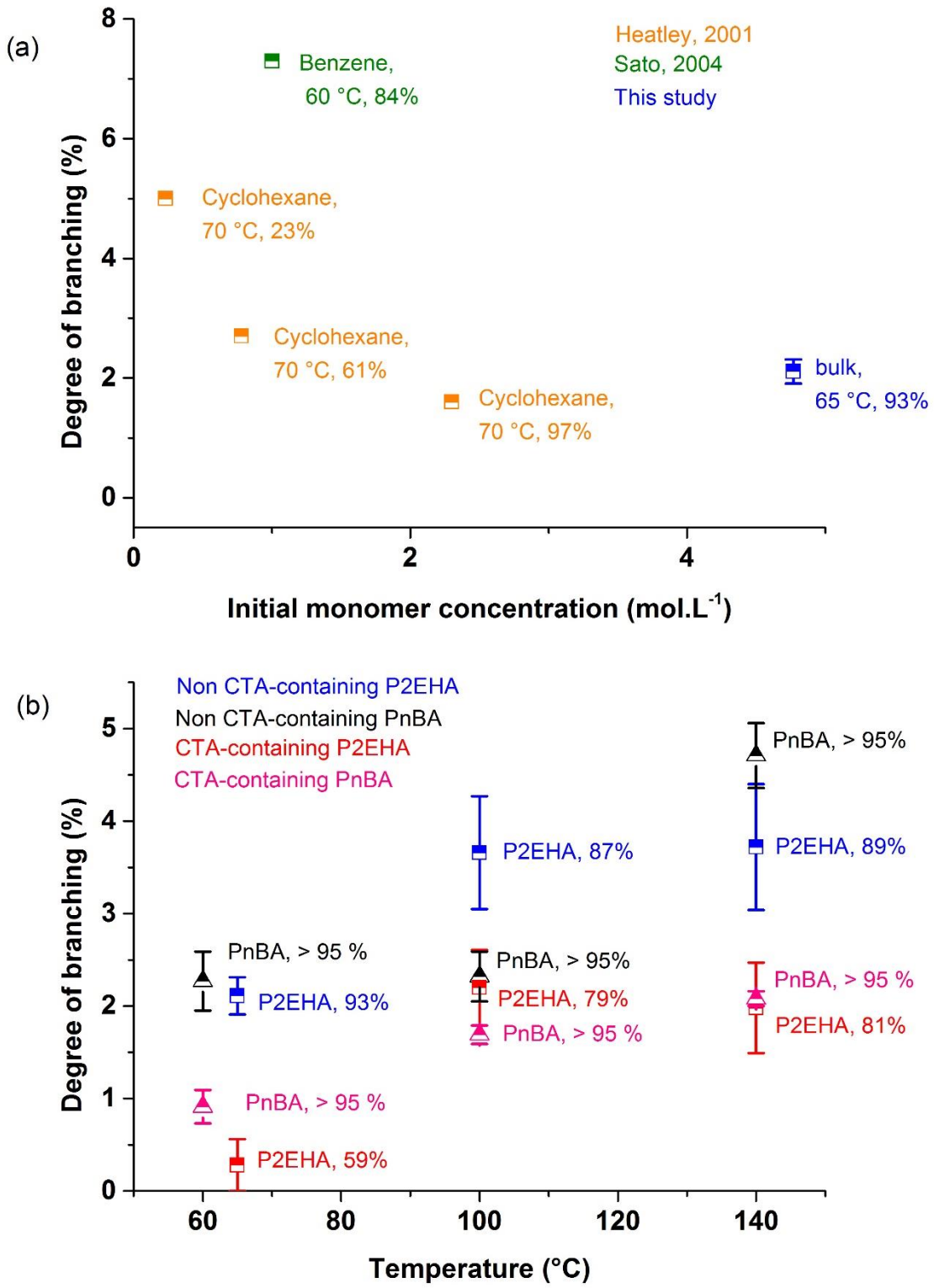

Figure 4.8: Comparisons of degree of branching, *DB*, obtained in this and previous studies. (a) Effect of initial monomer concentration at similar temperature for P2EHA, where literature data is from Heatley *et al.* [7] and *Sato et al.* [4] (b) Effect of temperature and CTA for P2EHA (this study) and P*n*BA (Gaborieau *et al.* [21]) in otherwise similar conditions (bulk, same CTA/monomer and initiator/monomer). In both cases the final conversion is given.

4.3.6 Rate coefficients

Historically it has been assumed in determining k_{bb}/k_p from *DB* values that [M] stays approximately constant throughout an experiment. In a lot of experiments this has not been the case, including the present work, in which bulk experiments were carried out to high conversion and then the polymer isolated for analysis. This means that during an experiment the monomer concentrating is decreasing, and so the balance between SPR propagation, of frequency k_p[M], and backbiting, k_{bb}, is constantly changing, and thus the instantaneous *DB* is contantly changing; specifically, it will increase as conversion increases, and thus the cumulative *DB* will also increase. In view of this, Nikitin *et al.* derived Eq. (4.4) for cumulative *DB* [46], as determined in this work:

$$DB\ (\%) = \frac{k_{\mathrm{bb}}\ 100\ ln\left(\frac{[\mathrm{M}]_0}{[\mathrm{M}]_\mathrm{e}}\right)}{k_\mathrm{p}([\mathrm{M}]_0 - [\mathrm{M}]_\mathrm{e})} \tag{4.4}$$

Here $[M]_0$ and $[M]_e$ are the monomer concentrations at the start and end, respectively, of a polymerization. This equation assumes negligible loss of MCRs by transfer, β-scission and termination, i.e., that all MCRs become a branch site. It also assumes negligible occurrence of LCB, i.e., it assumes all branches are formed by backbiting. Our earlier study on PAA was the first to apply this equation to *DB* data [15].

There is a complication in applying Eq. (4.4) in the present work, which is that clearly it cannot be assumed that β-scission occurs to a negligible extent. To overcome this, we assume that all MCRs either propagate to give a branch site or undergo β-scission to give a terminal double bond. In this situation it would seem to us that Eq. (4.4) can be simply adapted as follows:

$$DB\ (\%)\ + D\beta S\ (\%) = \frac{k_{\mathrm{bb}}\ 100\ ln\left(\frac{[\mathrm{M}]_0}{[\mathrm{M}]_\mathrm{e}}\right)}{k_\mathrm{p}([\mathrm{M}]_0 - [\mathrm{M}]_\mathrm{e})} \tag{4.5}$$

This equation has all the assumptions of Eq. (4.4) apart from that regarding β-sicssion. However, it does additionally assume that there is negligible consumption of macronomoner by propagation. It is felt that these assumptions are reasonable. Obviously the use of either Eq.(4.4) or (4.5) assumes that accurate values of $[M]_e$ have been obtained. In our study we were not able to prove that the residual monomer signals in ^{13}C NMR spectroscopy are quantitative. For this reason our final conversions may be overestimated.

Eq. (4.5) enables determination of k_{bb}/k_p for our bulk E2HA data. The Arrhenius plot of the resulting values is Figure A.4.11. For no-CTA data the Arrhenius fit is

$$k_{bb}/k_p \text{ (mol L}^{-1}) = 5.5 \times 10^1 \, e^{-\frac{20.6 \times 10^3}{RT}} \quad (65\ ^\circ\text{C} < \theta < 140\ ^\circ\text{C}) \qquad (4.6a)$$

Here T is temperature in K and q in °C. Strictly speaking Eq. (4.5) should not be used for polymer made with CTA, as it assumes that MCRs do not undergo transfer to CTA. Nevertheless we still analyzed our CTA data in this way, obtaining

$$k_{bb}/k_p \text{ (mol L}^{-1}) = 9.6 \times 10^0 \, e^{-\frac{15.7 \times 10^3}{RT}} \quad (65\ ^\circ\text{C} < \theta < 140\ ^\circ\text{C}) \qquad (4.6b)$$

We stress that Eq. (4.6b) does not actually give true values of k_{bb}/k_p for systems with CTA. Rather, it gives values that incorporate the patching reaction, which of course acts to lower the apparent rate of backbiting. Nevertheless we present Eq. (4.6b), as it may be used to estimate $DB + D\beta S$ for systems with the present concentration of DDM, which was approximately 10 mol % relative to monomer.

It is also important to note that it has been proven previously that macroradical formed by β-scission are consummed. Consequantly, k_{bb}/k_p (calculated with Eq. (4.5) are underestimated).

To obtain individual values of k_{bb}, the value of k_p is needed. This was calculated according to Equation (7) [29], which was obtained from PLP-SEC experiments over the indicated temperature range:

$$k_p \text{ (L mol}^{-1} \text{ s}^{-1}) = 9.1 \times 10^6 \, e^{-\frac{1901}{T}} \quad (10\ ^\circ\text{C} < \theta < 60\ ^\circ\text{C}) \qquad (4.7)$$

Only the no-CTA points were treated this way, as the aim is to obtain the true value of $k_{bb,}$ not an apparent value due to the occurrence of patching. Our k_{bb} results are presented in Figure 4.9 while the ensuing Arrhenius parameters – activation energy, E_a, and pre-exponential factor, A – are given in Table 4.12, with errors given in Table A.4.5. Table 4.12 also includes values from a variety of literature studies.

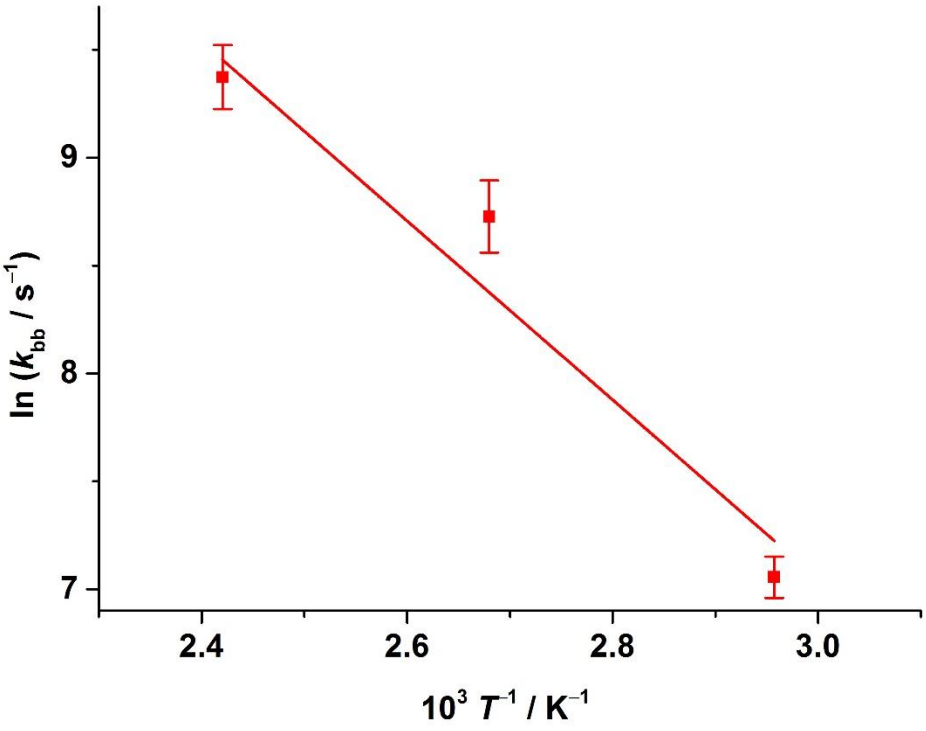

Figure 4.9: Arrhenius plot of backbiting rate coefficient, k_{bb}, of 2EHA, as obtained from experiments without CTA.

Table 4.13: Frequency factor, A, and activation energy, E_a, of backbiting rate coefficient, k_{bb}, for different acrylates. The measurement temperature range, method and solvent are indicated.

Acrylate	***A*** **(10^8 s^{-1})**	***E*a** **(kJ mol^{-1})**	***θ* range (°C)**	**Reference**	**Method**	**Solvent**	k_{bb} **at 50 °C (10^2 s^{-1})**†
dodecyl (DA)	2.1	35.2	0 – 60	[19]	SP-PLP-EPR	toluene	4.3
2EHA	4.4	35.9	65 – 140	this study	NMR	none	6.9
*n*BA	0.35	29.3	–16 – 60	[47]	NMR	heptane*	6.4
*n*BA	320	52.3	60 – 140	[14]	NMR	*p*-xylene*	1.1
*n*BA	0.48	31.7	–10 – 40	[48]	PLP-SEC	none	3.6
*n*BA	1.6	34.7	0 – 60	[49]	SP-PLP-EPR	toluene	3.9
methyl (MA)	1.5	33.2	0 – 60	[19]	SP-PLP-EPR	toluene	6.4
AA#	5.1	36.4	5 – 40	[50]	SP-PLP-EPR	water	6.7
AA	9.9	38.0	20 – 75	[16]	NMR	water	7.1
AA	29	42.1	50 – 90	[15]	NMR	water/THF	4.5

† Calculated from given Arrhenius parameters.# Determined from k_{bb} values tabulated in Appendix 2 [50].
* Some experiments carried out in bulk, some in the given solvent.

It is clear from Table 4.12 that all but one of the previous determinations of k_{bb} have been at lower temperatures than the present work. Further, the previous *n*BA study [14] over a similar temperature range stands out in Table 4.12 for having inexplicably high Arrhenius parameters. For these reasons no other data is presented in Figure 4.9 – it would just be to compare our results with a set of extrapolations. Instead, in Figure 4.10 – which will shortly be discussed – we compare the extrapolated fit of our results with the fits of some other results over the temperature range of their measurement.

Values of k_{bb} at 50 °C for each Arrhenius fit are given in Table 4.12, and it is clear there is good agreement in most cases. However an obvious conculsion to draw from Table 4.12 is that it is difficult to obtain Arrhenius parameters for k_{bb} with high accuracy. In this context it is evident that the values from the present work sit very comfortably within historical averages. Indeed, of the five determinations of $E_a(k_{bb})$ by NMR, the present one looks to be the most accurate.

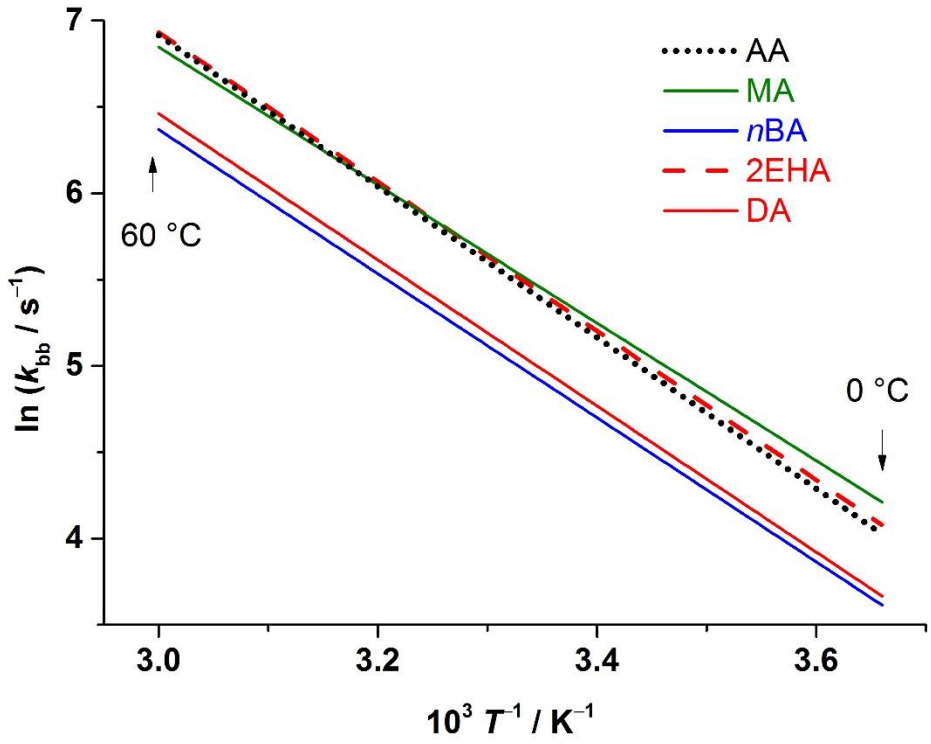

Figure 4.10: Arrhenius fits of backbiting rate coefficients, k_{bb}, for acrylic acid[50] (AA), methyl acrylate[19], *n*-butyl acrylate [49] (*n*BA), 2EHA (present work) and dodecyl acrylate [19] (DA). All of these literature results were obtained by SP-PLP-EPR, as opposed to the use of NMR in the present work. The temperature range is that from the SP-PLP-EPR studies.

It is evident from Table 4.12 that the technique of SP-PLP-EPR delivers k_{bb} with the highest precision of the four methods so far used, as the four values of $E_a(k_{bb})$ obtained this way are within the relatively small range of 33.2 – 36.4 kJ mol^{-1}. Arguably this is not surprising, as the technique probes the radicals most directly: a single-pulse PLP experiment is carried out within an EPR cavity, meaning that the SPR and MCR concentrations can be monitored as the SPRs created by the laser pulse are converted into MCRs by backbiting. It is very pleasing that our $E_a(k_{bb})$ for 2EHA falls exactly within the narrow range of values found by SP-PLP-EPR, whereas values found previously by other techniques for other acrylates are outside it.

Given the above we have plotted in Figure 4.10 the Arrhenius fits from the four SP-PLP-EPR studies with that from the present work. Previously Kattner and Buback plotted just the MA, BA and DA values. Here we add also their fit for AA [50]. On the basis of these results it seems reasonable to make the tentative conclusion that there is family-type behavior in acrylate k_{bb}, with $E_a \approx 35$ kJ mol^{-1} and A weakly decreasing as the alkyl side group increases in size (as is reflected in the 50 °C value of table 4.12). We note that this is similar to acrylate [51] and methacrylate [52] k_p, except that there the variation of A goes in the opposite direction: E_a (of k_p) is constant but A increases as the alkyl side group becomes larger. On the other hand, Kattner and Buback have found that the rate coefficient for MCR propagation, k_p^t, shows the opposite trend, i.e., significantly decreasing A (with constant E_a) as the alkyl side group becomes larger [19]. This combined with decreasing [M] would seem to be the primary cause of MCR fraction increasing as acrylates become larger. Whether there is any significant variation of k_{bb} from acrylate to acrylate remains to be seen; in fact Kattner and Buback proposed the one Arrhenius fit for all acrylates [19]. We note that Heatley *et al*. found higher *DB* in P2EHA than in P*n*BA, and they interpreted this as being due to an increase in $A(k_{bb})$ because of P2EHA having greater free volume than PnBA, meaning that the tertiary CH is more accessible for backbiting [7]. If true this is consistent with the placement of 2EHA in Figure 4.10.

That our Arrhenius fit for k_{bb} nestles so well amongst the SP-PLP-EPR fits – see Figure 4.10 – is quite remarkable given all the differences between the experiments: EPR versus NMR, PLP versus steady-state, solution versus bulk, low versus extended conversion, and high versus low temperature. Concerning the last difference, there are two important points to make. The first is that our k_{bb} were obtained from our k_{bb}/k_p values using an Arrhenius fit for k_p that was obtained over a much lower temperature range, viz. 10 – 60 °C [29]. Given that we extrapolate this fit to 140 °C to obtain k_{bb}, the consistency of these k_{bb} with literature values is outstanding.

In particular, all it would take is for $A(k_p)$ to be too large by a factor of 2 – which is a relatively small error – and then our $A(k_{bb})$ would be smaller by a factor of 2, placing it perfectly in agreement with the BA and DA data of Figure 4.10. The second point is to be aware that, because of the high temperature, this is the first occasion in which *β*-scission has been taken into account in order to determine k_{bb}/k_p. The flipside of this is that when our k_{bb} values are used, it must be remembered that these give $DB + D\beta S$, and that $D\beta S$ is only negligible at low temperature, estimated to be around 70 °C and below for 2EHA.

4.4 Conclusions

For many decades the kinetics of acrylate polymerization were a mystery. Around the turn of the century there emerged definitive proof that branching occurs in the polymerization of *n*-butyl acrylate [10]. This was soon followed by a call to arms from van Herk [53], who correctly sensed that chain transfer to polymer was at the heart of all the mysteries. Progress has been rapid in the 16 years since then. This work makes another contribution to this progress, and there are several elements that we feel elevate this paper above mere "stamp collecting", i.e., routine repetition of past practices. The first is the exceptionally clear identification of *β*-scission products in our ESI-MS analyses of P2EHA made at high temperature. The second is the quantification of the level of *β*-scission by ^{13}C NMR. The third is that both *β*-scission and branching are accounted for in determining k_{bb}/k_p. Important in this process is the use – for only the second time – of an equation from Nikitin *et al*.[46] that allows for experiments to be carried out over a range of conversion, as opposed to being limited just to low conversions. Finally, the k_{bb} values that we obtain are the first reported for 2EHA and are in outstanding agreement with the most recent – and seemingly most accurate – literature values,[19] ones obtained by a completely different method. For all these reasons we feel confident in recommending our methodology for future work. With more studies like these, the acrylate enigma will be fully transformed into a powerful revelation.

4.5 References

[1] A.B. Lopez, J.C. de la Cal, J.M. Asua, Highly Hydrophobic Coatings from Waterborne Latexes, Langmuir, 32 (2016) 7459-7466.

[2] M.D. Gower, R.A. Shanks, The effect of varied monomer composition on adhesive performance and peeling master curves for acrylic pressure-sensitive adhesives, Journal of Applied Polymer Science, 93 (2004) 2909-2917.

[3] D.J. Haloi, N.K. Singha, Synthesis of Poly(2-ethylhexyl acrylate)/Clay Nanocomposite by In Situ Living Radical Polymerization, Journal of Polymer Science Part a-Polymer Chemistry, 49 (2011) 1564-1571.

[4] E. Sato, T. Emoto, P.B. Zetterlund, B. Yamada, Influence of mid-chain radicals on acrylate free radical polymerization: Effect of ester alkyl group, Macromolecular Chemistry and Physics, 205 (2004) 1829-1839.

[5] J. Vandenbergh, T. Junkers, Synthesis of Macromonomers from High-Temperature Activation of Nitroxide Mediated Polymerization (NMP)-made Polyacrylates, Macromolecules, 46 (2013) 3324-3331.

[6] P.M. Wood-Adams, J.M. Dealy, A.W. deGroot, O.D. Redwine, Effect of molecular structure on the linear viscoelastic behavior of polyethylene, Macromolecules, 33 (2000) 7489-7499.

[7] F. Heatley, P.A. Lovell, T. Yamashita, Chain transfer to polymer in free-radical solution polymerization of 2-ethylhexyl acrylate studied by NMR spectroscopy, Macromolecules, 34 (2001) 7636-7641.

[8] C. Plessis, G. Arzamendi, J.M. Alberdi, M. Agnely, J.R. Leiza, J.M. Asua, Intramolecular Chain Transfer to Polymer in the Emulsion Polymerization of 2-Ethylhexyl Acrylate, Macromolecules, 34 (2001) 6138-6143.

[9] P. Castignolles, R. Graf, M. Parkinson, M. Wilhelm, M. Gaborieau, Detection and quantification of branching in polyacrylates by size-exclusion chromatography (SEC) and melt-state 13C NMR spectroscopy, Polymer, 50 (2009) 2373-2383.

[10] N.M. Ahmad, F. Heatley, P.A. Lovell, Chain transfer to polymer in free-radical solution polymerization of n-butyl acrylate studied by NMR spectroscopy, Macromolecules, 31 (1998) 2822-2827.

[11] N. Ballard, J.C. de la Cal, J.M. Asua, The role of chain transfer agent in reducing branching content in radical polymerization of acrylates, Macromolecules, 48 (2015) 987-993.

[12] B. Wenn, G. Reekmans, P. Adriaensens, T. Junkers, Photoinduced acrylate polymerization: Unexpected reduction in chain branching, Macromol. Rapid Commun., 36 (2015) 1479-1485.
[13] N.M. Ahmad, B. Charleux, C. Farcet, C.J. Ferguson, S.G. Gaynor, B.S. Hawkett, F. Heatley, B. Klumperman, D. Konkolewicz, P.A. Lovell, K. Matyjaszewski, R. Venkatesh, Chain transfer to polymer and branching in controlled radical polymerizations of n-butyl acrylate, Macromol. Rapid Commun., 30 (2009) 2002-2021.
[14] S. Hamzehlou, N. Ballard, Y. Reyes, A. Aguirre, J.M. Asua, J.R. Leiza, Analyzing the discrepancies in the activation energies of the backbiting and beta-scission reactions in the radical polymerization of n-butyl acrylate, Polym. Chem., 7 (2016) 2069-2077.
[15] J.-B. Lena, A.K. Goroncy, J.J. Thevarajah, A.R. Maniego, G.T. Russell, P. Castignolles, M. Gaborieau, Effect of transfer agent, temperature and initial monomer concentration on branching in poly(acrylic acid): A study by 13C NMR spectroscopy and capillary electrophoresis, Polymer, 114 (2017) 209-220.
[16] N.F.G. Wittenberg, C. Preusser, H. Kattner, M. Stach, I. Lacík, R.A. Hutchinson, M. Buback, Modeling acrylic acid radical polymerization in aqueous solution, Macromol. React. Eng., 10 (2016) 95-107.
[17] J. Loiseau, N. Doerr, J.M. Suau, J.B. Egraz, M.F. Llauro, C. Ladaviere, Synthesis and characterization of poly(acrylic acid) produced by RAFT polymerization. Application as a very efficient dispersant of CaCO3, kaolin, and TiO2, Macromolecules, 36 (2003) 3066-3077.
[18] L. Couvreur, C. Lefay, J. Belleney, B. Charleux, O. Guerret, S. Magnet, First nitroxide-mediated controlled free-radical polymerization of acrylic acid, Macromolecules, 36 (2003) 8260-8267.
[19] H. Kattner, M. Buback, Termination, Propagation and Transfer Kinetics of Midchain Radicals in Methyl, Acrylate and Dodecyl Acrylate Homopolymerization, Macromolecules, (2017).
[20] C. Barner-Kowollik, T.P. Davis, M.H. Stenzel, Probing mechanistic features of conventional, catalytic and living free radical polymerizations using soft ionization mass spectrometric techniques, Polymer, 45 (2004) 7791-7805.
[21] M. Gaborieau, S.P.S. Koo, P. Castignolles, T. Junkers, C. Barner-Kowollik, Reducing the degree of branching in polyacrylates via midchain radical patching: A quantitative melt-state NMR study, Macromolecules, 43 (2010) 5492-5495.
[22] M. Buback, G.T. Russell, P. Vana, Elucidation of Reaction Mechanisms: Conventional Radical Polymerization, in: C. Barner-Kowollik, T. Gründling, J. Falkenhagen, S. Weidner

(Eds.) Mass Spectrometry in Polymer Chemistry, Wiley-VCH Verlag & Co. KGaA, Weinheim, Germany, 2012, pp. 319-372.
[23] T. Junkers, S.P.S. Koo, T.P. Davis, M.H. Stenzel, C. Barner-Kowollik, Mapping poly(butyl acrylate) product distributions by mass spectrometry in a wide temperature range: Suppression of midchain radical side reactions, Macromolecules, 40 (2007) 8906-8912.
[24] S.P.S. Koo, T. Junkers, C. Barner-Kowollik, Quantitative product spectrum analysis of poly(butyl acrylate) via electrospray ionization mass spectrometry, Macromolecules, 42 (2009) 62-69.
[25] M. Gaborieau, T.J. Causon, Y. Guillaneuf, E.F. Hilder, P. Castignolles, Molecular weight and tacticty of oligoacrylates by capillary electrophoresis - mass spectrometry, Aus. J. Chem., 63 (2010) 1219-1226.
[26] C.M. Guttman, K.M. Flynn, W.E. Wallace, A.J. Kearsley, Quantitative mass spectrometry and polydisperse materials: Creation of an absolute molecular mass distribution polymer standard, Macromolecules, 42 (2009) 1695-1702.
[27] P. Castignolles, Transfer to Polymer and Long-Chain Branching in PLP-SEC of Acrylates, Macromol. Rapid Commun., 30 (2009) 1995-2001.
[28] L. Couvreur, G. Piteau, P. Castignolles, M. Tonge, B. Coutin, B. Charleux, J.P. Vairon, Pulsed-laser radical polymerization and propagation kinetic parameters of some alkyl acrylates, Macromolecular Symposia, 174 (2001) 197-207.
[29] T. Junkers, M. Schneider-Baumann, S.P.S. Koo, P. Castignolles, C. Barner-Kowollik, Determination of Propagation Rate Coefficients for Methyl and 2-Ethylhexyl Acrylate via High Frequency PLP-SEC under Consideration of the Impact of Chain Branching, Macromolecules, 43 (2010) 10427-10434.
[30] A.B. Pangborn, M.A. Giardello, R.H. Grubbs, R.K. Rosen, F.J. Timmers, Safe and convenient procedure for solvent purification, Organometallics, 15 (1996) 1518-1520.
[31] J.P.A. Heuts, T.P. Davis, G.T. Russell, Comparison of the Mayo and chain length distribution procedures for the measurement of chain transfer constants, Macromolecules, 32 (1999) 6019-6030.
[32] R.A. Hutchinson, D.A. Paquet, J.H. McMinn, Determination of free-radical chain-transfer rate coefficients by pulsed-laser polymerization, Macromolecules, 28 (1995) 5655-5663.
[33] D. Massiot, F. Fayon, M. Capron, I. King, S. Le Calve, B. Alonso, J.O. Durand, B. Bujoli, Z.H. Gan, G. Hoatson, Modelling one- and two-dimensional solid-state NMR spectra, Magnetic Resonance in Chemistry, 40 (2002) 70-76.

[34] G.B. Smith, G.T. Russell, The Cutthroat Competition Between Termination and Transfer to Shape the Kinetics of Radical Polymerization, Macromolecular Symposia, 248 (2007) 1-11.
[35] G.B. Smith, G.T. Russell, M. Yin, J.P.A. Heuts, The effects of chain length dependent propagation and termination on the kinetics of free-radical polymerization at low chain lengths, European Polymer Journal, 41 (2005) 225-230.
[36] Z.M. Gu, J.Y. Ma, X.G. Zhao, J. Wu, D.L. Zhang, Reduction of nitriles to amines in positive ion electrospray ionization mass spectrometry, Rapid Communications in Mass Spectrometry, 20 (2006) 2969-2972.
[37] M. Strohalm, "mMass - Open Source Mass Spectrometry Tool", in.
[38] J. Chiefari, J. Jeffery, R.T.A. Mayadunne, G. Moad, E. Rizzardo, S.H. Thang, Chain transfer to polymer: A convenient route to macromonomers, Macromolecules, 32 (1999) 7700-7702.
[39] A.M. Zorn, T. Junkers, C. Barner-Kowollik, Synthesis of a Macromonomer Library from High-Temperature Acrylate Polymerization, Macromol. Rapid Commun., 30 (2009) 2028-2035.
[40] J. Chiefari, J. Jeffrey, R.T.A. Mayadunne, G. Moad, E. Rizzardo, S.H. Thang, Chain Transfer to Polymer: A Convenient Route to Macromonomers, Macromolecules, 32 (1999) 7700-7702.
[41] S. Beuermann, M. Buback, C. Schmaltz, Termination rate coefficients of butyl acrylate free-radical homopolymerization in supercritical CO2 and in bulk, Industrial & Engineering Chemistry Research, 38 (1999) 3338-3344.
[42] M. Buback, M. Egorov, A. Feldermann, Chain-length dependence of termination rate coefficients in acrylate and methacrylate homopolymerizations investigated via the SP-PLP technique, Macromolecules, 37 (2004) 1768-1776.
[43] T. Junkers, C. Barner-Kowollik, The Role of Mid-Chain Radicals in Acrylate Free Radical Polymerization: Branching and Scission, Journal of Polymer Science Part a-Polymer Chemistry, 46 (2008) 7585-7605.
[44] J.P.A. Heuts, G.T. Russell, The nature of the chain-length dependence of the propagation rate coefficient and its effect on the kinetics of free-radical polymerization. 1. Small-molecule studies, European Polymer Journal, 42 (2006) 3-20.
[45] C. Plessis, G. Arzamendi, J.R. Leiza, H.A.S. Schoonbrood, D. Charmot, J.M. Asua, A Decrease in Effective Acrylate Propagation Rate Constants Caused by Intramolecular Chain Transfer, Macromolecules, 33 (2000) 4-7.

[46] A.N. Nikitin, R.A. Hutchinson, G.A. Kalfas, J.R. Richards, C. Bruni, The Effect of Intramolecular Transfer to Polymer on Stationary Free-Radical Polymerization of Alkyl Acrylates, 3-Consideration of Solution Polymerization up to High Conversions, Macromolecular Theory and Simulations, 18 (2009) 247-258.
[47] C. Plessis, G. Arzamendi, J.M. Alberdi, A.M. van Herk, J.R. Leiza, J.M. Asua, Evidence of Branching of Poly(butyl acrylate) Produced in Pulsed-Laser Polymerization Experiments, Macromol. Rapid Commun., 24 (2003) 173-177.
[48] A.N. Nikitin, R.A. Hutchinson, M. Buback, P. Hesse, Determination of Intramolecular Chain Transfer and Midchain Radical Propagation Rate Coefficients for Butyl Acrylate by Pulsed Laser Polymerization, Macromolecules, 40 (2007) 8631-8641.
[49] J. Barth, M. Buback, P. Hesse, T. Sergeeva, Termination and Transfer Kinetics of Butyl Acrylate Radical Polymerization Studied via SP-PLP-EPR, Macromolecules, 43 (2010) 4023-4031.
[50] J. Barth, W. Meiser, M. Buback, SP-PLP-EPR Study into Termination and Transfer Kinetics of Non-Ionized Acrylic Acid Polymerized in Aqueous Solution, Macromolecules, 45 (2012) 1339-1345.
[51] C. Barner-Kowollik, S. Beuermann, M. Buback, P. Castignolles, B. Charleux, M.L. Coote, R.A. Hutchinson, T. Junkers, I. Lacik, G.T. Russell, M. Stach, A.M. van Herk, Critically evaluated rate coefficients in radical polymerization - 7. Secondary-radical propagation rate coefficients for methyl acrylate in the bulk, Polym. Chem., 5 (2014) 204-212.
[52] S. Beuermann, M. Buback, T.P. Davis, R.G. Gilbert, R.A. Hutchinson, A. Kajiwara, B. Klumperman, G.T. Russell, Critically evaluated rate coefficients for free-radical polymerization, 3. Propagation rate coefficients for alkyl methacrylates, Macromolecular Chemistry and Physics, 201 (2000) 1355-1364.
[53] A.M. van Herk, Pulsed Initiation Polymerization Applied to Acrylate Monomers: Sources of Experimental Failure, Macromol. Rapid Commun., 22 (2001) 687-689.

Chapter 5

Conclusions

Over the course of this research project, the mechanism of radical polymerization of acrylic acid (AA) (hydrophilic monomer) and 2-ethylhexyl acrylate (2EHA) (hydrophobic monomer) was studied in depth. Poly(acrylic acid) (PAA) and poly(2-ethylhexyl acrylate) (P2EHA) were synthesized at various temperatures in the presence and absence of a chain transfer agent (CTA). P2EHAs were analysed by electrospray ionization-mass spectrometry (ESI-MS), thermogravimetric analysis (TGA), differential scanning calorimetry (DSC) and ^{13}C melt-state NMR spectroscopy. PAAs were analysed by ESI-MS, ^{1}H and ^{13}C solution-state NMR spectroscopy, capillary electrophoresis and Taylor dispersion analysis (TDA). ESI-MS analyses proved that in the cases of both AA and 2EHA polymerization, the transfer to a CTA occurs efficiently at various temperatures (from 50 °C to 90 °C for AA polymerization and from 4 °C to 140 °C for 2EHA polymerization). CTA-capped polymers were observed as the dominant species in all ESI-MS spectra of CTA-containing polymers. This confirmed the results observed by Hutchinson *et al.*: the transfer to a CTA does not depend on the temperature [1].

ESI-MS analyses have revealed that 2EHA radical polymerization is more complex than AA polymerization as (i) *β*-scission occurs at all temperatures, which was not observed previously and (ii) from 4 °C to 65 °C termination (by combination) products are observed. ESI-MS analyses of PAAs have only shown CTA-capped polymers. The average degrees of branching (*DB*) and of *β*-scission (*DβS*) (only for P2EHA) were measured by ^{13}C melt-state and solution-state NMR spectroscopy for P2EHA and PAA respectively. As ^{13}C NMR spectroscopy is not as sensitive as ESI-MS analysis, unsaturated double bonds due to *β*-scission were observed only in polymers obtained at 65 °C and above. *DβS* increases with the polymerization temperature and is reduced by the presence of a CTA. This confirms previous literature results for poly(*n*-butyl acrylate) (P*n*BA) [2, 3].

The presence of branches was observed between 50 °C and 90 °C for AA polymerization and between 65 °C and 140 °C for P2EHA, confirming previous literature results [4-7]. As was observed in the case of radical polymerization of *n*-butyl acrylate, the presence of a CTA considerably reduces *DB* [8, 9]. This is likely due to either the patching effect – a transfer of hydrogen radical between the CTA and the midchain radical (MCR) – or a reduction of the number of backbiting steps, because in the presence of a CTA the polymerization occurs for a shorter time.

This observed difference in *DB* could be strengthened by two factors. The first factor is that the reactions typically occur with an uncontrollable exotherm (even in relatively dilute solution) and therefore the temperature of the reaction leads to differences in the *DB* from what may be expected. This process will be enhanced when the solution is viscous and may lead to the differences between samples with and without CTA. The second factor is that high conversion is reached more quickly in the absence of CTA [5, 7]. This leads to an increase in *DB*, which is bigger at high conversion.

The *DB* increases with temperature because the frequency of backbiting and of intermolecular transfer to polymer (leading to the formation of MCRs) is higher at high temperature. In the case of 2EHA polymerization, this increase of *DB* is not observed above 100 °C. This is because the fragmentation of MCRs by *β*-scission becomes important. The *DB* observed in AA and 2EHA polymerization was compared with previous results in the literature. These comparisons show some consistency of the results obtained over this study. The *DB*s observed in this study do not vary with the initial monomer concentration. This indicates that the formation of branches by intermolecular transfer is not negligible [10], due to high monomer conversion. However, even though *DB*s of P2EHAs and of P*n*BAs were measured and compared previously, the effect of transfer agent and reaction temperature on *DB* of P2EHAs was never studied and the DβS was never defined or calculated. The quantification of *β*-scission products was carried out only by ESI-MS.

It is important to note that the accuracy of the *DB* obtained in AA polymerization is lowered by the presence of non-soluble PAA fractions (in D_2O), whose branching is not detected [11]. The backbiting rate coefficients k_{bb} were obtained from *DB* at high monomer conversion. Nikitin *et al*. were able to link the *DB* to the ratio of backbiting to propagation rates coefficients, taking into account the effect of monomer conversion [12]. The obtained Arrhenius equation was consistent with previous literature results obtained by pulsed laser polymerization (PLP) coupled with size exclusion chromatography (SEC) [13, 14]. Arrhenius fits were obtained with a correlation above 0.9, demonstrating the validity of Nikitins equation, which was never used before.

The dispersity of electrophoretic mobility in non-CTA-containing PAA, which is directly related to the heterogeneity of branching [15], was determined by capillary electrophoresis in the critical condition (CE-CC). As basic buffers were used, PAAs were analysed as poly(sodium acrylate) (PNaA). It is known that PNaAs can be separated by branching using

CE-CC [16]. The heterogeneity of branching in linear PNaA and of PNaAs synthesized by nitroxide mediated polymerization (NMP) initiated with a multifunctional initiator (alkoxyamine inimer) was determined previously [15]. Our study proved that neither the polymerization temperature nor the initial monomer concentration significantly influences the heterogeneity of branching. However, the heterogeneity increases with the diversity of branching structures as it was expected.

To better understand the mechanism of separation of polyelectrolyte by CE, further CE-CC analyses of branched PNaA were carried out. Electropherograms of PNaAs obtained in sodium borate buffers exhibit two peaks, which were not identified until now. The relation between the electrophoretic mobility and the structure was determined using a so-called slope plot [17]. Linear, 3-arm star and hyperbranched PNaAs were analysed in sodium borate buffer at different concentrations (from 110 to 300 mmol L^{-1}). The variation of electrophoretic mobility μ_{ep} with the buffer concentration was much more important for the sharp peak than for the broad peak. As the analyses of the linear PNaA lead to similar variations of μ_{ep} for the broad peak, it was identified as a slightly branched chains population while the sharp peak was identified as a highly branched chains population. Previously, PNaAs had been separated by branching in sodium borate buffer at only 110 mmol L^{-1} [15, 16]. At this buffer concentration, highly branched polymers exhibit a lower μ_{ep} than slightly branched polymers. At higher buffer concentration, the separation is inverted. This could be because branched polyacrylates (negatively charged) can easily complex with a positively charged counter ion (sodium in this case). At higher buffer concentration, branched polyacrylates might complex with the borate (negatively charged) rather than the sodium. As a result, the overall charge might be increased, and then μ_{ep} (which is proportional to the ratio of the absolute value of the charge to the friction) is higher than for the unbranched species, which may not complex the borate as effectively. Based on these results, the heterogeneity of branching was determined in optimal conditions: with sodium borate buffer concentration of 300 mmol L^{-1}. At this buffer concentration, broad and sharp peaks are completely resolved. It was not possible to use a buffer concentration lower than 110 mmol.L^{-1} as some pressure mobilization experiments have demonstrated the adsorption of PNaA on the capillary. The heterogeneity of branching of both sharp and broad peaks was determined separately for PNaAs synthesized by conventional radical polymerization as well as 3-arm star and hyperbranched PNaAs. The branching of the sharp peak is very homogeneous. Most of the heterogeneity of branching is due to the broad peak. As it is a slightly branched chains population, both linear and branched species are likely to be

present, which might not be the case for the highly branched chains population. As CE-CC analysis is carried out with a UV detector, the area of each peak is proportional to the concentration of the corresponding species (Beer-Lambert law). By comparing the peak areas, the contribution of broad and sharp peaks was calculated. The contribution of the sharp peak is highest in the hyperbranched PNaA, which has the highest *DB*. This confirms the identification thate sharp peak corresponds to a highly branched chain population. The effect of addition of silver nitrate in the buffer on the separation's selectivity was tested, but μ_{ep} remains in the same range when the silver nitrate concentration is varied from 0 to 100 mmol L^{-1}. This was not the expected effect [18]. This is most likely to be because the complexation of boric acid (or borate) is stronger than the complexation of silver by PNaA.

As it is proven that SEC is an inaccurate method of size determination for PAA – errors of 100 % are reported in the literature [19] – size-based characterization using alternative methods needs to be tested. The main focus of future work should consist of firstly measuring the diffusion coefficient *D* and the hydrodynamic radius of PAA by TDA, and then measuring the M_n of CTA-containing PAAs by quantifying the fraction of the CH_2 chain end using ^1H solution-state NMR spectroscopy analysis. From these results, it should be possible to discuss the influence of the temperature on the transfer to a CTA. Some work has already been initiated and is presented in Chapter 5.

References

[1] R.A. Hutchinson, D.A. Paquet, J.H. McMinn, Determination of free-radical chain-transfer rate coefficients by pulsed-laser polymerization, Macromolecules, 28 (1995) 5655-5663.

[2] S.P.S. Koo, T. Junkers, C. Barner-Kowollik, Quantitative product spectrum analysis of poly(butyl acrylate) via electrospray ionization mass spectrometry, Macromolecules, 42 (2009) 62-69.

[3] T. Junkers, S.P.S. Koo, T.P. Davis, M.H. Stenzel, C. Barner-Kowollik, Mapping poly(butyl acrylate) product distributions by mass spectrometry in a wide temperature range: Suppression of midchain radical side reactions, Macromolecules, 40 (2007) 8906-8912.

[4] E. Sato, T. Emoto, P.B. Zetterlund, B. Yamada, Influence of mid-chain radicals on acrylate free radical polymerization: Effect of ester alkyl group, Macromolecular Chemistry and Physics, 205 (2004) 1829-1839.

[5] F. Heatley, P.A. Lovell, T. Yamashita, Chain transfer to polymer in free-radical solution polymerization of 2-ethylhexyl acrylate studied by NMR spectroscopy, Macromolecules, 34 (2001) 7636-7641.

[6] C. Plessis, G. Arzamendi, J.M. Alberdi, M. Agnely, J.R. Leiza, J.M. Asua, Intramolecular chain transfer to polymer in the emulsion polymerization of 2-ethylhexyl acrylate, Macromolecules, 34 (2001) 6138-6143.

[7] N.F.G. Wittenberg, C. Preusser, H. Kattner, M. Stach, I. Lacík, R.A. Hutchinson, M. Buback, Modeling acrylic acid radical polymerization in aqueous solution, Macromolecular Reaction Engineering, 10 (2016) 95-107.

[8] M. Gaborieau, S.P.S. Koo, P. Castignolles, T. Junkers, C. Barner-Kowollik, Reducing the degree of branching in polyacrylates via midchain radical patching: A quantitative melt-state NMR study, Macromolecules, 43 (2010) 5492-5495.

[9] N. Ballard, J.C. de la Cal, J.M. Asua, The role of chain transfer agent in reducing branching content in radical polymerization of acrylates, Macromolecules, 48 (2015) 987-993.

[10] N.M. Ahmad, F. Heatley, P.A. Lovell, Chain transfer to polymer in free-radical solution polymerization of n-butyl acrylate studied by NMR spectroscopy, Macromolecules, 31 (1998) 2822-2827.

[11] J.-B. Lena, A.K. Goroncy, J.J. Thevarajah, A.R. Maniego, G.T. Russell, P. Castignolles, M. Gaborieau, Effect of transfer agent, temperature and initial monomer concentration on

branching in poly(acrylic acid): A study by 13C NMR spectroscopy and capillary electrophoresis, Polymer, 114 (2017) 209-220.
[12] A.N. Nikitin, R.A. Hutchinson, G.A. Kalfas, J.R. Richards, C. Bruni, The Effect of Intramolecular Transfer to Polymer on Stationary Free-Radical Polymerization of Alkyl Acrylates, 3-Consideration of Solution Polymerization up to High Conversions, Macromolecular Theory and Simulations, 18 (2009) 247-258.
[13] J. Barth, W. Meiser, M. Buback, SP-PLP-EPR study into termination and transfer kinetics of non-ionized acrylic acid polymerized in aqueous solution, Macromolecules, 45 (2012) 1339-1345.
[14] H. Kattner, M. Buback, Termination, Propagation and Transfer Kinetics of Midchain Radicals in Methyl, Acrylate and Dodecyl Acrylate Homopolymerization, Macromolecules, (2017).
[15] J.J. Thevarajah, A.T. Sutton, A.R. Maniego, E.G. Whitty, S. Harrisson, H. Cottet, P. Castignolles, M. Gaborieau, Quantifying the heterogeneity of chemical structures in complex charged polymers through the dispersity of their distributions of electrophoretic mobilities or of compositions, Analytical Chemistry, 88 (2016) 1674-1681.
[16] A.R. Maniego, D. Ang, Y. Guillaneuf, C. Lefay, D. Gigmes, J.R. Aldrich-Wright, M. Gaborieau, P. Castignolles, Separation of poly(acrylic acid) salts according to topology using capillary electrophoresis in the critical conditions, Analytical and Bioanalytical Chemistry, 405 (2013) 9009-9020.
[17] A. Ibrahim, S.A. Allison, H. Cottet, Extracting Information from the Ionic Strength Dependence of Electrophoretic Mobility by Use of the Slope Plot, Analytical Chemistry, 84 (2012) 9422-9430.
[18] A. Ezhova, K. Huber, Specific interactions of Ag+ ions with anionic polyacrylate chains in dilute solution, Macromolecules, 47 (2014) 8002-8011.
[19] I. Lacík, M. Stach, P. Kasák, V. Semak, L. Uhelská, A. Chovancová, G. Reinhold, P. Kilz, G. Delaittre, B. Charleux, I. Chaduc, F. D'Agosto, M. Lansalot, M. Gaborieau, P. Castignolles, R.G. Gilbert, Z. Szablan, C. Barner-Kowollik, P. Hesse, M. Buback, SEC analysis of poly(acrylic acid) and poly(methacrylic acid), Macromolecular Chemistry and Physics, 216 (2015) 23-37.

Chapter 6

Further size-based characterization of poly(acrylic acid) using alternative methods to size exclusion chromatography

6.1 Introduction

As explained previously, the presence of long chain branching (LCB) leads to ineffective separation of branched polymers, such as PAA [1] and P2EHA [2], in terms of molar mass. Specifically, two polymers of different *M* can have the same hydrodynamic volume, V_h, due to branching: a branched chain of larger *M* will have the same V_h as a less branched (or even linear) chain of smaller *M*. This has long been known as a problem with size-exclusion chromatography. Historically there has been a lot of effort to resolve this issue for polyethylene given the massive importance of low density polyethylene (LDPE) as a commercial product. However, it is now recognized that this is also a problem for acrylates, and for this reason there has been focus on this aspect of the problem for the best part of two decades. One broad approach for solving this problem is deconvolution of SEC chromatograms. This is highly mathematical and involves knowledge of the branching distribution and its effect on elution volumes. The other broad approach is to develop other methods for characterization of acrylate polymers. These yield alternative information about polyacrylates, which may either indirectly shed light on the molar mass, or else obviate the need to know it. In this chapter of my thesis I will consider the latter approach for PAA. The considerations should be applicable to hydrophilic polymers in general.

6.1.1 Measurement of the diffusion coefficient using Taylor dispersion analysis

Different methods to measure the diffusion coefficient, *D*, of a particle are known. These methods can be divided into two categories. One of them includes free diffusion [3], sedimentation [4], dynamic light scattering [5] and Taylor dispersion analysis (TDA), and allows computing an average diffusion coefficient over a full sample. The other category includes methods for which the retention is related to the diffusion of the analyte, such as SEC [6] or field flow fractionation [7]: these can be used to calculate *D* in separated zones.

It is important to note that *D* is related to the hydrodynamic diameter d of the polymer according to Eq. (6.1).

$$D = \frac{K_B T}{3\pi\eta d} \tag{6.1}$$

Where η is the viscosity of the solution and *d* is the hydrodynamic diameter.

6.1.1.1 Description of the method

Based on the works of Taylor [8] and Aris [9], TDA is a method in which the dispersion coefficient of a solute plug in an open tube under Poiseuille laminar flow is calculated. Due to a parabolic velocity profile, molecules injected in a narrow band at the inlet end of the tube move with different velocities depending on their position in the tube cross section. The dispersion of the solute plug depends on the molecular diffusion that redistributes the molecules over the cross section of the tube. When the method was first developed by Taylor, the solute concentration at different positions in the tube at a given time needed to be measured. Then, a few years later, fast-flow-through chromatographic detectors allowed the calculation of the dispersion coefficient from the distribution of solute concentration at a given position along the tube (the outlet) as a function of time.

TDA is applicable to particles of any molar mass. As an absolute method, no calibration is needed and the concentration of the analyte does not need to be known if it is low enough for *D* to correspond to the high dilution limit. This has been applied to measure *D* of solutes in gaseous [10] and liquid [11] phases. Capillary zone electrophoresis instrumentation, which allows the detection of a concentration at a given location inside the column, was shown to be suited for TDA [12]. In 2007, Cottet *et al.* carried out some TDA analyses of sample mixtures and established equations to calculate *D*. Then, they verified the validity of these equations on experimental mixtures of polymeric and small molecules [13]. In 2008, Le Saux *et al.* demonstrated the possibility of performing TDA after a CE separation for analysis of a mixture of polymers [14].

6.1.1.2 Theory

Combination of the dispersive velocity profile with the molecular diffusion leads to a specific mechanism of dispersion [14]. It is described by the Taylor-Aris-Gloray equation [15], in which the plate height *H* of an analyte unretained in a capillary column of radius *R* is related to the eluent velocity *u* and the molecular diffusion coefficient *D* as follows:

$$H = \frac{2D}{u} + \frac{R^2 u}{24D} \tag{6.2}$$

The plate height H is related to the elution time t_r and the temporal variance σ_s^2 of the elution peak as follows:

$$H_S = L\frac{\sigma^2}{t_r^2} \tag{6.3}$$

If the elugram provides a Gaussian-shaped peak, it can be considered that the full width at half maximum (FWHM) is equal to the temporal variance. Eq. 6.3 then becomes:

$$H_S = L\frac{FWHM}{t_r^2} \tag{6.4}$$

To determine the diffusion coefficient, it is possible to perform experiments at various carrier velocities. For each velocity, H is calculated and the graph $H = f(u)$ is plotted. The slope S is determined and D can be calculated with Eq. 6.5:

$$D = \frac{R^2}{24S} \tag{6.5}$$

6.1.2 Fraction of CH_2 chain end determined by ^{1}H NMR spectroscopy

From ^{1}H NMR spectroscopy analyses of PAA, it is possible to quantify the fraction of terminal CH_2 (adjacent to a COOH group in the last monomer unit of the chain), $X_{CH2\ term}$. $X_{CH2\ term}$ is defined as the number of CH_2-COOH terminals per monomer unit (i.e., it is a fraction). It can be calculated by comparing the integrals of the CH_2 a or b signals (defined in Scheme 6.1) with the main-chain CH_2 signal, and its value is between 0 and 1. These groups can be obtained by transfer to CTA, transfer to solvent, disproportionation or transfer to polymer. Scheme 6.1 summarizes the reactions leading to terminal CH_2 groups. By comparing the evolution of $X_{CH2\ term}$ of PAAs synthesized with and without CTA with the temperature, information related to the activation energy of transfer in comparison to propagation can be extracted.

6.1.3 Aim of this chapter

The two methods described above have been tested on CTA- and non-CTA-containing PAAs. The aim was to determine both accurately and precisely the diffusion coefficient by TDA. From $X_{CH2\ term}$, as obtained from NMR results, the aim was to calculate the difference of activation energy between transfer and propagation rate coefficients. Even though these aims were not fully realized because part of this work failed, the potential application of these methods has led to results that merit description and will allow future research to be carried out.

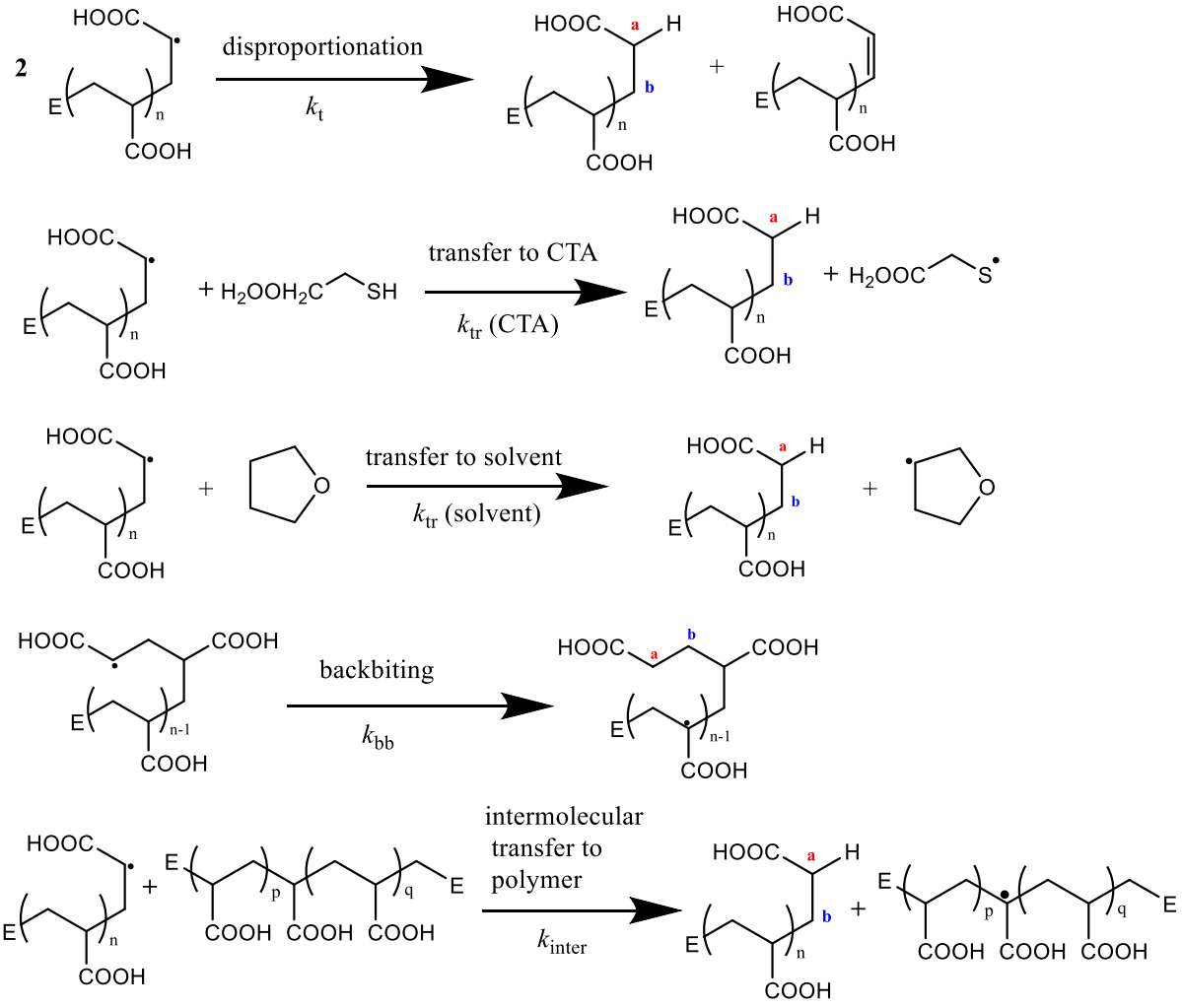

Scheme 6.1: Showing reactions leading to a terminal CH_2, where E represents an end group. In this work THF and thioglycolic acid were used as examples of solvent and CTA respectively, hence showing them above.

6.2 Materials and methods

6.2.1 Materials

Milli-Q water was used. Boric acid (≥ 98 %) was purchased from BDH AnalaR, Merck Pty Ltd. Sodium hydroxide pellets and dimethyl sulfoxide (DMSO) were provided by Sigma-Aldrich. Deuterium oxide (99.9 % D) was supplied by Cambridge Isotope Laboratory Inc. The linear, hyperbranched and 3-arm star PNaAs were obtained from PSS (Mainz, Germany), as described in [16]. Acrylic acid (AA, 99 %) and 4,4'-azobis(4-cyanovaleric acid) (75 %+) were supplied by Sigma-Aldrich.

6.2.2 Synthetic methods

Linear and hyperbranched PAA were synthesized as described in [16]. The synthesis of PAA by conventional radical polymerization is described in [17] and in Chapter 2.

6.2.3 Capillary electrophoresis and pressure mobilization

Free-solution capillary electrophoresis (CE) and pressure mobilization (PM) experiments were carried out using an Agilent 7100 CE (Agilent Technologies, Waldbronn, Germany) instrument equipped with a UV detector. Polyimide-coated fused silica high sensitivity capillaries (50 μm internal diameter) were obtained from Agilent. The capillary (62.3 cm total length, 53.8 cm effective length) was initially pre-treated by flushing with 1 M NaOH for 10 min, then with 0.1 M NaOH, then Milli-Q water and finally sodium borate buffer for 5 min each at the start of the series of experiments. An oligo(sodium acrylate) was separated [18] in NB110 and NB300 at pH 9.2 to validate the capillary and the instrument before each session. The mobile phase for poly(sodium acrylate) (PNaA) analysis was NB300 at pH 9.2. Some tests to check potential adsorption of PNaA on the capillary were carried out using NB110 and NB300 at pH 9.2 on PAAs synthesized at 90 °C with and without CTA. Results are presented in Chapter 3 and in Appendix 2. Because CTA-containing PAAs adsorb on the capillary when NB110 at pH 9.2 is used as the mobile phase (on Figure A-6-1 in Appendix 2, a peak of adsorption is observed), the 300 mM concentration was preferred for this study. CE was undertaken by applying 30 kV at 25 °C. PM was carried out at five different pressures: 100, 90, 80, 70 and 60 mbar (without electric field). For PM, the sample was mixed with the background electrolyte by varying the electric field. This involved ramping the voltage up to 30 kV and

then down to −30 kV and back up to 0 kV over the first 4 min of separation. The mixing of the PNaA with the mobile phase is due to the electroneutrality of the solution needing to be maintained at all times, even during the ramping process. Details are given in the study by Thevarajah *et al.* [19]. Each injection was done in triplicate. To calculate H_s and u, the average values of t_r and FWHM were taken and their *SD* values were neglected. Values of t_r, FWHM, H_s, u and correlation coefficients of Gaussian fits are given in Tables A.6.1 to A.6.3 in Appendix 2. Only the *SD* of the slope was considered to determine *D*. Details are provided in Appendix 2 (see Eq. (A.6.1) to (A.6.5)).

6.2.4 Solution-state NMR spectroscopy

6.2.4.1 Conditions for analyses

Spectra of PAAs synthesized by conventional radical polymerization with and without CTA were acquired in D_2O at 26 °C (^{1}H NMR spectra) on an Agilent 400 MR with Varian 7600-AS auto-sampler, equipped with a OneNMR probe and variable temperature capabilities, operating at Larmor frequencies of 399.84 MHz. The concentration was 3 g L^{-1}. One-dimensional ^{1}H NMR spectra were acquired with 16,384 data points, 100 scans, 16 ppm spectral width (6,410.3 Hz), 10 s relaxation delay, 2.556 s acquisition time and a 90° flip angle.

6.2.4.2 T_1 measurement

A full inversion recovery experiment was carried out to measure the T_1 of each proton. In total, 32 values of τ were used. To obtain quantitative spectra, full recovery of the spins needs to occur. Results are presented below.

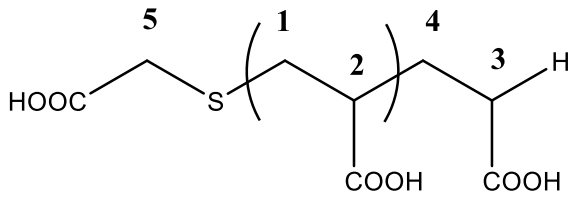

Scheme 6.2: Structure of CTA-containing PAA with carbon atoms numbered.

Table 6.1: T_1 measurements of ^{1}H NMR signals for CTA-containing PAA.

Signal	T_1 (s)	Error*
1	0.3589	0.006436
2	0.6987	0.0071
3	2.13	0.01276
4	1.958	0.01063
5	2.168	0.01088
6 (residual HOD)	16.64	0.4747

*The error was obtained with the Wnmr software package (Agilent Technology)

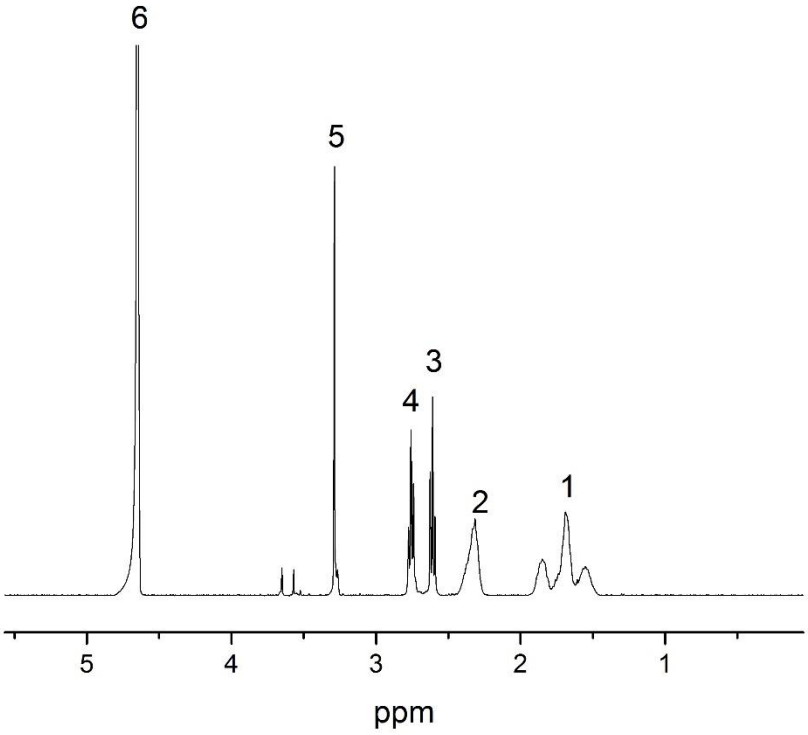

Figure 6.1: ^{1}H NMR spectrum of PAA synthesized at 50 °C with CTA. The measurement was carried out in D_2O at 3 g L^{-1}.

6.2.4.3 Calculation of X_{CH2}

$X_{CH2\ term}$ was quantified in percentage of monomer units by comparing the integrals, *I*, of signals a or b (defined in Scheme 1) at 2.88 and 2.75 ppm respectively and of the main chain CH_2 at 1.65 to 1.95 ppm as follows:

$$X_{CH2\ term} = \frac{100\ I\ (a)}{I(a) + I\ (main\ chain\ CH2)} \tag{6.6}$$

$$X_{CH2\ \text{term}} = \frac{100\ I\ (b)}{I(b) + I\ (main\ chain\ CH2)} \tag{6.7}$$

The *SD* of $X_{\text{CH2 term}}$ was calculated based on the *SNR* of the signals of protons a and b using Eq. (6.8) [20]:

$$SD = \frac{238}{SNR^{1.28}} \tag{6.8}$$

Results are given in Table A.6.4 in Appendix 2.

6.3 Results and discussions

Diffusion coefficients and fraction of CH_2 chain end were determined for all PAAs synthesized by conventional polymerization. The diffusion coefficient of the hyperbranched and linear PAAs were calculated as references.

6.3.1 Diffusion coefficients

First, it is important to note that, as expected, TDA works for PNaAs. As observed in Figure 6.2 and in Figures A.6.2 and A.6.3 of Appendix 2, the linear fits $H = f(u)$ all have a correlation coefficient better than 0.95.

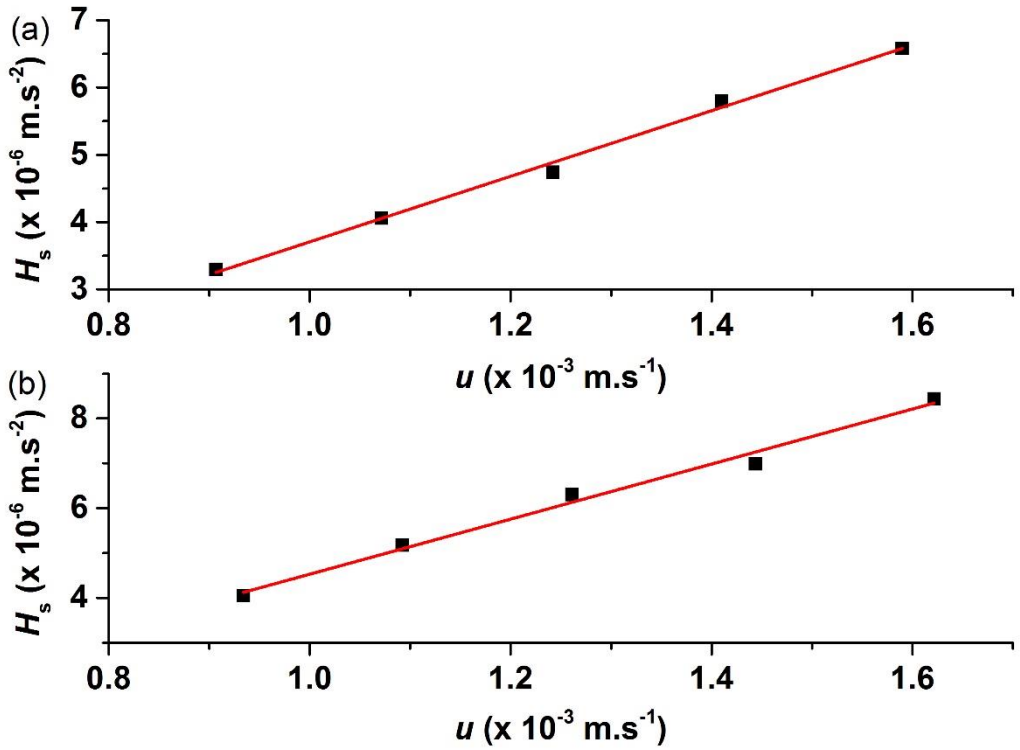

Figure 6.2: $H_s = f(u)$ obtained by TDA for (a) linear PNaA, and (b) hyperbranched PNaA.

Figure 6.3 shows the evolution of *D* with the synthesis temperature and initial monomer concentration. Both the size and degree of branching (*DB*) are expected to influence the value of *D*, which is expected to decrease with size but to increase with *DB* [21]. Naturally, the linear PNaA has the lowest *D* as it does not have any branches. Its M_n was measured by SEC as 39 000 g mol^{-1}. The PNaAs synthesized with CTA at 70 and 90 °C have a DP_n around 10, whilst the CTA-containing PNaA synthesized at 50 °C has a DP_n close to 5. This explains the difference between the *D* of CTA- and non-CTA-containing PNaA obtained at 50 °C. At 70 and 90 °C, a smaller increase in *D* is observed when the synthesis is carried out with a CTA.

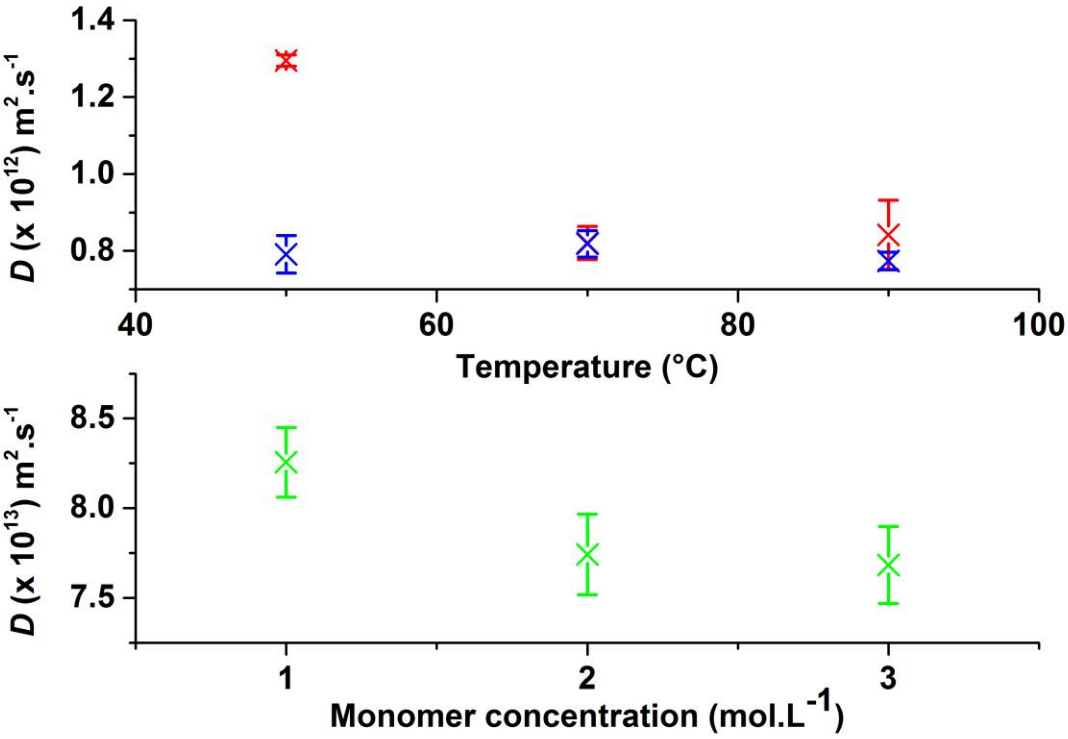

Figure 6.3: Diffusion coefficient of PNaAs synthesized by conventional radical polymerization as a function of temperature (upper graph) and initial monomer concentration (lower graph). Red crosses represent CTA-containing PNaAs and blue points represent non-CTA-containing PNaAs. On the lower graph, green crosses represent PNaAs synthesized at 90 °C by conventional radical polymerization without CTA.

Several hypotheses are possible to explain these results. First, the size might not affect the diffusion coefficient above a certain DP_n. Second, the branching plays a role: as a higher *DB* is observed at 70 and 90 °C, the value of *D* of non-CTA-containing PNaA could be increased due to the higher value of *DB*. However, the most likely hypothesis is the imprecision of these measurements. As only five points were used, the standard deviation of the slope of the graphs $H = f(u)$ leads to measurements of *D* with limited precision. Considering this, it is not possible at this stage to have a formal conclusion from these analyses. More experiments need to be carried out to obtain more data. From Figure 6.3, it is observed that the diffusion coefficient is likely to decrease with the initial monomer concentration. As no variation of *DB* was observed between these three PNaAs, this is probably due to the size: higher M_n is obtained at high monomer concentration, and thus lower *D*.

Table 6.2: Diffusion coefficients of PNaAs.

Polymer	Diffusion coefficient, *D* ($m^2.s^{-1}$)	Slope	*SD* (slope)	*SD* (*D*)	Correlation coefficient
PAA synthesized at 50 °C with CTA $[AA]_0$=2M	1.30×10^{-12}	8.29×10^{-4}	9.29×10^{-6}	1.45×10^{-14}	0.9995
PAA synthesized at 50 °C without CTA $[AA]_0$=2M	7.91×10^{-13}	5.06×10^{-4}	3.12×10^{-5}	4.88×10^{-14}	0.98495
PAA synthesized at 70 °C with CTA $[AA]_0$=2M	8.20×10^{-13}	5.25×10^{-4}	2.79×10^{-5}	4.35×10^{-14}	0.98882
PAA synthesized at 70 °C without CTA $[AA]_0$=2M	8.17×10^{-13}	5.24×10^{-4}	2.21×10^{-5}	3.46×10^{-14}	0.99289
PAA synthesized at 90 °C with CTA $[AA]_0$=2M	8.42×10^{-13}	5.39×10^{-4}	1.91×10^{-5}	9.06×10^{-14}	0.9552
PAA synthesized at 90 °C without CTA $[AA]_0$=1M	8.25×10^{-13}	5.28×10^{-4}	1.24×10^{-5}	1.94×10^{-14}	0.99778
PAA synthesized at 90 °C without CTA $[AA]_0$=2M	7.75×10^{-13}	4.95×10^{-4}	1.44×10^{-5}	2.25×10^{-14}	0.99664
PAA synthesized at 90 °C without CTA $[AA]_0$=3M	7.69×10^{-13}	4.92×10^{-4}	1.38×10^{-5}	2.15×10^{-14}	0.99688
Linear PNaA	7.61×10^{-13}	4.87×10^{-4}	1.91×10^{-5}	2.98×10^{-14}	0.99389
Hyperbranched PNaA	9.59×10^{-13}	6.13×10^{-4}	3.68×10^{-5}	5.75×10^{-14}	0.98574

However, the use of CE equipment introduces a nonideality that has not been considered. The Taylor and Aris method assumes that the mean fluid velocity *u* (fluid velocity averaged over the cross section of the capillary) is a constant and steady-state value. As the centrifugation of commercial CE instruments requires the fluid flows along a capillary to stop for the solute to be injected, there is an initial acceleration of the fluid after injection as the flow rate is increased from zero to the steady-state value. This is called the "ramping up" effect in the velocity [22].

The conditions for Eq. 6.2 to be valid can be determined by using dimensionless quantities: (i) τ, the ratio of the residence time to the time required for a solute to diffuse a distance equal to the radius of the capillary, and (ii) the Peclet number, *Pe*, which describes the relative rates

of mass transfer along the axis of the capillary due to convection and diffusion. The quantities τ and *Pe* are defined as follows:

$$\tau = \frac{Dt_r}{R^2} \tag{6.9}$$

$$Pe = \frac{uR}{D} \tag{6.10}$$

Taylor showed the validity of Eq. 6.2 if (i) τ is greater than the time required to decrease variation in radial concentration and $\tau >> 0.14$, and (ii) diffusion in the axial direction is greater than the convection ($Pe >> 7$) [23]. Even though these conditions cannot be predicted, τ and *Pe* were determined. The results are in Table A-6-4 in Appendix 2. It clearly appears that some corrections will be required at $0.1 < \tau < 0.2$, which does not meet the condition to use Eq. 6.2. In future, Eqs. 6.11 to 6.13 will need to be used [22].

$$D + \frac{R^2u^2}{48D} = \frac{1}{4}u^2t_r\left(-1 + \sqrt{1 + \frac{4\sigma^2}{t_r^2}}\right) \tag{6.11}$$

$$t_r = t_{r,obs}\left(1 - \left(\frac{V_i}{2\pi R^2 l}\right)\right) \tag{6.12}$$

$$\sigma^2 = \sigma_{obs}^2 - \frac{t_{r,obs}^2}{12}\left(\frac{V_i}{\pi R^2 l}\right)^2 \tag{6.13}$$

Here V_i is the volume of the injection plug.

6.3.2 Fraction of CH_2 chain ends

Figure 6.4 shows that the terminal CH_2 signals are not visible in the NMR spectra of non-CTA-containing PAAs. The other ^{1}H NMR spectra of PAA are presented in Figure A.6.5. Their X_{CH2} is thus below the limit of detection by NMR. This suggests that the reactions of disproportionation and transfer to THF do not occur to a major extent, which is as expected – acrylate termination is known to be predominantly by combination. However, as these PAA polymers are branched, backbiting and intermolecular transfer to polymer occur, leading to MCRs and terminal CH_2. X_{CH2} should be equal to or higher than the degree of branching and thus should be detected (see Figure A.6.5 in Appendix 2). At this stage, there is no definitive explanation for this observation. It could be that the terminal CH_2 might overlap with other signals. It could also be that the ^{13}C NMR experiments to measure *DB* had a better limit of

detection than the present ^{1}H NMR experiments, although it is admitted this is opposite to usual practice.

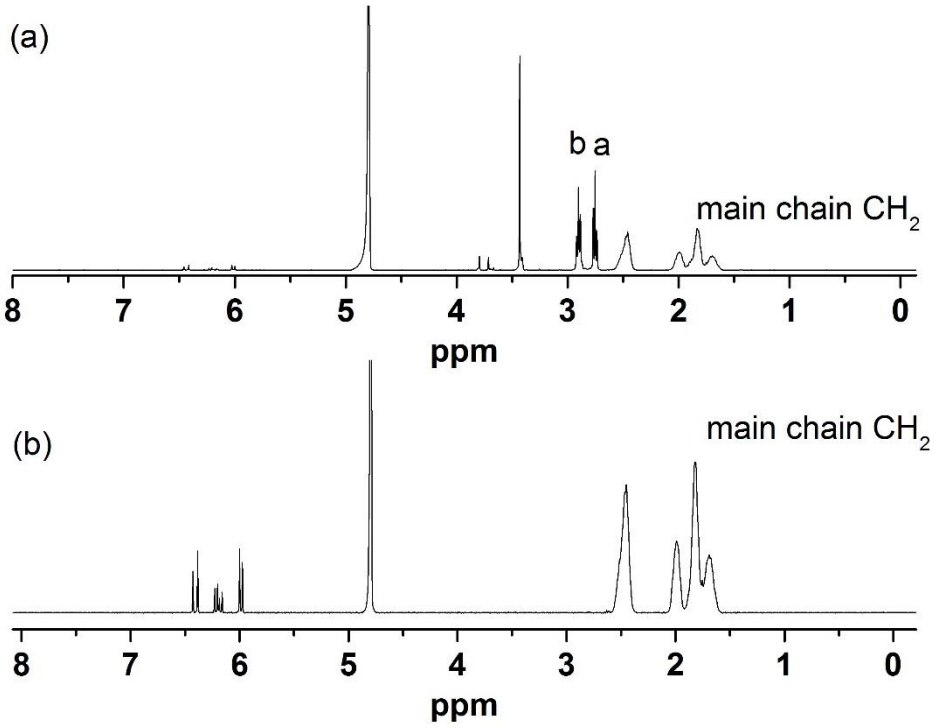

Figure 6.4: ^{1}H NMR spectra of PAA made at 50 °C and analysed in D_2O (a) CTA-containing PAA, (b) non-CTA-containing PAA.

Figure 6.5 shows that the $X_{CH2\ term}$ decreases significantly with temperature when PAAs are synthesized with CTA. This means that the transfer to thioglycolic acid efficiency decreases from 50 °C to 90 °C, which suggests that the activation energy of SPR propagation is larger than that of transfer to thioglycolic acid. Consequently, the efficiency of transfer from acrylic acid to thioglycolic acid decreases with temperature. This would also suggest that the patching effect occurs more at 50 °C than at 90 °C. However, the difference of *DB* between CTA- and non-CTA-containing PAA is more important at 90 °C. Consequently, the decrease of *DB* in the presence of a CTA is more likely due to the reduction in the number of backbiting events compared with propagation, rather than the patching effect. However, these results need to be treated with caution as (i) there is uncertainty around the determined conversion, which influences the $X_{CH2\ term}$, as the size of a polymer depends on the conversion [24], and (ii) they are not consistent with the results observed for the transfer from dodecanethiol to alkyl

methacrylates [25]. However, it could be that acrylates are opposite to methacrylates in this regard.

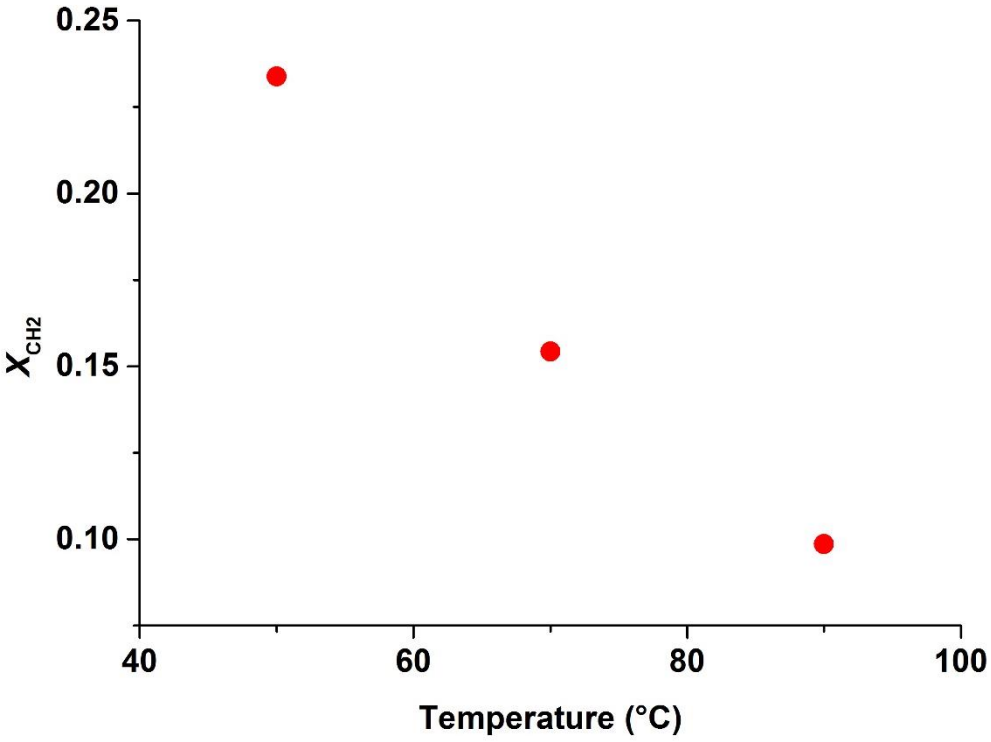

Figure 6.5: $X_{\mathrm{CH2\ term}}$ calculated from Eq. (6.5) as a function of temperature.

6.3.3 Estimation of the activation energy of transfer to thioglycolic acid

As explained in Chapter 1, if a polymer has been synthesized in a system containing a CTA that reacts irreversibly with the polymer chain, its degree of polymerization, DP_{n}, can be expressed as follows:

$$\frac{1}{\overline{DP_n}} = \frac{1}{\overline{DP_n^0}} + \frac{k_{\mathrm{tr}}}{k_{\mathrm{p}}}\frac{[\mathrm{CTA}]}{[\mathrm{M}]} \tag{6.14}$$

Here DP_{n}^0 is the degree of polymerization that is obtained in the absence of CTA, M is monomer, and k_{tr} and k_{p} are the transfer and SPR propagation rate coefficients respectively.

Moreover, if it is reasonably assumed that termination, transfer to THF and the effect of branching (DB < 0.4 % for the CTA-containing PAA) on $X_{\mathrm{CH2\ term}}$ are negligible (noting that here 'term' denotes 'terminal' rather than 'termination'), Eq. 6.14 becomes:

$$X_{CH2\ term} = \frac{k_{\mathrm{tr}}}{k_{\mathrm{p}}}\frac{[\mathrm{CTA}]}{[\mathrm{M}]} \tag{6.15}$$

This is just the so-called transfer limit of the Mayo equation. Substituting Arrhenius expressions for the rate coefficients into Eq. 6.15 it is obtained that

$$\ln(X_{CH2\ term}) = \ln(A_{\mathrm{tr}}) - \ln(A_{\mathrm{p}}) + ln\frac{[\mathrm{CTA}]}{[\mathrm{M}]} + \left(\frac{E_{\mathrm{a,p}} - E_{\mathrm{a,tr}}}{RT}\right) \qquad (6.16)$$

Here A and E_{a} are pre-exponential factor and activation energy respectively.

Figure 6.6 is an Arrhenius plot for ln ($X_{\mathrm{CH2\ term}}$). The linear fit parameters are in Table A.7.6 in Appendix 2.

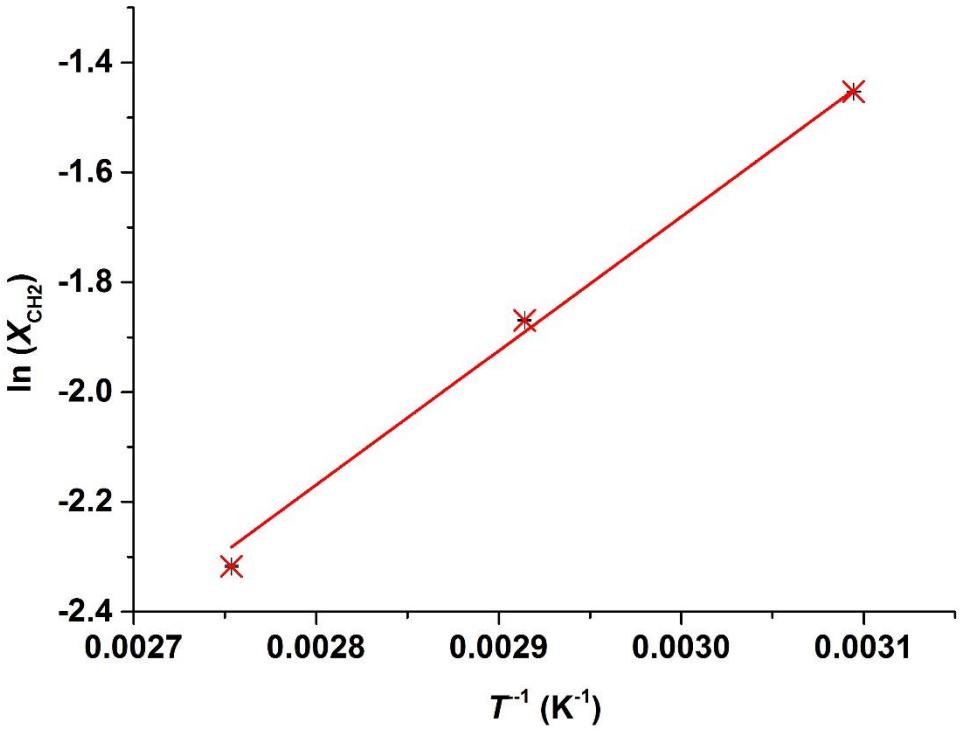

Figure 6.6: Arrhenius plot of $X_{\mathrm{CH2\ term}}$.

According to Figure 6.6, $E_{\mathrm{a,p}} - E_{\mathrm{a,tr}} \approx 20$ kJ mol^{-1}. This is physically implausible, because it is known that $E_{\mathrm{a,p}} = 17$ kJ mol^{-1} for *n*-alkyl acrylates in bulk [26], and it may be even lower for AA in water [24]. So the result of Figure 6.6 implies a negative activation energy for transfer of thioglycolic acid to AA, which cannot be correct. One possible problem with the analysis here is the implicit assumption of constant [CTA]/[M] in all experiments (see Eq. 6.16). While experiments were carried out so that this ratio was the same at the start of all experiments, clearly it would vary to a different extent during the course of experiments. That said, it would be surprising if this effect is of a large enough magnitude to explain the results here. To eliminate such uncertainty, it is recommended that future experiments of this type should start

with the same [CTA]/[M] but be restricted to a low range of conversion rather than being carried out to high conversion.

6.4 Conclusions and future work

This work has demonstrated the potential of alternative methods to SEC for characterization of PAA and PNaA.

The Taylor dispersion analysis allows the determination of the diffusion coefficient of molecules and it can be applied to PNaA. In future work, (i) the non-ideality of CE equipment needs to be considered, and (ii) by measuring the intrinsic viscosity, the hydrodynamic radii need to be determined.

The DP_n of PAA can be estimated by quantifying the fraction of CH_2 terminals by ^{1}H NMR. The accuracy of this method is, however, limited: some polymer chains with other end groups, not detected by ^{1}H NMR due to the low frequency of these end groups, may exist and may bias these results. At this stage, the use of this method is uncertain. Even though it has been proven that backbiting occurs, leading to CH_2 terminal groups, these were not detected in the non-CTA-containing PAAs, which nevertheless are branched to a detectable extent. It could be that the signal of the CH_2 terminal groups of non-CTA-containing PAAs might overlay that for main-chain CH_2. Furthermore, even for CTA-containing PAAs an implausible variation of C_T with temperature was obtained.

Even though the present studies are incomplete, some consistent results have been obtained. The ^{1}H NMR results showed that the CTA-containing PAAs synthesized at 50 °C have a much lower M_n than the other CTA-containing PAAs, and this is reinforced by the values of *D*. The three PNaAs synthesized at 90 °C without CTA have the same *DB* (see Chapter 2), and a small decrease in *D* is observed at high monomer concentration, which is expected because the chain length increases with the monomer concentration.

6.5 References

[1] I. Lacík, M. Stach, P. Kasák, V. Semak, L. Uhelská, A. Chovancová, G. Reinhold, P. Kilz, G. Delaittre, B. Charleux, I. Chaduc, F. D'Agosto, M. Lansalot, M. Gaborieau, P. Castignolles, R.G. Gilbert, Z. Szablan, C. Barner-Kowollik, P. Hesse, M. Buback, SEC analysis of poly(acrylic acid) and poly(methacrylic acid), Macromolecular Chemistry and Physics, 216 (2015) 23-37.

[2] P. Castignolles, Transfer to polymer and long-chain branching in PLP-SEC of acrylates, Macromolecular Rapid Communications, 30 (2009) 1995-2001.

[3] H.K. Schachman, Ultracentrifugation, diffusion, and viscometry, Methods in Enzymology, 4 (1957) 32-103.

[4] K.E. Vanholde, R.L. Baldwin, Rapid attainment of sedimentation equilibrium, Journal of Physical Chemistry, 62 (1958) 734-743.

[5] V. Roger, H. Cottet, L. Cipelletti, A New Robust Estimator of Polydispersity from Dynamic Light Scattering Data, Analytical Chemistry, 88 (2016) 2630-2636.

[6] A.C. Vanasten, R.J. Vandam, W.T. Kok, R. Tijssen, H. Poppe, Determination of the compositional heterogeneity of polydisperse polymer samples by the coupling of size-exclusion chromatography and thermal field-flow fractionation, Journal of Chromatography A, 703 (1995) 245-263.

[7] J.C. Giddings, F.J.F. Yang, M.N. Myers, Flow field-flow fractionation - versatile new separation method, Science, 193 (1976) 1244-1245.

[8] G. Taylor, DIispersion of soluble matter in solvent flowing slowly through a tube, Proceedings of the Royal Society of London Series a-Mathematical and Physical Sciences, 219 (1953) 186-203.

[9] R. Aris, On the dispersion of a solute in a fluid flowing through a tube, Proceedings of the Royal Society of London Series a-Mathematical and Physical Sciences, 235 (1956) 67-77.

[10] J.C. Giddings, S.L. Seager, Rapid determination of gaseous diffusion coefficients by means of gas chromatography apparatus, Journal of Chemical Physics, 33 (1960) 1579-1580.

[11] E. Grushka, E.J. Kikta, Extension of chromatographic broadening method of measuring diffusion-coefficients to liquid-systems .1. Diffusion-coefficients of some alkylbenzenes in chloroform, Journal of Physical Chemistry, 78 (1974) 2297-2301.

[12] M.S. Bello, R. Rezzonico, P.G. Righetti, Use of Taylor-Aris Dispersion for measurement of a solute diffusion-coefficient in thin capillaries, Science, 266 (1994) 773-776.

[13] H. Cottet, J.P. Biron, M. Martin, Taylor dispersion Analysis of mixtures, Analytical Chemistry, 79 (2007) 9066-9073.
[14] T. Le Saux, H. Cottet, Size-based characterization by the coupling of capillary electrophoresis to Taylor dispersion analysis, Analytical Chemistry, 80 (2008) 1829-1832.
[15] H.A. Claessens, J.H.M. Vandenberg, Measurements of diffusion-coefficients in liquids, Journal of High Resolution Chromatography & Chromatography Communications, 5 (1982) 437-438.
[16] A.R. Maniego, D. Ang, Y. Guillaneuf, C. Lefay, D. Gigmes, J.R. Aldrich-Wright, M. Gaborieau, P. Castignolles, Separation of poly(acrylic acid) salts according to topology using capillary electrophoresis in the critical conditions, Analytical and Bioanalytical Chemistry, 405 (2013) 9009-9020.
[17] J.-B. Lena, A.K. Goroncy, J.J. Thevarajah, A.R. Maniego, G.T. Russell, P. Castignolles, M. Gaborieau, Effect of transfer agent, temperature and initial monomer concentration on branching in poly(acrylic acid): A study by 13C NMR spectroscopy and capillary electrophoresis, Polymer, 114 (2017) 209-220.
[18] M. Gaborieau, T.J. Causon, Y. Guillaneuf, E.F. Hilder, P. Castignolles, Molecular weight and tacticty of oligoacrylates by capillary electrophoresis - mass spectrometry, Australian Journal of Chemistry, 63 (2010) 1219-1226.
[19] J.J. Thevarajah, J.C. Bulanadi, M. Wagner, M. Gaborieau, P. Castignolles, Towards a less biased dissolution of chitosan, Analytica Chimica Acta, 935 (2016) 258-268.
[20] K. Klimke, M. Parkinson, C. Piel, W. Kaminsky, H.W. Spiess, M. Wilhelm, Optimisation and application of polyolefin branch quantification by melt-state 13C NMR spectroscopy, Macromolecular Chemistry and Physics, 207 (2006) 382-395.
[21] M. Schmidt, D. Nerger, W. Burchard, Quasi-elastic light-scattering from branched polymers .1. Polyvinylacetate and polyvinylacetate-microgels prepared by emulsion polymerization, Polymer, 20 (1979) 582-588.
[22] U. Sharma, N.J. Gleason, J.D. Carbeck, Diffusivity of solutes measured in glass capillaries using Taylor's analysis of dispersion and a commercial CE instrument, Analytical Chemistry, 77 (2005) 806-813.
[23] G. Taylor, Conditions under which dispersion of a solute in a stream of solvent can be used to measure molecular diffusion, Proceedings of the Royal Society of London Series a-Mathematical and Physical Sciences, 225 (1954) 473-477.

[24] N.F.G. Wittenberg, C. Preusser, H. Kattner, M. Stach, I. Lacík, R.A. Hutchinson, M. Buback, Modeling acrylic acid radical polymerization in aqueous solution, Macromolecular Reaction Engineering, 10 (2016) 95-107.
[25] A. Ibrahim, S.A. Allison, H. Cottet, Extracting Information from the Ionic Strength Dependence of Electrophoretic Mobility by Use of the Slope Plot, Analytical Chemistry, 84 (2012) 9422-9430.
[26] C. Barner-Kowollik, S. Beuermann, M. Buback, P. Castignolles, B. Charleux, M.L. Coote, R.A. Hutchinson, T. Junkers, I. Lacik, G.T. Russell, M. Stach, A.M. van Herk, Critically evaluated rate coefficients in radical polymerization - 7. Secondary-radical propagation rate coefficients for methyl acrylate in the bulk, Polymer Chemistry, 5 (2013) 204-212.

APPENDIX 1

Publications, Conferences, Service and Funding

A1.1 List of publications

J.-B. Lena, A.K. Goroncy, J.J. Thevarajah, A.R. Maniego, G.T. Russell, P. Castignolles, M. Gaborieau, Effect of transfer agent, temperature and initial monomer concentration on branching in poly(acrylic acid): A study by ^{13}C NMR spectroscopy and capillary electrophoresis, Polymer, 114 (2017) 209-220.

J.-B. Lena, M. Deschamps, N.F. Sciortino, S.L. Masters, M.A. Squire, G.T. Russell, Effect of transfer agent and temperature on branching and β-scission in radical polymerization of 2-ethylhexyl acrylate, Macromolecular Chemistry & Physics, Accepted (macp.201700579).

J.-B. Lena, A.R. Maniego, J.J. Thevarajah, G.T. Russell, S. L. Masters, P. Castignolles, M. Gaborieau, Characterization of the branching in hydrophilic polyacrylates using capillary electrophoresis, Journal of Chromatography A, Manuscript in preparation.

A1.2 Conferences contributions

RACI 35 Australian Polymer Symposium

Gold Coast, QLD, Australia, 12-15 July 2015

Poster presentation: "*Effect of Transfer Agent, Initial Monomer Concentration and Temperature on Branching in Poly(Acrylic Acid): NMR Spectroscopy and Capillary Electrophoresis Study"*

RACI NSW Polymer Workshop 2015

Sydney, NSW, Australia, 20 November 2015

Oral presentation: "*Characterization of Branching in Poly(acrylic acid) by ^{13}C NMR Spectroscopy and Capillary Electrophoresis"*

RACI Physical Chemistry 2016 meeting

Christchurch, New Zealand, 2-5 February 2016

Poster presentation: "*Characterization of Poly(Acrylic Acid) Branching by Capillary Electrophoresis"*

IUPAC-PSK-40 Conference on advanced polymeric materials

Jeju, South Korea, 4-7 October 2016

Oral presentation: "*Characterization of Branching in Poly(acrylic acid) by ^{13}C NMR Spectroscopy and Capillary Electrophoresis"*

Poster presentation: "*Separation of Poly(sodium acrylate) by Branching using Capillary Electrophoresis"*

University of Canterbury Chemistry Postgraduate Student Showcase

University of Canterbury, New Zealand, 30 November 2016

Oral presentation: *"Further Characterization of Branching in Water Soluble Polyelectrolyte Using Capillary Electrophoresis"*

A1.3 Professional membership and service

Professional memberships:

2015–2017: New Zealand Institute of Chemistry (NZIC) student member

Paid services:

2015–2017: Lab demonstrating for Chemistry undergraduate labs (CHEM111, CHEM112)

A1.4 Funding received

March 2014:	UC Doctoral Scholarship	
March 2015:	Evan’s Fund (Hardship)	($677)
September 2015:	Evan’s Fund (Hardship)	($697)
March 2016:	Evan’s Fund (Hardship)	($803)
May 2016:	Departmental Travel grant	($1000)
May 2016:	New Zealand Institute of Chemistry Travel Grant	($200)
September 2016:	Evan’s Fund (Hardship)	($1000)
March 2017:	Evan’s Fund (Hardship)	($200)
May 2017:	Departmental Travel Grant	($2000)

APPENDIX 2

Supplementary data

A2.1. Chapter 2: Effect of temperature, initial monomer concentration, and presence of CTA on the branching in poly(acrylic acid)

A2.1.1 Synthesis of PAA

Table A.2.1: Reaction times

Temperature	Reaction time	Half-time for decomposition of 4,4'-azobis(4-cyanovaleric acid) *
50 °C	24 h	96.6 h
70 °C	6 h	5.40 h
90 °C	1 h	24.9 min

* Calculated using a frequency factor of 6.21×10^{15} s^{-1} and an activation energy of 132.9 kJ mol^{-1} [1].

A2.1.2 Monomer conversion

Monomer conversion in acrylic acid polymerization is commonly determined in the literature using ^{1}H NMR spectroscopy[2, 3] and gravimetry [4-8] but also by HPLC[9], UV absorbance at 260 nm, near-infrared (NIR) spectroscopy[7, 10] (or NIR checked by ^{1}H NMR[11]) and calorimetry[12].

In the case of PAA synthesized at 50 °C with CTA and $[AA]_0$ = 2 M, the gravimetry indicated an average conversion of only 66 %, but with a standard deviation of 20 % (n = 3). The low precision of this gravimetric measurement may add to a low accuracy because of the presence of both THF and water to evaporate in the gravimetry. The monomer conversion was also measured by solution-state ^{1}H NMR, and the conversion was found to be high (Table S-2). The discrepancy between the values determined by gravimetry and ^{1}H NMR is large, with values of 66 % (gravimetry, large error) and 98 % by ^{1}H NMR on the same sample. The large conversion observed by NMR spectroscopy was thus confirmed by a completely different method, namely free-solution capillary electrophoresis (CE).

CE of pure acrylic acid monomer leads to 3 fully resolved peaks (dashed line on figure S-2). The sodium acrylate is likely the peak at 2.5×10^{-8} m^2 V^{-1} s^{-1}. The peak at 3.30×10^{-8} m^2 V^{-1} s^{-1} is likely from poly(sodium acrylate) generated by autopolymerization. It should be noted that the bottle of acrylic acid used for this experiment was different from the one used for the polymerization (it was provided by Aldrich and the purity was better than

99%). The small peak at 2.05×10^{-8} m^2 V^{-1} s^{-1} could be either a dimer or an inhibitor. The preliminary study to determine the monomer conversion was performed with a fused-silica capillary of about 60 cm total length and with sodium borate at pH = 9.2 as buffer at a concentration close to 100 mmol L^{-1}. The conversion was determined as the ratio of the polymer peak area to the polymer, monomer and dimer peak areas. The UV absorption (Beer-Lambert) coefficient of the monomer is expected to be higher than that of the carboxylate (chromophore) moiety of the polymer. The peak attributed to the dimer may be another species such as the inhibitor. For both these reasons, we expect these conversion values to be an underestimate of the monomer conversion. The monomer conversion determined by CE is higher than 88 % in the presence of thiol and consistent with that determined by NMR spectroscopy. The monomer conversion is expected to be higher at least for the polymerization in the absence of thiol, since the rate of polymerization is generally observed to be higher in the absence of transfer agent.

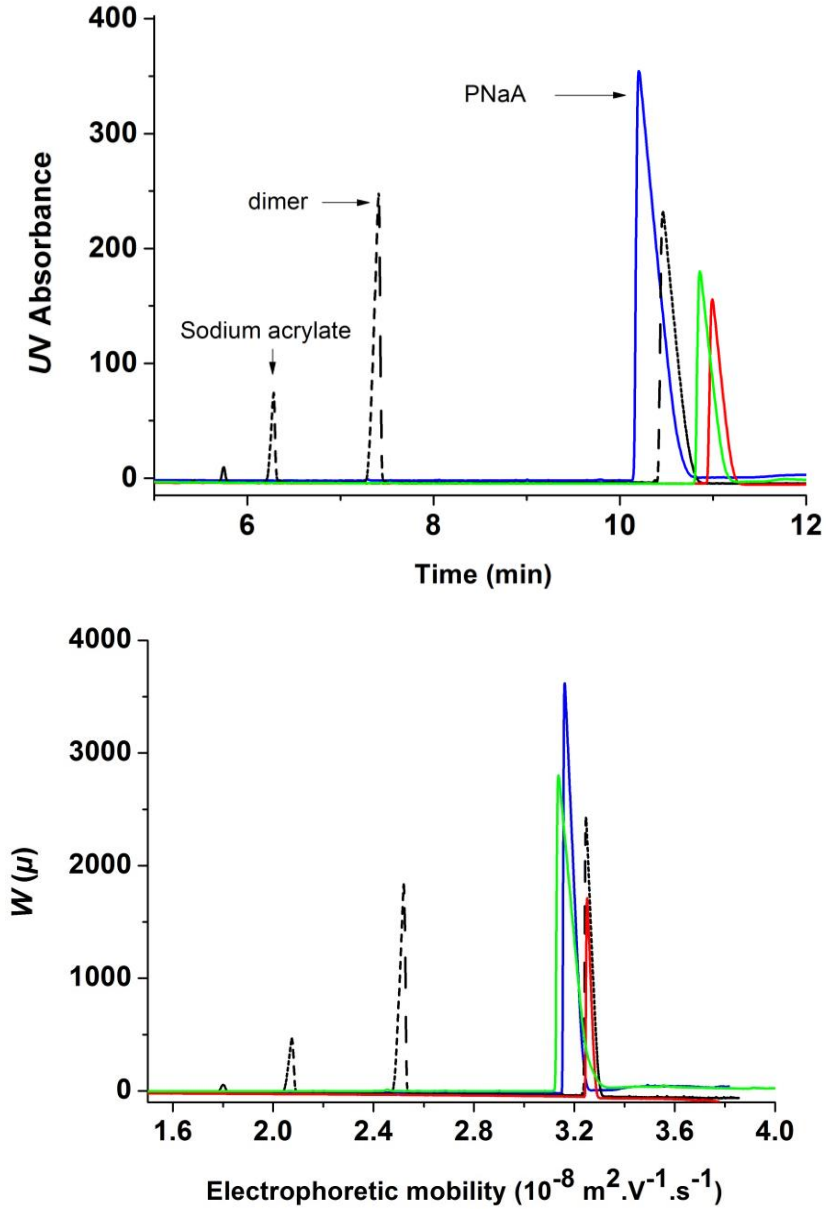

Figure A.2.1: Separation of sodium acrylate and poly(sodium acrylate) by capillary electrophoresis (CE) shown as raw electropherogram (top) and distribution of electrophoretic mobility (bottom). Acrylic acid (black dashed line) was prepared at 2 $g.L^{-1}$ in 1 mM aqueous NaOH spiked with DMSO. PAAs synthesized at 50 °C, 70 °C and 90 °C with CTA (red, green and blue lines, respectively) were injected as crude medium diluted by a factor of 100 with water.

Table A.2.2: Monomer conversion determined by CE and ^{1}H NMR spectroscopy. The values used to determine the residual monomer concentrations are in bold.

Polymer (PAA) synthesis conditions	Conversion by NMR (%)	*SNR* (residual monomer) NMR	*SD* (%) of the residual monomer in NMR	Conversion by CE (%)	SD (%) of the conversion by CE (%, ***n***=3)	$[M]_e$ values (mol.L^{-1}) used to calculate k_{bb}
50 °C with a CTA and at $[AA]_0$ = 2M	98.0	38	0.04	**99.3**	0.2	1.4×10^{-2}
50 °C without a CTA and at $[AA]_0$ = 2M	**93.8**	240	0.1			1.2×10^{-1}
70 °C with a CTA and at $[AA]_0$ = 2M	98.8	24	0.05	**99.0**	0.6	2.0×10^{-2}
70 °C without a CTA and at $[AA]_0$ = 2M	**97.4**	58	0.05			5.2×10^{-2}
90 °C with a CTA and at $[AA]_0$ = 2M	>99.9 *			**88.4**	4.0	2.3×10^{-1}
90 °C without a CTA and at $[AA]_0$ = 2M	**97.6**	61	0.05			4.8×10^{-2}
90 °C without a CTA and at $[AA]_0$ = 1M	**99.9**	5.2	0.03			1.0×10^{-3}
90 °C without a CTA and at $[AA]_0$ = 3M	**98.9**	25	0.04			3.3×10^{-2}

*No residual monomer was observed by ^{1}H NMR spectroscopy.

A2.1.3 NMR spectroscopy

A2.1.3.1 Two-dimensional NMR of PAA

In order to identify the signals and to check if some signals of impurities were overlapping with the quantified signals, the COSY and HSQC NMR analyses of PAA were carried out (see Figure S7).

It was shown that nothing was overlapping with the main-chain CH signal (42 ppm) and the branching signal (48 ppm).

COSY and HSQC spectra were acquired at 26 °C in D_2O on an Agilent 400 MR with Varian 7600-AS auto-sampler, equipped with OneNMR probe and variable temperature capabilities, operating at a Larmor frequency of 399.84 MHz for ^{1}H and 100.55 MHz for ^{13}C. 2D HSQC (^{1}H, ^{13}C) spectra were acquired with (1024, 1024) data points, 32 scans, (6404.0 Hz, 20 090.97 Hz) spectral width, (0.1501 s, 0.0048 s) acquisition time, 4.5 s relaxation delay, and with the pulse program bsHSQCAD. The 2D COSY (^{1}H, ^{1}H) spectra were acquired with (1150, 128) data points, 1 scan, (7662.04 Hz, 7608.80 Hz) spectral width, (0.1501 s, 0.0048 s) acquisition time, 1.0 s relaxation delay, and with the pulse program gCOSY.

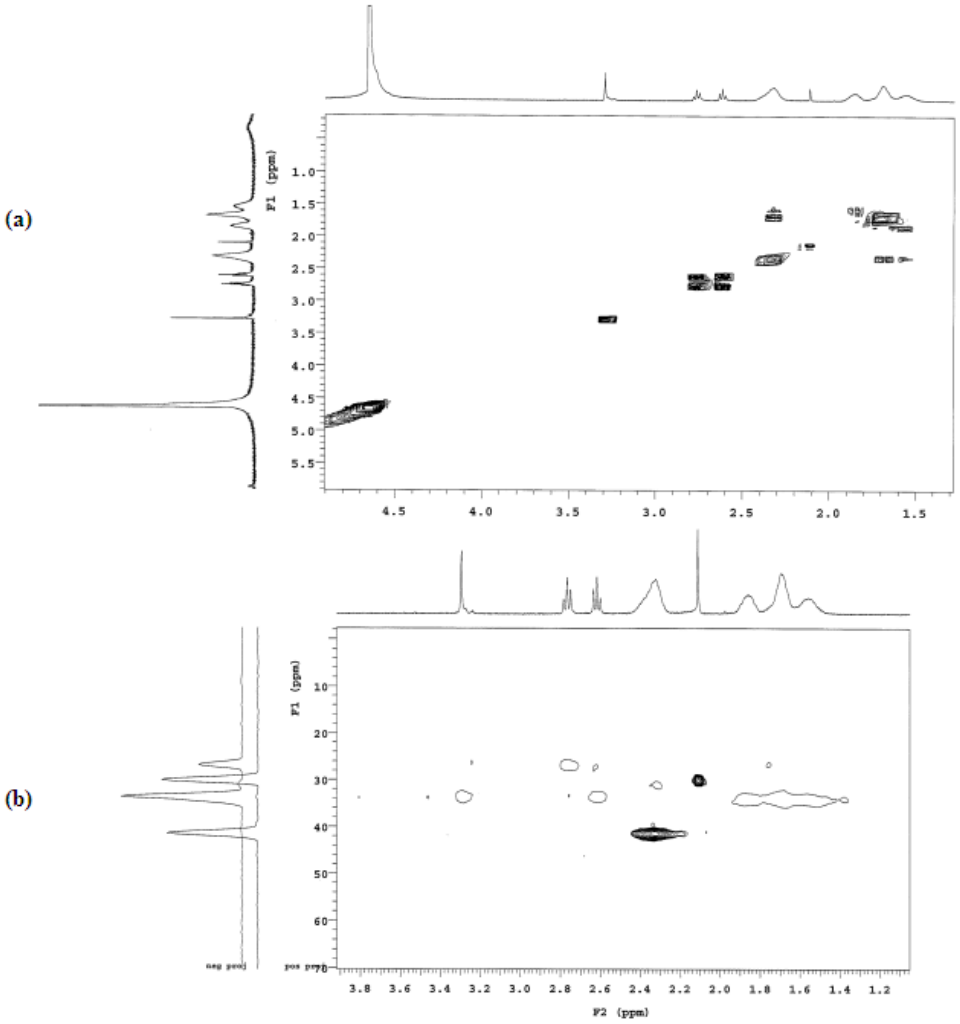

Figure A.2.2: Two-dimensional NMR of CTA-containing PAA synthesized at 70 °C, analysed in D_2O: (a) COSY; (b) HSQC, white shapes represent CH_2 and black shapes represent CH and CH_3.

A2.1.3.2 One-dimensional NMR of PAA

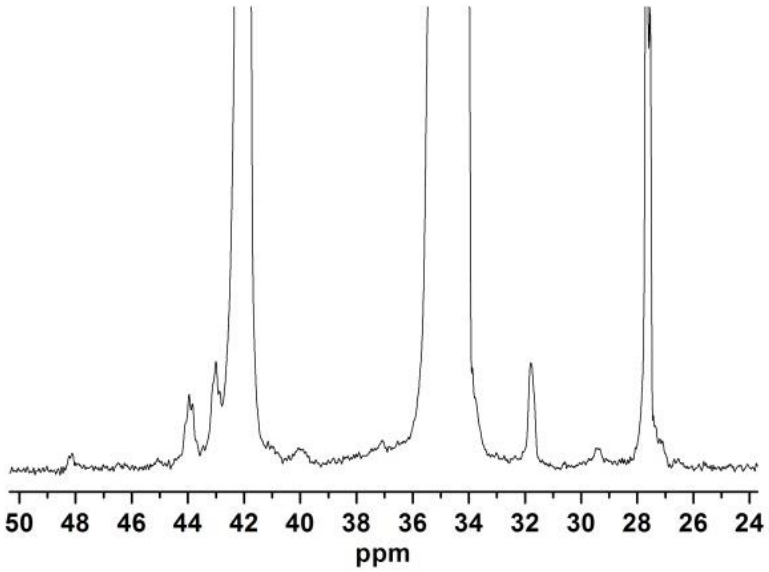

Figure A.2.3: Partial ^{13}C NMR spectrum of PAA synthesized at 70 °C with CTA, analysed at 750 g L^{-1} in D_2O. The signals of C adjacent to the sulfur and of main-chain CH are overlapping.

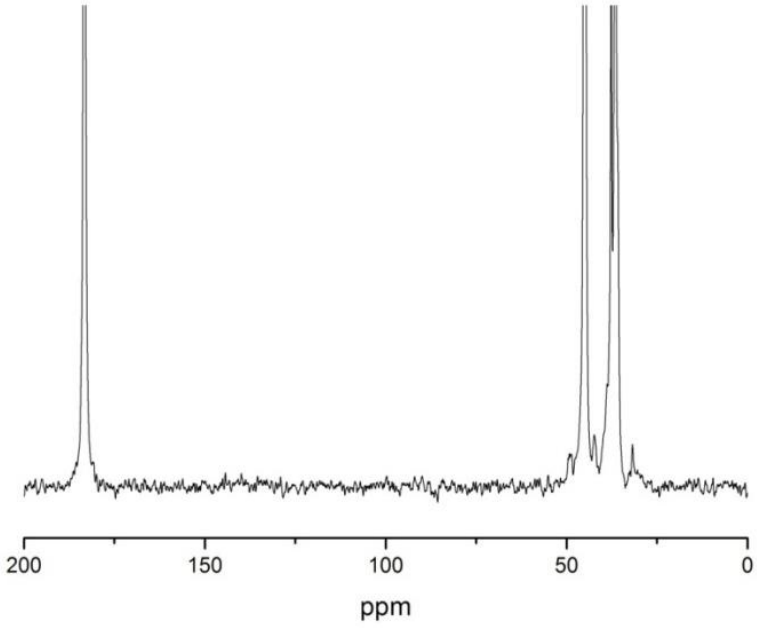

Figure A.2.3: ^{13}C NMR spectrum of PAA provided by Sigma-Aldrich, analysed at 27 g L^{-1} in D_2O (with 1 mol eq. of NaOD and 0.5 mol eq. of DCl) at room temperature.

A2.1.3.3 Degree of branching (*DB*): equations and results

Table A.2.3: *DBs* of PAAs calculated with different equations and their relative standard deviation (RSD) based on the signal-to-noise ratio (SNR) of the Cq (calculated using Eq. (2.7) in chapter 2).

PAA synthesis	DB (%) from Eq. (2.3) or Eq. (A.2.2)*	DB (%) from Eq. (2.5) (underestimate)	DB (%) from Eq. (2.4) (overestimate)	DB (%) from Eq. (2.6)	SNR	RSD (%)
90 °C with CTA and at $[AA]_0$ = 2 M	–	0.36	0.37	0.37	9.22	13.9
70 °C with CTA and at $[AA]_0$ = 2 M	–	0.31	0.33	0.32	8.16	16.4
50 °C with CTA and at $[AA]_0$ = 2 M	–	0.21	0.25	0.23	5.85	24.8
90 °C without CTA and at $[AA]_0$ = 2 M	1.32	–	–	1.28	7.15	19.2
70 °C without CTA and at $[AA]_0$ = 2 M	0.83	–	–	0.83	7.55	17.9
50 °C without CTA and at $[AA]_0$ = 2 M*	Below 0.61*	–	–	–	2.62	–
90 °C without CTA and at $[AA]_0$ = 1 M	1.36	–	–	1.37	9.28	13.8
90 °C without CTA and at $[AA]_0$ = 3 M	1.16	–	–	1.17	6.94	20.0
Sigma-Aldrich	–	–	–	1.13	16.75	6.45

* For the PAA synthesized at 50 °C without CTA, the *SNR* was below 3, i.e. below the limit of detection (LOD).

Because the SNR was below 3 and so below the level of detection for the PAA synthesized at 50 °C with a CTA, it is not possible to confirm whether this polymer is branched or not. To estimate a maximum possible degree of branching, the *SNR* of the main chain CH signal and that of of the C_q signal were compared as follows (Eq. (A.2.1)).

$$DB(\%) = \frac{100 \cdot I(\mathrm{C}_q)}{I(\mathrm{C}_q)+I(\mathrm{CH})} = \frac{100}{1+\frac{I(\mathrm{CH})}{I(\mathrm{C}_q)}} \qquad (A.2.1)$$

Figure A.2.5 shows that *SNR*(CH) / *SNR*(C_q) ≈ *I*(CH) / *I*(C_q), meaning that Eq. (A.2.2) provides an estimation for a maximum potential *DB:*

$$DB_{max}\ (\%) = \frac{100}{1+\frac{SNR(\mathrm{CH})}{SNR\,(C_q)}} \qquad (A.2.2)$$

This equation was used for this one particular case.

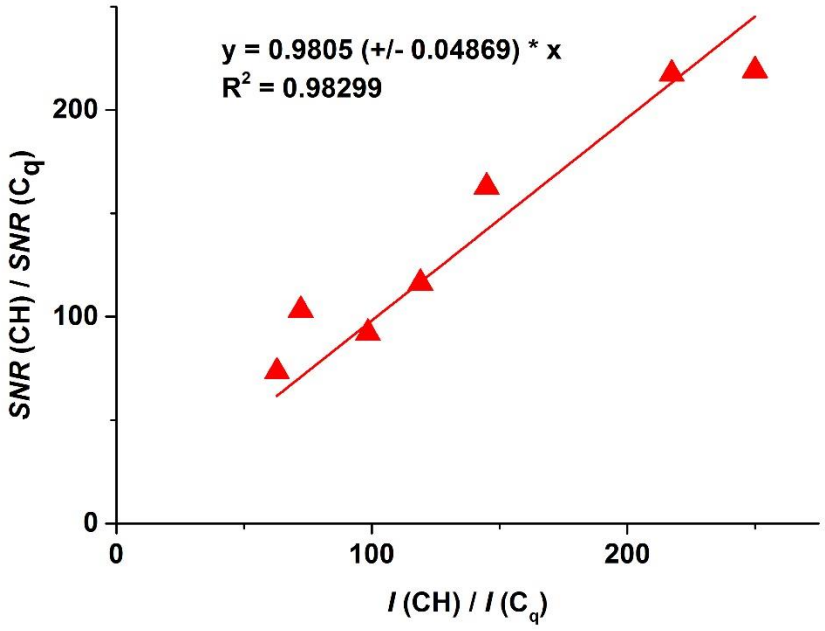

Figure A.2.4: Ratio of the *SNR*s of the backbone CH and Cq signals as a function of the ratio of their integrals for the experiments of this work

A2.1.3.4 Effect of the contamination by deuterium oxide

A ^{1}H NMR analysis of the D_2O used to run the different analyses showed that this solvent has been contaminated with PAA (see figure A.2.6). In order to test the effect of the contamination on the study, a ^{13}C NMR analysis was run under the same conditions as the quantitative analyses of PAA. Figure A.2.7 shows that the contamination has a negligible impact on a regular spectrum. On the ^{13}C NMR spectrum of the contaminated D_2O, the main chain CH and main chain COOH signals have *SNR* values around 4 and 6 respectively, which is less than 1 % of the *SNR* of the same signals on regular spectra. So, the error potentially induced by the contamination on the *DB* is much lower than the calculated error bar of *DB*.

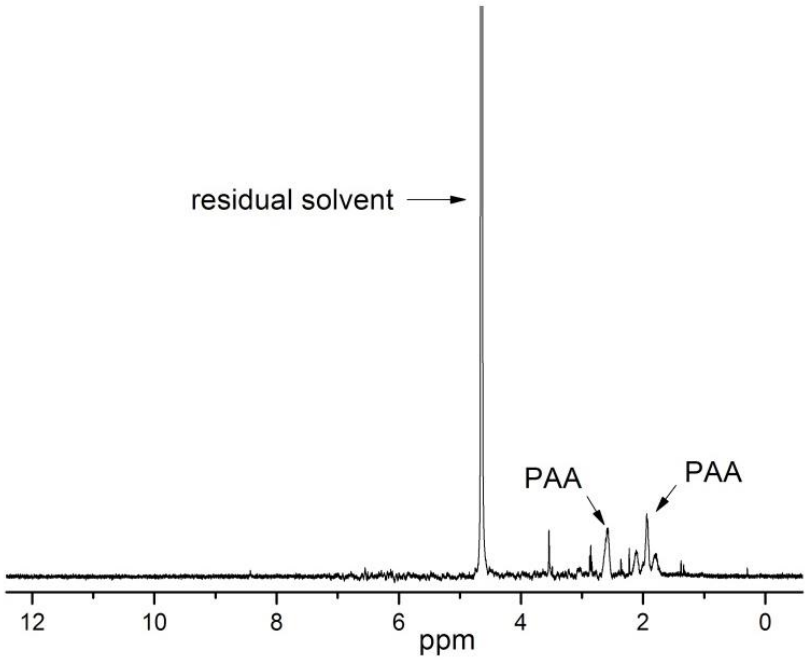

Figure A.2.5: ^{1}H NMR spectrum of the contaminated D_2O

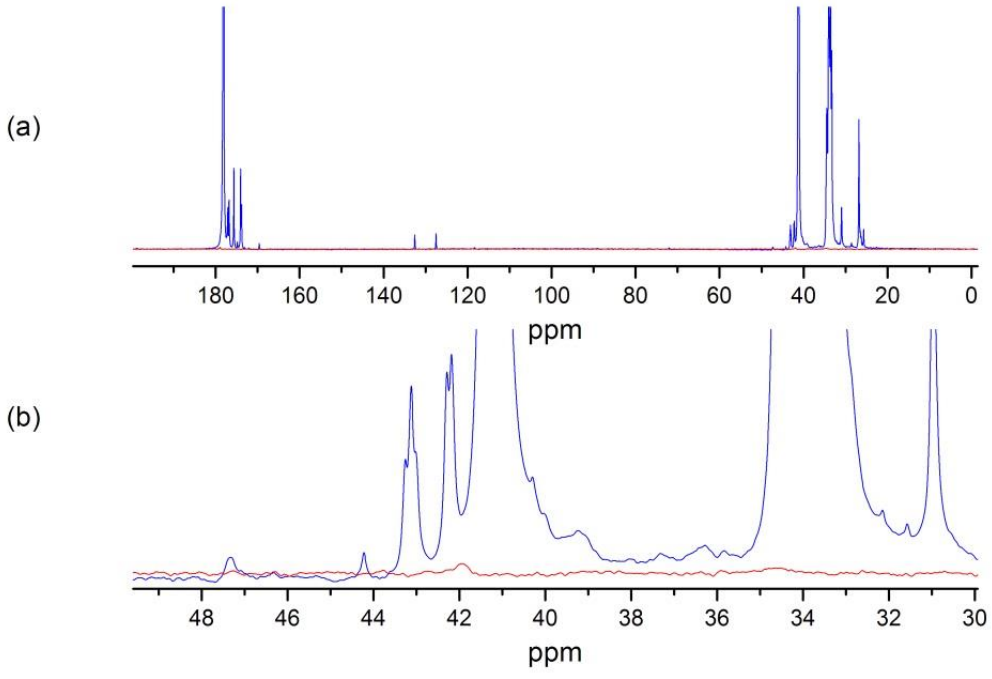

Figure A.2.6: Full (a) and partial (b) ^{13}C NMR spectra of PAA synthesized at 90 °C with thiol and [AA]0=2 M (blue line) and of the contaminated D_2O (red line)

A2.1.3.5 Probing the dissolution of PAA in D_2O

Dissolution of analytes can be analysed by NMR spectroscopy [13].

The noise was measured in 2 steps. First, the *SNR* was measured using the ACD/Lab software and then the height of the signals was measured with the Origin 9.0 software. The peak area was also measured with the Origin 9.0 software by integration of the signal.

The uncertainty of the normalized *PNR* was calculated based on the uncertainty of the concentration of analyte, neglecting the error on the number of scans and the peak area (Eq. A.2.3). The error in the mass was based on the last digit appearing on the scale (mg), and the error in the measured volume was calculated by weighing 1 mL of MilliQ water 5 times, each taken with 5 different 1 mL plastic syringes ($SD_{1\ mL\ syringes}$ = 0.016936 mL). In the case of the thiol-containing PAA synthesized at 70 °C, there is also an uncertainty in the peak area due tot overlapping between main chain CH and C_{thiol} signals.

$$Uncertainty\ (normalized\ PNR) = |Normalized\ PNR_{max} - Normalized\ PNR_{min}| \qquad (A.2.3)$$

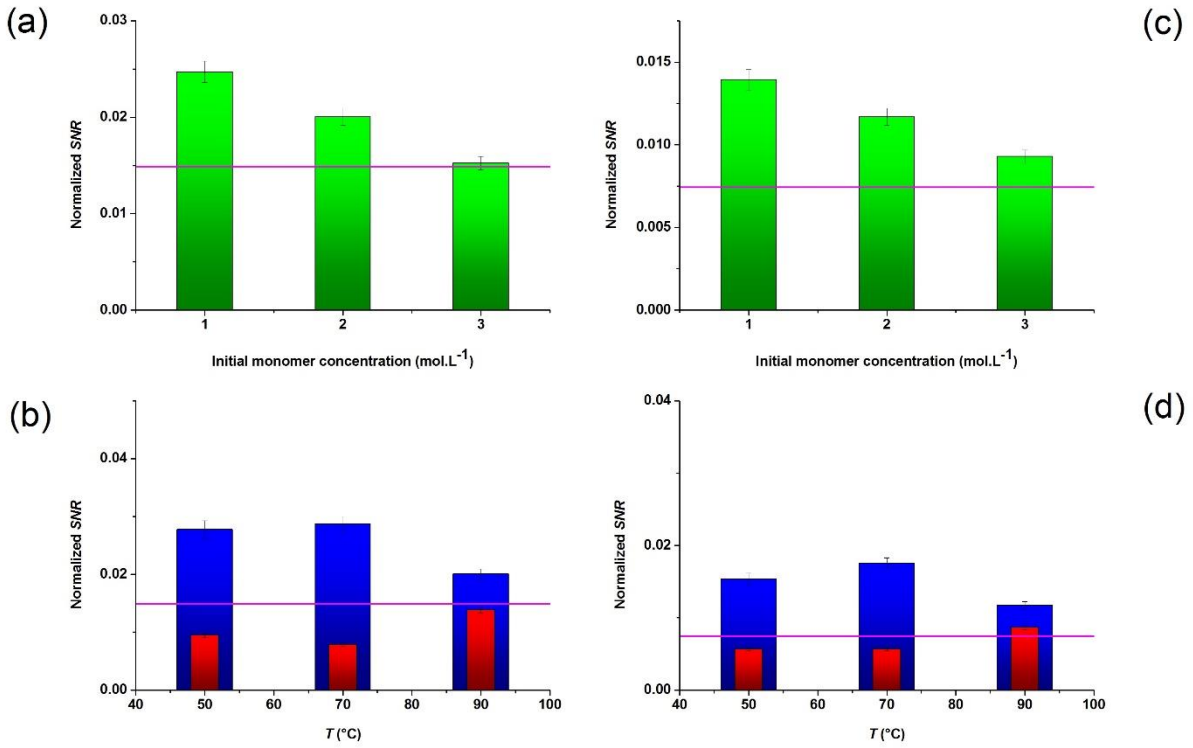

Figure A.2.7: Normalized *SNR* of the different PAAs synthesized by conventional radical polymerization. Green bars represent the PAAs synthesized at 90 °C without CTA at different initial monomer concentrations, red and blue bars represent the PAAs synthesized at

$[AA]_0$=2 M at different temperatures, with and without CTA, respectively. Graphs (a) and (b) represents the results obtained with the backbone COOH signal, (c) and (d) graphs represent the results obtained with the backbone CH signal. Magenta lines represent the SNR values obtained for the linear PNaA.

A2.1.3.6 Remaining ^{13}C NMR Spectra

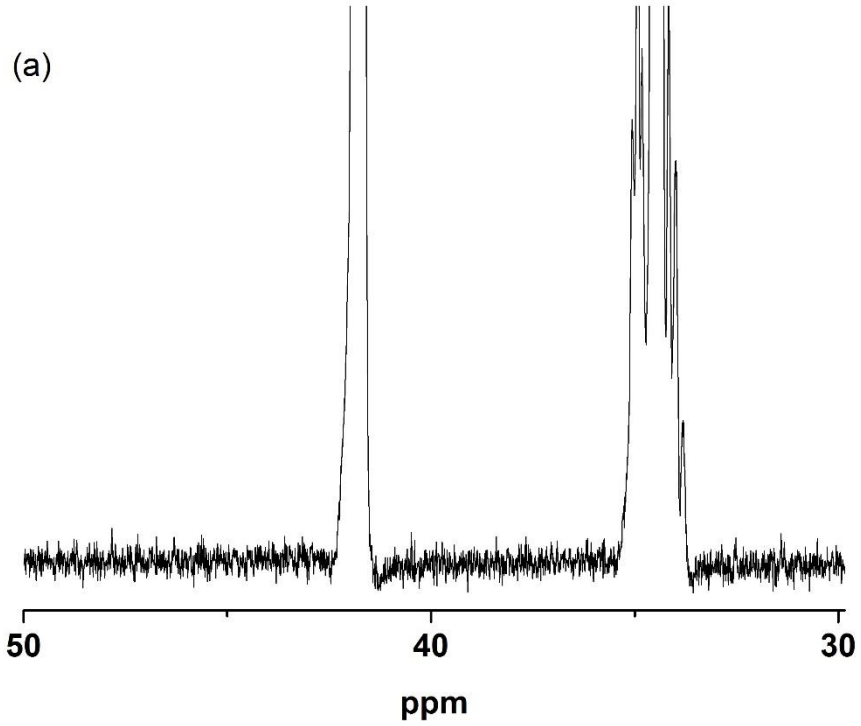

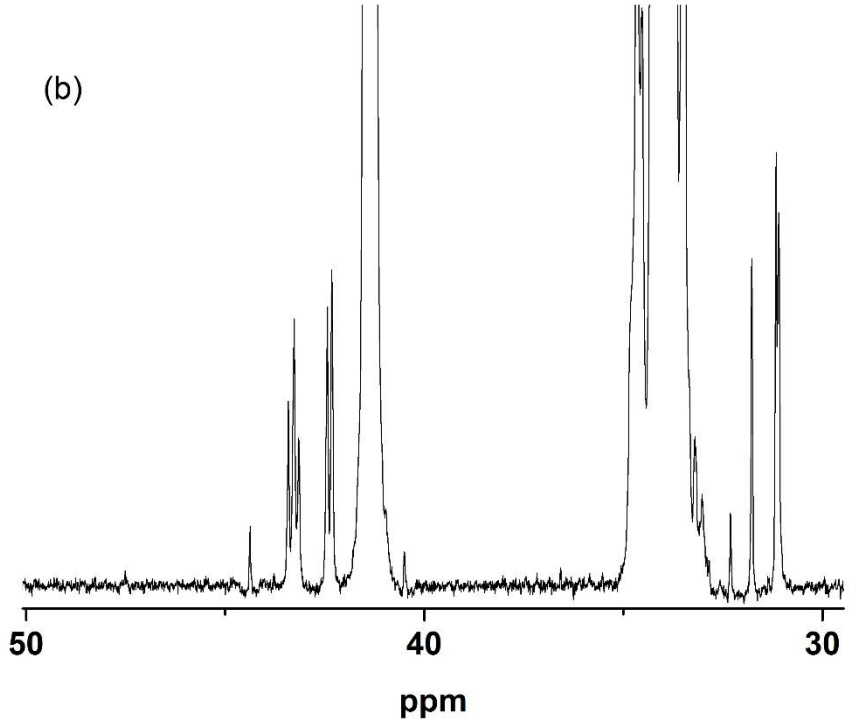
(b)
50
40
30
ppm

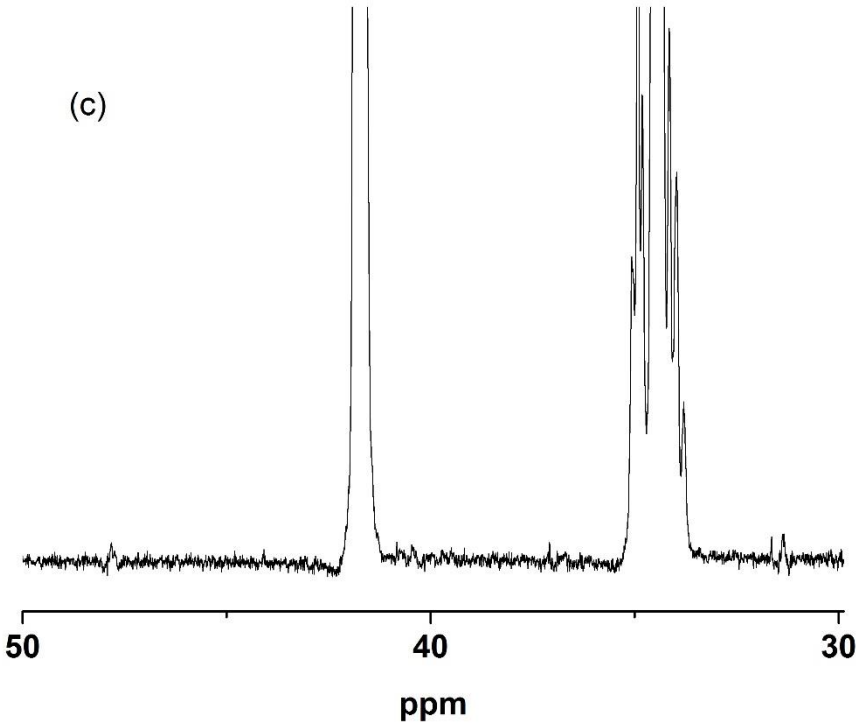
(c)
50
40
30
ppm

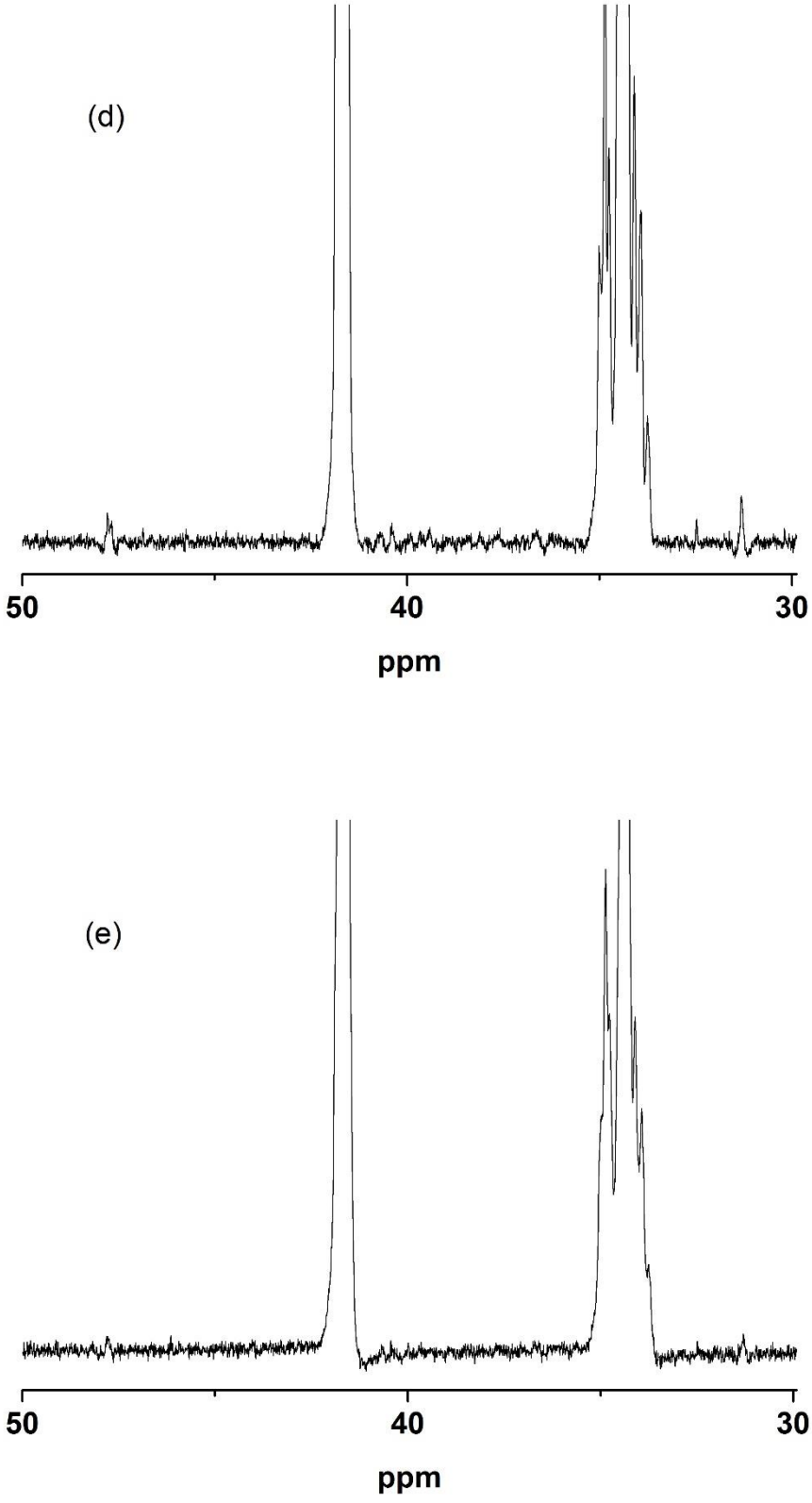

Figure A.2.8: Partial ^{13}C NMR Spectra of PAA not shown previously. (a) PAA synthesized at 50 °C without a CTA, (b) PAA synthesized at 50 °C with a CTA, (c) PAA synthesized at 70

°C without a CTA, (d) PAA synthesized at 90 °C without a CTA and $[AA]_0$=1M, (e)) PAA synthesized at 90 °C without a CTA and $[AA]_0$=3M

A2.1.4 Backbiting rates coefficients

A2.1.4.1 Parameters used for the linear fits

The values of the backbiting rate coefficients were estimated using Eq. (2.10) as well as the values of the propagation rate coefficient estimated from Eq. (A.2.4) (already given in the introduction). The final monomer conversion $[M]_e$ was calculated based on the monomer conversion estimated using CE for the polymer synthesized in the presence of CTA, and using ^{1}H NMR spectroscopy for the polymer synthesized in the absence of CTA.

$$k_p(L.mol^{-1}.s^{-1}) = 3.2\ 10^7 e^{-\frac{1564}{T}}(0.11 + (1-0.11)e^{-3w'_{AA}}) \quad \text{(A. 2.4)}$$

In Eq. (A.2.4), w'_{AA} is the wt. fraction of AA solution on a polymer-free basis. The average value of w'_{AA} over the polymerization process was used in order to calculate k_p using Arrhenius equation as follows:

$$\ln\ (k) = \ln(A) - \frac{E_A}{RT} \quad \text{(A. 2.5)}$$

where k is the kinetic rate coefficient, A is the frequency factor (same unit as k), E_A is the activation energy (J mol^{-1}), R is the ideal gas constant (J K^{-1} mol^{-1}), T is the temperature (K).

Table A.2.4: Kinetic rate coefficients calculated with Eq. (1.20))

Presence of a CTA	***T* (K)**	**$[M]_0$ (mol.L^{-1})**	**k_p (L.mol^{-1}.s^{-1})**	**k_{bb} (s^{-1})**	**ln(k_{bb})**	**k_{bb} (s^{-1}) (from Eq. (A.2.6))**	**Δk_{bb} (%) with Wittenberg**
yes	223.15	2	2.12×10^5	2.12×10^2	5.36		
yes	243.15	2	2.80×10^5	3.98×10^2	5.99		
yes	263.15	2	3.60×10^5	1.09×10^3	7.00		
no	223.15	2	2.11×10^5	4.41×10^2	6.09	7.04×10^3	176
no	243.15	2	2.79×10^5	1.24×10^3	7.12	1.61×10^4	171
no	263.15	2	3.61×10^5	2.49×10^3	7.82	3.35×10^4	172
no	263.15	1	3.92×10^5	7.71×10^2	6.65		
no	263.15	3	3.35×10^5	2.56×10^3	7.85		

The slope and intercepts were calculated with the Origin 9.0 software.

$$k_{bb}\,(s^{-1}) = 9.94 \times 10^{8}\,(s^{-1})\,e^{-\frac{4576}{T/K}} \qquad (A.2.6)$$

$$RSD\,(\ln k_{bb}) = \frac{RSD\,(DB)}{k_{bb}} \qquad (A.2.7)$$

Table A.2.5: Linear fit parameters for the different Arrhenius plots of k_{bb}, where the slope refers to the activation energy and the intercept to the ln (A) where A is the frequency factor.

	k_{bb} (s^{-1}) from this study in the absence of CTA	k_{bb} (s^{-1}) from this study in the absence of CTA excluding the polymerization at 90 °C and 1 M monomer	k_{bb} (s^{-1}) from this study in the presence of CTA	k_{bb} (s^{-1}) of Wittenberg *et al*. study **[7, 11]**
slope (−E_A/R ($J.mol^{-1}$))	−3737	−5066	−4777	−4576
Standard error (slope)	1933	244	86	
Intercept (ln (A (s^{-1}))	17.8	21.8	20.1	20.7
Standard error (intercept)	5.5	0.7	2.4	
Correlation coefficient R^2	0.56	0.996	0.97	

A2.1.5 Capillary electrophoresis

A2.1.5.1 Determination of the optimal injection concentrations

Preliminaries studies to determine the optimal injection concentrations were performed with a fused-silica capillary of about 60 cm total length and with sodium borate as buffer at a concentration close to 100 mmol L^{-1}. For each sample, the concentrations of PAA and NaOH decreased by the same factor from their initial values through the sample dilution with water.

Table A.2.6: Concentrations of injected PAAs without overloading

PAA sample synthesis	Concentration (g L^{-1}) at which no overloading occurs	Concentration of NaOH (mmol L^{-1})
50 °C with CTA, $[AA]_0$ = 2 M	6.67	10.0
50 °C without CTA, $[AA]_0$ = 2 M	0.208	0.313
70 °C with CTA, $[AA]_0$ = 2 M	1.67	2.50
70 °C without CTA, $[AA]_0$ = 2 M	0.833	1.25
90 °C with CTA, $[AA]_0$ = 2 M	1.67	2.50
90 °C without CTA, $[AA]_0$ = 1 M	0.833	1.25
90 °C without CTA, $[AA]_0$ = 2 M	0.833	1.25
90 °C without CTA, $[AA]_0$ = 3 M	0.417	0.625

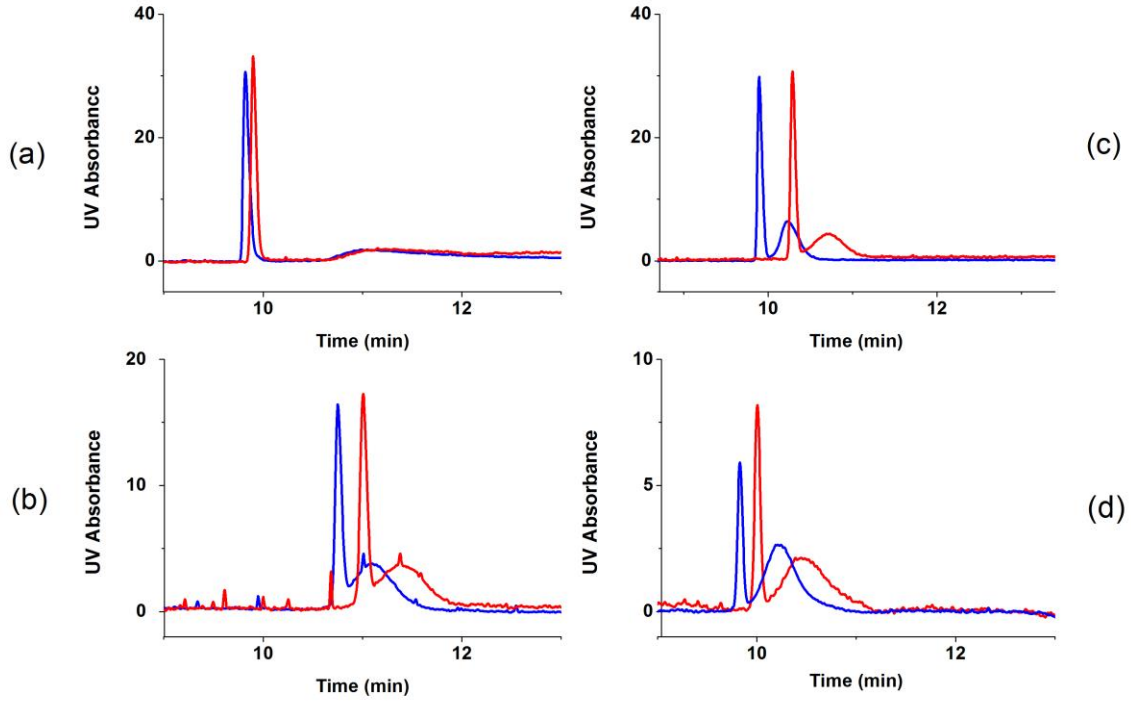

Figure A.2.9: PAA synthesized at (a) 90 °C with CTA and $[AA]_0$ = 2 mol L^{-1}, (b) 90 °C without CTA and $[AA]_0$=1 mol L^{-1}, (c) 90 °C without CTA and $[AA]_0$ = 2 mol L^{-1}, (d) 90 °C without CTA and $[AA]_0$=3 mol L^{-1}. In all raw electropherograms, all PAA are injected at two different concentrations: the concentration at which no overloading occurs (see Table A.2.5) (blue line) and half of that value (red line).

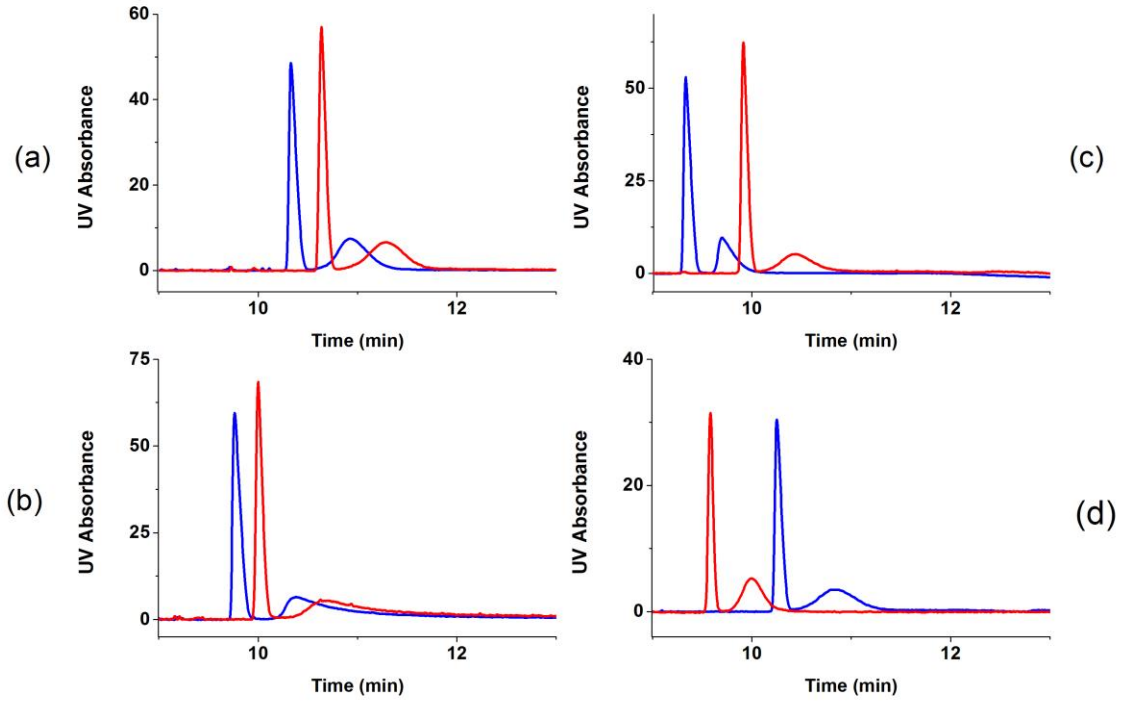

Figure A.2.10: PAA synthesized at (a) 50 °C with CTA and $[AA]_0$=2 mol L^{-1}, (b) 70 °C with CTA and $[AA]_0$=2 mol L^{-1}, (c) 50 °C without CTA and $[AA]_0$=2 mol L^{-1}, (d) 70 °C without CTA and $[AA]_0$=2 mol L^{-1} . In all raw electropherograms, all PAA are injected at two different concentrations: the concentration at which no overloading occurs (see Table A.2.5) (blue line) and half that value (red line).

A2.1.5.2 Dispersities of the distributions of electrophoretic mobilities

The dispersities of the distributions of electrophoretic mobilities, which are related to the heterogeneity of branching, are given by Eqs. (A.2.8) to (A.2.11) [14]. They are all ratios of moments of different orders of the weight distribution of electrophoretic mobilities $W(\mu)$. Eq. (A.2.12) gives the weight average electrophoretic mobility [14].

$$D(W(\mu),1,0) = \frac{[\sum_z W(\mu_z)\mu_z(\mu_{z+1}-\mu_z)][\sum_z W(\mu_z){\mu_z}^{-1}(\mu_{z+1}-\mu_z)]}{[\sum_z W(\mu_z)(\mu_{z+1}-\mu_z)]^2} \quad (A.2.8)$$

$$D(W(\mu),2,0) = \frac{[\sum_z W(\mu_z){\mu_z}^2(\mu_{z+1}-\mu_z)]\,[\sum_z W(\mu_z)(\mu_{z+1}-\mu_z)]}{[\sum_z W(\mu_z)\mu_z(\mu_{z+1}-\mu_z)]^2} \quad (A.2.9)$$

$$D(W(\mu),3,0) = \frac{[\sum_z W(\mu_z){\mu_z}^3(\mu_{z+1}-\mu_z)]\,[\sum_z W(\mu_z)\mu_z(\mu_{z+1}-\mu_z)]}{[\sum_z W(\mu_z){\mu_z}^2(\mu_{z+1}-\mu_z)]^2} \quad (\text{A. 2.10})$$

$$D_\sigma = \left[\frac{[\sum_z W(\mu_z)(\mu_z-\mu_w)^2(\mu_{z+1}-\mu_z)]}{[\sum_z W(\mu_z)(\mu_{z+1}-\mu_z)]}\right]^{0.5} \quad (A.\,2.11)$$

$$\mu_w = \frac{[\sum_z W(\mu_z)\mu_z(\mu_{z+1}-\mu_z)]}{[\sum_z W(\mu_z)(\mu_{z+1}-\mu_z)]} \quad (A.\,2.12)$$

A2.1.5.3 Reproducibility of the electrophoretic mobility distributions obtained from injections of PNaA at different pHs

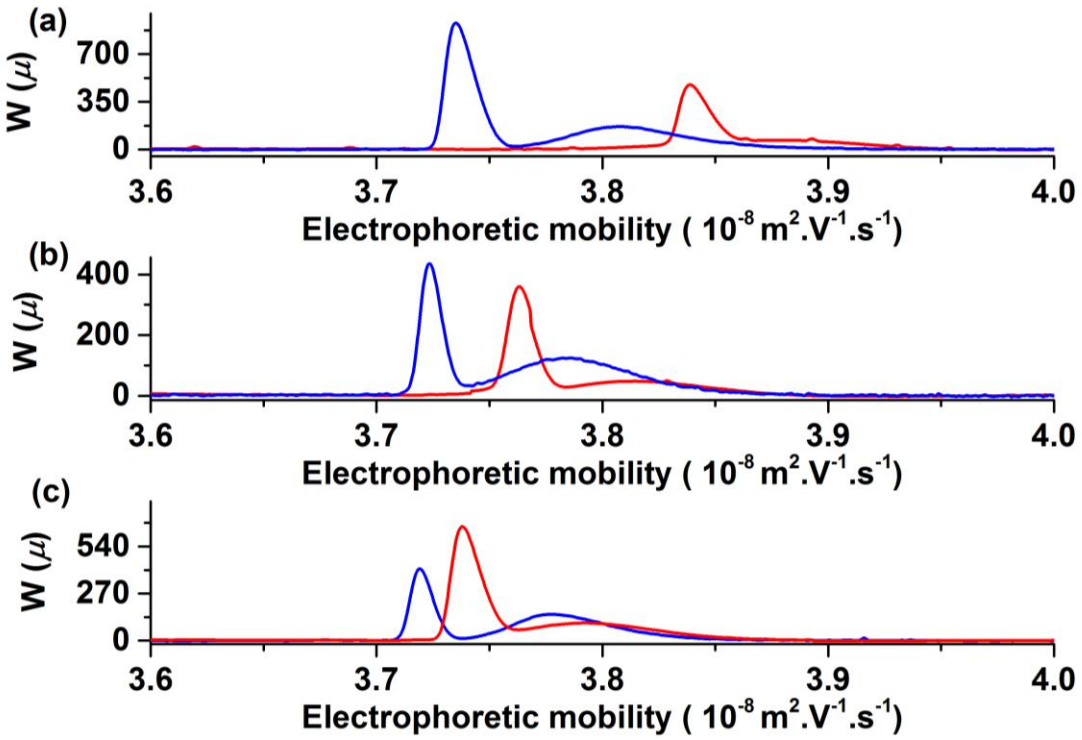

Figure A.2.11: Electrophoretic mobility distributions of PNaA synthesized at 70 °C without CTA and $[AA]_0$=2 M (a), PNaA synthesized at 90 °C without CTA and $[AA]_0$=1 M (b), PNaA synthesized at 90 °C without CTA and $[AA]_0$=2 M (c). The PNaA were injected at pH between 4 and 5 (blue line) or between 8 and 9 (red line).

Table A.2.7: Values of the dispersities and weight-average of the electrophoretic mobility distributions of PNaAs, with their average and standard deviation *SD*

Sample synthesis		$\boldsymbol{D(W(\mu),1,0)}$	$\boldsymbol{D(W(\mu),2,0)}$	$\boldsymbol{D(W(\mu),3,0)}$	$\boldsymbol{D_\sigma}$	$\boldsymbol{\mu_w}$ **(m^2 V^{-1} s^{-1})**
50 °C without CTA and $[AA]_0$ = 2 M		1.00011	1.00011	1.00011	3.94×10^{-10}	3.76×10^{-8}
		1.00012	1.00012	1.00012	4.07×10^{-10}	3.72×10^{-8}
		1.00012	1.00012	1.00013	4.14×10^{-10}	3.73×10^{-8}
	average	1.000116667	1.000117	1.00012	4.05×10^{-10}	3.73515×10^{-8}
	SD	4.71405×10^{-6}	4.71×10^{-6}	8.16×10^{-6}	8.64×10^{-12}	1.6631×10^{-10}
70 °C without CTA and $[AA]_0$ = 2 M		1.00013	1.00013	1.00013	4.36×10^{-10}	3.77×10^{-8}
		1.00012	1.00012	1.00012	4.21×10^{-10}	3.79×10^{-8}
		1.00013	1.00013	1.00013	4.25×10^{-10}	3.75×10^{-8}
	average	1.000126667	1.000127	1.000127	4.27×10^{-10}	3.77×10^{-8}
	SD	4.71405×10^{-6}	4.71×10^{-6}	4.71×10^{-6}	6.07×10^{-12}	1.69056×10^{-10}
90 °C without CTA and $[AA]_0$ = 2 M		1.00013	1.00013	1.00013	4.30×10^{-10}	3.72×10^{-8}
		1.00012	1.00012	1.00012	4.05×10^{-10}	3.74×10^{-8}
		1.0001	1.0001	1.0001	3.82×10^{-10}	3.76×10^{-8}
	average	1.000116667	1.000117	1.000117	4.06×10^{-10}	3.74123×10^{-8}
	SD	1.24722×10^{-5}	1.25×10^{-5}	1.25×10^{-5}	1.96×10^{-11}	1.6696×10^{-10}
90 °C without CTA and $[AA]_0$ = 1 M		1.00014	1.00014	1.00014	4.43×10^{-10}	3.72×10^{-8}
		1.00012	1.00012	1.00012	4.07×10^{-10}	3.72×10^{-8}
		1.00011	1.00011	1.00011	3.95×10^{-10}	3.74×10^{-8}
	average	1.000123333	1.000123	1.000123	4.15×10^{-10}	3.72857×10^{-8}
	SD	1.24722×10^{-5}	1.25×10^{-5}	1.25×10^{-5}	2.02×10^{-11}	8.3467×10^{-11}

90 °C without CTA and $[AA]_0$ = 3 M		1.00012	1.00012	1.00012	4.16×10^{-10}	3.79×10^{-8}
		1.0001	1.0001	1.0001	3.81×10^{-10}	3.78×10^{-8}
		1.00012	1.00012	1.00012	4.22×10^{-10}	3.79×10^{-8}
	average	1.000113333	1.000113	1.000113	4.07×10^{-10}	3.78657×10^{-8}
	SD	9.42809×10^{-6}	9.43×10^{-6}	9.43×10^{-6}	1.79×10^{-11}	8.06687×10^{-11}
Linear PNaA **[15]**		1.00001	1.00001	1.00001	1.40×10^{-10}	3.86×10^{-8}
		1.00001	1.00001	1.00001	1.48×10^{-10}	3.86×10^{-8}
		1.00001	1.00001	1.00001	1.42×10^{-10}	3.88×10^{-8}
	average	1.00001	1.00001	1.00001	1.44×10^{-10}	3.86489×10^{-8}
	SD	0	0	0	3.43×10^{-12}	1.33498×10^{-10}

A2.2 Chapter 3: Further characterization of the branching in hydrophilic poly(acrylates) using capillary electrophoresis

A2.2.1 Pressure mobilization

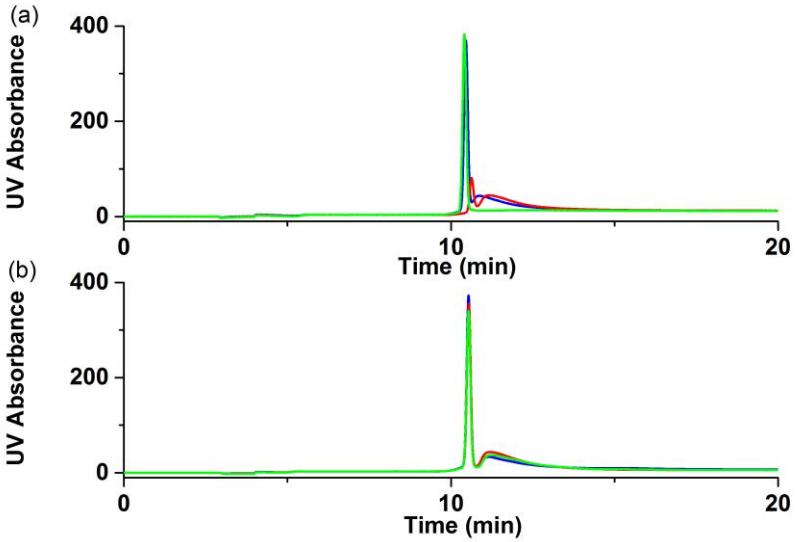

Figure A.3.1: Elugrams of pressure mobilization of Linear PNaA injected in sodium borate at (a) 25 mmol L^{-1} and (b) 50 mmol L^{-1}. Each injection was carried out in triplicate.

A broad peak is observed when linear PNaA is injected with sodium borate at 75, 50, and 25 mmol L^{-1}. This means that below 110 mmol L^{-1}, PNaA absorbs on the capillary when it is injected in sodium borate. Consequently, results obtained at low buffer concentrations are not reliable.

Table A.3.1: Correlation coefficient (triplicates) of Gaussian fits for chromatograms of different PNaA

	Correlation coefficient R^2	Correlation coefficient R^2	Correlation coefficient R^2	Average	*SD*
PNaA synthesized at 90 °C without CTA and at $[AA]_0$ = 2 M and analysed in NB110	0.9316	0.88091	0.85623	0.88958	0.031374
PNaA synthesized at 90 °C without CTA and at $[AA]_0$ = 2 M and analysed in NB300	0.99942	0.9996	0.99961	0.999543	8.73×10^{-5}
Linear PNaA analysed in NB110	0.99678	0.99641	0.99612	0.996437	2.70×10^{-4}
Hyperbranched PNaA analysed in NB110	0.99732	0.99729	0.99424	0.996283	0.001445
Hyperbranched PNaA analysed in NB300	0.99912	0.99945	0.99931	0.99929	0.00014

Capillary electrophoresis

A2.2.1.1 Independence of optimal PNaA concentration on buffer concentration

Table A.3.2: Peak areas of oligoacrylates injected in sodium borate at different concentration

Oligomer and buffer	Peak area	Peak area	Peak area	Average	*SD*
AA1 in NB25	1.61×10^{-7}	1.58×10^{-7}	1.51×10^{-7}	1.57×10^{-7}	4.18994×10^{-9}
AA1 in NB50	1.39×10^{-7}	1.29×10^{-7}	1.39×10^{-7}	1.36×10^{-7}	4.71405×10^{-9}
AA1 inNB110	1.36×10^{-7}	8.74×10^{-8}	1.03×10^{-7}	1.09×10^{-7}	2.02603×10^{-8}
AA1 in NB300	1.25×10^{-7}	1.25×10^{-7}	1.13×10^{-7}	1.21×10^{-7}	5.65685×10^{-9}
AA1 RAFT in NB25	5.20×10^{-7}	5.84×10^{-7}	5.32×10^{-7}	5.45×10^{-7}	2.77769×10^{-8}
AA1 RAFT in NB50	4.97×10^{-7}	4.26×10^{-7}	4.28×10^{-7}	4.50×10^{-7}	3.30084×10^{-8}
AA1 RAFT in NB110	4.66×10^{-7}	4.07×10^{-7}	4.09×10^{-7}	4.27×10^{-7}	2.73537×10^{-8}
AA1 RAFT in NB300	3.74×10^{-7}	3.75×10^{-7}	3.60×10^{-7}	3.70×10^{-7}	6.84755×10^{-9}
AA2 RAFT in NB25	1.18×10^{-6}	1.01×10^{-6}	9.82×10^{-7}	1.06×10^{-6}	8.74884×10^{-8}
AA2 RAFT in NB50	8.95×10^{-7}	7.27×10^{-7}	6.91×10^{-7}	7.71×10^{-7}	8.89044×10^{-8}
AA2 RAFT in NB110	8.70×10^{-7}	7.63×10^{-7}	7.54×10^{-7}	7.96×10^{-7}	5.26899×10^{-8}
AA2 RAFT in NB300	6.62×10^{-7}	6.71×10^{-7}	6.55×10^{-7}	6.63×10^{-7}	6.54896×10^{-9}

A2.2.1.2 Peak Identification

Table A.3.3: Mobilities of PNaA in sodium borate

Polymers and buffer	μ_{ep} ($\times 10^8$ m^2 V^{-1} s^{-1}) (max)	μ_{ep} ($\times 10^8$ m^2 V^{-1} s^{-1}) (max)	μ_{ep} ($\times 10^8$ m^2 V^{-1} s^{-1}) (max)	μ_{ep} ($\times 10^8$ m^2 V^{-1} s^{-1}) (max)	μ_{ep} ($\times 10^8$ m^2 V^{-1} s^{-1}) (avge)	Normal-ized μ_{ep}	*SD* μ_{ep} (normalized)
Linear PNaA in NB 110	3.85	3.85	3.88		3.86	1	0.0284
Hyperbranched PNaA (sharp peak) in NB110	3.7	3.71	3.74	3.73	3.72	1	0.0312
Hyperbranched PNaA (broad peak) in NB110	3.78	3.78	3.82	3.82	3.8	1	0.0400
3-arm star PNaA (sharp peak) in NB110	3.78	3.81	3.87		3.82	1	0.0748
3-arm star PNaA (broad peak) in NB110	3.76	3.77	3.8		3.78	1	0.0339

Linear PNaA in NB300	3.8	3.80	3.83		3.81	0.987	0.0283
Hyperbranched PNaA (sharp peak) in NB300	4.27	4.25	4.22		4.25	1.14	0.0364
Hyperbranched PNaA (broad peak) in NB300	3.98	3.98	3.98		3.98	1.05	0.0200
3-arm star PNaA (sharp peak) in NB300	4.23	4.26	4.28		4.256666667	1.11	0.0580
3-arm star PNaA (broad peak) in NB300	3.82	3.82	3.89		3.84	1.02	0.0500
Linear PNaA in NB200	3.78	3.79	3.85		3.81	0.999	0.0451
Hyperbranched PNaA (sharp peak) in NB200	3.66	3.66	3.74	3.72	3.70	0.99328	0.0535
Hyperbranched PNaA (broad peak) in NB200	3.58	3.6	3.68	3.59	3.61	0.951	0.0596
3-arm star PNaA (sharp	3.87	3.89	3.91		3.89	1.02	0.0537

peak) in NB200						
3-arm star PNaA (broad peak) in NB200	3.60	3.60	3.64	3.61	0.957	0.0359
Linear PNaA in NB150	3.75	3.79	3.78	3.77	0.978	0.0311
Hyperbranched PNaA (sharp peak) in NB150	3.75	3.77	3.78	3.77	1.01	0.0283
Hyperbranched PNaA (broad peak) in NB150	3.77	3.78	3.8	3.78	0.996	0.0325
3-arm star PNaA (sharp peak) in NB150	3.68	3.7	3.72	3.70	0.969	0.0537
3-arm star PNaA (broad peak) in NB150	3.62	3.64	3.65	3.64	0.963	0.0295

Linear PNaA in NB250	3.66	3.68	3.68	3.67	0.952	0.0236
Hyperbranched PNaA (sharp peak) in NB250	3.76	3.78	3.79	3.78	1.02	0.0283
Hyperbranched PNaA (broad peak) in NB250	3.61	3.63	3.65	3.63	0.955	0.0363
3-arm star PNaA (sharp peak) in NB250	3.79	3.81	3.81	3.80	0.996	0.0468
3-arm star PNaA (broad peak) in NB250	3.54	3.57	3.57	3.56	0.942	0.0311

Standard deviation of a ratio:

$$SD\left(\frac{A}{B}\right) = SD(A) + SD(B) \qquad (A.3.1)$$

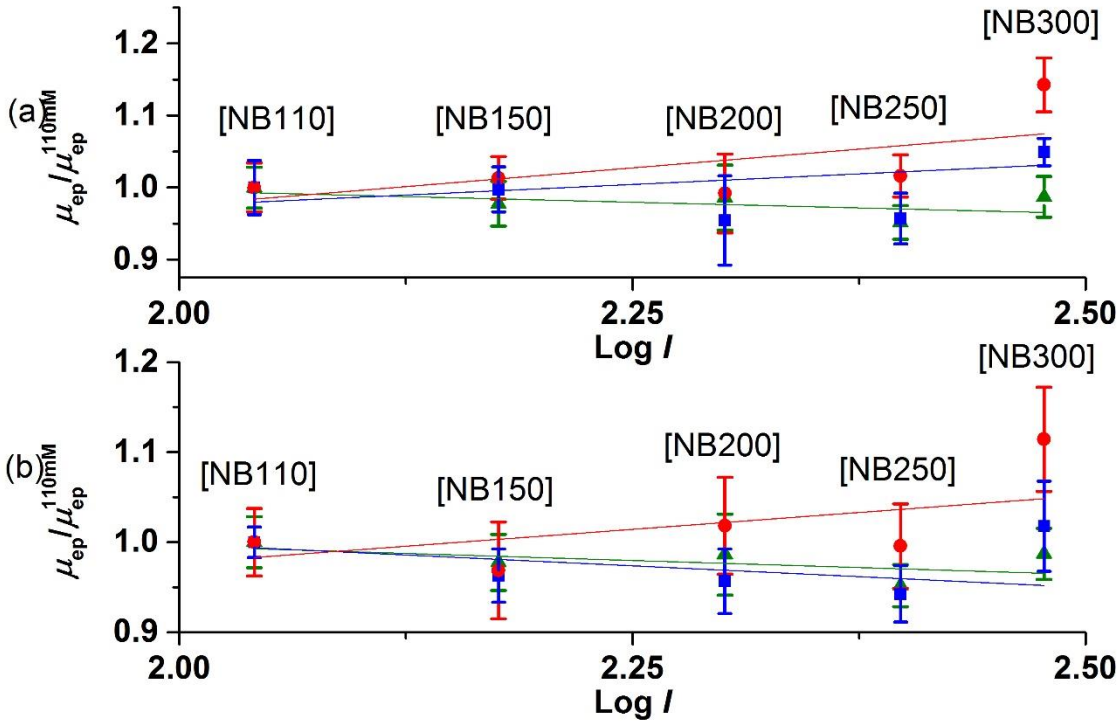

Figure A.3.2: Logarithmic dependence of the electrophoretic mobility with the ionic strength for (a) hyperbranched PNaA and (b) 3-arm star PNaA. Red circles represent the sharp peak, blue squares the broad peaks, and green triangles the linear PNaA. Fits were drawn.

Table A.3.4: Linear fits parameters for the logarithmic dependence of the electrophoretic mobility on the ionic strength

Population	*S* value (including injection in NB300)	Correlation coefficient R^2 (including injections in NB300)	*S* value (excluding injections in NB300)	*SD* (*S*)	Correlation coefficient R^2 (excluding injection in NB300)
Linear PNaA	0.06266	0.07626	0.12647	0.03363	0.81418
Hyperbranched PNaA (sharp peak)	−0.11767	0.02816	−0.03176	0.03633	−0.08518
Hyperbranched PNaA (broad peak)	0.20799	0.22811	0.13801	0.04291	0.75697
3-arm star PNaA (sharp peak)	−0.14987	0.10766	−0.01315	0.07432	−0.47689
3-arm star PNaA (broad peak)	0.09621	0.1495	0.16543	0.02972	0.90904

Injection of PNaA in CAPS:

The injections in ammonium acetate and in CAPS were not as repeatable as they were in sodium borates but the difference in phenomena are still observed: the sharp peak exhibits a lower mobility than the broad peak at each buffer concentration. The electropherogram of PNaA in ammonium acetate exhibits two peaks, which proves that neither of the peaks is a complex between polyacrylate and borate. The mobility of the broad peak is always higher than that of the sharp peak when PNaA is injected in CAPS (from 25 to 300 mmol L^{-1}).

Injection of PNaA in ammonium acetate and of PNaA with sodium acrylate in sodium borate:

It should be noted that the bottle of acrylic acid used for this experiment was different from the one used for the polymerization (it was provided by Aldrich and the purity was better than 99%). The preliminary study to identify both peaks (injection of PNaA with acrylic acid and injection of PNaA in ammonium acetate) was performed with a fused-silica capillary of about 60 cm total length and with sodium borate at pH = 9.2 as buffer at concentration close to 100 mmol L^{-1}.

A2.2.1.3 Selectivity:

Standard deviation of the selectivity is given by:

$$SD\left(\frac{1}{|A-B|}\right) = \frac{SD(A)+SD(B)}{|A-B|^2} \qquad (A.3.2)$$

Table A.3.5: Inverse of difference of mobility (*IDM*) of PNaA at different sodium borate concentration

Polymers and buffers	*IDM* (broad/sharp)	*SD*
Hyperbranched PNaA in NB25	1.82	0.0908
3-arm star PNaA in NB25	1.88	0.0309
Hyperbranched PNaA in NB300	3.75	0.1445
3-arm star PNaA in NB300	2.42	0.157
Hyperbranched PNaA in NB110	13.0	3.05
3-arm star PNaA in NB110	23.1	14.5
Hyperbranched PNaA in NB50	3.41	0.264
3-arm star PNaA in NB50	6.52	2.40
Hyperbranched PNaA in NB200	15.0	9.10
3-arm star PNaA in NB200	3.61	0.230
Hyperbranched PNaA in NB75	10.0	7.48
3-arm star PNaA in NB75	11.1	12.9
Hyperbranched PNaA in NB150	60.0	44.9
3-arm star PNaA in NB150	15.8	3.59
Hyperbranched PNaA in NB250	6.82	0.669
3-arm star PNaA in NB250	4.11	0.199

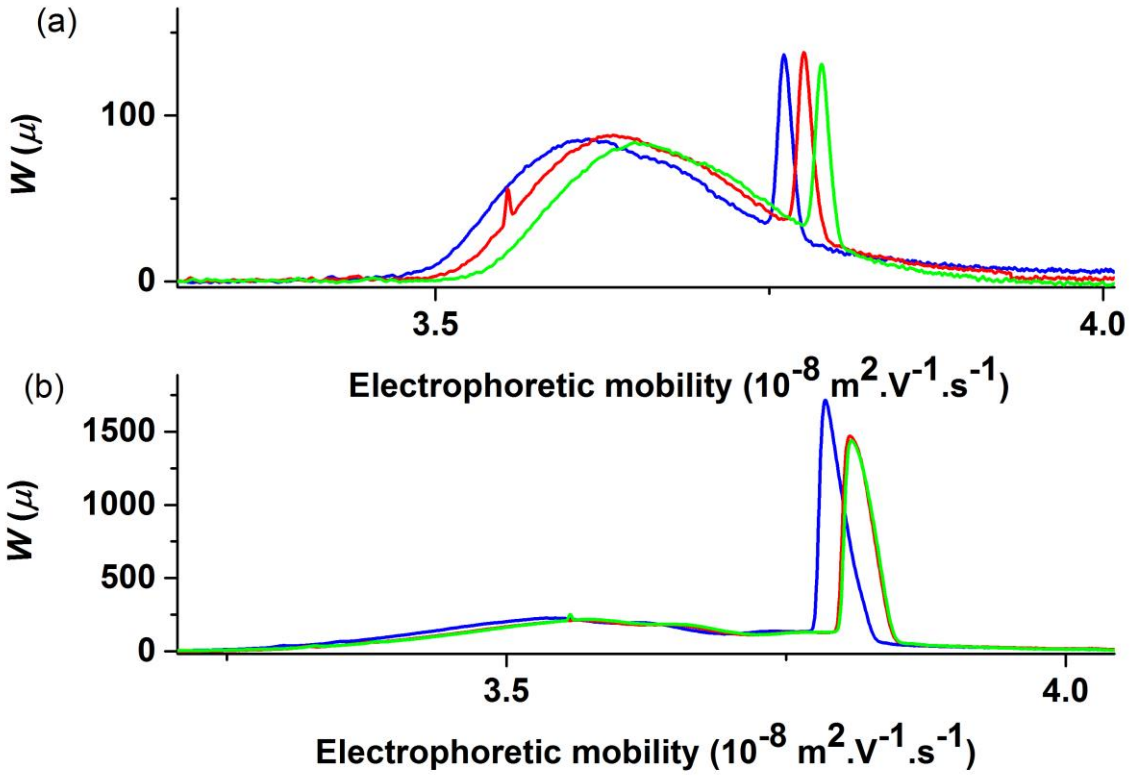

Figure A.3.3: (a) Hyperbranched and (b) 3-arm star PNaA injected using [NB250] as background electrolyte. Each experiment has been carried out in triplicate.

Table A.3.6: Electrophoretic mobilities of PNaA in sodium borate with and without silver nitrate

Buffers / Polymers	μ_{ep} ($\times 10^8$ m^2 $V^{-1}.s^{-1}$) (maximum)	μ_{ep} ($\times 10^8$ m^2 V^{-1} s^{-1}) (maximum)	μ_{ep} ($\times 10^8$ m^2 $V^{-1}.s^{-1}$) (maximum)	μ_{ep} ($\times 10^8$ m^2 V^{-1} s^{-1}) (average)	normalized μ_{ep}	SD
NB110						
Linear PNaA	3.85	3.85	3.88	3.86	1.00	0.0283
Hyperbranched PNaA (sharp peak)	3.7	3.71	3.74	3.72	1.00	0.0340
Hyperbranched PNaA (broad peak)	3.78	3.78	3.82	3.79	1.00	0.0377
3-arm star PNaA (sharp peak)	3.78	3.81	3.87	3.82	1.00	0.0748
3-arm star PNaA (broad peak)	3.76	3.77	3.8	3.78	1.00	0.0340
NB110+Ag (1×10^{-6} M)						
Linear PNaA	3.78	3.81	3.82	3.80	0.985	0.0311
Hyperbranched PNaA (sharp peak)	3.72	3.74	3.74	3.73	1.00	0.0264
Hyperbranched PNaA (broad peak)	3.85	3.85	3.85	3.85	1.01	0.0189
3-arm star PNaA (sharp peak)	3.63	3.64	3.64	3.64	0.952	0.0421
3-arm star PNaA (broad peak)	3.63	3.64	3.64	3.64	0.963	0.0217

Buffers and polymers	μ_{ep} ($\times 10^8$ m^2 $V^{-1}.s^{-1}$) (maximum)	μ_{ep} ($\times 10^8$ m^2 V^{-1} s^{-1}) (maximum)	μ_{ep} ($\times 10^8$ m^2 $V^{-1}.s^{-1}$) (maximum)	μ_{ep} ($\times 10^8$ m^2 V^{-1} s^{-1}) (average)	normalized μ_{ep}	SD
NB110+Ag (2×10^{-6} M)						
Linear PNaA	3.8	3.82	3.84	3.82	0.990	0.0305
Hyperbranched PNaA (sharp peak)	3.59	3.6	3.63	3.61	0.970	0.0340
Hyperbranched PNaA (broad peak)	3.7	3.7	3.7	3.7	0.975	0.0189
3-arm star PNaA (sharp peak)	3.61	3.61	3.61	3.61	0.945	0.0374
3-arm star PNaA (broad peak)	3.57	3.57	3.57	3.57	0.945	0.0170
NB110+Ag (100×10^{-6} M)						
Linear PNaA	3.75	3.77	3.80	3.77	0.978	0.0347
Hyperbranched PNaA (sharp peak)	3.58	3.60	3.63	3.60	0.970	0.0376
Hyperbranched PNaA (broad peak)	3.65	3.69	3.72	3.69	0.971	0.0475
3-arm star PNaA (sharp peak)	3.60	3.61	3.61	3.61	0.944	0.0421
3-arm star PNaA (broad peak)	3.55	3.55	3.55	3.55	0.940	0.0170

Table A.3.7: Peak areas of PNaAs in NB110 with and without silver

Polymers and silver nitrate concentration	Peak area	Peak area	Peak area	Average	*SD*
Linear PNaA, $[AgNO_3]$ = 0 mmol L^{-1}	1.22×10^{-7}	7.40×10^{-8}	4.78×10^{-8}	8.13×10^{-8}	3.07×10^{-8}
Linear PNaA, $[AgNO_3]$ = 1 mmol L^{-1}	1.00×10^{-7}	9.44×10^{-8}	8.34×10^{-8}	9.27×10^{-8}	7.03×10^{-9}
Linear PNaA, $[AgNO_3]$ = 2 mmol L^{-1}	1.15×10^{-7}	1.15×10^{-7}	1.15×10^{-7}	1.15×10^{-7}	2.02×10^{-10}
Linear PNaA, $[AgNO_3]$ = 100 mmol L^{-1}	1.70×10^{-7}	1.43×10^{-7}	1.43×10^{-7}	1.52×10^{-7}	1.30×10^{-8}
3-arm star PNaA, $[AgNO_3]$ = 0 mmol L^{-1}	2.45×10^{-6}	2.57×10^{-6}	1.57×10^{-6}	2.20×10^{-6}	4.44×10^{-7}
3-arm star PNaA, $[AgNO_3]$ = 1 mmol L^{-1}	2.14×10^{-6}	1.97×10^{-6}	2.13×10^{-6}	2.08×10^{-6}	7.54×10^{-8}
3-arm star PNaA, $[AgNO_3]$ = 2 mmol L^{-1}	1.79×10^{-6}	2.02×10^{-6}	2.03×10^{-6}	1.95×10^{-6}	1.12×10^{-6}
3-arm star PNaA, $[AgNO_3]$ = 100 mmol L^{-1}	1.37×10^{-6}	1.49×10^{-6}	1.30×10^{-6}	1.39×10^{-6}	7.65×10^{-8}
Hyperbranched PNaA, $[AgNO_3]$ = 0 mmol L^{-1}	1.97×10^{-6}	1.92×10^{-6}	1.72×10^{-6}	1.87×10^{-6}	1.07×10^{-7}
Hyperbranched PNaA, $[AgNO_3]$ = 1 mmol L^{-1}	2.13×10^{-6}	1.80×10^{-6}	1.91×10^{-6}	1.95×10^{-6}	1.35×10^{-7}
Hyperbranched PNaA, $[AgNO_3]$ = 2 mmol L^{-1}	1.79×10^{-6}	1.34×10^{-6}	1.31×10^{-6}	1.48×10^{-6}	2.19×10^{-7}
Hyperbranched PNaA, $[AgNO_3]$ = 100 mmol L^{-1}	2.14×10^{-6}	1.73×10^{-6}	1.63×10^{-6}	1.83×10^{-6}	2.22×10^{-7}

A2.2.1.4 Dispersity of branching

Table A.3.8: Dispersity of electrophoretic mobility $D(W(\mu),1,0)$ of linear, 3-arm star and hyperbranched PNaAs in diffferent buffer concentrations.

Buffers	Polymers	$\boldsymbol{D(W(\mu),1,0)}$	$\boldsymbol{D(W(\mu),1,0)}$	$\boldsymbol{D(W(\mu),1,0)}$	Average	*SD*
NB110	Linear PNaA	1.00001	1.00001	1.00001	1.00001	0.00000
	3-arm star PNaA	1.00113	1.00162	1.00067	1.00114	0.00039
	Hyperbranched PNaA	1.00040	1.00049	1.00035	1.00041	0.00006
	Linear PNaA	1.00002	1.00003	1.00003	1.00003	0.00000
NB150	3-arm star PNaA	1.00148	1.00140	1.00174	1.00154	0.00015
	Hyperbranched PNaA	1.00049	1.00043	1.00042	1.00045	0.00003
NB200	Linear PNaA	1.00003	1.00023	1.00015	1.00014	0.00008
	3-arm star PNaA	1.00288	1.00195	1.00223	1.00235	0.00039
	Hyperbranched PNaA	1.00068	1.00050	1.00049	1.00056	0.00009
NB250	Linear PNaA	1.00002	1.00002	1.00002	1.00002	0.00000
	3-arm star PNaA	1.00192	1.00180	1.00193	1.00188	0.00006
	Hyperbranched PNaA	1.00112	1.00074	1.00036	1.00074	0.00031
NB300	Linear PNaA	1.00001	1.00001	1.00002	1.00001	0.00000
	3-arm star PNaA	1.00306	1.00297	1.00370	1.00324	0.00032
	Hyperbranched PNaA	1.00108	1.00094	1.00091	1.00098	0.00007

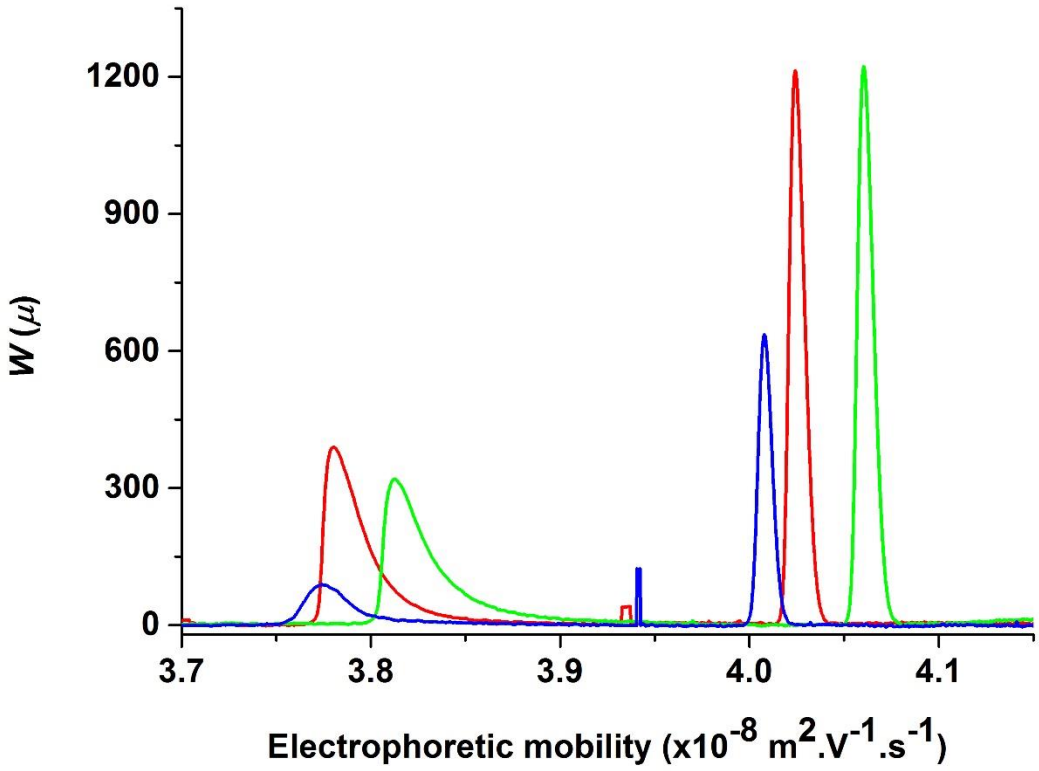

Figure A.3.4: Electropherogram of PNaAs synthesized by conventional radical polymerization at 50 °C (blue line), 70 °C (green line) and 90 °C (red line) without CTA at $[AA]_0$ = 2 M in NB300. Both peaks are resolved. A third peak is observed at 50 °C with CTA, which could be identified as the residual thiol.

Table A.3.9: Dispersities of PNaAs injected in [NB300]

Polymers		$\boldsymbol{D(W(\mu), 1, 0)}$ of the broad peak	$\boldsymbol{D(W(\mu), 2, 0)}$ of the broad peak	$\boldsymbol{D(W(\mu), 3, 0)}$ of the broad peak	$\boldsymbol{D_\sigma}$ of the broad peak	$\boldsymbol{D(W(\mu), 1, 0)}$ of the sharp peak	$\boldsymbol{D(W(\mu), 2, 0)}$ of the sharp peak	$\boldsymbol{D(W(\mu), 3, 0)}$ of the sharp peak	$\boldsymbol{D_\sigma}$ of the sharp peak
PNaA synthesized at 50 °C without CTA and at $[AA]_0$=2M		1.00001	1.00001	1.00001	2.23×10^{-10}	1	1	1	4.15×10^{-11}
		1.00013	1.00013	1.00013	5.27×10^{-10}	1	1	1	3.76×10^{-11}
		1.00005	1.00005	1.00005	2.65×10^{-10}	1	1	1	3.71×10^{-11}
	Average	1.000063333	1.000063333	1.000063333	3.38×10^{-10}	1	1	1	3.87×10^{-11}
	SD	4.98888×10^{-5}	4.98888×10^{-5}	4.98888×10^{-5}	1.34×10^{-10}	0	0	0	1.96×10^{-12}
PNaA synthesized at 70 °C without CTA and at $[AA]_0$=2M		1.00004	1.00005	1.00005	2.57×10^{-10}	1	1	1	4.23×10^{-11}
		1.00007	1.00007	1.00007	3.24×10^{-10}	1	1	1	4.30×10^{-11}
		1.00008	1.00009	1.00009	3.56×10^{-10}	1	1	1	4.61×10^{-11}
	Average	1.000063333	1.00007	1.00007	3.12×10^{-10}	1	1	1	4.38×10^{-11}
	SD	1.69967×10^{-5}	1.63299×10^{-5}	1.63299×10^{-5}	4.11×10^{-11}	0	0	0	1.67×10^{-12}
PNaA synthesized at 90 °C without CTA and at $[AA]_0$=2M		1.00002	1.00002	1.00003	1.94×10^{-10}	1	1	1	4.69×10^{-11}
		1.0001	1.00011	1.00011	3.90×10^{-10}	1	1	1	4.19×10^{-11}
		1.00005	1.00005	1.00005	2.86×10^{-10}	1	1	1	4.17×10^{-11}
	Average	1.000056667	1.00006	1.000063333	2.9×10^{-10}	1	1	1	4.35×10^{-11}
	SD	3.29983×10^{-5}	3.74166×10^{-5}	3.39935×10^{-5}	8.01×10^{-11}	0	0	0	2.39×10^{-12}

PNaA synthesized at 90 °C without CTA and at $[AA]_0$=1M		1.00005	1.00005	1.00005	2.80×10^{-10}	1	1	1	4.65×10^{-11}
		1.00002	1.00002	1.00002	2.33×10^{-10}	1	1	1	3.90×10^{-11}
		1.00003	1.00003	1.00003	2.33×10^{-10}	1	1	1	3.91×10^{-11}
	Average	1.000033333	1.000033333	1.000033333	2.49×10^{-10}	1	1	1	4.15×10^{-11}
	SD	1.24722×10^{-5}	1.24722×10^{-5}	1.24722×10^{-5}	2.23×10^{-11}	0	0	0	3.52×10^{-12}
PNaA synthesized at 90 °C without CTA and at $[AA]_0$=3M		1.00004	1.00004	1.00004	2.61×10^{-10}	1	1	1	4.00×10^{-11}
		1.00005	1.00005	1.00005	2.88×10^{-10}	1	1	1	3.63×10^{-11}
		1.00003	1.00003	1.00003	2.07×10^{-10}	1	1	1	5.99×10^{-11}
	Average	1.00004	1.00004	1.00004	2.52×10^{-10}	1	1	1	4.54×10^{-11}
	SD	8.16497×10^{-6}	8.16497×10^{-6}	8.16497×10^{-6}	3.36×10^{-11}	0	0	0	1.04×10^{-11}
Linear PNaA		1.00001	1.00001	1.00001	1.16	-	-	-	-
		1.00001	1.00001	1.00001	1.17	-	-	-	-
		1.00001	1.00001	1.00001	1.18				
	Average	1.00001	1.00001	1.00001	8.16×10^{-10}	-	-	-	-
	SD	0	0	0	1.14×10^{-12}	-	-	-	-

3-arm star PNaA		1.00153	1.00153	1.00153	1.52×10^{-9}	1	1	1	8.30×10^{-11}
		1.00175	1.00174	1.00173	1.64×10^{-9}	1	1	1	9.54×10^{-11}
		1.00171	1.00017	1.00169	1.60×10^{-9}	1	1	1	8.70×10^{-11}
	Average	1.00166	1.00166	1.00165	1.59×10^{-9}	1	1	1	8.85×10^{-11}
	SD	9.57×10^{-5}	9.10×10^{-5}	8.64×10^{-5}	4.99×10^{-11}	0	0	0	5.17×10^{-12}
		1.00035	1.00035	1.00035	5.57×10^{-10}	1	1	1	8.23×10^{-11}
Hyperbranched PNaA		1.00048	1.00048	1.00048	8.90×10^{-10}	1.00001	1.00001	1.00001	1.01×10^{-10}
		1.00043	1.00043	1.00043	8.31×10^{-10}	1	1	1	8.10×10^{-11}
	Average	1.00042	1.000423	1.000423	7.59×10^{-10}	1.000003	1.000003	1.000003	8.81×10^{-11}
	SD	5.35×10^{-5}	5.73×10^{-5}	5.73×10^{-5}	1.45×10^{-10}	4.71×10^{-6}	4.71×10^{-6}	4.71×10^{-6}	9.14×10^{-12}

Table A.3.10: Percentage of the broad peak in the total area of both broad and sharp peaks of PNaAs.

Samples	Contribution of the broad peak (%)	*SD*
PNaA synthesized at 50 °C without CTA and at $[AA]_0$=2M	34.4	5.9
PNaA synthesized at 70 °C without CTA and at $[AA]_0$=2M	44.1	1.2
PNaA synthesized at 90 °C without CTA and at $[AA]_0$=2M	47.7	0.43
PNaA synthesized at 90 °C without CTA and at $[AA]_0$=1M	60.4	0.63
PNaA synthesized at 90 °C without CTA and at $[AA]_0$=3M	80.8	7.7

A2.3 Chapter 4: Effect of transfer agent and polymerization temperature on branching and β-scission in poly(2-ethylhexyl acrylate)

A2.3.1 Synthesis of Polu(2-ethylhexyl acrylate)

A2.3.1.1 Conversions of P2EHAs obtained with a thermal initiator

Even though P2EHAs were dried on a Schlenk line for 5 days, an important quantity of residual monomer was observed in the ^{13}C NMR spectra. Consequently, the conversion was determined by multiplying the conversion determined gravimetrically by the conversion obtained by ^{13}C NMR spectroscopy. It should be be noted that the residual monomer signals observed by ^{13}C NMR spectroscopy may not be quantitative. Consequently, the conversion determined by ^{13}C NMR spectroscopy might be slightly overestimated. Values were determined by comparing the main chain CH signal with the average value of the 3 residual monomer signals. Results are in Table A.4.1.

Table A.4.1: Final monomer conversion obtained for P2EHAs synthesized with thermal initiator.

Polymers	Conversion obtained by gravimetry	Conversion obtained by ^{13}C NMR spectroscopy	Used final conversion
P2EHA-1	88%	92%	81%
P2EHA-2	>99.9%	89%	89%
P2EHA-3	93%	85%	79%
P2EHA-4	98%	89%	87%
P2EHA-5	96%	63%	59%
P2EHA-6	97%	96%	96%

A2.3.1.2 Conversions of P2EHAs obtained with a redox initiator

The conversion in polymerizations carried out at 4 and 25 °C could not be determined by gravimetry due to the presence of iron sulphate. Therefore, ^{1}H NMR spectroscopy was used. For the P2EHAs synthesized with CTA, the signals of residual monomer were compared with the main chain CH signal, and the conversion was calculated using Eq. (A.4.1).

$$conversion(\%) = \frac{H_1 \times 100}{\frac{H_2}{3} + H_1} \quad \text{(A. 4.1)}$$

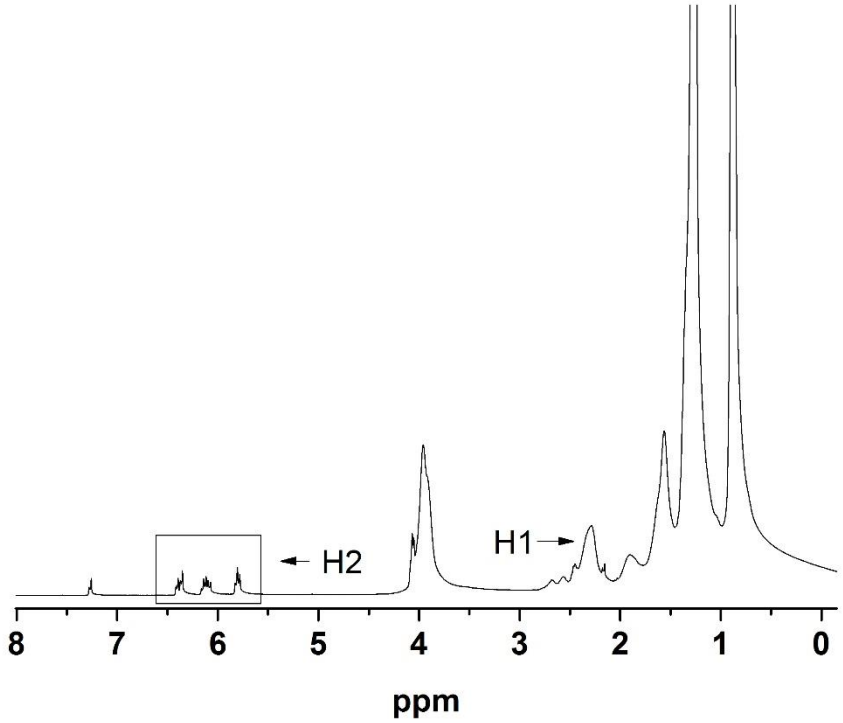

Figure A.4.1: Partial ^{1}H NMR spectrum of P2EHA synthesized at 4 °C with CTA, analysed at 58 g L^{-1} in $CDCl_3$.

This method was not applied to measure the conversion of P2EHAs synthesized at 4 and 25 °C without CTA due to the low solubility of the polymers in $CDCl_3$. When such measurements were tried, no conversion above 15 % was obtained using Eq. (A.4.1). Consequently, a calibration curve in the absence of polymer was generated, using three solutions of 2-ethylhexyl acrylate in $CDCl_3$ at 144 g L^{-1}, 96 g L^{-1} and 72 g L^{-1}. The peak area to noise ratio (*PNR*) – defined as the absolute peak area divided by the noise – was measured for one of the monomer signals (shown in Figure A.4.2) and plotted versus the concentration of 2EHA. Figure A.4.3 shows the calibration curve. The *PNR* can be used to measure the concentration of a solute in a deuterated solvent as the peak area is proportional to the amount of sample and the noise is used as a scaling factor to put all spectra on the same scale. The *PNR* was calculated is in [16].

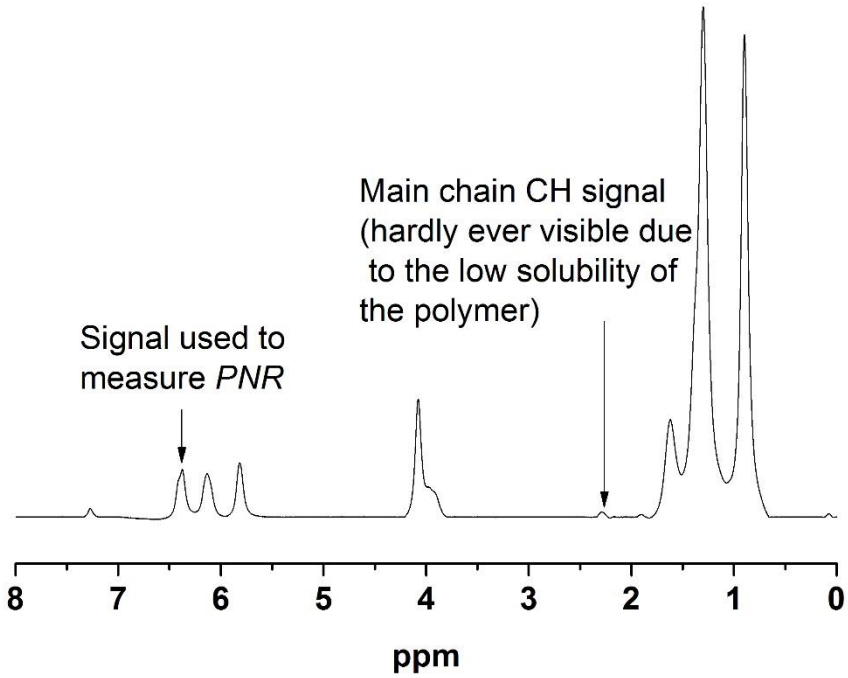

Figure A.4.2: Partial ^{1}H NMR spectrum of P2EHA synthesized at 25 °C with a CTA, analysed at 132 g L^{-1} in $CDCl_3$.

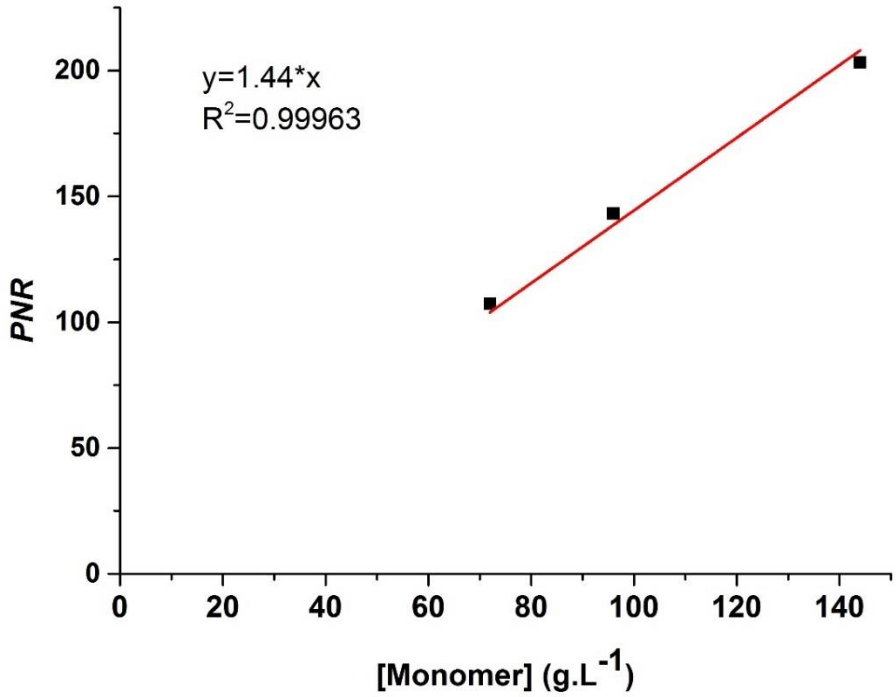

Figure A.4.3: Calibration curve: *PNR* plotted against 2EHA concentration.

After polymerization and before drying the polymer on the Schlenk line, an aliquot of P2EHA was taken and diluted in $CDCl_3$. This solution, whose concentration in P2EHA was known, was analysed by ^1H NMR spectroscopy and the *PNR* of the residual monomer signal at 6.5 ppm was measured and, using the calibration curve, the concentration of residual monomer was determined. The total concentration (monomer + polymer) was considered as 61 % of the total concentration of the solution as, at the start of the reaction, 5.5 g of 2EHA and 2.2 g of iron (II) sulphate were added. The change of weight due to the oxidation of iron (II) into iron (III) was neglected.

A2.3.2 Thermal analyses

A2.3.2.1 Differential scanning calorimetry

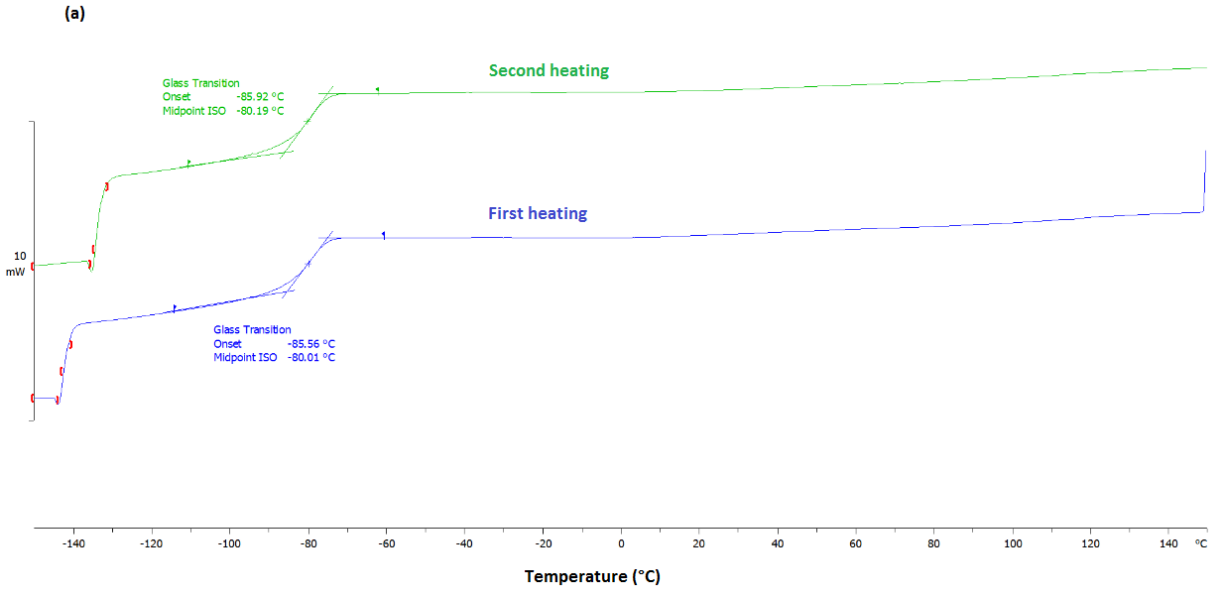

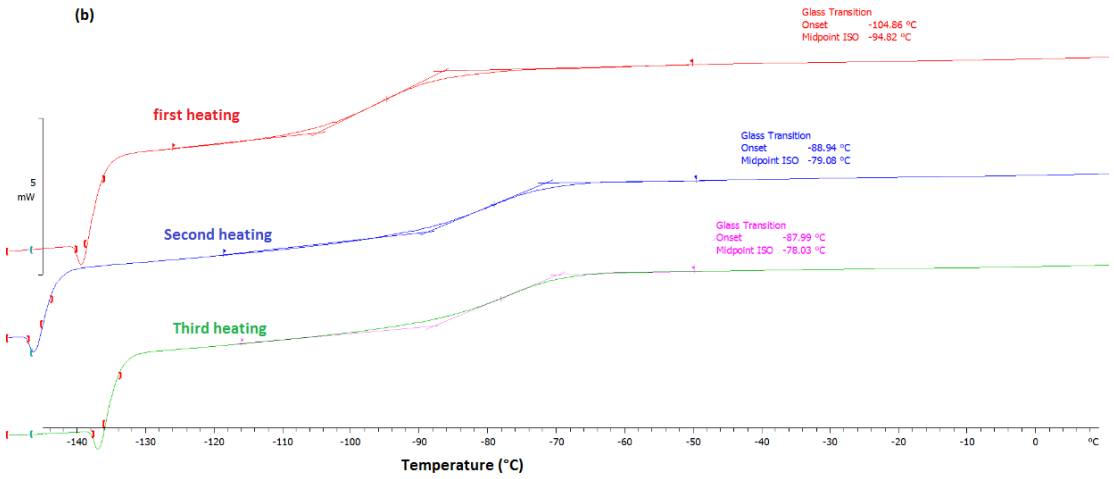

(c)

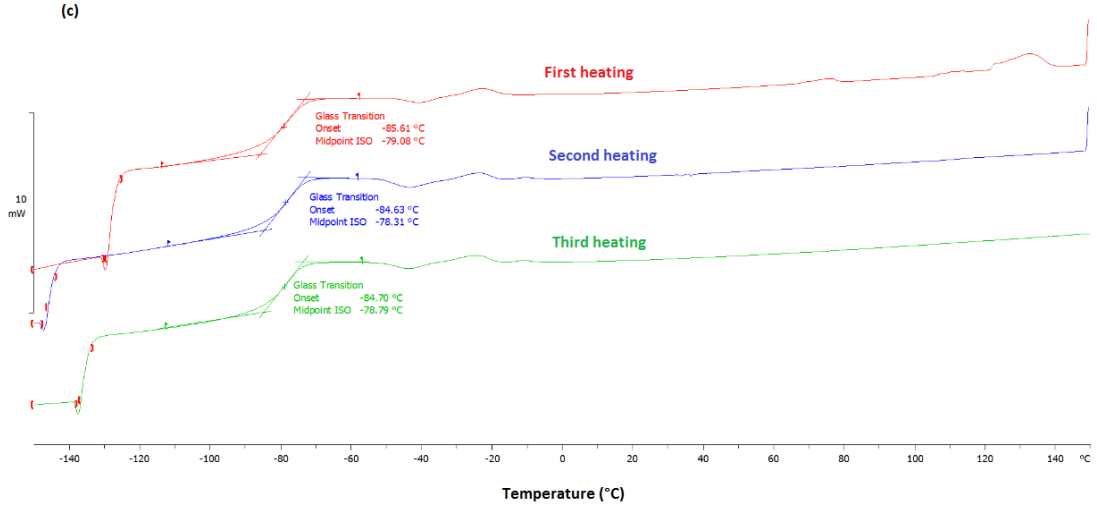
First heating
Glass Transition
Onset -85.61 °C
Midpoint ISO -79.08 °C
Second heating
Glass Transition
Onset -84.63 °C
Midpoint ISO -78.31 °C
Third heating
Glass Transition
Onset -84.70 °C
Midpoint ISO -78.79 °C
10
mW
-140 -120 -100 -80 -60 -40 -20 0 20 40 60 80 100 120 140 °C
Temperature (°C)

(d)

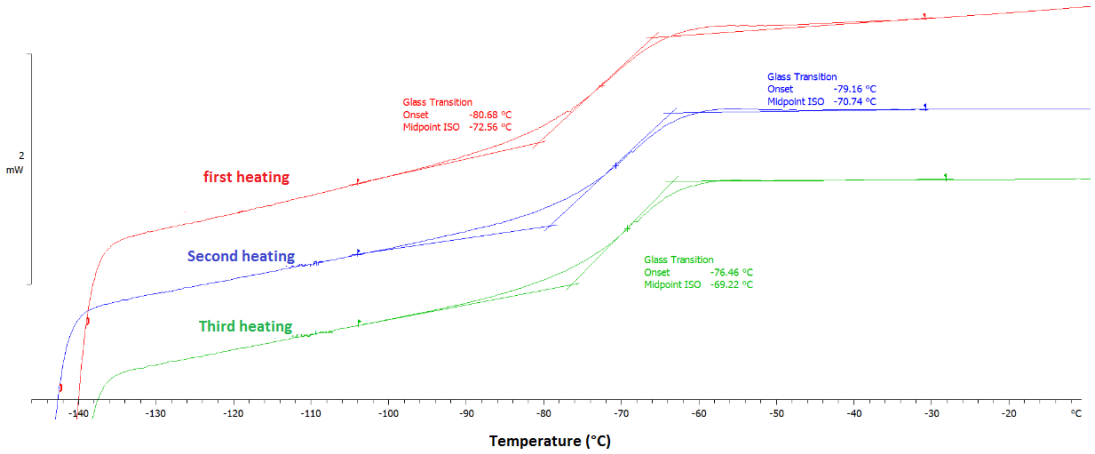
Glass Transition
Onset -80.68 °C
Midpoint ISO -72.56 °C
Glass Transition
Onset -79.16 °C
Midpoint ISO -70.74 °C
first heating
Second heating
Third heating
Glass Transition
Onset -76.46 °C
Midpoint ISO -69.22 °C
2
mW
-140 -130 -120 -110 -100 -90 -80 -70 -60 -50 -40 -30 -20 °C
Temperature (°C)

(e)

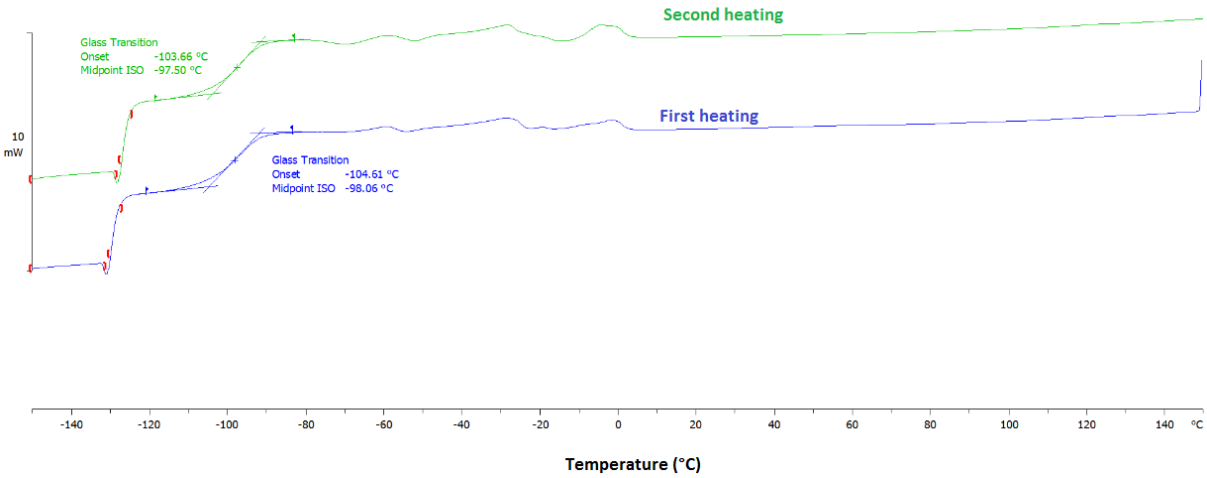
Second heating
Glass Transition
Onset -103.66 °C
Midpoint ISO -97.50 °C
First heating
10
mW
Glass Transition
Onset -104.61 °C
Midpoint ISO -98.06 °C
-140 -120 -100 -80 -60 -40 -20 0 20 40 60 80 100 120 140 °C
Temperature (°C)

(f)

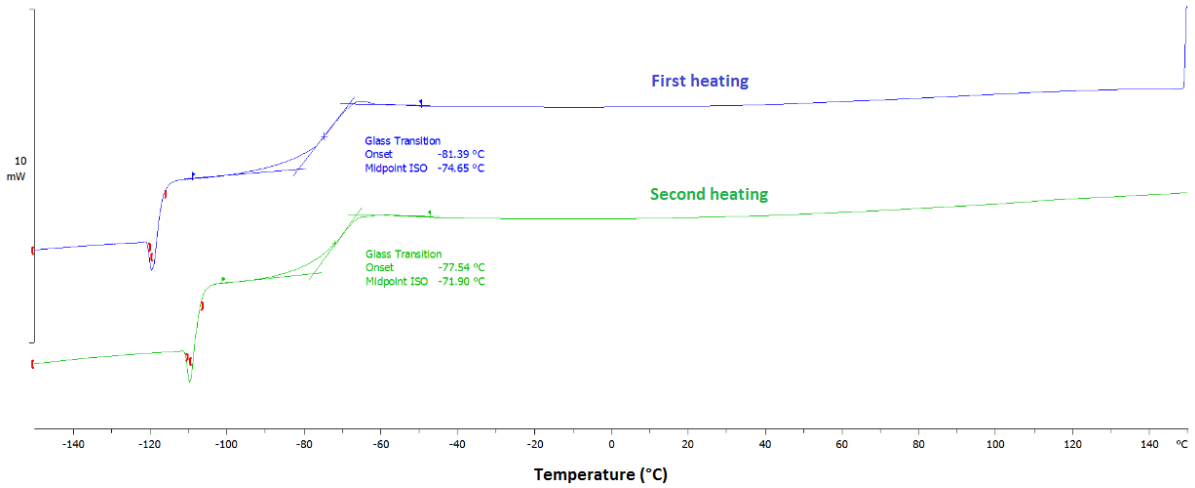
First heating
10
mW
Glass Transition
Onset -81.39 °C
Midpoint ISO -74.65 °C
Second heating
Glass Transition
Onset -77.54 °C
Midpoint ISO -71.90 °C
-140 -120 -100 -80 -60 -40 -20 0 20 40 60 80 100 120 140 °C
Temperature (°C)

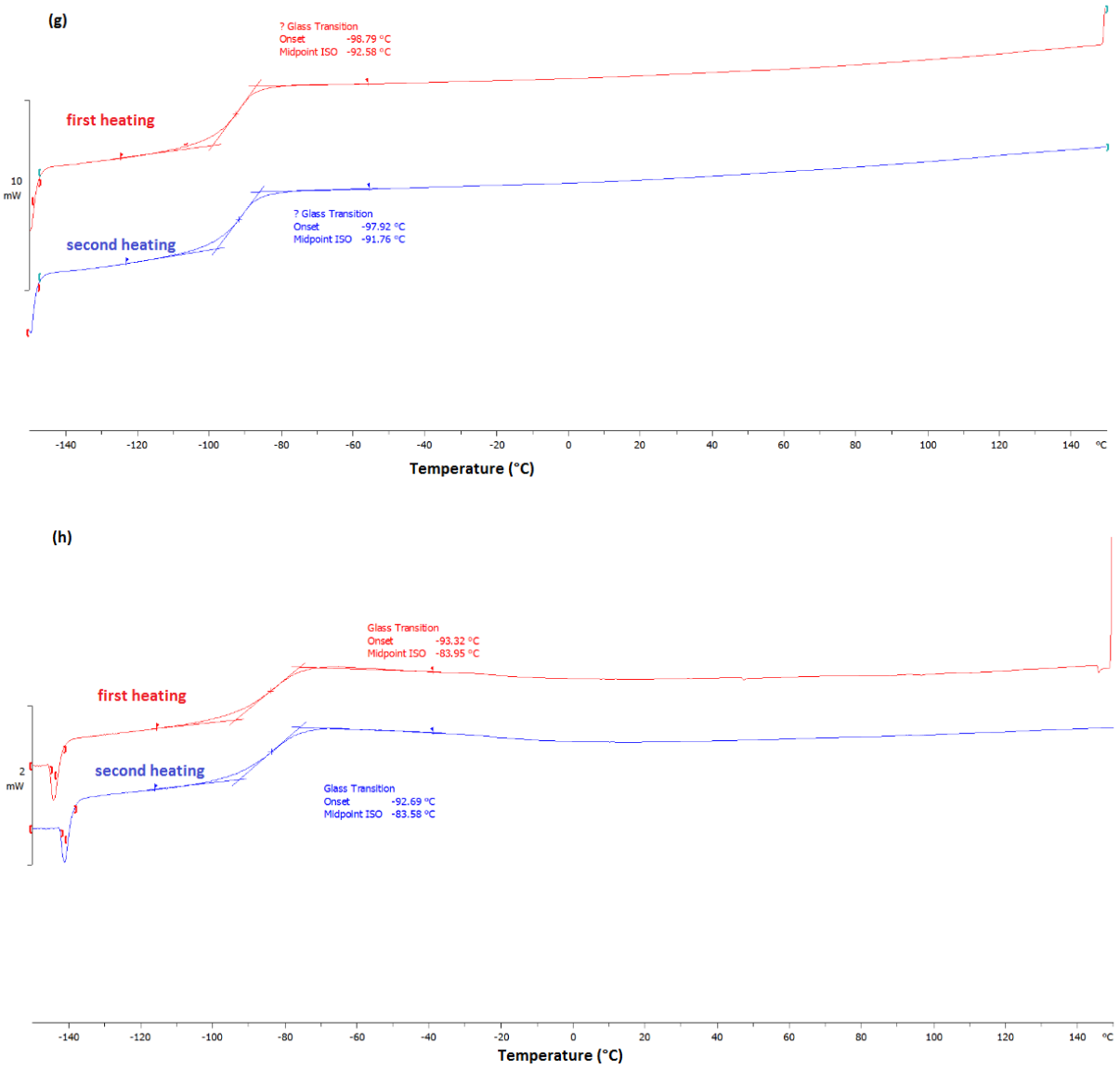

Figure A.4.4: DSC analyses of P2EHA synthesized at (a) 4 °C with CTA, (b) 4 °C without CTA, (c) 25 °C with CTA, (d) 25 °C without CTA, (e) 65 °C with CTA, (f) 65 °C without CTA, (g) 100 °C with CTA, (h) 100 °C without CTA, (i) 140 °C with CTA, (j) 140 °C without CTA.

A2.3.2.2 Thermogravimetric analysis

The decomposition temperature was defined as the temperature at the onset of the significant weight loss. In some cases, a small gap is observed at around 100 °C due to hydration loss. This decrease was not considered in measuring the decomposition temperature. Results are presented in Table A.4.2 and Figures A.4.5 to A.4.7.

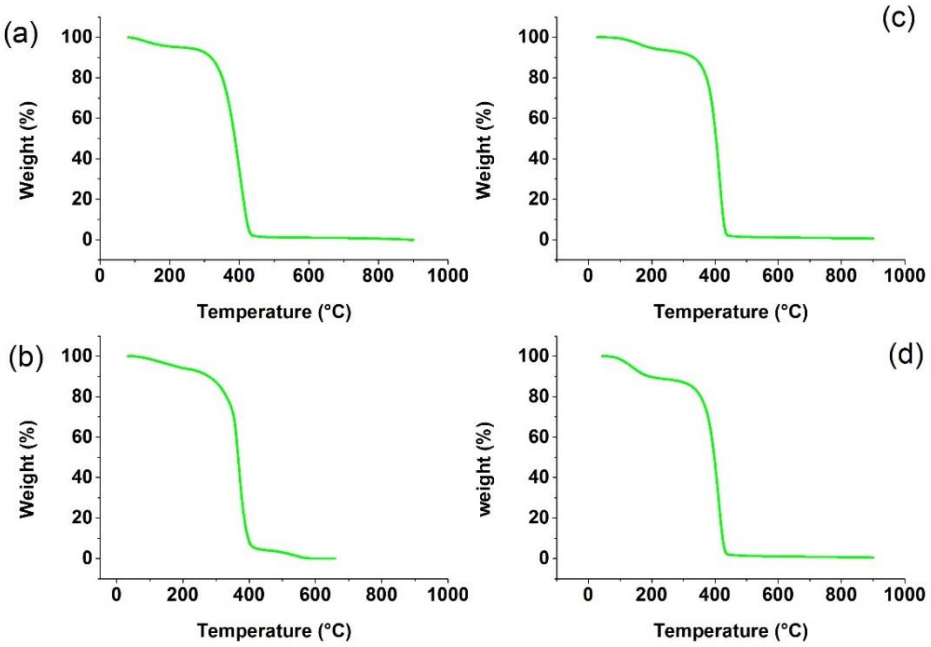

Figure A.4.5: TGA analyses of P2EHA synthesized at (a) 140 °C without CTA, (b) 100 °C without CTA, (c) 140 °C with CTA, 100 °C with CTA.

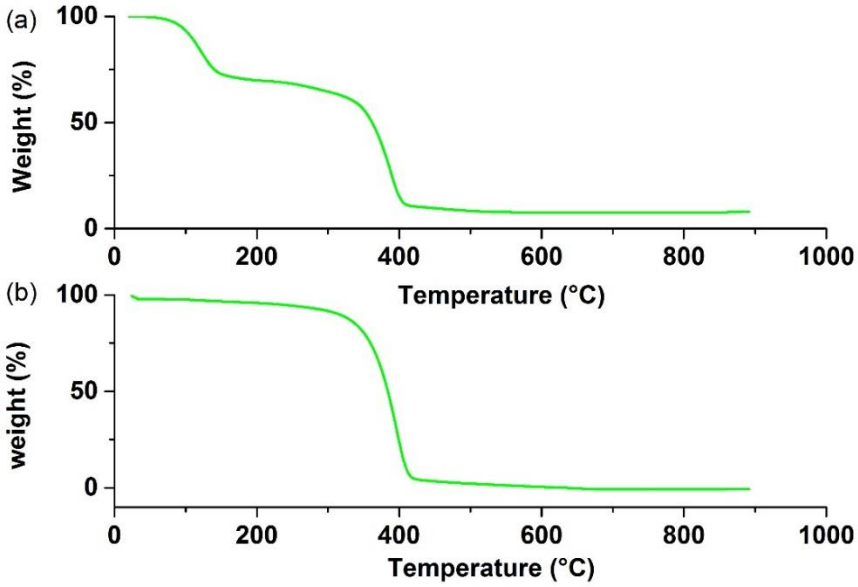

Figure A.4.12: TGA analyses of P2EHA synthesized at (a) 65 °C with CTA, (b) 65 °C without CTA.

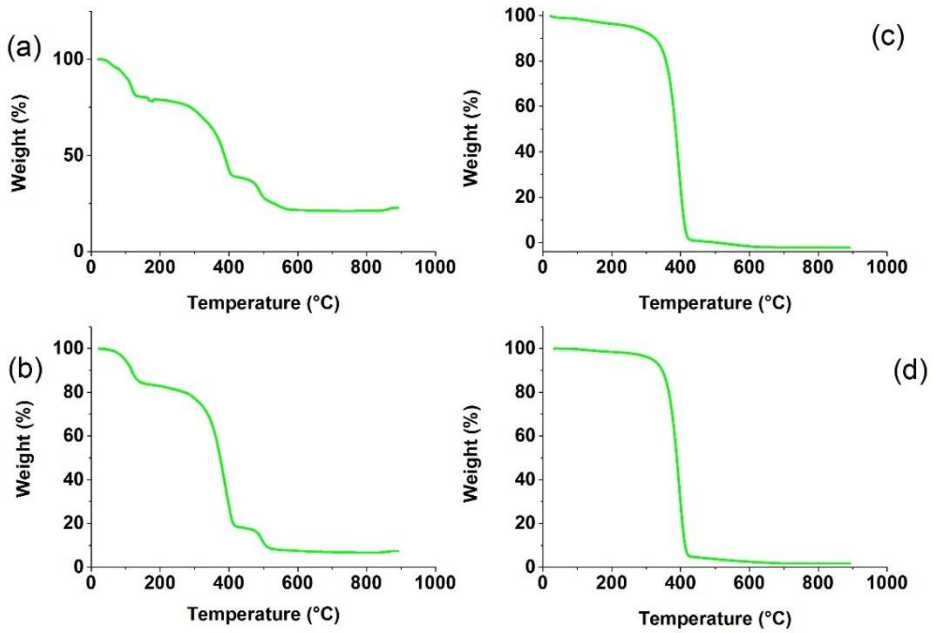

Figure A.4.13: TGA analyses of P2EHA synthesized at (a) 25 °C without CTA, (b) 4 °C without CTA, (c) 25 °C with CTA, (d) 4 °C with CTA.

Table A.4.2: T_g and degradation temperatures of P2EHAs.

Sample	Decomposition temperature	Glass transition temperature
P2EHA-1	385 °C	-87 °C
P2EHA-2	350 °C	-77 °C
P2EHA-3	375 °C	-92 °C
P2EHA-4	345 °C	-84 °C
P2EHA-5	355 °C	-97 °C
P2EHA-6	350 °C	-72 °C
P2EHA-7	380 °C	-79 °C
P2EHA-8	315 °C	-69 °C
P2EHA-9	360 °C	-80 °C
P2EHA-10	345 °C	-78 °C

A2.3.3 NMR spectroscopy

A2.3.3.1 Sample packing for melt-state NMR analyses

Table A.4.3 presents the conditions for ^{13}C melt-state NMR spectroscopy analysis (NMR spectrometer and sample packing) of each P2EHA.

Table A.4.3: Packing of P2EHA for each ^{13}C melt-state NMR experiments.

Sample	NMR spectrometers	Packing
P2EHA-1	Bruker 850 MHz double resonance ^{1}H-^{13}C MAS 4 mm probe	KelF (PTCFE) liquid insert inside ZrO_2 rotor with KelF caps
P2EHA-2	Bruker 850 MHz double resonance ^{1}H-^{13}C MAS 4 mm probe	ZrO2 rotor with BN caps
P2EHA-3	Bruker 850 MHz double resonance ^{1}H-^{13}C MAS 4 mm probe	KelF (PTCFE) liquid insert inside ZrO_2 rotor with KelF caps
P2EHA-4	Bruker 850 MHz double resonance ^{1}H-^{13}C MAS 4 mm probe	ZrO2 rotor with BN caps
P2EHA-5	Bruker 850 MHz double resonance ^{1}H-^{13}C MAS 4 mm probe	KelF (PTCFE) liquid insert inside ZrO_2 rotor with KelF caps
P2EHA-6	Bruker 850 MHz double resonance ^{1}H-^{13}C MAS 4 mm probe	ZrO2 rotor with BN caps
P2EHA-7	Bruker 400 MHz	KelF (PTCFE) liquid insert inside ZrO_2 rotor with KelF caps
P2EHA-8	Bruker 400 MHz	ZrO_2 rotor with BN caps
P2EHA-9	-	-
P2EHA-10	-	-

A2.3.3.2 Fit for NMR spectrum of P2EHA

Figure A.4.8 shows an original ^{13}C NMR spectrum of P2EHA and its reconstituted fit obtained with the DMfit software package [17].

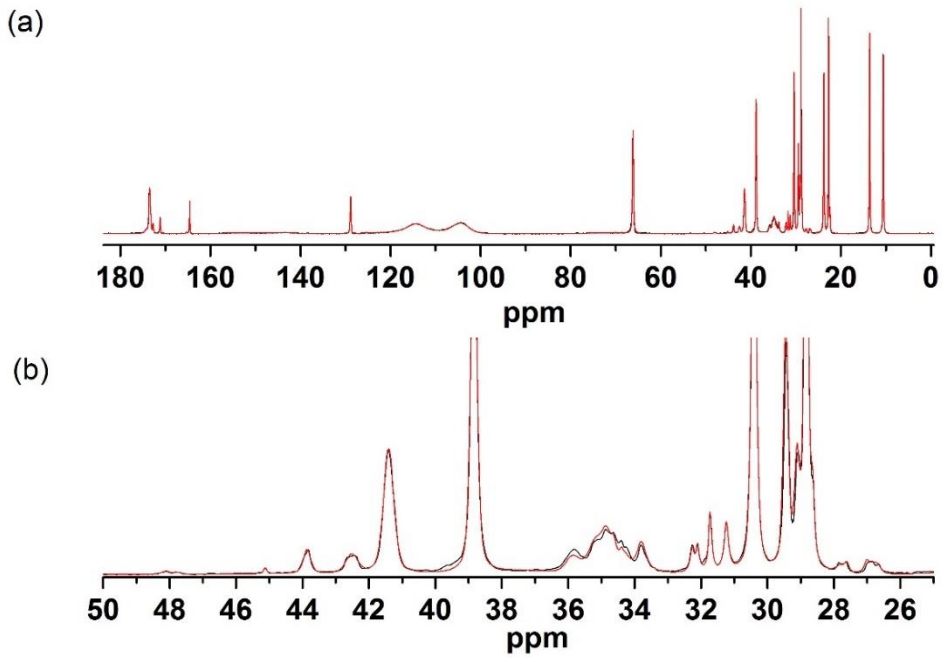

Figure A.4.8: Fitted spectrum of P2EHA synthesized at 100 °C with CTA. The black line is the obtained spectrum and the red line is that calculated with DMfit. (a) Full spectrum; (b) partial spectrum.

A2.3.3.3 Degree of branching and β-scission (*DB* and *DβS*): equations and results

Table A.4.4: *DB* and *DβS* of P2EHAs and their relative standard deviation (*RSD*).

Sample	*DB* (%) from Eq. (4.1)	RSD (%)	*DB* (%) from Eq. (4.2)	*RSD* (%)	*DβS* (%)	*RSD* (%)
P2EHA-1	1.98	0.49	1.65	0.42	1.68	0.25
P2EHA-2	3.72	0.68	3.10	0.59	2.98	0.31
P2EHA-3	2.20	0.41	1.86	0.35	1.27	0.29
P2EHA-4	3.66	0.61	3.26	0.56	1.78	0.29
P2EHA-5	Below 0.56*	-	Below 0.47*	-	0.71	0.17
P2EHA-6	2.11	0.20	1.95	0.19	-	-
P2EHA-7	-	-	-	-	-	-
P2EHA-8	-	-	-	-	-	-

* As on the ^{13}C NMR spectra of P2EHA-5 the C_q signal was below the limit of detection (SNR < 3), it was not possible to confirm, based on this analysis, that this polymer is branched. However, according to the literature, poly(alkyl acrylate)s synthesized at 65 °C are branched [18, 19]. Based on the error on the amplitude it was possible to obtain a spectrum for this *DB*.

The three RSD columns were calculated from the DMfit program. It includes calculation of the error on each fitted parameter, using the values of the chi-square and of the partial derivatives of the fitted function at the fitting set of parameters. A good approximation of the error on the peak area is obtained by the error on the peak intensity, while keeping its position and width fixed once optimised (the error on which is usually small, as expected for well defined peaks). The error on the ratio of peak intensities is determined with Maple built-in error propagation routines.

Figures A.4.9 and A.4.10 show the absence of branches and β-scission, respectively, in P2EHAs obtained at 25 °C.

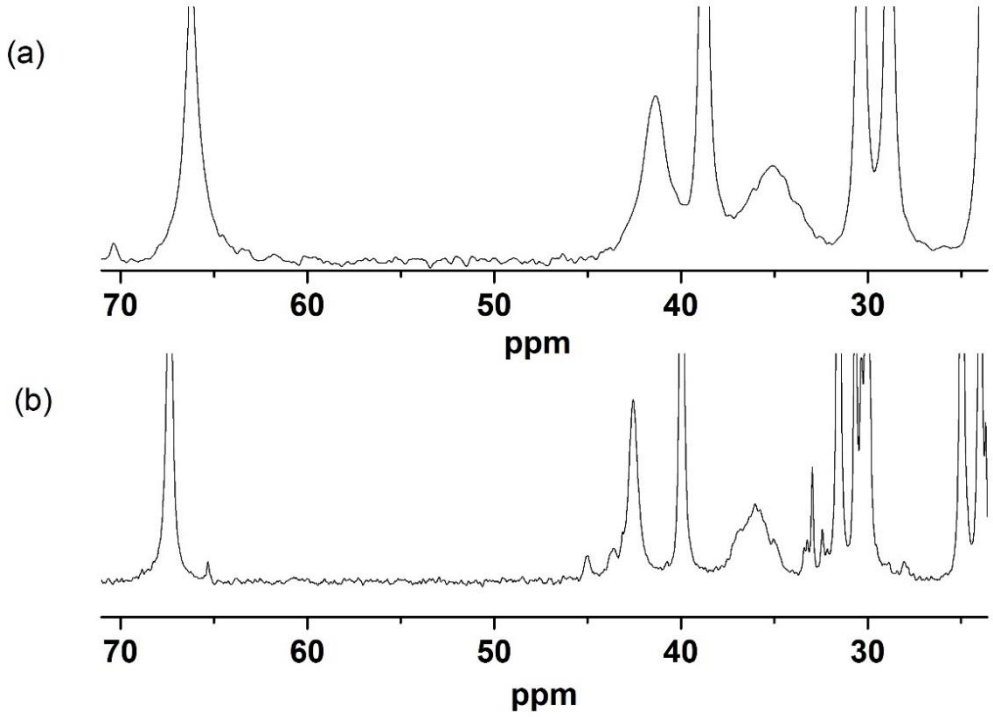

Figure A.4.9: Partial ^{13}C solid-state NMR spectra (23 – 71 ppm) at 50 °C of P2EHA synthesized at 25 °C (a) without CTA and (b) with CTA.

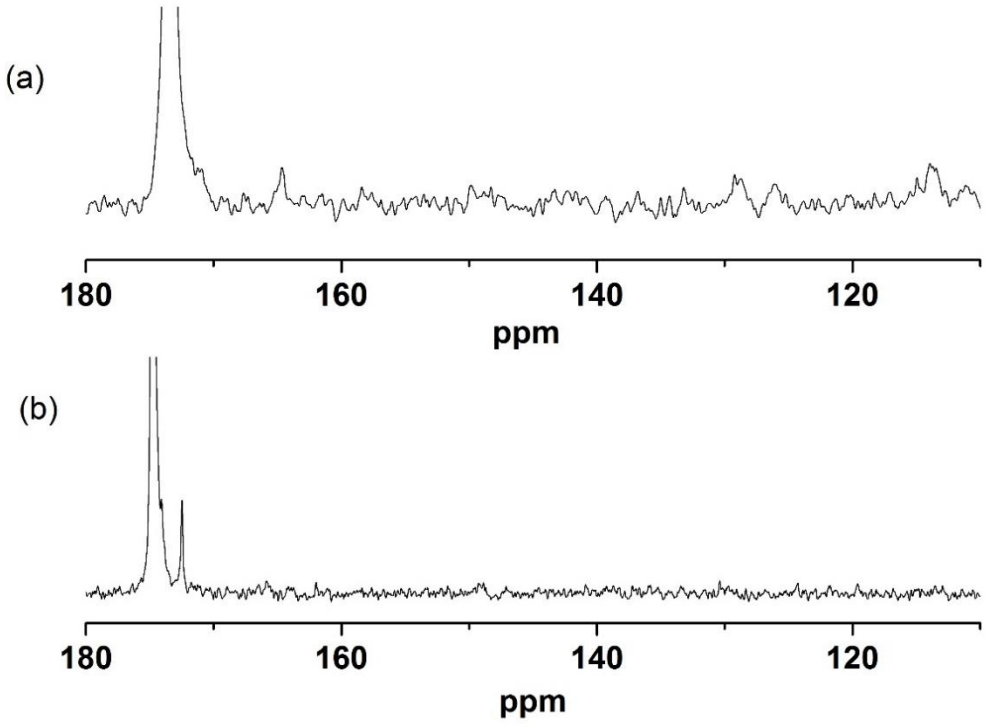

Figure A.4.10: Partial ^{13}C solid-state NMR spectra (110 – 180 ppm) at 50 °C of P2EHA synthesized at 25 °C (a) without CTA and (b) with CTA.

A2.3.4 Rate coefficients

Values of k_{bb}/k_p for polymerizations both with and without CTA were calculated from Equation (4.5); $[M]_0$ was calculated using the molar mass and the density of the 2EHA; $[M]_e$ was estimated using the final conversion (see Table A.4.1). The Arrhenius plot of these values is below.

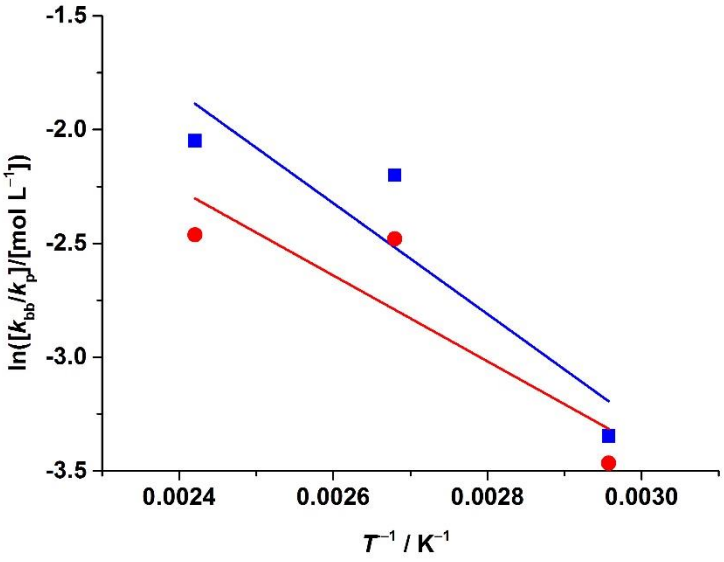

Figure A.4.11: Arrhenius plot of k_{bb}/k_p values of this work. Blue squares: without CTA; red circles: with CTA; lines: respective best fits.

The Arrhenius fits from Figure A.4.11 are:

$$\text{No CTA: } k_{bb}/k_p\,(\text{mol L}^{-1}) = e^{4.013}\, e^{-\frac{2437}{T}} \quad (65\,^{\circ}\text{C} < \theta < 140\,^{\circ}\text{C}) \qquad \text{(A. 4.2a)}$$

$$\text{With CTA: } k_{bb}/k_p\,(\text{mol L}^{-1}) = e^{2.265}\, e^{-\frac{1887}{T}} \quad (65\,^{\circ}\text{C} < \theta < 140\,^{\circ}\text{C}) \qquad \text{(A. 4.2b)}$$

Values from Eq. (A.4.22) were converted into k_{bb} using Eq. (4.7)[20] of the main text, where the Arrhenius plot of the resulting k_{bb} values is also given. This treatment was only done for the values from Equation (A.4.2a) (no CTA). The parameters from linear fitting with the Origin 9.0 software package are given in the table below.

Table A.4.5: Linear-fit parameters for the Arrhenius plot of k_{bb} for 2EHA without CTA, where the slope contains the activation energy, E_a, and the intercept contains the frequency factor, A.

Slope, $(-E_a/R)$/(J mol^{-1})	Standard error of slope	Intercept, ln(A/s^{-1})	Standard error of intercept	Correlation coefficient, R^2
–4 322.77	894.90	19.90	2.49	0.92

A2.3.5 Remaining NMR and ESI-MS spectra

Here we include all NMR and ESI-MS spectra not earlier included

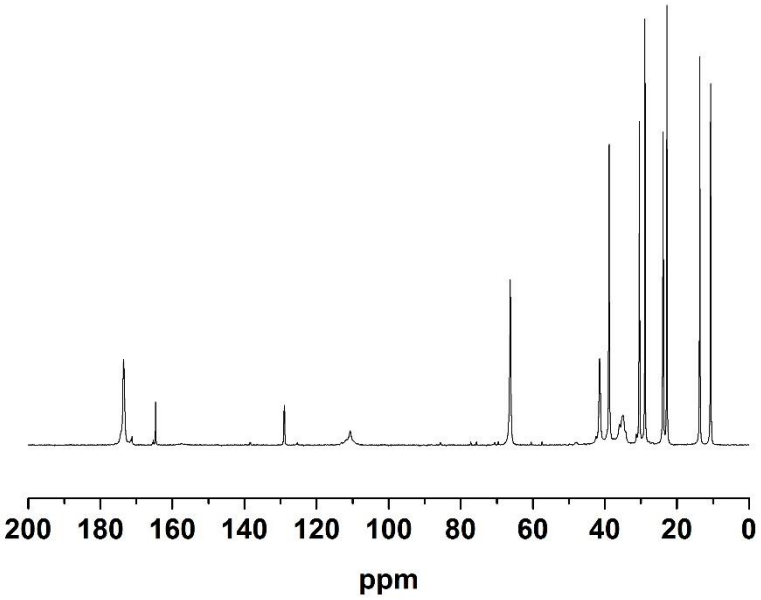

(a)

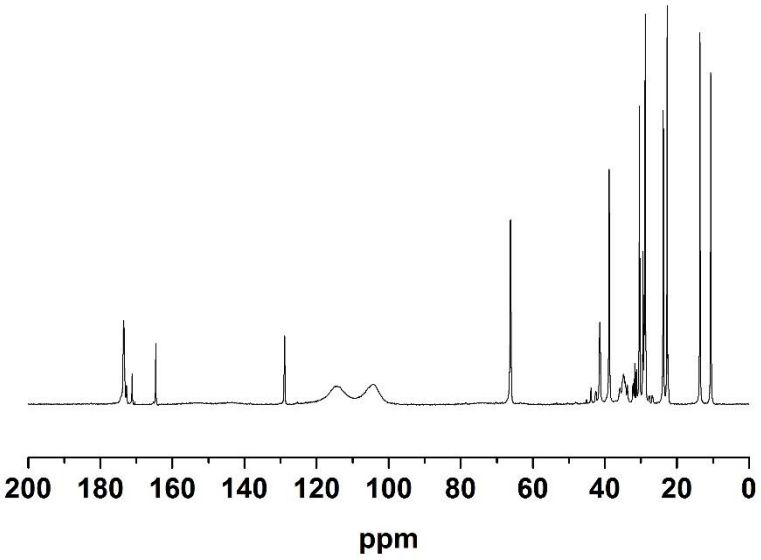

(b)

Figure A.4.12: ^{13}C NMR spectra of P2EHA synthesized at 100 °C (a) without CTA and (b) with CTA.

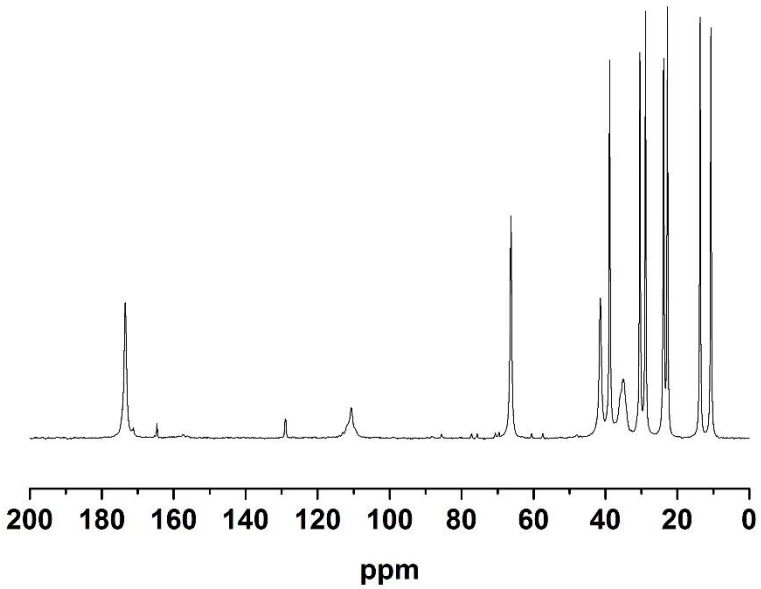

(a)

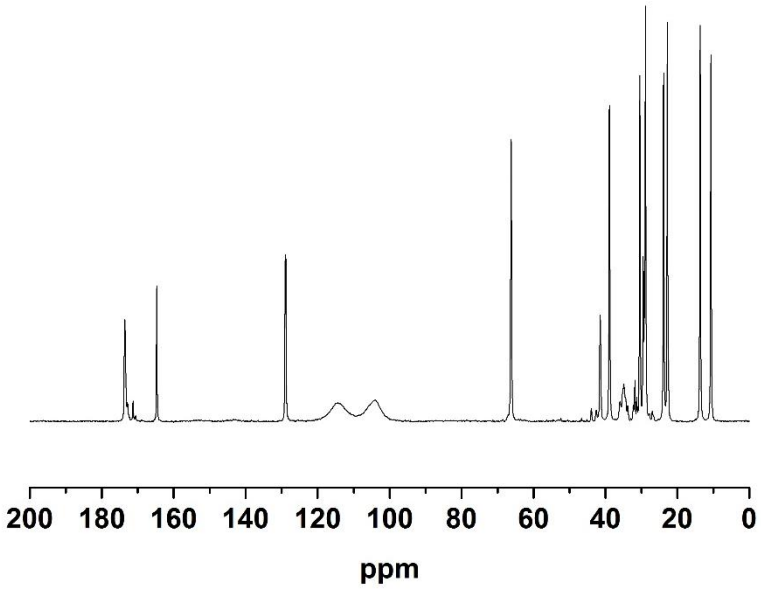

(b)

Figure A.4.13: ^{13}C NMR spectra of P2EHA synthesized at 65 °C (a) without CTA and (b) with CTA.

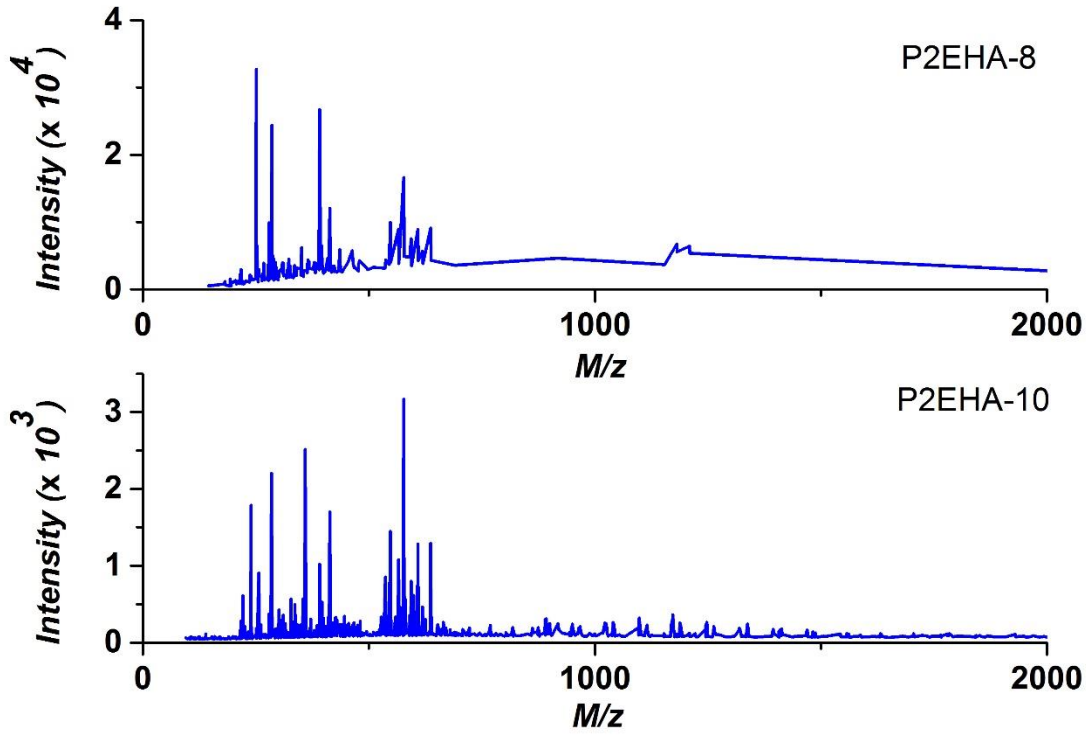

Figure A.4.14: Full ESI-MS spectra of samples P2EHA-8 and -10, which were synthesized without CTA at 25 and 4 °C, respectively.

A2.4 Chapter 6: Future work: size-based characterization of PAA using alternative methods to SEC

A2.4.1 Diffusion coefficients

A2.4.1.1 Adsorption of PNaA on the capillary:

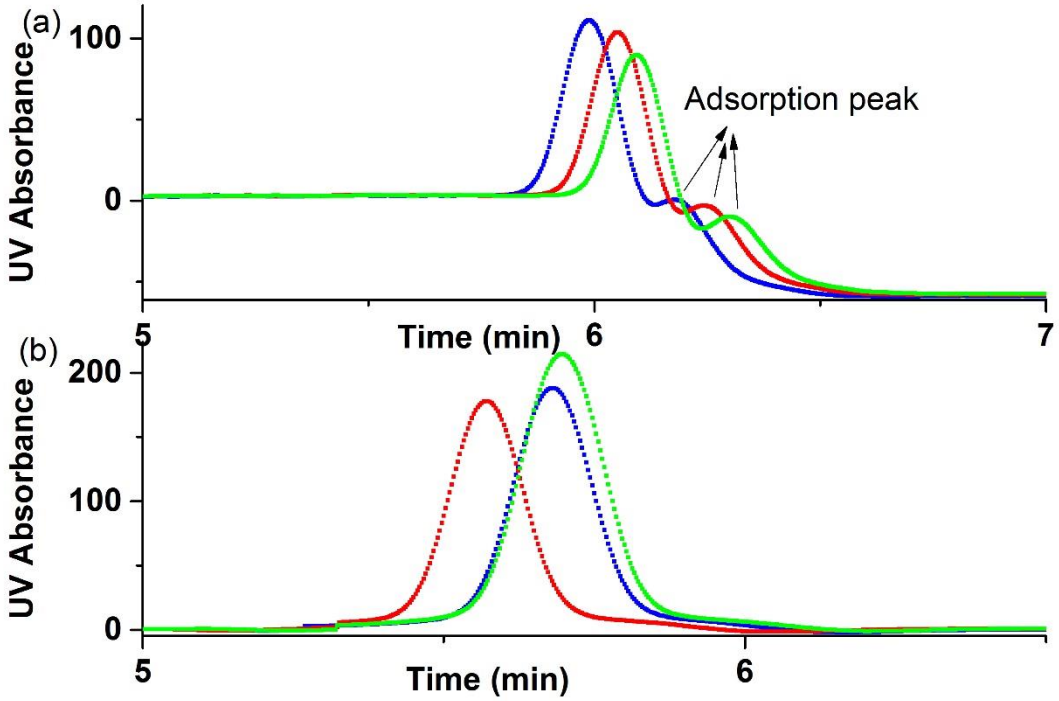

Figure A.6.1: PM experiments: injection of PNaA synthesized at 90 °C with CTA with (a) [NB110] and (b) [NB300] as mobile phase

From Figure A.6.1, it is clearly shown that CTA-containing PNaAs adsorb on the capillary in the mobile phase if [NB110] is used, and do not if [NB300] is used. In chapter 3, it is clearly stated that non-CTA-containing PNaAs do not adsorb in the capillary if the mobile phase is [NB110] or higher sodium borate concentration.

A2.4.1.2 Calculation of diffusion coefficients

Table A.6.1: Gaussian fit FWHM values for all PM experiments.

Polymers	Internal pressure (mbar)	FWHM	FWHM	FWHM	FWHM (Average)	FWHM (*SD*)
PAA synthesized at 50 °C without CTA $[AA]_0$=2M	100	0.14012	0.13987	0.13918	0.13972	0.000398
	90	0.15261	0.14563	0.15208	0.15011	0.003173
	80	0.14921	0.16375	0.14772	0.15356	0.007231
	70	0.18693	0.17072	0.18844	0.18203	0.008021
	60	0.2097	0.18343	0.1881	0.19374	0.011443
PAA synthesized at 70 °C without CTA $[AA]_0$=2M	100	0.13714	0.14028	0.14063	0.13935	0.001569
	90	0.1527	0.15332	0.1461	0.15071	0.003267
	80	0.15151	0.14845	0.15778	0.15258	0.003883
	70	0.17592	0.18414	0.17279	0.17762	0.004786
	60	0.19978	0.18476	0.18809	0.19088	0.006441
PAA synthesized at 90 °C without CTA $[AA]_0$=2M	100	0.14745	0.1339	0.14814	0.14316	0.006556
	90	0.15734	0.14427	0.15026	0.15062	0.005342
	80	0.17338	0.15871	0.15675	0.16295	0.007421
	70	0.19672	0.17843	0.18033	0.18516	0.008211
	60	0.21618	0.20474	0.19293	0.20462	0.009492
PAA synthesized at 90 °C without CTA $[AA]_0$=1M	100	0.14269	0.14257	0.14289	0.14272	0.000132
	90	0.14369	0.14137	0.1454	0.14349	0.001652
	80	0.1646	0.16992	0.156	0.16351	0.005735
	70	0.17274	0.1913	0.17079	0.17828	0.009243
	60	0.18564	0.18908	0.18504	0.18659	0.00178
PAA synthesized at 90 °C without CTA $[AA]_0$=3M	100	0.13577	0.13427	0.13647	0.13550	0.000918
	90	0.15121	0.14061	0.14208	0.14463	0.004689
	80	0.168	0.15718	0.14991	0.15836	0.007432
	70	0.18716	0.16698	0.16905	0.17440	0.009065
	60	0.20824	0.20296	0.19234	0.20118	0.006612
PAA synthesized at 50 °C with CTA $[AA]_0$=2M	100	0.20392	0.19763	0.20185	0.20113	0.002617
	90	0.2214	0.22102	0.22045	0.22096	0.00039
	80	0.23885	0.24267	0.22195	0.23449	0.009003
	70	0.26221	0.22979	0.25028	0.24743	0.013388
	60	0.24973	0.24911	0.26534	0.25473	0.007509
PAA synthesized at 70 °C with CTA $[AA]_0$=2M	100	0.15029	0.14647	0.14718	0.14798	0.001659
	90	0.16421	0.16577	0.15136	0.16045	0.006457
	80	0.19467	0.17757	0.1833	0.18518	0.007106
	70	0.2076	0.18807	0.18407	0.19325	0.01028
	60	0.22235	0.21393	0.22065	0.21900	0.003635
	100	0.1482	0.14809	0.15258	0.14962	0.002091
	90	0.15156	0.15944	0.15085	0.15395	0.003893

PAA synthesized at 50 °C with CTA $[AA]_0$=2M	80	0.19796	0.17917	0.2002	0.19244	0.00943
	70	0.18518	0.18919	0.18882	0.18773	0.001809
	60	0.20056	0.19316	0.22026	0.20466	0.011437
Lin PNaA	100	0.13678	0.13932	0.14403	0.14004	0.003004
	90	0.15654	0.15704	0.15711	0.15690	0.000254
	80	0.16096	0.16277	0.17096	0.16490	0.004351
	70	0.19122	0.18848	0.19017	0.18996	0.001129
	60	0.21478	0.21531	0.21649	0.21553	0.000715
Hyperbranched PNaA	100	0.17603	0.17108	0.17029	0.17247	0.00254
	90	0.17231	0.18523	0.18257	0.18004	0.00557
	80	0.21643	0.21176	0.21098	0.21306	0.002406
	70	0.23456	0.23536	0.23234	0.23409	0.001278
	60	0.26005	0.26127	0.23657	0.25263	0.011367

Table A.6.2: Retention times for all PM experiments

Polymers	Internal pressure (mbar)	t_r (s)	t_r (s)	t_r (s)	t_r (s) (Average)	t_r (s) (*SD*)	t_r^2
PAA synthesized at 50 °C without CTA $[AA]_0$=2M	100	346.2	346.2	348.6	347	1.131371	120409
	90	379.2	379.2	379.8	379.4	0.282843	143944.4
	80	424.8	429	424.8	426.2	1.979899	181646.4
	70	504	505.2	510	506.4	2.592296	256441
	60	583.8	581.4	579.6	581.6	1.720465	338258.6
PAA synthesized at 70 °C without CTA $[AA]_0$=2M	100	349.2	346.2	347.4	347.6	1.232883	120825.8
	90	379.8	380.4	381	380.4	0.489898	144704.2
	80	421.2	431.4	432	428.2	4.955805	183355.2
	70	495	504.6	492	497.2	5.374012	247207.8
	60	587.4	583.8	575.4	582.2	5.027922	338956.8
PAA synthesized at 90 °C without CTA $[AA]_0$=2M	100	348.6	349.2	349.8	349.2	0.489898	121940.6
	90	375	373.8	367.8	372.2	3.149603	138532.8
	80	433.8	429	438	433.6	3.676955	188009
	70	503.4	494.4	511.8	503.2	7.104928	253210.2
	60	588	589.2	580.2	585.8	3.989987	343161.6
PAA synthesized at 90 °C without CTA $[AA]_0$=1M	100	348.6	349.2	349.2	349	0.282843	121801
	90	364.2	376.8	378	373	6.241795	139129
	80	435.6	434.4	438.6	436.2	1.766352	190270.4
	70	505.8	504.6	507	505.8	0.979796	255833.6
	60	582.6	573.6	579.6	578.6	3.741657	334778
PAA synthesized at 90 °C without CTA $[AA]_0$=3M	100	333	334.2	332.4	333.2	0.748331	111022.2
	90	376.8	375.6	377.4	376.6	0.748331	141827.6
	80	432	429.6	432.6	431.4	1.296148	186106
	70	496.8	491.4	500.4	496.2	3.698648	246214.4
	60	590.4	591.6	583.8	588.6	3.429286	346450
PAA synthesized at 50 °C with CTA $[AA]_0$=2M	100	331.2	332.4	333	332.2	0.748331	110356.8
	90	378	378	378	378	0	142884
	80	436.2	435.6	436.2	436	0.282843	190096
	70	492	489.6	492	491.2	1.131371	241277.4
	60	586.8	581.4	592.2	586.8	4.409082	344334.2
PAA synthesized at 70 °C with CTA $[AA]_0$=2M	100	336	340.2	340.8	339	2.135416	114921
	90	378.6	378.6	375	377.4	1.697056	142430.8
	80	432	432.6	440.4	435	3.826225	189225
	70	495.6	488.4	492.6	492.2	2.952965	242260.8
	60	588	591	589.2	589.4	1.232883	347392.4
	100	339	345.6	343.8	342.8	2.785678	117511.8

PAA synthesized at 50 °C with CTA $[AA]_0$=2M	90	375	380.4	377.4	377.6	2.209072	142581.8
	80	434.4	433.2	433.8	433.8	0.489898	188182.4
	70	490.2	487.2	489.6	489	1.296148	239121
	60	572.4	589.8	588.6	583.6	7.934734	340589
Linear PNaA	100	337.8	339	338.4	338.4	0.489898	114514.6
	90	381.6	381.6	381.6	381.6	5.68E-14	145618.6
	80	433.2	431.4	433.2	432.6	0.848528	187142.8
	70	501.6	502.2	502.2	502	0.282843	252004
	60	592.8	592.8	593.4	593	0.282843	351649
Hyperbranched PNaA	100	331.2	331.8	331.8	331.6	0.282843	109958.6
	90	371.4	373.2	372.6	372.4	0.748331	138681.8
	80	427.2	426	426.6	426.6	0.489898	181987.6
	70	493.8	494.4	492.6	493.6	0.748331	243641
	60	579.6	583.8	576	579.8	3.187475	336168

Table A.6.3: H_s, u and correlation coefficients for the Gaussian fits for all PM experiments.

Polymers	Internal pressure (mbar)	H_s (m s^{-2})	u (m s^{-1})	Correlation coefficient	Correlation coefficient	Correlation coefficient
PAA synthesized at 50 °C without CTA $[AA]_0$=2M	100	6.24×10^{-7}	0.00155	0.99888	0.99901	0.99911
	90	5.61×10^{-7}	0.001418	0.9993	0.99903	0.99925
	80	4.55×10^{-7}	0.001262	0.99906	0.99899	0.99902
	70	3.82 × 10-7	0.001062	0.99938	0.9998	0.99935
	60	3.08×10^{-7}	0.000925	0.99877	0.99933	0.99921
PAA synthesized at 70 °C without CTA $[AA]_0$=2M	100	6.2×10^{-7}	0.001548	0.99939	0.99911	0.99913
	90	5.6×10^{-7}	0.001414	0.99917	0.99908	0.99917
	80	4.48×10^{-7}	0.001256	0.99908	0.99876	0.99897
	70	3.87×10^{-7}	0.001082	0.99949	0.99952	0.99947
	60	3.03×10^{-7}	0.000924	0.99913	0.99899	0.99912
PAA synthesized at 90 °C without CTA $[AA]_0$=2M	100	6.32×10^{-7}	0.001541	0.99912	0.99945	0.99931
	90	5.85×10^{-7}	0.001445	0.99896	0.99861	0.99883
	80	4.66×10^{-7}	0.001241	0.99927	0.99877	0.9993
	70	3.93×10^{-7}	0.001069	0.99848	0.99806	0.99755
	60	3.21×10^{-7}	0.000918	0.99841	0.99815	0.99826
PAA synthesized at 90 °C without CTA $[AA]_0$=1M	100	6.3×10^{-7}	0.001542	0.99908	0.99911	0.99905
	90	5.55×10^{-7}	0.001442	0.99895	0.99903	0.99878
	80	4.62×10^{-7}	0.001233	0.99938	0.99926	0.99953
	70	3.75×10^{-7}	0.001064	0.99936	0.99934	0.99927
	60	3.00×10^{-7}	0.00093	0.99822	0.99787	0.99811
PAA synthesized at 90 °C without CTA $[AA]_0$=3M	100	6.57×10^{-7}	0.001615	0.99936	0.99947	0.99932
	90	5.49×10^{-7}	0.001429	0.99861	0.9987	0.99879
	80	4.58×10^{-7}	0.001247	0.9994	0.99962	0.99971
	70	3.81×10^{-7}	0.001084	0.99912	0.99957	0.9996
	60	3.12×10^{-7}	0.000914	0.9982	0.99796	0.99812
PAA synthesized at 50 °C with CTA $[AA]_0$=2M	100	9.81×10^{-7}	0.00162	0.99758	0.99719	0.99721
	90	8.32×10^{-7}	0.001423	0.99882	0.9989	0.99888
	80	6.64×10^{-7}	0.001234	0.9989	0.99897	0.99772
	70	5.52×10^{-7}	0.001095	0.99891	0.99849	0.99869
	60	3.98×10^{-7}	0.000917	0.9992	0.99921	0.99927
PAA synthesized at 70 °C with CTA $[AA]_0$=2M	100	6.93×10^{-7}	0.001587	0.9975	0.99524	0.99612
	90	6.06×10^{-7}	0.001426	0.99644	0.99615	0.99395
	80	5.26×10^{-7}	0.001237	0.9972	0.98722	0.98922
	70	4.29×10^{-7}	0.001093	0.99799	0.9969	0.99599
	60	3.39×10^{-7}	0.000913	0.99727	0.99654	0.99713
PAA synthesized at 50 °C with CTA $[AA]_0$=2M	100	6.85×10^{-7}	0.001569	0.99594	0.99495	0.98921
	90	5.81×10^{-7}	0.001425	0.98969	0.98945	0.98474
	80	5.5×10^{-7}	0.00124	0.99157	0.98647	0.98705
	70	4.22×10^{-7}	0.0011	0.99884	0.99898	0.99872
	60	3.23×10^{-7}	0.000922	0.99602	0.99538	0.99618

Linear PNaA	100	6.58×10^{-7}	0.00159	0.99853	0.99842	0.99755
	90	5.8×10^{-7}	0.00141	0.99883	0.99875	0.99869
	80	4.74×10^{-7}	0.001244	0.9971	0.9968	0.99832
	70	4.06×10^{-7}	0.001072	0.99839	0.99849	0.99789
	60	3.3×10^{-7}	0.000907	0.99712	0.99813	0.99717
Hyperbranched PNaA	100	8.44×10^{-7}	0.001622	0.9958	0.99801	0.99558
	90	6.98×10^{-7}	0.001445	0.99672	0.99666	0.99626
	80	6.3×10^{-7}	0.001261	0.99648	0.99649	0.99619
	70	5.17×10^{-7}	0.00109	0.99559	0.99534	0.99524
	60	4.04×10^{-7}	0.000928	0.99646	0.99622	0.99614

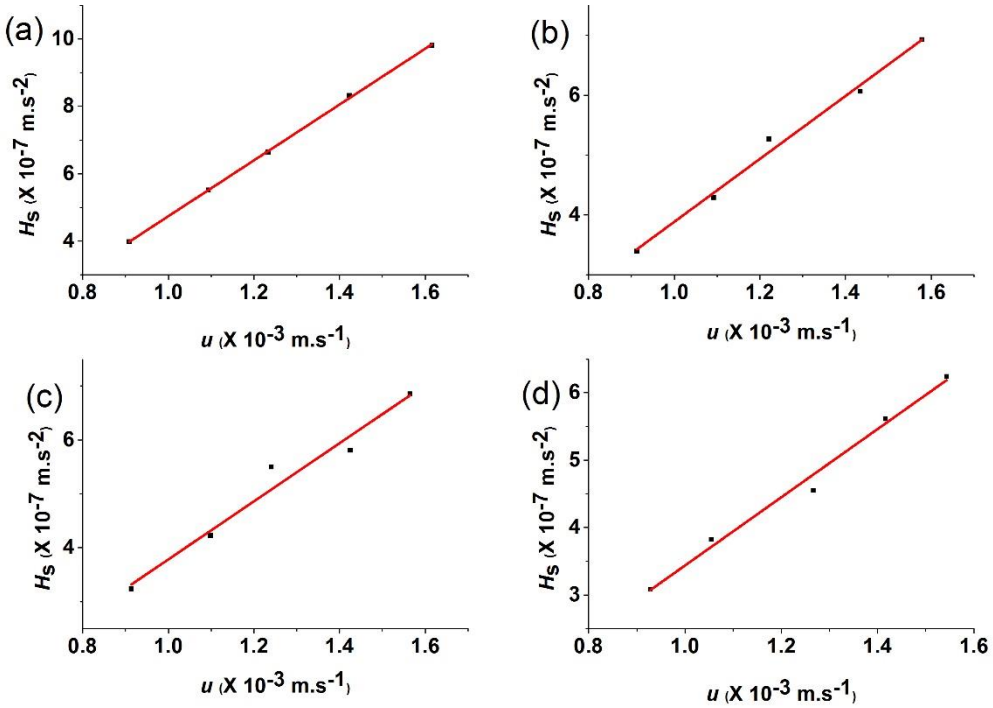

Figure A.6.2: H_s = f (u) obtained by TDA for PNaA synthesized by conventional radical polymerization at (a) 50 °C with CTA, (b) 70 °C with CTA, (c) 90 °C with CTA, (d) 50 °C without CTA.

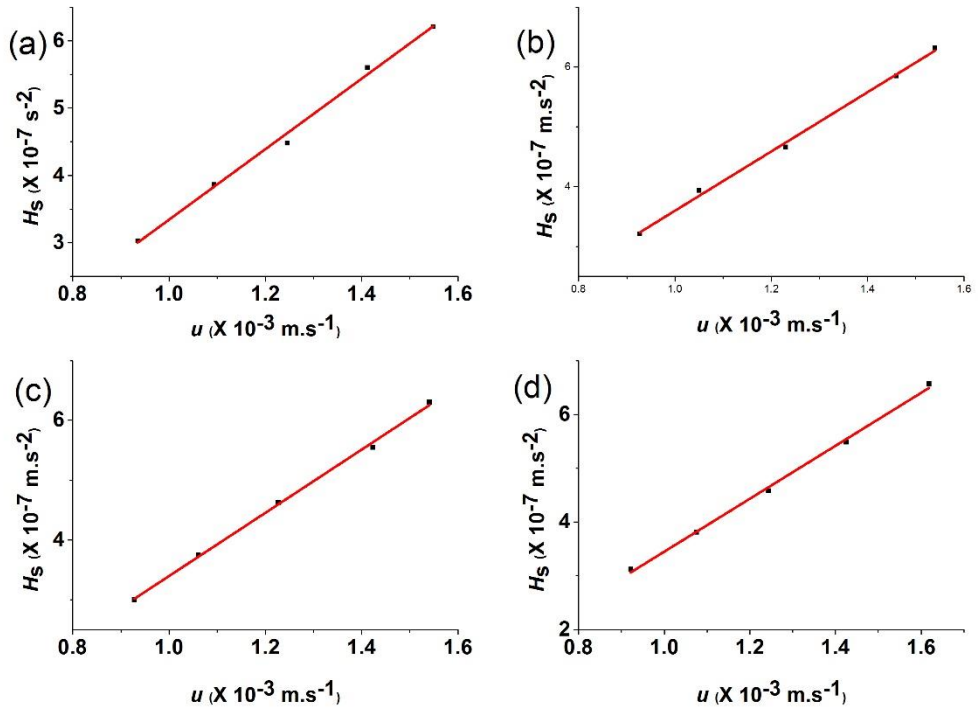

Figure A.6.3: H_s = f (u) obtained by TDA for PNaA synthesized by conventional radical polymerization at (a) 70 °C without CTA, (b) 90 °C without CTA, (c) 90 °C without CTA and $[AA]_0$=1M, (d) 90 °C without CTA and $[AA]_0$=3M.

The standard deviation of the slope was calculated with Eqs. (A.6.1) to (A.6.5)

$$Slope_{max} = Slope + SD(slope) \quad (A.6.1)$$

$$Slope_{min} = Slope - SD(slope) \quad (A.6.2)$$

$$D_{max} = \frac{R^2}{24 \times Slope_{min}} \quad (A.6.3)$$

$$D_{min} = \frac{R^2}{24 \times Slope_{max}} \quad (A.6.4)$$

$$SD\ (D) = \frac{D_{min} + D_{max}}{2} \quad (A.6.5)$$

Table A.6.4: τ and *Pe* calculated with Eq. (6.8) and (6.9)

Polymers	Internal pressure (mbar)	τ	*Pe*
PAA synthesized at 50 °C without CTA $[AA]_0$=2M	100	0.109814	9.80×10^4
	90	0.120068	8.96×10^4
	80	0.134878	7.98×10^4
	70	0.160259	6.71×10^4
	60	0.184058	5.85×10^4
PAA synthesized at 70 °C without CTA $[AA]_0$=2M	100	0.11379	9.46×10^4
	90	0.124528	8.64×10^4
	80	0.140175	7.68×10^4
	70	0.162763	6.61×10^4
	60	0.190589	5.65×10^4
PAA synthesized at 90 °C without CTA $[AA]_0$=2M	100	0.108137	9.95×10^4
	90	0.115259	9.34×10^4
	80	0.134273	8.01×10^4
	70	0.155826	6.91×10^4
	60	0.181405	5.93×10^4
PAA synthesized at 90 °C without CTA $[AA]_0$=1M	100	0.115247	9.34×10^4
	90	0.123172	8.74×10^4
	80	0.144042	7.47×10^4
	70	0.167025	6.44×10^4
	60	0.191065	5.63×10^4
PAA synthesized at 90 °C without CTA $[AA]_0$=3M	100	0.102405	1.05×10^5
	90	0.115744	9.30×10^4
	80	0.132586	8.12×10^4
	70	0.152502	7.06×10^4
	60	0.1809	5.95×10^4
PAA synthesized at 50 °C with CTA $[AA]_0$=2M	100	0.172062	6.25×10^4
	90	0.195784	5.50×10^4
	80	0.225825	4.76×10^4
	70	0.254416	4.23×10^4
	60	0.303932	3.54×10^4
PAA synthesized at 70 °C with CTA $[AA]_0$=2M	100	0.111281	9.67×10^4
	90	0.123886	8.69×10^4
	80	0.142794	7.54×10^4
	70	0.161571	6.66×10^4
	60	0.193478	5.56×10^4
PAA synthesized at 90 °C with CTA $[AA]_0$=2M	100	0.115402	9.32×10^4
	90	0.127117	8.46×10^4
	80	0.146037	7.37×10^4
	70	0.16462	6.54×10^4
	60	0.196466	5.48×10^4

Linear PNaA	100	0.103028	1.04×10^5
	90	0.116181	9.26×10^4
	80	0.131708	8.17×10^4
	70	0.152837	7.04×10^4
	60	0.180543	5.96×10^4
Hyperbranched PNaA	100	0.127142	8.46×10^4
	90	0.142785	7.54×10^4
	80	0.163566	6.58×10^4
	70	0.189255	5.69×10^4
	60	0.222306	4.84×10^4

A2.4.2 Fraction of chain end

A2.4.2.1 Values of $X_{CH2\ term}$

Table A.6.5: $X_{CH2\ term}$ calculated for the CTA-containing PAAs

PAA synthesis	$X_{CH2\ term}$ from Eq. (5)	$X_{CH2\ term}$ from Eq. (6)	*SNR*	*RSD* (%)
50 °C with CTA and at $[AA]_0 = 2$ M	0.234	0.245	618	0.00016
70 °C with CTA and at $[AA]_0 = 2$ M	0.154	0.157	404	0.00017
90 °C with CTA and at $[AA]_0 = 2$ M	0.0985	0.0110	270	0.00020

A2.4.2.2 Determination of the LOD

As SNR varies linearly with $X_{CH2\ term}$ (see Figure A.6.1), it is possible to calculate the LOD, corresponding to $SNR = 3$.

LOD: $X_{CH2\ term} = 0.0011$. Consequently, terminal CH_2 due to the branching should be detected for the non-CTA-containing PAAs.

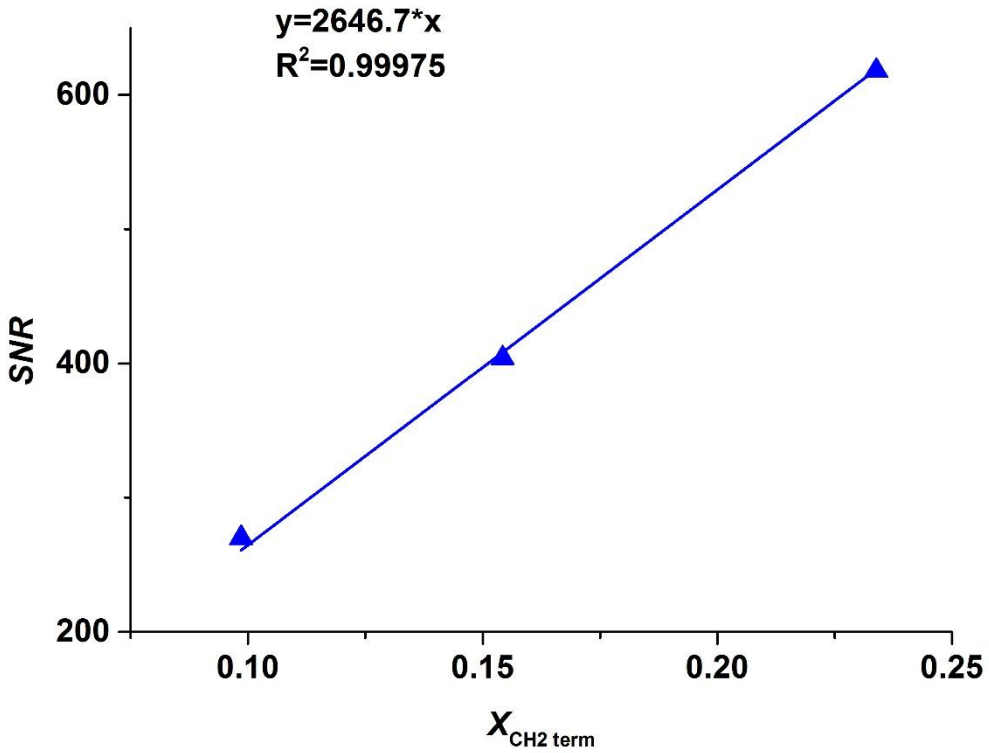

Figure A.6.4: *SNR* plotted against $X_{\text{CH2 term}}$

A2.4.3 Estimation of the activation energy of transfer to thioglycolic acid

Table A.6.6: Linear fit parameters for the Arrhenius plot of $X_{\text{CH2 term}}$

Slope	Intercept	Correlation coefficient
2441.4	-9.00052	0.9944

A2.4.4 Remaining ^{1}H NMR spectra

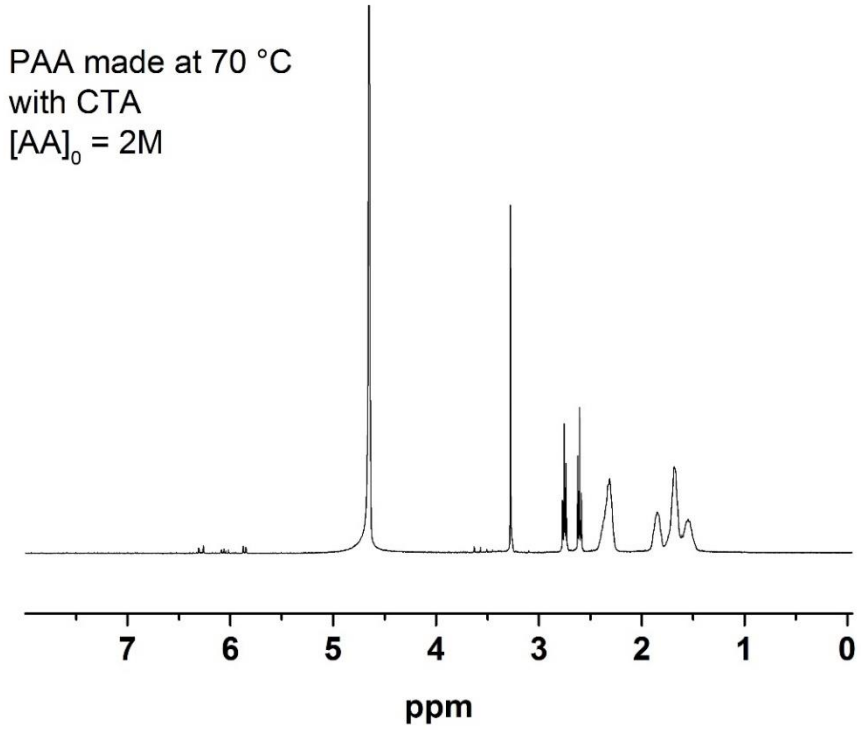

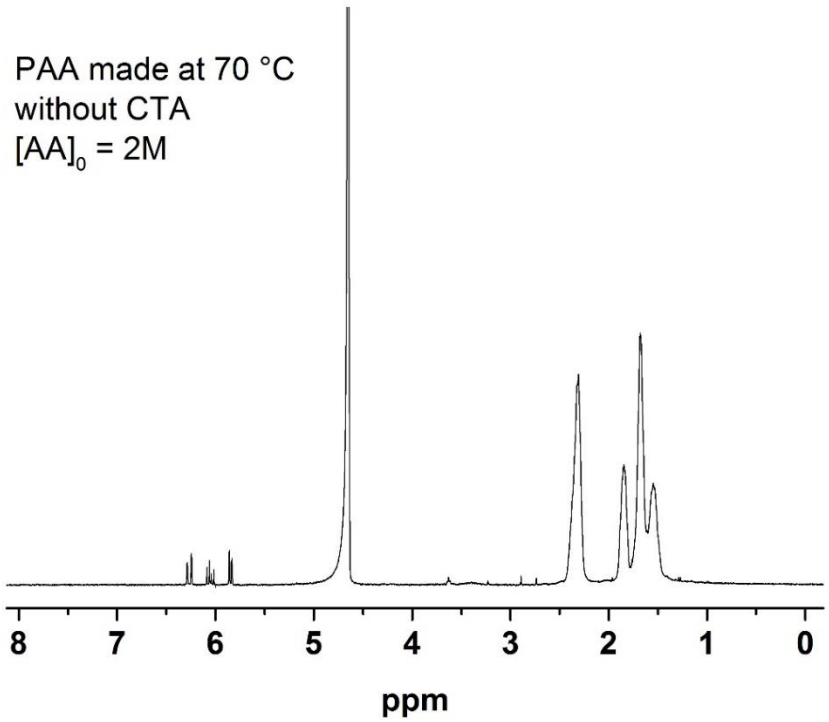
PAA made at 70 °C
without CTA
[AA]0 = 2M
8
7
6
5
4
3
2
1
0
ppm

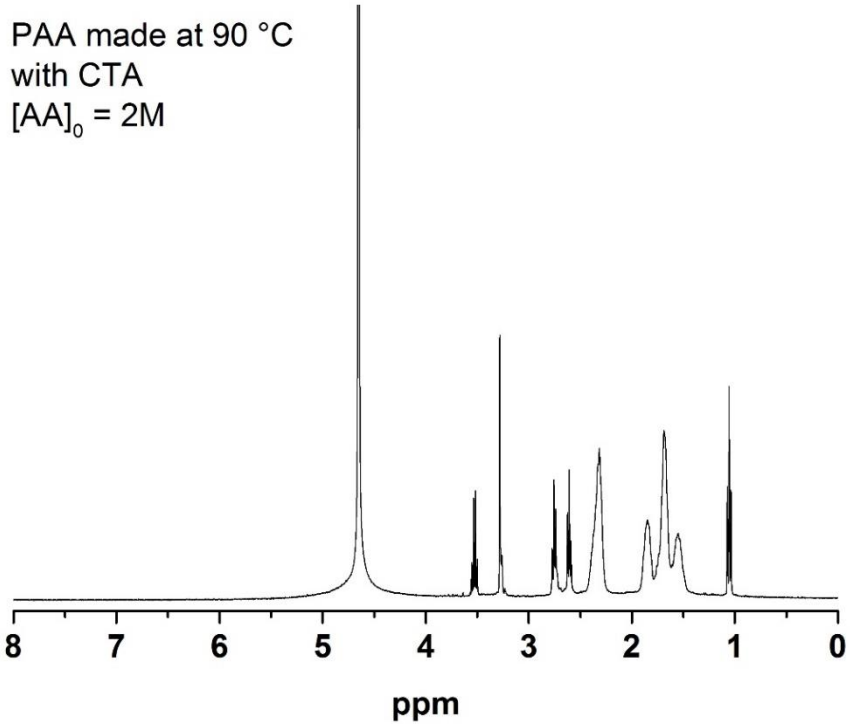
PAA made at 90 °C
with CTA
[AA]0 = 2M
8
7
6
5
4
3
2
1
0
ppm

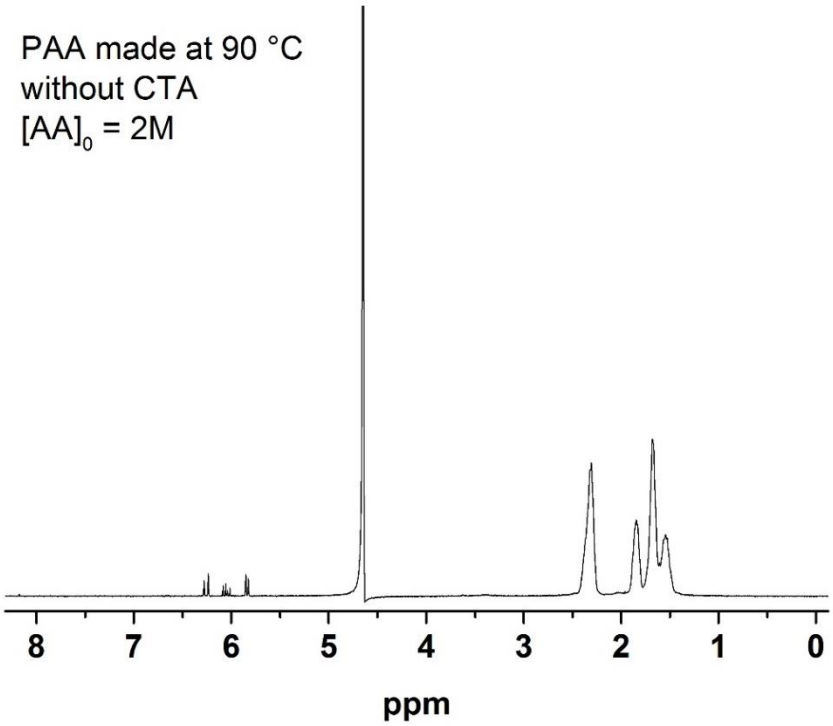
PAA made at 90 °C
without CTA
[AA]0 = 2M
8
7
6
5
4
3
2
1
0
ppm

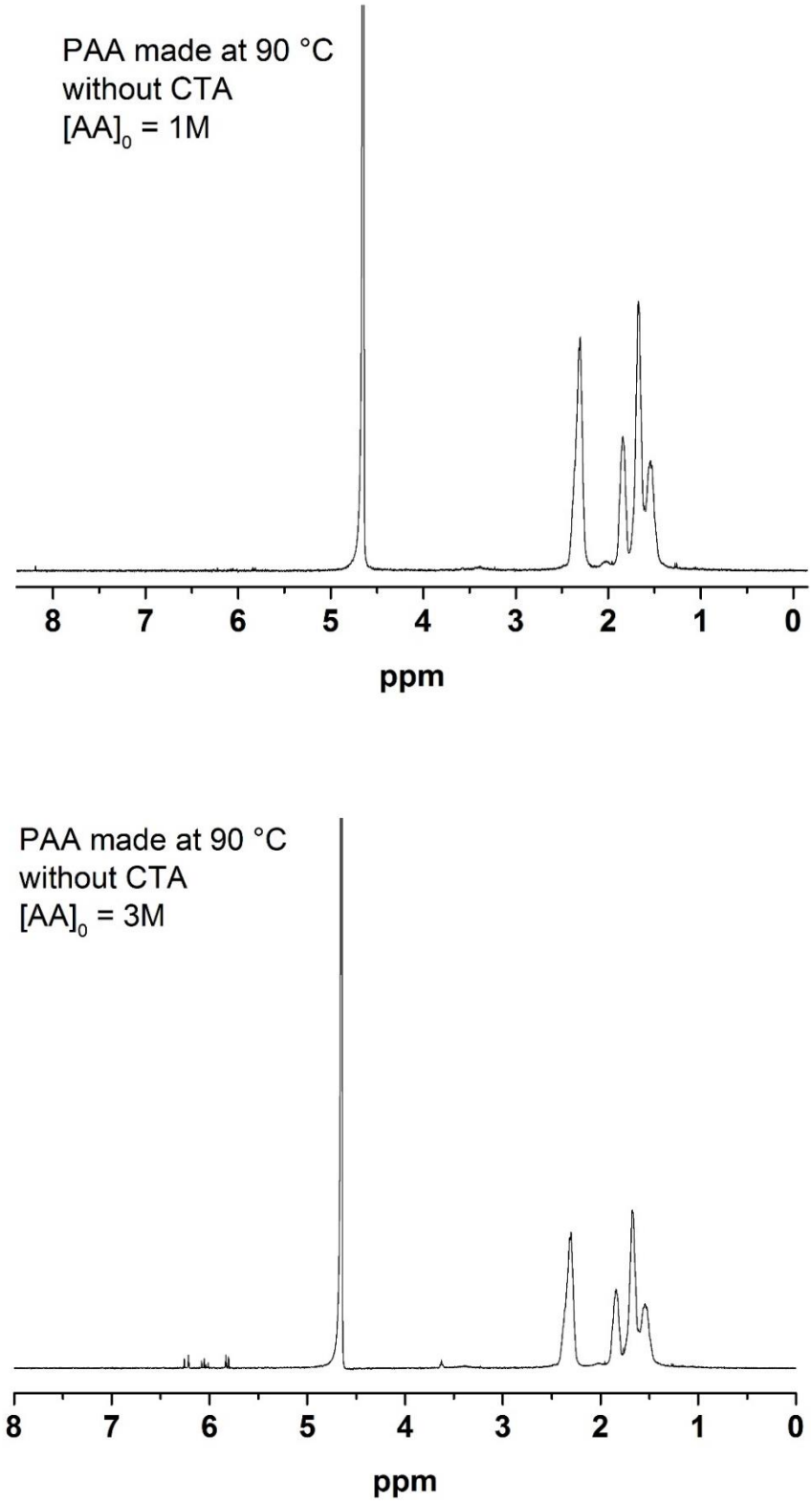

Figure A.6.5: ^{1}H NMR spectra of PAA analyzed at 25 °C in D2O

A2.5 References

[1] D.C. Blackley, A.C. Haynes, Kinetics of thermal-decomposition of 4,4'-azobis-(4-cyanopentanoic acid) and its salts in aqueous-solution, Journal of the Chemical Society - Faraday Transactions I, 75 (1979) 935-941.

[2] C. Loubat, B. Boutevin, Telomerization of acrylic acid with thioglycolic acid - Effect of the solvent on the C-T value, Polymer Bulletin, 44 (2000) 569-576.

[3] F.A. Plamper, H. Becker, M. Lanzendorfer, M. Patel, A. Wittemann, M. Ballauff, A.H.E. Muller, Synthesis, characterization and behavior in aqueous solution of star-shaped poly(acrylic acid), Macromolecular Chemistry and Physics, 206 (2005) 1813-1825.

[4] I. Lacik, S. Beuermann, M. Buback, PLP-SEC study into the free-radical propagation rate coefficients of partially and fully ionized acrylic acid in aqueous solution, Macromolecular Chemistry and Physics, 205 (2004) 1080-1087.

[5] F.D. Kuchta, A.M. van Herk, A.L. German, Propagation kinetics of acrylic and methacrylic acid in water and organic solvents studied by pulsed-laser polymerization, Macromolecules, 33 (2000) 3641-3649.

[6] H.L. Wang, H.R. Brown, Self-initiated photopolymerization and photografting of acrylic monomers, Macromolecular Rapid Communications, 25 (2004) 1095-1099.

[7] J. Barth, W. Meiser, M. Buback, SP-PLP-EPR study into termination and transfer kinetics of non-ionized acrylic acid polymerized in aqueous solution, Macromolecules, 45 (2012) 1339-1345.

[8] S. Khanlari, M.A. Dube, Effect of pH on Poly(acrylic acid) Solution Polymerization, Journal of Macromolecular Science Part a-Pure and Applied Chemistry, 52 (2015) 587-592.

[9] J. Loiseau, N. Doerr, J.M. Suau, J.B. Egraz, M.F. Llauro, C. Ladaviere, Synthesis and characterization of poly(acrylic acid) produced by RAFT polymerization. Application as a very efficient dispersant of CaCO3, kaolin, and TiO2, Macromolecules, 36 (2003) 3066-3077.

[10] J.-N. Ollagnier, T. Tassaing, S. Harrisson, M. Destarac, Application of online infrared spectroscopy to study the kinetics of precipitation polymerization of acrylic acid in supercritical carbon dioxide, Reaction Chemistry & Engineering, 1 (2016) 372-378.

[11] N.F.G. Wittenberg, C. Preusser, H. Kattner, M. Stach, I. Lacík, R.A. Hutchinson, M. Buback, Modeling acrylic acid radical polymerization in aqueous solution, Macromolecular Reaction Engineering, 10 (2016) 95-107.

[12] K.S. Anseth, R.A. Scott, N.A. Peppas, Effects of ionization on the reaction behavior and kinetics of acrylic acid polymerizations, Macromolecules, 29 (1996) 8308-8312.
[13] S. Schmitz, A.C. Dona, P. Castignolles, R.G. Gilbert, M. Gaborieau, Assessment of the extent of starch dissolution in dimethyl sulfoxide by 1H NMR spectroscopy, Macromolecular Bioscience, 9 (2009) 506-514.
[14] J.J. Thevarajah, A.T. Sutton, A.R. Maniego, E.G. Whitty, S. Harrisson, H. Cottet, P. Castignolles, M. Gaborieau, Quantifying the heterogeneity of chemical structures in complex charged polymers through the dispersity of their distributions of electrophoretic mobilities or of compositions, Analytical Chemistry, 88 (2016) 1674-1681.
[15] A.R. Maniego, D. Ang, Y. Guillaneuf, C. Lefay, D. Gigmes, J.R. Aldrich-Wright, M. Gaborieau, P. Castignolles, Separation of poly(acrylic acid) salts according to topology using capillary electrophoresis in the critical conditions, Analytical and Bioanalytical Chemistry, 405 (2013) 9009-9020.
[16] J.-B. Lena, A.K. Goroncy, J.J. Thevarajah, A.R. Maniego, G.T. Russell, P. Castignolles, M. Gaborieau, Effect of transfer agent, temperature and initial monomer concentration on branching in poly(acrylic acid): A study by 13C NMR spectroscopy and capillary electrophoresis, Polymer, 114 (2017) 209-220.
[17] D. Massiot, F. Fayon, M. Capron, I. King, S. Le Calve, B. Alonso, J.O. Durand, B. Bujoli, Z.H. Gan, G. Hoatson, Modelling one- and two-dimensional solid-state NMR spectra, Magnetic Resonance in Chemistry, 40 (2002) 70-76.
[18] M. Gaborieau, T.J. Causon, Y. Guillaneuf, E.F. Hilder, P. Castignolles, Molecular weight and tacticty of oligoacrylates by capillary electrophoresis - mass spectrometry, Aus. J. Chem., 63 (2010) 1219-1226.
[19] F. Heatley, P.A. Lovell, T. Yamashita, Chain transfer to polymer in free-radical solution polymerization of 2-ethylhexyl acrylate studied by NMR spectroscopy, Macromolecules, 34 (2001) 7636-7641.
[20] T. Junkers, M. Schneider-Baumann, S.P.S. Koo, P. Castignolles, C. Barner-Kowollik, Determination of Propagation Rate Coefficients for Methyl and 2-Ethylhexyl Acrylate via High Frequency PLP-SEC under Consideration of the Impact of Chain Branching, Macromolecules, 43 (2010) 10427-10434.